Evaluation des risques d'altération d'origine thermo-hydro-mécanique des pierres du patrimoine bâti

Asaad Alomari

UNIVERSITÉ D'ORLÉANS

ÉCOLE DOCTORALE ENERGIE, MATERIAUX, SCIENCES DE LA TERRE ET DE L'UNIVERS

Centre de Recherche sur la Matière Divisée CRMD FRE CNRS 3520

THÈSE présentée par:

Asaad ALOMARI

Soutenance prévue le :¨**18 Juin 2014**˝

pour obtenir le grade de : **Docteur de l'université d'Orléans**

Discipline/ Spécialité : Génie Civil

Evaluation des risques d'altération d'origine thermo-hydro-mécanique des pierres du patrimoine bâti

THÈSE dirigée par :

Muzahim AL-MUKHTAR	Professeur, Université d'Orléans
Kevin BECK	Maitre de conférences, Université d'Orléans
Xavier BRUNETAUD	Maitre de conférences, Université d'Orléans

RAPPORTEURS :

Anne PANTET	Professeur, Université du Havre
Beatriz MENENDEZ	Maître de conférences HDR, Université de Cergy-Pontoise

---

JURY:

Joelle RISS	Professeur, Université de Bordeaux
Anne PANTET	Professeur, Université de le Havre
Beatriz MENENDEZ	Maître de conférences HDR, Université de Cergy-Pontoise
Akos TOROK	Professeur, Université de Budapest, Hongrie
Muzahim AL-MUKHTAR	Professeur, Université d'Orléans
Kevin BECK	Maître de conférences, Université d'Orléans
Xavier BRUNETAUD	Maître de conférences, Université d'Orléans

Centre Val de Loire UNIVERSITÉ
Spirit of the Loire Valley

UNIVERSITY OF ORLEANS

UNIVERSITE D'ORLEANS

DOCTORALE SCHOOL FOR ENERGY, MATERIALS, EARTH AND UNIVERS SCIENCES

Research Center in Divided Matter CRMD FRE CNRS 3520

THESIS presented by:

Asaad ALOMARI

Date of thesis defence: ″**June 18th 2014**″

In partial fulfillment of the requirement for the degree:
Doctor of Philosophy from the University of Orleans

Speciality : Civil Engineering

Risk assessment of thermo-hydro-mechanical stone decay in built heritage

THESIS directed by:

Muzahim AL-MUKHTAR	Professor, University of Orleans
Kevin BECK	Associate Professor, University of Orleans
Xavier BRUNETAUD	Associate Professor, University of Orleans

RAPPORTEURS :

Anne PANTET	Professor, University du Havre
Beatriz MENENDEZ	Associate Professor HDR, University of Cergy-Pontoise

---

JURY:

Joelle RISS	Professor, University of Bordeaux
Anne PANTET	Professor, University of Le Havre
Beatriz MENENDEZ	Associate Professor HDR, University of Cergy Pontoise
Akos TOROK	Professor, University of Budapest, Hungary
Muzahim AL-MUKHTAR	Professor, University of Orleans
Kevin BECK	Associate Professor, University of Orleans
Xavier BRUNETAUD	Associate Professor, University of Orleans

Acknowledgements

In the beginning all my thanks and praises goes to my Lord “Allah” who help me to achieve my goal and to complete this research work. Also, it is a pleasure to thank all the people who gave me emotional support to continue my study.

Firstly I would like to introduce great thanks to my supervisor, Prof. Dr. **Muzahim Al-MUKHTAR** for his guidance, construction comments throughout this work, in addition, his valued time spending for reading the draft of this PhD research. Also, the efforts of Dr. **Kevin BECK** and of Dr. **Xavier BRUNETAUD** is highly appreciated whose help me for building this thesis to what it looks like now. A lot of thanks go to the members of the thesis committee, Dr. **Joelle RISS**, Dr. **Anne PANTET**, Dr. **Beatriz MENENDEZ** and Dr. **Akos TOROK** for their insightful comments, enthusiasm, recommendations and words of wisdom which enhanced my research work.

Sincere acknowledges are given to **the Ministry of Higher Education and Scientific Research of Iraq** and to **Mosul University** for their support as I made my doctoral study in the Polytechnic, Orleans University, France. I am grateful to all the staff from the laboratory of Research Center on the Divided Material (CRMD) especially, the director of the laboratory professor Dr. **Sylvie BONNAMY**. Also acknowledged are **Nicole NOURRY**, **Jennifer JUBIN** and **Jean-Michel MONFROY** for their help regarding administrative issues. This thesis would not have been the same without the emotional support of my Friend **Abdulrahman ALDAOOD** especially during the hard time of my staying in France.

I will never forget my professor who supports me to be field engineer, and take care a lot about me to get perfect in master degree then highlighted me in the PhD study. His name **Suhail Khattab** will stay forever in my mind.

The greatest thanks should go to the deceased's parents: **my father and my mother**, who are the reason for my existence in this life, and I ask God to have mercy on them and call them in paradise. I should not forget to extend the thanks to my brothers **Arshad**, **Arkam** and special thanks to my **sister**.

Last but not least, I would like to present my heartfelt thanks and love to my wife, for her care, support, affection in particular and encourage me. Great thanks and cordiality to my son **Saleh** and my princess my daughter **Maymuna**.

Contents

List of Figures

Chapter 1

Chapter 2

Chapter 3

List of Tables

Chapter 2

Chapter 3

Evaluation des risques d'altération d'origine thermo-hydro-mécanique des pierres du patrimoine bâti

Introduction générale

Introduction générale

L'étude présentée dans ce mémoire de thèse concerne le vieillissement des ouvrages en pierre calcaires. Les pierres calcaires poreuses sont des matériaux de construction qui furent et sont toujours beaucoup utilisés pour la réalisation de monuments prestigieux et emblématiques, dans quasiment toutes les cultures sédentaires. Les monuments historiques nous parviennent aujourd'hui dans un état très variable de conservation, compte tenu des moyens accordés ou non pour leur entretien, mais aussi notre souvent faible maîtrise des processus de dégradation, notamment sur le long terme. Les pierres calcaires poreuses et fines sont particulièrement prisées du fait de leurs qualités restées longtemps sans concurrence : résistance suffisante en parement, bonne capacité à être sculptées, aspect esthétique blanc et homogène, et disponibilité à peu près partout sur les continents. Cependant, ces qualités s'accompagnent de faiblesses qu'il convient de prendre en compte, à la fois durant la construction, mais aussi lors des phases d'entretien et de restauration : grande capacité de rétention d'eau, porosité complexe favorisant l'accumulation de sels, sensibilité au gel, présence d'une fraction argileuse parfois significative et donc induisant potentiellement des comportements hydriques pathogènes, résistances mécaniques médiocres en présence d'eau... C'est pourquoi ces pierres sont utilisées principalement en parement de façade, surtout lorsque ces parements sont ouvragés. Lorsqu'ils sont épais, les murs contiennent une partie intérieure faite de matériaux de remplissage issus de fragments de pierre de taille, de moellons, et d'autres déchets et remblais de construction, tandis que leurs soubassements utilisent des pierres moins sensibles à l'eau et plus résistantes, dite non-capillaires ; leurs parties supérieures sont par ailleurs protégées de l'eau gravitaire par une étanchéité. Malgré toutes ces attentions, les pierres calcaires poreuses s'altèrent, soit à cause d'une erreur de conception ou de réalisation (défaut d'étanchéité, pont capillaire...), soit pour des raisons accidentelles (incendies détruisant la toiture et donc la protection de la pierre, inondations...), soit tout simplement par l'action prolongée du temps, au sens temporel et climatique. C'est sur ce dernier point que cette étude se concentre. En partant de l'hypothèses que les anciens ont travaillé selon les règles de l'art connues alors, il s'agit

d'enrichir notre connaissance afin de transmettre notre patrimoine bâti en limitant l'impact socio-économique, car comprendre et maitriser l'origine des dégradations est la voie la moins coûteuse pour maintenir l'intégrité d'un ouvrage. Limiter les opérations de remplacement de tout ou partie d'un ouvrage permet en effet d'assurer la transmission de notre identité patrimoniale.

Les altérations des pierres résultent de leur interaction avec l'environnement. Etudier le vieillissement de la pierre in situ requiert donc que l'on s'intéresse au matériau, mais aussi au climat et plus particulièrement aux conditions météorologiques locales auxquelles il est soumis. L'existence d'un document décrivant et documentant les typologies d'altération (glossaire ICOMOS) montre que même si les climats diffèrent selon la situation géographique des ouvrages, et si les conditions locales d'exposition peuvent aussi jouer un rôle prépondérant, les typologies d'altérations restent globalement les mêmes. Cela ne signifie pas cependant que les origines soient les mêmes, ni que nous sachions y remédier. D'une manière générale, si la description des symptômes des dégradations des pierres commence à faire consensus, la recherche des sources pathogènes et des processus d'altération reste largement ouverte. De nombreuses hypothèses existent, des mécanismes sont proposés et documentés, mais très peu d'études quantitatives se sont attachées à tester leur véracité ou leur champ de validité.

Les études de durabilité sont par nature transdisciplinaires et complexes, car il s'agit de comprendre pourquoi un système a priori correctement dimensionné et initialement stable devient instable par la concomitance de facteurs externes répétés et/ou accidentels en lien avec des propriétés évolutives du matériau. Se limiter à l'étude d'un seul aspect, ou par une seule approche signifie risquer de passer à côté de couplages multi-physiques ou multi-échelles, sans oublier les nombreux domaines de la connaissance qui doivent intervenir : géologie, physico-chimie, mécanique, météorologie, histoire... Le Génie Civil est une discipline scientifique résolument appliquée et transversale, et particulièrement adaptée aux études de durabilité. C'est pourquoi le vieillissement des ouvrages est étudié ici sous l'angle du Génie Civil.

Deux sites historiques majeurs constituent le champ d'investigation et d'application de cette étude. Il s'agit du Château de Chambord, fleuron architectural du patrimoine bâti de

la Région Centre, et du site archéologique d'Al-Namrud en Irak et plus particulièrement de la Ziggurat. Dans le cas du site de Chambord, les matériaux étudiés sont le tuffeau, largement utilisé dans les parements de façade, et la pierre de Richemont, utilisée ponctuellement mais abondamment en substitution du tuffeau pour la restauration du château. Dans le cas du site d'Al-Namrud, deux pierres sont étudiées. L'une est issue de prélèvements in-situ sur des pierres supposées d'origine, l'autre correspond à celle qui pourrait être utilisée pour la restauration en raison de leur proximité géologique et géographique. Toutes ces pierres sont des pierres majoritairement calcaires, poreuses et fines, utilisées pour des parements exposés à des conditions climatiques difficiles. Le choix des deux sites permet de mettre en avant la différence de climat et son impact sur le vieillissement des pierres.

L'objectif de cette thèse est de proposer des méthodes quantitatives d'estimation des conséquences de l'interaction pierre / environnement en termes de durabilité. Il s'agit donc d'étudier le rôle des conditions climatiques dans l'évolution des propriétés des pierres. Les approches menées pour atteindre cet objectif touchent la caractérisation physico-chimique des pierres, la caractérisation de leurs propriétés de transfert et de rétention d'eau, la caractérisation de leur comportement thermo-hydrique ; cela concerne également la collecte de données météorologiques sur les deux sites, l'estimation des risques d'endommagement des pierres en réponse au climat via le calcul de fréquence de la condensation, de cycles de gel/dégel, de contrainte thermo-hydrique, l'estimation de la compatibilité entre les matériaux in situ et la pierre « candidate » pour la restauration. Enfin, une application préliminaire du carnet de santé numérique, développé pour le château de Chambord, est effectuée sur le site d'Al-Namrud utilisant un photomodèle 3D de la Ziggurat en vue de réaliser un diagnostic d'ouvrage.

Le manuscrit se compose de trois chapitres. Le premier est consacré à une synthèse bibliographique, le second traite aux pierres françaises, et le troisième aux pierres irakiennes.

Le chapitre s'attache à décrire et illustrer de manière synthétique les principales typologies d'altération, les principaux processus d'altération (physiques, biologiques, chimiques) proposés dans la littérature, ainsi que les facteurs environnementaux et les

propriétés de la pierre intervenants dans ces processus. Les processus de dégradation physiques ont été tout particulièrement approfondis, car sur eux reposent les estimations des risques d'endommagement étudiés dans les chapitres suivants.

Le second chapitre synthétise les études relatives aux pierres calcaires utilisées dans les parements du Château de Chambord : tuffeau et pierre de Richemont. Ce second chapitre débute par la description de toutes les procédures expérimentales exécutées : les caractérisations physico-chimiques et texturales impliquant DRX, ATG/ATD, chromatographie ionique, microscopie électronique et optique, et porosimétrie à l'eau et par intrusion de mercure ; les caractérisations des propriétés de transfert d'eau telles que les courbes de rétention d'eau, l'imbibition capillaire, l'absorption d'eau et la perméabilité à l'eau, et la dilatation hydrique ; les propriétés mécaniques par essais destructifs (compression et fendage) et non destructifs (ultra-sons) ; et la caractérisation thermo-hydrique du module élastique, du coefficient de Poisson et des déformations libres par extensométrie dans une cellule hydraulique à température et humidité contrôlée. Le second chapitre présente ensuite les risques d'endommagement des pierres consécutif à l'exposition aux fluctuations climatiques. Il s'agit ici d'évaluer la fréquence d'événements ponctuels tels que la condensation à la surface et dans la porosité des pierres, le gel-dégel, et la variation des contraintes hydro-thermiques au regard des limites imposées par la résistance en compression et en traction des pierres. Pour ces calculs, les données d'entrée sont d'une part les propriétés hydro-thermiques, mécaniques et texturales issues des caractérisations des pierres, et d'autre part des données climatiques issues de la station de Bricy située à 45 km de Chambord, et de quinzaine de capteurs insérés dans les pierres à différentes profondeurs, hauteurs et orientations. Enfin, la notion de degré de saturation critique est abordée afin de déterminer le degré de saturation des pierres minimal permettant au gel de devenir un facteur d'endommagement, et ce pour chacune des deux pierres. Ces estimations quantitatives du risque d'endommagement permettent de discuter du rôle des facteurs environnementaux, et ainsi de hiérarchiser les processus d'altération prédominants dans le cadre des pierres du Château de Chambord exposées au climat local.

Le troisième et dernier chapitre rend compte des études relatives à la pierre calcaire, dans sa version altérée et saine, utilisée dans la construction du site d'Al-Namrud et de la

pierre candidate à sa restauration. Les processus d'altérations auxquels sont soumises les pierres de la Ziggurat d'Al-Namrud sont examinés et discutés. Toutes les pierres sont caractérisées afin de vérifier a priori la compatibilité de la pierre candidate pour la restauration du site. Une estimation des risques d'endommagement de la pierre consécutif aux fluctuations climatiques est réalisée sur la base des caractérisations et des données météorologiques disponibles sur un site proche d'Al-Namrud. Le processus d'estimation des risques est similaire à celui employé dans le chapitre précédent, mais il est ici simplifié du fait de la moindre disponibilité des propriétés des pierres et des données météorologiques locales. Enfin, une première étape de constitution d'un carnet de santé numérique de la Ziggurat d'Al-Namrud est présentée, sous la forme d'un photomodèle 3D des parements dans lequel sont représentées les cartographies d'altérations, et la situation précédente d'enfouissement des pierres, ceci afin de poser les bases du diagnostic d'ouvrage.

Enfin, ce mémoire se termine par une conclusion synthétisant les différents chapitres et résumant les principaux apports scientifiques et méthodologiques. Sur ces bases, des perspectives de développement et de recherches futures sont proposées. Quatre annexes sont ajoutées à ce mémoire, il s'agit de quatre articles scientifiques publiés à ce jour issus de ce travail.

Résumé du chapitre 1

Résumé du chapitre 1

Ce chapitre est consacré à une synthèse bibliographique des principaux processus d'altération (physiques, biologiques, chimiques) expliquant les altérations des pierres en contact avec leur environnement, ainsi que les facteurs environnementaux et les propriétés de la pierre intervenant dans ces processus.

La première partie de ce chapitre traite des processus d'altération. Parmi ceux-ci, les premiers processus documentés sont appelés "physiques" et concernent la création de contraintes dans la pierre sans interaction chimique ou biologique avec la matrice. Il s'agit donc des contraintes thermiques et hydriques consécutives aux variations de température et d'humidité, du gel-dégel, et de la cristallisation de sels exogènes. Ces contraintes, si elles dépassent la résistance en traction ou compression de la pierre, peuvent être à l'origine d'une fissuration de la matrice et d'un éclatement ou désagrégation superficielle de la pierre. Chacun de ces processus est illustré soit par de la documentation issue de la littérature, soit grâce à des photographies prises durant ce travail. Le premier processus de dégradation physique présenté est celui relatif au gel-dégel, qui est considéré comme l'un des principaux processus d'endommagement des pierres de parement dans les régions humides et froides. L'influence de ce processus est profondément liée aux propriétés de la pierre, notamment à sa porosité et à sa texture, mais aussi comme tout processus physique, à sa résistance. Le degré de saturation en eau de la pierre est un facteur majeur, car la porosité remplie d'air agit comme vasque d'expansion pour limiter les effets induits par la cristallisation de la glace. Pour expliquer la création de contraintes mécaniques potentiellement pathogènes, plusieurs hypothèses existent : l'augmentation de volume de l'eau gelée, la pression de cristallisation de la glace, la migration d'eau liquide, et les éventuelles pressions induites hydrauliques par cette migration. Le deuxième processus d'altération physique présenté est celui relatif à l'attaque par les sels. La précipitation de sels est générée par l'évaporation de la solution interstitielle de la pierre. Si les différents ions nécessaires à la formation de sels expansifs potentiellement pathogènes proviennent de l'extérieur de la pierre, il s'agit bien d'un processus physique. Si tout ou partie des ces ions provient de la dissolution de la matrice de la pierre, il s'agit d'un processus chimique. La dégradation par les sels est

considérée comme très répandue dans le monde entier. Ce processus est particulièrement néfaste dans les zones côtières où les embruns marins charrient une grande quantité de sels dissous, lorsque des pierres sont en contact avec un sol pollué par les sels, notamment des sels de déverglaçage, des déjections d'animaux... Les ions considérés comme les plus pathogènes sont les chlorures, les sulfates, les nitrates et les carbonates. Ce chapitre passe en revue les études les plus significatives sur l'action des sels sur les pierres historiques. Les contraintes générées par les sels peuvent provenir de diverses origines : la pression de cristallisation à proprement parler, les pressions d'hydratation dues aux changement de phases des sels en fonction de l'humidité environnante, les pressions hydrauliques dues aux mouvements d'eau, et des dilatations différentielles, notamment thermiques, provenant d'une différence de coefficient de dilatation entre certains sels et la matrice de la pierre. Le processus suivant est celui relatif aux contraintes thermiques, qui proviennent de déformations empêchées ou différentielles entre la surface et le cœur, suite à une variation thermique. Comme l'origine des contraintes est ici directement liée aux variations climatiques, la notion de fatigue intervient pour estimer l'effet à long terme. Enfin, les différents minéraux constitutifs de la pierre possèdent parfois des coefficients de dilatation thermique différents, ce qui induit des dilatations différentielles potentiellement importantes. Le dernier processus physique présenté est celui relatif aux conséquences des variations de teneur en eau de la pierre, aussi appelées cycles d'humidification - séchage. De la même manière que pour les contraintes thermiques, des contraintes hydriques peuvent être induites par gradient avec le coeur, par dilatation empêchée, et par dilatations différentielle, notamment dans le cas où les pierres contiennent une fraction significative d'argiles gonflantes. Il faut ajouter à cela les contraintes hydrauliques induites par les mouvements d'eau. L'éventuelle dissolution de la matrice résultante de ces mouvements d'eau, ainsi que la reprécipitation consécutive associée, est davantage un phénomène chimique. Les processus chimiques de dégradation interviennent lorsque l'on peut observer une modification de la composition minéralogique des la pierre, ou de sa répartition. Ils sont principalement issus de réactions chimiques de dissolution, d'oxydation, d'hydratation et d'hydrolyse. Enfin, les derniers processus présentés sont biologiques, et concernent la croissance d'organismes biologiques tels que les mousses, les algues, les lichens, et qui

peuvent induire des dégradations via des processus physiques et chimiques. Par exemple, les racines peuvent fissurer la matrice de la pierre tandis que certains lichens peuvent attaquer la pierre avec une solution acide. Les processus chimiques et biologiques n'étant pas le sujet principal de cette recherche, leur documentation reste succincte.

La deuxième partie de ce premier chapitre s'attache à décrire les facteurs jouant sur la dégradation des pierres, qui sont constitués des propriétés des pierres (facteurs internes) et des agents extérieurs (facteurs externes). Les facteurs internes correspondent aux propriétés ayant un rôle révélé majeur dans le développement ou l'initiation des dégradations. il s'agit de la texture de la pierre, sa taille de grain, sa composition minérale, et les propriétés de sa porosité (valeur totale, distribution en taille des pores, connectivité). Les résultats de la littérature montrent que moins la microtexture est homogène, et plus la distribution en taille de grain est large, moins la pierre est résistante aux altérations. La présence de minéraux argileux dans la composition minérale de la pierre est un facteur augmentant la sensibilité aux altérations. Une distribution en taille de pore étendue favorise la rétention d'eau de la pierre. Une plus grande connectivité des pores favorise les mouvements d'eau et la sensibilité au gel. La porosité totale agit à l'échelle de l'intensité de l'endommagement. Les pierres qui possèdent une faible conductivité hydraulique sont moins sensible aux sels tandis qu'une forte capacité de rétention d'eau limite la cinétique de séchage et donc la sensibilité aux sels. Les pierres possédant une faible conductivité thermique subissent davantage de gradient thermique, et donc sont plus sensibles aux variations de température, phénomène amplifié par une forte absorption des rayonnements solaire (i.e. albédo élevé). Hormis les pollutions, les facteurs extérieurs sont principalement liés aux conditions climatiques qui règnent au contact de la pierre. Il s'agit de l'humidité relative, de la température, du vent, des précipitations et des radiations solaires. Ces différents paramètres jouent de manière répétée par leurs variations, et sur de très longues périodes. La fatigue du matériau induite par ces variations rend complexe l'appréhension de leur impact. De plus, ces facteurs extérieurs engendrent un gradient de leurs homologues dans la pierre, qui peut être à l'origine d'un endommagement sous la surface de la pierre, et donc particulièrement difficile à diagnostiquer. Ajouté à l'effet purement cyclique, une température haute favorise le séchage, lui-même à l'origine des phénomènes de

précipitation des sels. Les précipitations, principalement sous la forme de pluie, sont des vecteurs pour l'apport de polluants dans la pierre ou la formation d'une solution acide. De plus, les pluies diffuses favorisent les réactions avec le substrat tandis que les pluies abondantes augmentent la dissolution de surface. Finalement, le vent tend à augmenter la cinétique de séchage et ainsi la sensibilité aux sels. Il est de plus un vecteur de dépôt de polluant par voie sèche, et d'érosion lorsqu'il est chargé de particules fines et abrasives.

L'élément récurrent dans les processus d'altérations reste principalement l'eau. Tout ce qui favorise ses mouvements et son accumulation rend a priori la pierre plus sensible à son environnement. La condensation et le gel-dégel, à la fois en surface en en profondeur de la pierre, sont directement liés à la fois aux conditions environnementales et aux propriétés de la pierre. Enfin, les variations climatiques engendrent des dilatations empêchées qui se traduisent par des contraintes thermo-hydriques pouvant être à l'origine d'une fatigue de la pierre. Ces différences processus clé sont étudiés et évalués quantitativement en termes d'estimation des risques d'endommagement dans les chapitres suivants.

Résumé du chapitre 2

Résumé du chapitre 2

Ce chapitre traite des études relatives aux pierres calcaires utilisées dans les parements du Château de Chambord : tuffeau et pierre de Richemont. La caractérisation du tuffeau et de la pierre de Richemont commence par une description générale de leur provenance, de leur composition et de leurs caractéristiques d'un point de vue géologique, ainsi que des principaux ouvrages ayant fait appel à ces pierres. L'étude pétrographique qui suit, et qui utilise les résultats de DRX, d'ICP OES et d'ATG/ATD montre les différences minéralogiques entre les deux pierres. Le tuffeau est une pierre majoritairement calcaire (49 %) à forte teneur en silice, et possédant une proportion significative de minéraux argileux, tandis que la pierre de Richemont est presque purement calcaire (95 %) et sans argile. La microtexture des deux pierres observée au MEB équipé d'une microsonde EDX montre quant à elle que le tuffeau comporte une gamme de taille et de morphologie de grains beaucoup plus large que la pierre de Richemont, qui se révèle ainsi à la fois plus fine et plus homogène. La caractérisation de la porosité utilise dans un premier temps la mesure des densités réelles et apparentes par pesée hydrostatique. La porosité totale du tuffeau (45%) se révèle supérieure à celle de la pierre de Richemont (29 %). Pour obtenir la distribution en tailles des pores, c'est la porosimétrie par intrusion de mercure qui est utilisée. Le tuffeau se caractérise par une distribution plutôt bimodale : un premier pic centré sur 8 µm et un deuxième sur 0,01 µm. La pierre de Richemont est davantage monomodale avec un pic centré sur 2 µm et un épaulement à 0,6 µm. Les propriétés de transfert d'eau sont représentées d'abord par la capacité de rétention d'eau, utilisant plusieurs méthodes selon la succion recherchée : les solutions salines pour des succions supérieures à 2,7 MPa (moins de 98 % d'humidité relative), les solutions osmotiques entre 1,5 et 0,1 MPa, et les plaques tensiométriques entre 0,01 et 0,001 MPa. Pour les deux pierres, les courbes de rétention d'eau montrent relativement peu d'hystérésis. La capacité de rétention d'eau du tuffeau est beaucoup plus élevée que celle de la pierre de Richemont, et réclame des humidités relatives plus faibles pour s'installer. L'absorption d'eau à 48h à pression atmosphérique atteint 27 % pour le tuffeau, soit plus du double de la pierre de Richemont (12 %). L'absorption capillaire se caractérise à la fois par la prise de poids et le suivi du front

d'imbibition capillaire en surface des échantillons. En fin d'imbibition capillaire, la prise de poids du tuffeau est 60 % plus élevée après un temps deux fois plus court. La perméabilité à l'eau est mesurée en soumettant un échantillon de pierre à un gradient de pression hydraulique, et en mesurant le débit résultant en régime permanent. La perméabilité du tuffeau (3.10-7 m.s-1) s'est révélée nettement plus élevée que celle de la pierre de Richemont (5,4.10-8 m.s-1). Les propriétés mécaniques ont été mesurées par compression simple et par traction indirecte ou fendage, à la fois à l'état sec et à l'état saturé. La résistance du tuffeau atteint près de 12 MPa en compression à l'état sec, et 10 % de cette valeur en traction. Dans les deux cas, les valeurs calculées à l'état saturées chutent de 60 % par rapport à l'état sec. Pour la pierre de Richemont, la résistance atteint près de 20 MPa en compression et toujours 10 % de cette valeur en traction. Sa chute de résistance à l'état saturé est identique au tuffeau pour la traction, mais moins dramatique en compression (35 %). La vitesse de propagations des ondes de compression a été mesurée par ultrason pour chacune des pierres à l'état sec. Elle atteint 1600 m.s-1 pour le tuffeau contre 2600 m.s-1 pour la pierre de Richemont.

La deuxième partie de ce chapitre s'intéresse à l'évaluation des risques d'endommagement des pierres dans leur environnement. Après une courte description des caractéristiques du Château de Chambord, les données climatiques utilisées pour cette étude sont présentées. Il s'agit de données récoltées à partir d'une station météorologique placée sur la terrasse de la tour du Chaudron du château durant 17 mois, ainsi que celles issues d'une station de base militaire située à Bricy (45 Km de Chambord) durant 39 ans. La fréquence d'acquisition des données de la station située à Chambord est plus élevée, ce qui rend ces données précieuses si la période d'acquisition s'avère représentative du climat local, ce qui s'est confirmé. Ajoutées aux données météorologiques, des valeurs de température et d'humidité issues de capteurs placés dans les pierres de la tour du Chaudron, à différentes profondeur, hauteur et orientation ont été acquises durant 3 ans. L'ensemble de ces données climatiques conduisent à conclure que le climat de Chambord est tempéré et humide. Les données des capteurs proches de la surface des pierres sont similaires à celles dans l'air. Leur amplitude de variation diminue avec la profondeur, les données à cœur étant particulièrement stables. Ces informations caractérisant le climat et sa conséquence directe

dans la pierre sont utilisées en tant que sollicitation pour l'estimation des risques d'endommagement. Le premier risque étudié est celui relatif à la condensation, à la fois à la surface des pierres, mais aussi dans la porosité de la pierre. La condensation en surface intervient lorsque la température de surface de la pierre est inférieure ou égale au point de rosée de l'air environnant, tandis que la condensation dans la porosité tient compte du rayon de pore via la notion d'humidité relative critique. A Chambord, la fréquence annuelle de jours avec au moins un évènement de condensation en surface s'élève à environ 31 %. A l'intérieur de la pierre, les fréquences de condensations diminuent avec la profondeur, et augmente pour les petits rayons de pores. Ainsi, de part sa distribution en taille de pores, la pierre de Richemont se montre trois fois moins sujette à la condensation comparée au tuffeau. De la même manière que pour la condensation, les risques de gel-dégel sont étudiés à la fois en surface de la pierre et dans sa porosité. Le gel intervient lorsque la température passe sous zéro en surface et lorsque elle descend sous le point de gel dans la porosité en tenant compte des rayons de pores. De plus, le risque de gel est analysé en concomitance avec l'occurrence de pluie ou de condensation. A la surface, le gel intervient environ 10 % des jours. A l'intérieur des pierres, seuls les plus gros pores proches de la surface peuvent geler. Pour estimer le risque d'endommagement lié à l'occurrence du gel, une expérimentation en laboratoire à base de cycles de gel-dégel a été menée. Il s'agit de déterminer le degré de saturation en eau minimal entrainant un endommagement de la pierre. Les cycles choisis durent 24h avec une température variant de -18 à +32°C. Après le suivi, tous les indicateurs (porosité, vitesse du son, contrainte résiduelle à la traction) convergent pour confirmer que le degré de saturation critique est de 85 % pour chaque pierre, et ce, indépendamment du nombre de cycles, ce qui conduit à conclure qu'il s'agit d'une propriété intrinsèque de ces pierres. Le dernier risque étudié est celui relatif aux contraintes générées par les dilatations empêchées, qu'elles soient d'origine thermique ou hydrique. Dans un premier temps, le travail s'est concentré sur le calcul des contraintes dites thermiques, dans les deux pierres, en se basant sur la réponse mécanique d'un milieu semi-infini (cas d'un mur épais) à une sollicitation thermique. Les calculs montrent que les contraintes d'origine thermique sont plus élevées dans la pierre de Richemont que dans le tuffeau, mais dans les deux cas bien inférieures à la résistance des pierres. Pour affiner ces

premiers calculs de contrainte, l'effet des dilatations hydriques empêchées ont été ajoutées aux dilatations thermiques. Il s'est de plus avéré que les différents paramètres élastiques rentrant en compte dans le calcul des contraintes sont très probablement dépendants à la fois de la température et de l'humidité. Avant le calcul des contraintes thermo-hydriques, une étape nécessaire préliminaire a donc consisté à mesurer les propriétés élastiques du tuffeau (Module élastique, coefficient de Poisson et dilatations libres) en fonction de la température et de l'humidité. Ce travail expérimental original a consisté à mesurer la réponse de jauges de déformations (rosettes) colées sur un échantillon inséré dans une cellule de chargement contrôlée par un circuit hydraulique, le tout à température et humidité contrôlée grâce à l'utilisation d'une enceinte climatique. Les températures prises en compte étaient de -8 ; 2 ; 20 ; et 40°C tandis que les humidités relatives étaient de 0 ; 7 ; 23 ; 80 et 100 %. Le plan d'expériences était factoriel complet, ce qui signifie que toutes les combinaisons possibles ont été réalisées. Pour chaque combinaison, la déformation libre, la déformation axiale sous chargement, ainsi que la déformation transversale résultante ont été mesurées afin d'en déduire les propriétés élastiques recherchées. La technique des plans d'expérience a ensuite été utilisée pour obtenir et valider statistiquement pour chaque propriété un modèle mathématique unique représentant toutes les réponses mesurées. C'est donc ce modèle représentant les propriétés élastiques qui est ensuite utilisé en complément des données climatiques pour calculer les contraintes induites par les dilatations thermohydriques empêchées. Ce calcul de contraintes thermohydriques a été réalisé selon plusieurs schémas. Dans un premier temps, l'amplitude journalière de variation des contraintes est comparée à la contrainte admissible dans le tuffeau. La variation journalière des contraintes thermohydriques montre que les risque d'endommagement restent faibles, même proche de la surface, car la marge de sécurité reste d'un facteur 12. Le deuxième schéma consiste calculer la différence entre la contrainte de surface avec la contrainte à cœur, c'est-à-dire à 250 mm de profondeur dans la pierre. Ce calcul est motivé par l'hypothèse que la plasticité et le fluage de la pierre permettent à celle-ci d'atteindre un équilibre mécanique à cœur, notamment du fait que les variations de température et d'humidité y sont très faibles. Cet état mécanique dit de référence sert donc de blanc pour les calculs, et permet ainsi de déterminer si la surface est en compression ou en traction par

rapport au cœur supposé non chargé. Cette contrainte différentielle est ensuite comparée à la résistance en traction ou en compression selon son signe. Dans ce deuxième schéma, les calculs montrent que les risques en compression sont du même ordre que dans le premier schéma. Par contre, les risques en traction deviennent plus critiques car la marge de sécurité est seulement d'un facteur 2, ce qui est très faible pour des phénomènes cycliques entrainant la fatigue des matériaux.

En conclusion de ce chapitre, différentes techniques de caractérisation complémentaires ont été appliquées pour obtenir les compositions minéralogiques, les propriétés de transfert d'eau, les propriétés de la porosité, les résistances mécaniques et les propriétés élastiques thermohydriques. Toutes ces propriétés servent soit dans le calcul des risques d'endommagement selon les différents processus de dégradation physique retenus, soit pour apporter un éclairage sur les résultats. Globalement, le tuffeau se montre a priori plus sensible que la pierre de Richemont aux agressions climatiques du fait d'une plus grande porosité, plus faibles résistances, moindre homogénéité minéralogique, gamme de pores plus étendus, capacité de rétention d'eau plus grande associée à des transferts d'eau plus rapides. L'effet des variations climatiques a été analysé en estimant la fréquence d'évènements de condensation, de gel-dégel, et en calculant les variations de contraintes mécaniques d'origine thermohydrique. Le climat tempéré et humide de Chambord favorise la condensation à la surface et dans la porosité des pierres. Les risques de gel sont faibles, et les risques d'endommagement par le gel aussi du fait de la valeur élevée du degré de saturation en eau critique. En utilisant l'état de la pierre à cœur comme référence mécanique, la fluctuation des contraintes d'origine thermohydriques engendre des contraintes de compression admissibles, tandis que les contraintes de traction résultantes se rapprochent dangereusement des limites de la pierre, soulignant le rôle probablement majeur de ce processus dans la dégradation des pierres à Chambord.

Résumé du chapitre 3

Résumé du chapitre 3

Le troisième et dernier chapitre est une application sur le site Irakien des méthodologies élaborées grâce à l'étude des pierres françaises. Il rend compte des études relatives à la pierre calcaire dans sa version altérée et saine, utilisée dans la construction du site d'Al-Namrud et de la pierre candidate à sa restauration. Dans un premier temps, Il s'agit de documenter le site et les faciès de dégradation observés in situ. Dans un deuxième temps, la collecte de données météorologiques est utilisée pour estimer les risques d'endommagement par processus physiques, notamment les contraintes thermiques. Enfin, ce chapitre pose les bases du carnet de santé numérique en réalisant une caractérisation comparatives des pierres historiques altérées et saines avec la pierre candidate à la restauration pour en déduire l'origine des dégradations et estimer la compatibilité de la pierre candidate pour la substitution des pierres du site, ainsi qu'un modèle 3D par photogrammétrie. Ce modèle est utilisé pour délimiter les différentes cartographies et ainsi proposer un exemple d'analyse représentative de l'utilisation du carnet de santé à des fins de diagnostic d'ouvrage.

Le site d'Al-Namrud est un ensemble de ruines assyriennes trois fois millénaire situé au Nord de l'Irak le long du Tigre, proche de la ville de Mossoul. Le climat local est continental-subtropical avec des étés très chauds et secs (plus de 45°C), des hivers froids et humides, et un gel occasionnel. Les matériaux utilisés pour la construction de la citée d'Al-Namrud sont la pierre calcaire poreuse sujette à cette étude, une pierre gypseuse verte et des briques argileuses. Les pierres de ce monument n'ont jamais été restaurées et présentent divers faciès d'altération : efflorescence, désagrégation sableuse, desquamations, parties manquantes, décoloration et érosion différentielle. Ces altérations sont illustrées par des photographies prises sur site.

En application des méthodologies développées pour estimer les risques climatiques à Chambord, les risques de condensation, de gel-dégel et de contraintes thermiques ont été évalués pour la Zigurrat d'Al-Namrud. La fréquence des évènement de condensation est calculée à partir de données météorologiques issues d'une station proche du site, et en supposant, faute de mieux, que la température de l'herbe puisse être un indicateur de la

température de surface des pierres. La fréquence annualisée de condensation sur la pierre atteint 28 % et se limite aux mois d'hiver. Par contre, la condensation dans la pierre reste très faible, ce qui laisse supposer que ce processus n'est pas discriminant sur ce site. Avec les mêmes indicateurs, les fréquences de gel sont estimées en surface et dans la porosité et atteignent au maximum 6 %, ce qui est faible mais non nul. Ainsi, l'action répétée du fait de la très longue durée d'application (3000 ans) de ces sollicitations pourrait tout de même en faire un processus pertinent via la prise en compte de la fatigue. Pour l'estimation des contraintes d'origine thermique, des mesures de températures ont été réalisées spécifiquement sur des pierres du site placées sur une toiture et dans l'air, notamment en tenant compte de l'orientation des faces de la pierre. Les températures maximales sur la face sud dépassent ponctuellement 55°C, ce qui provoque des gradients thermiques journaliers s'approchant de 30°C, avec une différence de température air-pierre atteignant 18°C. Avec ces valeurs climatiques, le calcul de la variation des contraintes provenant des dilatations thermiques empêchées montre que la contrainte admissible de la pierre est dépassée durant 25% de l'année. L'effet des contraintes thermiques semble particulièrement significatif et constitue probablement le processus majeur.

La pierre historique altérée a été caractérisée afin d'en préciser l'altération. La diffraction des rayons X, ajoutée à l'analyse chimique par chromatographie ionique confirment la présence de gypse dans toutes les pierres prélevées, avec une proportion allant de 0,2 à 1,6 %. La poussière prélevée sur site s'avère elle aussi polluée avec 3,4 % de gypse, et l'eau prélevée dans le puis du site s'est révélée saturée vis-à-vis du gypse. L'observation de la pierre altérée au MEB avec microsonde EDX montre la présence d'une croute argileuse allant jusqu'à 500 µm d'épaisseur. Cette couche argileuse s'est avérée contenir ponctuellement des cristaux de gypse, de même que le reste de la pierre. Globalement, les signes convergent pour confirmer le rôle potentiellement discriminant du gypse dans l'altération des pierres in situ. La pierre fraiche issue de la carrière d'Al-Mur proche d'Al-Namrud a été caractérisée et comparée à la pierre historique saine grâce à la DRX, l'ICP OES, porosimétrie par intrusion de mercure, et porosimétrie à l'eau. Leurs propriétés se sont révélées proches, ce qui suppose que la carrière d'Al-Mur a probablement

servi pour la construction de la Ziggurat. Cette pierre constitue donc un choix pertinent et durable pour remplacer les pierres trop endommagées pour être restaurées.

Une première étape de constitution du carnet de santé numérique de la Ziggurat d'Al-Namrud a été présentée, sous la forme d'un photomodèle 3D des parements. Le modèle 3D des murs de la Ziggurat a été obtenu par une technique reposant sur la photogrammétrie, avec une incertitude métrique de l'ordre de 1,5 %. Grâce à l'application de textures issues des photographies, ce modèle possède une apparence réaliste permettant d'aider à la délimitation des zones d'intérêt, notamment les altérations de surface de la pierre. Différents documents historiques montrent que la Ziggurat était restée jusque dans les années 1960 complètement enfouie, et ce pendant une durée inconnue. Depuis, elle a fait l'objet de campagnes successives d'excavation. La comparaison des cartographies d'altération et de situation précédente d'enfouissement des pierres, combinée à l'analyse des données de caractérisation des pierres altérées, montre que la partie récemment mise à nue est encore exempte de dégradations issues de processus physiques, alors que la partie mise à nue depuis plus longtemps est déjà très endommagée. Ceci laisse supposer que la récente mise à nue des pierres après excavation pourrait engendrer leur dégradation rapide si aucune précaution n'est prise.

Conclusion générale et perspectives

Conclusion générale

L'étude présentée dans ce mémoire de thèse concerne le vieillissement des ouvrages en pierre calcaire. Si les altérations des pierres résultent de leur interaction avec l'environnement, étudier le vieillissement de la pierre in situ demande donc à la fois de s'intéresser à la caractérisation du matériau, mais aussi aux conditions météorologiques locales auxquelles il est soumis. Parmi les processus de dégradation, les processus physiques (gél-dégel, condensation, dilatations thermo-hydriques) sont particulièrement difficiles à appréhender, notamment du fait de leur aspect cyclique pouvant générer la fatigue des matériaux sur le long terme. D'une manière générale, si la description des processus de dégradation physiques repose sur des bases théoriques reconnues, l'estimation du poids de ces processus, et de leur rôle dans les dégradations des pierres reste largement ouverte. L'objectif de cette thèse est d'étudier le rôle des conditions climatiques dans l'évolution des propriétés des pierres en estimant de manière quantitative le poids les différents processus d'altération physique.

Deux sites historiques majeurs constituent le champ d'investigation et d'application de cette étude. Il s'agit du Château de Chambord, et du site archéologique d'Al-Namrud en Irak. L'approche choisie pour évaluer les risques d'endommagement des pierres étudiées lorsqu'elles sont soumises au climat est la suivante :

1. Réalisation d'une synthèse bibliographique concernant la quantification de l'impact des processus de dégradation en soulignant les propriétés des pierres les plus influentes et les facteurs météorologiques les plus discriminants.
2. Réalisation d'une campagne de caractérisation multi-échelles des différentes pierres de Chambord en ciblant les propriétés physico-chimiques jugées majeures dans les processus d'altération.
3. Collecte des données météorologiques à Chambord par relevé de stations proches et par mesures in situ.
4. Réalisation de campagnes expérimentales d'estimation du poids de certains paramètres (ici gel-dégel) pour alimenter/compléter la phase d'estimation des risques.

5. Estimation du risque d'endommagement par utilisation des données météorologiques comme sollicitation dans le calcul de l'impact des différents processus, développement des approches de calculs lorsque nécessaires.
6. Application sur le site Irakien d'Al-Namrud : caractérisation des pierres de la Ziggurat, collecte des données météorologiques, estimation des risques.
7. Développement des bases d'un carnet de santé numérique de la Ziggurat d'Al-Namrud pour son diagnostic d'ouvrage.

Les étapes de caractérisation des propriétés des pierres, de collecte de données météorologiques, et d'estimation des risques sont itératives dans le sens où les données météorologiques collectées peuvent se révéler insuffisantes, où de nouvelles propriétés peuvent s'avérer pertinentes suite à de premières tentatives d'estimation des risques, et où la prise en compte de ces propriétés requiert un développement des méthodes de calcul.

La synthèse bibliographique dans le premier chapitre analyse les diverses altérations des pierres en contact avec leur environnement et leurs principaux processus (physiques, biologiques, chimiques). Les processus de dégradation physiques, axe principal de ce travail de recherche, sont les processus sur lesquels reposent les estimations de risque d'endommagement des chapitres suivants. Les processus physiques concernent les sollicitations d'origine climatiques. Il s'agit donc des contraintes thermiques et hydriques consécutives aux variations de températures et d'humidité, du gel-dégel, et de la cristallisation de sels exogènes. Les différents facteurs jouant sur la dégradation des pierres, constitués des propriétés des pierres (facteurs internes) et des agents extérieurs (facteurs externes), sont étudiés. Les facteurs internes correspondent aux propriétés telles que de la texture de la pierre, sa taille de grain, sa composition minérale, et les propriétés de sa porosité (valeur totale, distribution en taille des pores, connectivité). L'élément récurrent dans les processus d'altération restant principalement l'eau, toutes les propriétés qui favorisent ses mouvements et son accumulation rend a priori la pierre plus sensible à son environnement. Les facteurs extérieurs sont l'humidité relative, la température, le vent, les précipitations et des radiations solaires. Sur la base de cette synthèse, la condensation, le

gel-dégel, et les dilatations thermo-hydriques empêchées sont choisis comme processus physiques de dégradation clés pour le reste de l'étude.

Le second chapitre synthétise les études relatives aux pierres calcaires utilisées dans les parements du Château de Chambord : tuffeau et pierre de Richemont.

La caractérisation minéralogique du tuffeau et de la pierre de Richemont a été réalisée grâce à l'utilisation de la DRX, l'ICP OES et l'ATG/ATD. Le tuffeau est une pierre majoritairement calcaire (49 %) à forte teneur en silice, et possédant une proportion significative de minéraux argileux, tandis que la pierre de Richemont est presque purement calcaire (96 %) et sans argile. La microtexture des deux pierres observée au MEB équipé d'une microsonde EDX montre quant à elle que le tuffeau comporte une gamme de taille et de morphologie de grains beaucoup plus large que la pierre de Richemont, qui se révèle ainsi à la fois plus fine et plus homogène. La pesée hydrostatique a montré que la porosité totale du tuffeau (45%) est supérieure à celle de la pierre de Richemont (29 %). Grâce à la porosimétrie par intrusion de mercure, le tuffeau montre une distribution en taille de pores plutôt bimodale : un premier pic centré sur 8 µm et un deuxième sur 0,01 µm. La pierre de Richemont est davantage monomodale avec un pic centré sur 2 µm et un épaulement à 0,6 µm. La capacité de rétention d'eau du tuffeau est beaucoup plus élevée que celle de la pierre de Richemont. L'absorption d'eau à 48h à pression atmosphérique atteint 27 % pour le tuffeau, soit plus du double de la pierre de Richemont (12 %). En fin d'imbibition capillaire, la prise de poids du tuffeau est 60 % plus élevée après un temps deux fois plus court. La perméabilité du tuffeau (3.10-7 m.s-1) s'est révélée nettement plus élevée que celle de la pierre de Richemont (5,4.10-8 m.s-1). La résistance du tuffeau atteint près de 12 MPa en compression simple à l'état sec, et 10 % de cette valeur en traction par fendage. Dans les deux cas, les valeurs calculées à l'état saturées chutent de 60 % par rapport à l'état sec. Pour la pierre de Richemont, la résistance atteint près de 20 MPa en compression et toujours 10 % de cette valeur en traction. Sa chute de résistance à l'état saturé est identique au tuffeau pour la traction, mais moins dramatique en compression (35 %). La vitesse de propagations des ondes de compression atteint 1600 m.s-1 pour le tuffeau contre 2600 m.s-1 pour la pierre de Richemont.

L'évaluation des risques d'endommagement des pierres dans leur environnement a nécessité la collecte de données climatiques issues diverses sources (station installée sur le site, capteurs placés dans la pierre, station située à 45 Km de Chambord). Grâce à une étude statistique, les données météorologiques issues de la station in situ se sont révélées représentatives du climat et donc utilisable pour l'estimation des risques climatiques, malgré leur courte période d'acquisition (17 mois). L'ensemble de ces données confirme que le climat de Chambord est tempéré et humide. L'amplitude de variation des températures et des humidités fournis par les capteurs diminue avec la profondeur, les données à cœur étant particulièrement stables. Les données des capteurs et de la station sont utilisées conjointement comme sollicitation pour l'estimation des risques climatiques. La fréquence annualisée des jours avec au moins un évènement de condensation en surface des pierres atteint environ 31 % à Chambord, ce qui en fait un phénomène majeur. A l'intérieur de la pierre, les fréquences de condensations diminuent avec la profondeur, et augmente pour les petits rayons de pores. Ainsi, la pierre de Richemont se montre trois fois moins sujette à la condensation (30 %) comparée au tuffeau (90 %). A la surface des pierres, la fréquence annualisée de jours avec au moins un évènement de gel en présence d'eau est comprise entre 5 et 10 %. A l'intérieur des pierres, seuls les plus gros pores proches de la surface peuvent geler. Pour estimer le risque d'endommagement lié à l'occurrence du gel, une expérimentation en laboratoire à base de cycles de gel-dégel (cycle de -18 à 32°C sur 24h) a été menée. Après le suivi, tous les indicateurs (porosité, vitesse du son, contrainte résiduelle à la traction) convergent pour confirmer que le degré de saturation en eau minimal pour obtenir un endommagement est de 85 % pour chaque pierre, et ce, indépendamment du nombre de cycles, ce qui conduit à conclure qu'il s'agit d'une propriété intrinsèque de ces pierres. Le dernier risque étudié est celui relatif aux contraintes générées par les dilatations thermo-hydriques empêchées. Dans un premier temps, le travail s'est concentré sur le calcul des contraintes thermiques, dans les deux pierres. Les calculs montrent que ces contraintes sont plus élevées dans la pierre de Richemont que dans le tuffeau, mais dans les deux cas bien inférieures à la résistance des pierres. Pour affiner ces premiers calculs de contrainte d'origine climatique, l'effet des dilatations hydriques empêchées a été ajouté. Pour ce calcul, il a fallu mesurer les propriétés élastiques du tuffeau (Module élastique, coefficient de

Poisson et dilatations libres) en fonction de la température et de l'humidité. Ce travail expérimental original a consisté à mesurer la réponse de jauges de déformation (rosettes) collées sur un échantillon inséré dans une cellule de chargement contrôlée par un circuit hydraulique, le tout à température et humidité contrôlée grâce à l'utilisation d'une enceinte climatique. La déformation libre, la déformation axiale sous chargement, ainsi que la déformation transversale résultante ont été mesurées afin d'en déduire les propriétés élastiques recherchées. La technique des plans d'expérience a ensuite été utilisée pour obtenir et valider statistiquement pour chaque propriété un modèle mathématique unique représentant toutes les réponses mesurées. Ces modèles représentant les propriétés élastiques ont été utilisés en complément des données climatiques pour calculer les contraintes induites par les dilatations thermohydriques empêchées selon deux schémas. Le premier schéma relatif à l'estimation de l'amplitude journalière de variation des contraintes montre que les risques d'endommagement restent faibles, même proches de la surface, car la marge de sécurité reste d'un facteur 12. Le deuxième schéma, plus réaliste, est relatif au calcul de la contrainte différentielle entre la surface avec le cœur, c'est-à-dire à 250 mm de profondeur dans la pierre, du fait que la plasticité et le fluage de la pierre sont supposés permettre à celle-ci d'atteindre un équilibre mécanique à cœur. Cette contrainte différentielle, une fois comparée à la résistance en traction ou en compression selon son signe, montre que les risques en compression sont du même ordre que dans le premier schéma. Par contre, les risques en traction deviennent plus critiques car la marge de sécurité est seulement d'un facteur 2, ce qui peut être considéré comme faible pour des phénomènes cycliques entrainant la fatigue des matériaux. Ainsi, Le climat tempéré et humide de Chambord favorise la condensation à la surface et dans la porosité des pierres. Les risques de gel sont faibles, et les risques d'endommagement par le gel aussi du fait de la valeur élevée du degré de saturation en eau critique. En utilisant l'état de la pierre à coeur comme référence mécanique, la fluctuation des contraintes d'origine thermohydrique engendre des contraintes de compression admissibles, tandis que les contraintes de traction résultantes se rapprochent dangereusement des limites de la pierre, soulignant le rôle probablement majeur de ce processus dans la dégradation des pierres à Chambord.

Le troisième et dernier chapitre rend compte des études relatives à la pierre calcaire historique, dans sa version altérée et saine, utilisée dans la construction du site d'Al-Namrud et de la pierre candidate à sa restauration. Les pierres de ce monuments trois fois millénaire n'ont jamais été restaurées et présentent divers faciès d'altération : efflorescence, désagrégation sableuse, desquamations, parties manquantes, décoloration et érosion différentielle. En application des méthodologies développées pour estimer les risques climatiques à Chambord, les risques de condensation, de gel-dégel et de contraintes thermiques ont été évalués pour la Zigurrat d'Al-Namrud. Les risques liés à la condensation et au gel sont faibles mais non nuls, ce qui fait que la durée d'application de ces sollicitations pourrait tout de même en faire des paramètres pertinents via la prise en compte de la fatigue. L'effet des contraintes thermiques semble particulièrement significatif et constitue probablement le processus majeur. La pierre fraiche issue de la carrière d'Al-Mur proche d'Al-Namrud a été caractérisée et comparée à la pierre historique saine. Leurs propriétés se sont révélées proches, ce qui suppose que la carrière d'Al-Mur a probablement servi pour la construction de la Ziggurat. Cette pierre constitue donc un choix pertinent et durable pour remplacer les pierres trop endommagées pour être restaurées. Enfin, une première étape de construction du carnet de santé numérique de la Ziggurat d'Al-Namrud a été présentée, sous la forme d'un photomodèle 3D des parements. La comparaison des cartographies d'altérations et de situation précédente d'enfouissement des pierres, ajoutée aux données de caractérisation des pierres altérées, laisse supposer que la récente mise à nue des pierres après excavation pourrait engendrer leur dégradation si aucune précaution n'est prise.

Perspectives

Ces travaux de recherche ont permis de révéler des zones d'ombre dans la connaissance. Parmi celles qu’il semble pertinentes de parcourir pour affiner les résultats figurent les propositions suivantes :

1. Pour la condensation, les résultats pourraient être affinés en analysant l'effet spécifique des pluies, de la grêle, du brouillard et de la neige en combinaison avec la vitesse et la direction du vent.
2. Le degré de saturation critique vis-à-vis des risques d'endommagement par le gel est de 85 % pour les pierres testées, ce qui correspond à des humidités relatives d'équilibre très proches de 100%. Or, les capteurs thermo-hydriques utilisés ne sont pas précis pour les valeurs d'humidité élevées. Il faudrait donc développer des techniques de mesure in situ pour les hautes valeurs de saturation afin d'appréhender plus finement le risque lié au gel.
3. L'analyse des effets des dilatations empêchées repose ici sur l'utilisation de la notion de facteur de sécurité ou inversement marge de sécurité. Cette notion intègre notamment l'effet de fatigue du matériau. Il reste donc à quantifier comment fonctionne la fatigue thermo-hydrique des pierres pour mieux définir la sécurité à prendre en compte lors de l'estimation de l'effet de ces contraintes.
4. Malgré la mise en valeur des processus majeurs potentiellement responsables des altérations observées sur site, il n'a pas été possible de démontrer quel processus ou quelle combinaison de processus suffit pour déclencher les desquamations en plaques ou en feuillet. Même si des pistes sont proposées, la question reste ouverte.
5. Les caractérisations de pierre et le diagnostic d'altération de la Ziggurat d'Al-Namrud reposent sur un nombre faible de prélèvements in situ. Une campagne complémentaire de prélèvements serait nécessaire pour compléter ces études et consolider/compléter les conclusions.
6. L'ébauche d'un carnet de santé numérique proposée dans ce mémoire doit être complétée pour constituer une réelle base de données du site utilisable pour son diagnostic d'ouvrage. Cela requiert à la fois de collecter et de rassembler davantage d'informations, mais aussi d'utiliser une plateforme documentaire permettant l'organisation d'une base de données 3D, telle que NUBES.

Risk assessment of thermo-hydro mechanical stone decay in built heritage

General introduction

General introduction

The most famous monuments in the world have been constructed with stones. The preservation of these monuments, which are the symbols of ancient civilizations and prehistoric cultures across the world, is a great scientific challenge. Sedimentary rocks such as limestones have been commonly used in historical structures for many centuries as they are found all over the world. Limestones are aesthetically attractive, have pleasant light colors and are easy to cut and shape in various forms and designs. These features make limestones common building materials not only for archaeological sites and historic monuments but also for modern buildings. More recently, these stones have been used for wall cladding in order to provide a prestigious exterior wall area for buildings as well as to ensure better energy conservation. Limestones are known to be sensitive to weathering when they are exposed to outdoor environmental conditions. The degradation of limestones is caused by various physico-chemical and even biological weathering processes such as thermal stress, condensation, freezing, salt crystallization, and biological colonization.

Among the parameters influencing the decay of monuments such as the intrinsic properties of the stone, local environmental conditions have an essential impact in the weathering processes of stone. An understanding of the processes of stone weathering requires not only detailed knowledge of the physico-chemical behavior of stone during weathering, but also of cyclic variations in climatic conditions. The identification of such variations can provide essential information for better management, conservation, and future restoration work. The daily or seasonal variations in the local climatic conditions are major sources of decay for building stones. These variations can produce damaging effects which are generally invisible, but their constant action, repeated daily over long periods, can be highly destructive.

This research work in civil engineering concerns the durability of the building materials of two monuments:

- In France, the castle of Chambord and the two French limestones used in the construction and restoration of this castle: tuffeau and Richemont stone;

- In Iraq, the archaeological site of Al-Nimrud city and the historic limestones used in the construction of Al–Ziggurat and the fresh limestone (extracted from a quarry) considered as the original stone.

Objective of the research

Recently, great attention has been paid to the role of climatic conditions in the degradation of cultural heritage stones (Camuffo and Sturaro 2001; Bonazza et al., 2009a,b; Duthie, 2011; Gómez-Bolea et al., 2012; Ponziani et al., 2012; Al-Omari et al., 2012,2014a). A better understanding of this issue is crucial for the purpose of the preservation of built heritage, and involves a broad spectrum of knowledge encompassing geology, chemistry, physics, biology and engineering. The main objective of this PhD thesis is to study the behavior of stone monuments when exposed to natural environmental conditions. The research will focus on studying the effect of daily variations in the local climatic conditions on the degradation of two historic stone monuments, namely the castle of Chambord and Al-Nimrud city. The research will attempt to answer three main questions:

- What is the role of climatic conditions in the degradation of stone *in situ*?

- What are the weathering processes that damage the stones due to the daily variations in climatic conditions?

- What is the estimated damage risk to the stone due to the specific weathering process?

Therefore, the objectives of this study and the approach adopted to achieve them are:

- Determine the chemical and mineralogical composition of the studied limestones. To do this, different complementary techniques (X-ray diffraction, chemical analysis, thermo-gravimetric analysis, optical and electron microscopy) were used. In addition, the morphological characteristics of the pore space system of the limestones were identified through the analysis of results from total porosity and mercury intrusion porosimetry tests.

- Identify the thermal, mechanical and water transfer properties of the limestones. These properties include: linear thermal expansion coefficient, unconfined compressive and Brazilian tensile strength, ultrasonic pulse velocity, water retention curve, capillary imbibition coefficients, free absorption and water permeability coefficient. Determine the elastic behavior properties (elastic modulus and Poisson's ratio) and the dilation strain of the stones both in dry state and under different conditions of water saturation and temperature.
- Create mathematical models to estimate the elastic properties of soft tuffeau limestone for a wide range of temperature (-8 °C to 40 °C) and water saturation (0% to 100%), in an attempt to simulate the extreme, but realistic, range of stone temperatures and humidities that were measured *in situ*.
- Examine the risk of damage to the stones due to the main physical weathering processes caused by variations in climatic conditions: condensation, freezing-thawing action and thermal and hygrothermal stresses. To this end, statistical analyses were carried out: firstly, from the weather data recorded at different periods at meteorological stations located near Chambord castle and Al-Nimrud city; secondly, from the stone data (stone temperature and humidity) measured for three years using digital thermal-humidity sensors installed on the surface and at different depths inside the stones located on the east tower of Chambord castle.
- Identify the critical degree of water saturation that promotes degradation of the limestones due to freezing, through a series of laboratory tests. The results of these tests were coupled with the field observation of both air data and stone data in an attempt to determine the warning level of moisture that leads to the degradation of stones in the castle of Chambord.
- Define the origin of decay in the degradation observed on the historic limestone of Al-Nimrud monuments and find a suitable stone that can be used in the future restoration work of Al-Nimrud city.
- Construct a 3D model of Al-Ziggurat monument in order to accomplish the first step in establishing the digital health record of Al-Nimrud city.

Thesis layout

The research performed in this PhD thesis is presented in three main chapters:

The first chapter gives a general overview of the types of weathering faced by building stones in natural environments. In this overview, a brief definition of the three main weathering processes (physical, chemical and biological) is presented. Then some examples of stone degradation related to the different weathering processes are shown. Among the three weathering processes, the research focuses particularly on physical processes and describes the different forms of these weathering processes and their mechanisms in stone degradation. The main factors that affect stone degradation are divided into two groups: intrinsic factors represented by the properties of the stone, and extrinsic factors related to the surrounding environmental conditions.

The second chapter is devoted to the French limestones: tuffeau and Richemont stone. This chapter also lists all the techniques used in this research. The complete characterization (mineralogical, morphological, mechanical and water transfer properties) of the two stones and the methodologies used are presented. This chapter then focuses on assessing the damage risk to the two limestones of the castle of Chambord, through three weathering processes: condensation, freezing-thawing action, and thermal and hygrothermal stresses. This assessment is achieved through analysis of both weather and stone data. The weather data (air temperature, air relative humidity and rainfall) were recorded both from the local station placed on the roof of the east tower of the castle of Chambord and from the meteorological station at Bricy air base (45 km from the castle of Chambord). The stone data include stone temperature and humidity measured using digital thermal-humidity sensors installed on the surface and at different depths inside the stones on the walls of the east tower. The stone data include intrinsic properties such as the pore size distribution, the elastic properties and the stone strength properties. Mathematical models were built in order to estimate the elastic properties of tuffeau stone in the different conditions of water saturation and temperature encountered *in situ*. In addition, the determination of the critical degree of saturation concerning freezing damage of these two limestones is presented in this chapter.

The last chapter presented in this thesis is devoted to Iraqi limestones (weathered and unweathered historic limestones, and the fresh limestone extracted from

a quarry) that were used in the construction of the walls of Al-Ziggurat, an ancient monument in the archaeological site of Al-Nimrud city in the north of Iraq. The main damaging processes responsible for weathering of the stone are examined. Both the unweathered historic limestone and the fresh one were characterized in order to determine a suitable stone for future restoration work. In addition, the risk of damage to the limestone of Al-Nimrud monuments due to daily variations in the climatic conditions was assessed. To achieve this, weather data recorded at Mosul station (35 km from Al-Nimrud) were analyzed together with stone data (pore size distribution, thermal coefficient, elastic and mechanical properties). The last part of this chapter is dedicated to creating a 3D model of Al-Ziggurat walls, which is the first step required to build the digital health record of Al-Nimrud monuments for conservation purposes.

The thesis concludes with a summary of the main results obtained during this research and with the future perspectives of this work.

The appendices contain the four papers based on this research that have already been published in international journals.

Chapter 1

Weathering of building stones in natural environments

CHAPTER 1

Weathering of building stones in natural environments

The majority of historical and cultural heritage buildings are made of natural stone. The health of these buildings depends on many parameters, namely:

- Intrinsic stone properties and the durability of the stones used in the construction;
- Extrinsic factors, mainly environmental conditions of the building stones.

In terms of the rehabilitation of cultural heritage buildings, the choice of a non-durable or non-compatible building material (stone and/or mortar) for replacement in restoration work may decrease or increase the aesthetics of the building and the degradation of original stones during the weathering process. As a result, it can increase the cost related to the reconstruction and conservation of these cultural heritage buildings. In the present work, the role of mortar is not taken into consideration. This chapter is devoted to the presentation of different types of weathering processes that are encountered on building stones in natural environments. A significant part of this chapter focuses on the mechanisms and the main factors that affect the degradation of building stone. These factors involve both intrinsic stone properties and extrinsic factors represented by the surrounding environmental conditions.

1. Definition of weathering

Weathering is the term that describes all the processes that lead to the decay of materials such as rocks or building stones in the environment near the earth's surface. This definition is quite general and does not mention the major types of physical, chemical and biological weathering processes which are responsible for the degradation of stones. Therefore, in relation to the degradation of the stones analyzed in this PhD, Selby's definition (Selby, 1993) is more accurate *"... the process of alteration and breakdown of soil and rock material at and near the Earth's surface by physical, chemical and biotic processes"*. It should be pointed out that these three weathering processes can interfere with each other, thus accelerating the action of weathering. For example, chemical weathering

tends to weaken stone, thereby making it easier to break. Likewise, physical weathering creates additional surface area that is prone to chemical attack. In this way, the two processes can work together. Moreover, the alternation of wetting-drying cycles has a strong correlation with all the other weathering processes. Without water, there is no chemical reaction (i.e. no chemical weathering), no frozen water and no salt phase transition (i.e. limited effects of physical weathering), and no biological life (i.e. no biological weathering).

In this study, the main emphasis will be on describing physical weathering, then chemical weathering and biological weathering. We will concentrate particularly on the most important aspects of the main types of degradation and the factors affecting them.

1.1. Physical weathering

Physical weathering is a set of different processes: thermal stress, freeze-thaw action, wetting-drying cycles and salt crystallization. These processes break and disintegrate the stone into smaller pieces without changing the stone's mineral composition. Following a brief description of the main types of physical weathering affecting the stones on historic and archaeological buildings, a discussion about weathering processes will be presented.

1.1.1. Weathering due to freezing-thawing process

The freezing-thawing process is generally reported as an important factor causing the physical weathering of stone. In cold, wet regions, where the stone is subjected to freezing and thawing cycles at least once a year, the freezing-thawing process is considered to be the main weathering process responsible for stone damage (Bayram, 2012). The freezing-thawing process is a powerful weathering factor which has been used in the laboratory to test the durability of building stone (Janshidi et al., 2013). The variation in the resistance of stone to freezing-thawing action is vast and depends on the intrinsic stone properties: mechanical strength, porosity and porosimetric characteristics such as pore size distribution, pore shapes, and tortuosity (Amoroso and Fassina, 1983; Nakamura, 1996; Prick, 1997; Thomachot & Matsuoka, 2007).

Moreover, the amount of water within the stones plays a significant role in determining the damage intensity produced by frost action. In partially saturated stone, there are many empty pores (filled by air which is a compressible fluid) with free space to damp the pressure generated by liquid water when freezing occurs. Thus, saturated stone can be damaged by frost action although its mechanical strength is high, while partially saturated can resist this damage, even if its mechanical strength is lower (William, 1967). This concept led researchers to investigate what the critical degree of water saturation in porous material is at which frost damage occurs (Fagerlund, 1977a,b; Prick, 1995, 1997; Chen et al., 2004; Li et al., 2012; Al-Omari et al., 2013b). Some of the main patterns of degradation that can be observed due to freezing-thawing are: frost wedging, Fig. I-1; delamination & deep cracking, Fig. I-2; granular disintegration & contour scaling, Fig. I-3.

Fig. I-1. Frost wedging, Pikes peak, Colorado (Granite). (available online).

Fig. I-2. Delamination of a gravestone possibly by frost action, Cathedral Graveyard, Scotland (Sandstone). (ICOMOS-ISCS 2008).

1.1.1.1. Mechanisms of stone damage by freezing-thawing process

Although the freezing-thawing process has the potential to be a powerful weathering factor, the exact mechanisms involved in freezing-thawing weathering are harder to define. In fact, there are four main physical mechanisms that are considered capable of disintegrating the stone by frost action:

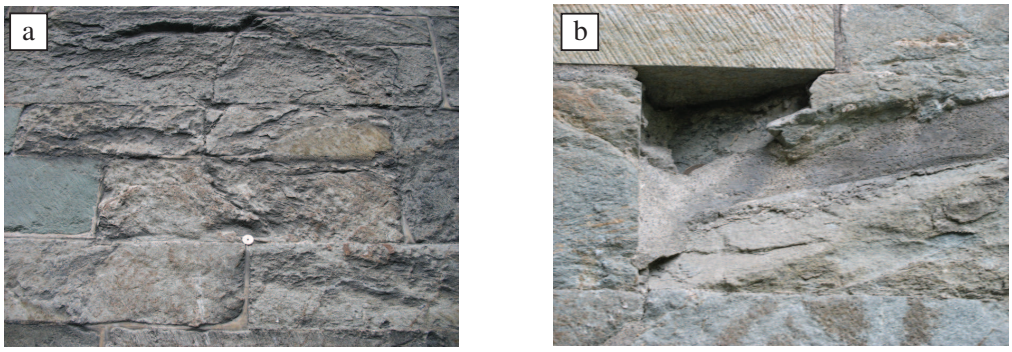

Fig. I-3. Degradation of stone due to freezing-thawing, (a) granular disintegration and (b) contour scaling, the Nidaros Domkirke, Trondheim, Norway (schists), (Angeli M., 2007).

1.1.1.1.a. Water volume expansion pressure

It is well known that when water turns to ice, its volume increases by 9%. This volume increase generates great pressure within the pore network of the stone which may exceed the tensile strength of the stone and cause it to fracture.

1.1.1.1.b. Ice crystallization pressure

Ice crystallization pressure is generated during the growth of ice crystals. It requires a sufficient amount of water to increase the growth of ice crystals (i.e. further crystallization pressure).

1.1.1.1.c. Migration of unfrozen water

When the stone containing water is exposed to sub-zero temperatures, the water freezes at different rates depending on the size of the pores in which the water is contained. The water in the smaller pores requires a lower temperature to freeze. During freezing, the unfrozen water migrates towards the frozen water and produces more ice crystals, i.e. more crystallization pressure (Prick, 1995; Chen et al., 2004).

1.1.1.1.d. Hydraulic pressure

If the surface of a stone contains a higher amount of water than the core, this surface will be exposed to freezing first when freezing occurs, forming a seal. Then the water

freezes at the core of the stone. Consequently, the pressure generated makes the remaining water flow towards the less saturated pores. If there is not enough space for this water to flow then hydraulic pressure will be generated and may cause damage to the stone (Powers, 1945).

1.1.2. Weathering due to salt attack

As saline solutions evaporate within a stone, damage to the stone is caused by salt weathering because of crystal growth. Conversely, the salt crystals can deliquesce if they absorb humidity from the surrounding environment. These phase transitions have traditionally been considered as effective weathering processes that induce damage in stones. In general, salt weathering falls under the category of physical weathering processes. However, in some cases this weathering process may be accompanied by some chemical reactions. For example, the host stone's minerals may release some cations (Na^+, K^+, Ca^{++} and Mg^{++}) due to dissolution by water and they may react with acid rain or polluted rain containing anions (SO_4^{--}, …), and finally cause damage to the stone by salt weathering. In this respect, stone degradation by salt weathering is thus halfway between physical and chemical weathering processes.

Salt weathering is one of the most destructive agents of archaeological sites all over the world (Lopez-Arce and Garcia-Guinea, 2005). This is due to the fact that there are diverse sources contributing to the presence of salts within the stone: underground soil containing salts, salts generated from the geological origin of the stone, wind transferring marine salt spray (Moropoulou et al., 1995), salts from pigeon or bat droppings (Hosono et al., 2006), de-icing treatment and air pollution in urban environments (Baptista et al., 2011). Incompatible building materials (mortar, concrete, etc.) and inappropriate treatments (i.e. sulphate-bearing mortars and magnesium-rich stone, which lead to extensive weathering by magnesium sulphate crystallization) are other sources to consider (López-Arce et al., 2009). Many salt ions are responsible for salt weathering; the predominant ones are chlorides, sulfates, nitrates, and carbonates (La Iglesia et al., 1994; Torfs and Van Grieken, 1997; Lopez-Arce et al., 2008).

From a fluid mechanics point of view, it is well known that the superficial tension, density and viscosity of saline solutions are strongly salt-concentration dependent. Therefore, when the salt concentration is high in the porous medium of stone, the kinetic potential is low and, as a result, the stone may exhibit more damage. In the experimental work by Van et al. (2007), salt weathering tests were conducted on two porous limestones having nearly the same total porosity. The accelerated weathering test was performed using imbibition-drying cycles with two different concentrations of sodium chloride solutions (30 g/l and 300g/l). The increase in salt concentration from 30 g/l to 300 g/l changed the behavior of both stones during the course of the test cycles. The stones tested with 300 g/l of NaCl were deteriorated, exhibiting two different damage intensities in the vertical dimension: the lower part of the stone was exposed to greater damage than the upper part. This is due to the increase in the viscosity and density of the salt solutions, and consequently, their kinetic potential to penetrate into the stone is reduced; in other words the salt will concentrate in the lower part of the stone, causing more damage.

In the same context, Angeli et al. (2010) investigated the evolution of stone damage by salt weathering performed by imbibition/drying cycles on a fine-grained detritic limestone mainly composed of calcite (90%) and quartz (10%). Two concentrations of sodium sulfate solution (5% and 12%) at room temperature were used. These variables were selected for the purpose of investigating the effect of salt concentration in the salt weathering processes at constant temperature. Figure (I-4) shows different decay patterns for the two cases. The decay of the stone ranged from fine crumbling (i.e. granular disintegration) to coarse crumbling and contour scaling when the salt solution was increased from 5% to 12%. They concluded that increasing the salt concentration not only affected the quantity of damage, but also changed the stone decay patterns. They attributed this change in failure mode to the fact that the increase in the concentration of the salt solution results in greater penetration of the salt solution within the stone's pores. During evaporation, the solution inside the stone will crystallize over a longer period than the solution near the surface, and this process provides sufficient time for crystallization pressure to take place, thereby enhancing the stone damage. Various other decay patterns can be related to salt weathering: efflorescence, Figure (I-5), honeycomb, Figure (I-6),

stone detachment in different forms, granular disintegration, Figure (I-7), contour scaling and sanding.

Fig. I-4. Different stone decay patterns due to salt weathering (sodium sulfate), fine crumbling at 5% salt concentration (*right*), coarse crumbling and contour scaling at 12% salt concentration (*left*).

Fig. I-5. Efflorescence, Crypt of the Cathedral of Cádiz, Spain (Limestone) (Vázquez et al., 2011).

Fig I-6. Honeycomb, St. Leonardo's church, Portugal (Sandstone) (Ludovico-Marques et al., 2012).

Fig. I-7. Granular disintegration by salt weathering, Al-Nimrud monument, Iraq (Limestone).

1.1.2.1. Mechanisms of stone damage by salt weathering

The effectiveness of salt weathering depends on the intrinsic stone properties, but also on salt composition and concentration, environmental conditions, temperature, and relative humidity. The stone properties such as porosity, permeability and capillary kinetics strongly affect the salt damage potential (Wark et al., 2006; Yu and Oguchi, 2010). However, there are four mechanisms that damage the stone by salt weathering:

1.1.2.1.a. Crystallization pressure

Salt crystallization pressure is the most widely accepted mechanism by which salts cause damage to stone. The mechanism is directly related to the degree of salt saturation in the saline solution. During evaporation, the concentration of ions exceeds the saturation point and salt crystals will form. Whenever the saturation increases, then the growth of salt crystals will exert more crystallization pressure (i.e. more damage to the stone).

1.1.2.1.b. Hydration pressure

The main cause of salt damage by hydration pressure is due to the transition of salt hydration phases. Many salts are unstable by nature and can take different forms depending on the presence of water within their structure. For example, calcium sulfate can absorb moisture and turn to gypsum with a volume expansion of 42%, while on hydration, thenardite Na_2SO_4 can turn to mirabilite $Na_2SO_4.10H_2O$ with a volume increase of about 300% (Price and Brimblecombe, 1994).

1.1.2.1.c. Hydraulic pressure

Hydraulic pressure can be generated when the salt-water system undergoes a phase transition. On crystallization, the volume of the precipitated salt plus the remaining solution can exceed the volume of the original salt solution, and on the assumption that stone is a closed system, this expansion in volume can exert hydraulic pressure. In fact stone is an open system, and consequently the risk of salt damage by hydraulic pressure in many cases is limited and occurs only in special conditions: for instance, when the salt solution

evaporates so quickly that the crystallization rate exceeds the drainage rate of liquid water, then hydraulic pressure may be generated (McMahon et al., 1992).

1.1.2.1.d. Thermal expansion

When there is a high temperature variation, it is expected that the salt within the stone will thermally expand and cause damage to stone without moisture. This is due to the fact that certain salts have a thermal expansion coefficient that exceeds the coefficients of stone minerals. Thus, the dilation of the salt minerals within the finer pores can exert sufficient pressure to cause damage to the stone.

1.1.3. Weathering due to thermal stress

Thermally induced stresses to the stone are known to be important agents in stone degradation. This is due to the high changes in temperature. Temperature variation can damage the stone by producing thermal stress which can cause fatigue or cracks if it is higher than the stone strength. If the sun is the main source of heat, then the damage generated is due to so-called insolation weathering. Although this type of weathering is more active in hot desert environments, it also occurs in cold environments where the daily variation in stone surface temperature can reach 35-40 ºC under mid-European climates (Weiss, 1992). A good example of stone damage by thermal stress is the case of granular disintegration and loss of relief observed on the building stone of Carrara marble (Weiss et al., 2004), Figure (I-8), cleavage planes observed on marble (Zeisig et al., 2004), Figure (I-9), and crack networks on marble sculpture, Figure (I-10). It should be noted that thermal dilation behavior is strongly enhanced by simultaneous changes in both temperature and moisture, and consequently the stone damage is more effective (Koch and Siegesmund, 2004). This is due to the simple fact that moisture reduces the tensile strength of the stone.

The main stone properties that control the degradation mechanism by thermal stress are albedo and thermal conductivity of the stone. Stones with a darker color (i.e. low albedo) and with a high thermal expansion coefficient (i.e. low thermal conductivity) are more sensitive to temperature variations (Warke and Smith, 1998) and, of course, strongly vulnerable to thermal stress.

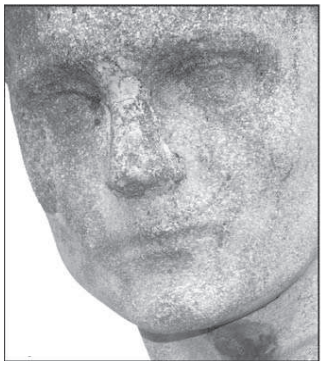

Fig. I-8. Granular disintegration and loss of relief, Pantheon cemetery, Hungary (Carrara marble) (Weiss et al., 2004).

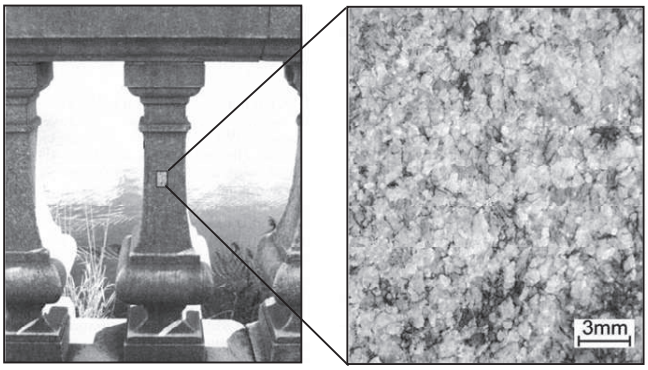

Fig. I-9. Cleavage planes due to thermal stress, Marmorpalais in Potsdam, Germany (marble) (Zeisig et al., 2002).

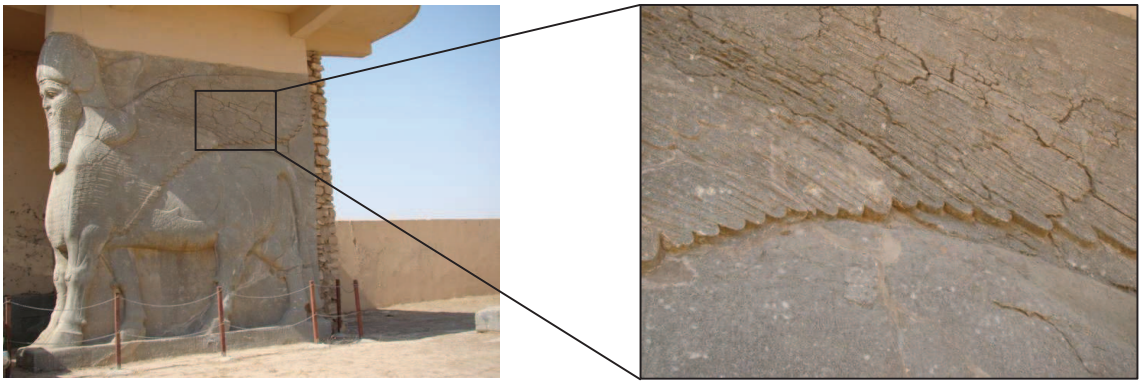

Fig. I-10. Crack network on historic sculpture, Al-Nimrud monument, Iraq (Marble).

1.1.3.1. Mechanism of stone damage by thermal stress

1.1.3.1.a. Thermal gradient

The damage caused by thermal stress is not only related to the magnitude of the stone temperature reached at the surface, but also to the internal temperature gradient. The temperature gradient is fully controlled by the thermal conductivity of the stone. Stone with a low thermal conductivity has a non homogeneous temperature in depth when it is submitted to heating. This results in a steeper thermal gradient and, hence greater thermal stress that causes damage to the stone.

1.1.3.1.b. Thermal fatigue

Again, stone with a low thermal conductivity is associated with low rates of cooling and heating. In this case, the temperature of the surface and subsurface will be different during cooling and heating stages. On cooling, the surface temperature will drop while the subsurface temperature continues to rise. Due to the fact that the subsurface is warmer than the surface, compressive stresses will be generated as the surface contracts and the subsurface expands. During heating, there are some developments of tensile stresses between the surface and the subsurface. This occurs because the surface expands more rapidly than the subsurface. Lastly, stone subjected to these repeated compressive and tensile stresses may suffer from fatigue, especially stones with a low thermal conductivity and low albedo (Warke and Smith, 1994).

1.1.3.1.c. Differential thermal expansion

Differential thermal expansion is directly related to the types of minerals contained in the stone. Because the minerals have different thermal expansion coefficients, this will cause differences in the expansion rates between the minerals, resulting in stresses which in turn damage the stone if they are in excess of the stone strength.

1.1.4. Weathering due to wetting-drying alternation

The alternation of wetting-drying can induce severe damage due to the dissolution of stone minerals, the reduction of the free energy of grain material which weakens the resistance, and the transport of air pollutants into porous media.

As is well known, the most weathered parts of stones are found near the stone surface. This will result in moisture, diffusion and transport taking place in the area between the stone and the atmosphere. The weathering processes that depend on moisture and changes in moisture are, therefore, likely to take place at the surface or very close to the stone surface. Moreover, a strong correlation exists between physical weathering processes and the existence of water. Therefore, it is vital to identify the ways by which water can be present within the stone. The presence of water within building stones can be due to one of the following sources: by capillary rise from ground water or by penetration

from driven rains in the case of the liquid phase, and by condensation in the case of water vapor phase.

1.1.4.1. Mechanism of stone damage by wetting-drying

The degradation of stone by alternate wetting-drying is related to the expansion and contraction of stone grains by the physical mechanism of capillary tension. It well known that the free water within the stone pores is under surface tension. This tension increases during drying, causing compression stresses on the surrounding grains and consequently shrinkage of the stone, causing disintegration of the stone.

The other phenomenon of stone degradation by wetting-drying is hygric expansion. In many cases, stones containing minerals with a high swelling potential are strongly altered by hygric expansion when subjected to alternating wetting-drying cycles (Weiss et al., 2004; Sebastian et al., 2008; Benavente et al., 2008; Colas et al., 2011). Clay minerals are the most responsible for producing damage to stone by hydric expansion. This is due to the expansion of clay minerals after wetting. For example, montmorillonite can expand to several times its original volume on wetting and then exerts sufficient pressure to damage the object containing it.

1.2. Chemical weathering

In chemical weathering processes, it is not only the fabric and the structure of the stone that are changed; the alteration also involves the chemical and mineralogical composition of the stone. The most common processes responsible for chemical weathering are: dissolution, oxidation, hydration, and hydrolysis. A good example of chemical weathering is the formation of a black crust on the stone surfaces, Figures (I-11 and I-12).

There is a strong correlation between climate and chemical weathering. This correlation can be explained by the role of rainfall and temperature in chemical reaction processes. Rainfall reacts with the sulfate oxides (SO_x) present in the polluted atmosphere, producing acid rain, which in turn reacts with the stone's constitutive minerals, generating a black crust on the outer stone surfaces (Maravelaki-Kalaitzaki and Biscontin, 1999).

Fig. I-11. Black crust at Ducale Place in Venice, Italy (Limestone) (Maravelaki-Kalaitzaki and Biscontin, 1999).

Fig. I-12. Black crust at cathedral of Granada, Portada del perdon, Spine (limestone) (Maravelaki-Kalaitzaki and Biscontin, 1999).

Temperature is the crucial factor that controls the rate and the intensity of chemical reactions. A rise in temperature of 10 ºC increases many chemical reactions by a factor of 2 (Connors, 1990). Depending on the prevailing climate, regions are classified as arid, semi-arid, humid and cold. In arid regions evaporation exceeds wetting via rainfall, thus the risk of chemical reactions occurring will be limited, as the stone is mostly dry, while in cold regions the influence of chemical weathering is inhibited since the water inside the stone, if any, is in a frozen state, and again there is no chance of a chemical reaction. Given the harsh climate in dry and cold regions, physical weathering processes are more dominant.

1.3. Biological weathering

Biological weathering denotes the presence of biological organisms: mosses, algae, and lichen on the stone surface which cause bio-deterioration through both physical and chemical processes (Sterflinger, 2010; Docampo et al., 2011; Zucconi et al., 2012). These simple living organisms grow on the outer surface of stone once the appropriate outdoor environment is available (i.e. high relative humidity). Organisms, and in particular fungi, can contribute to the deterioration of stone surfaces in the external environment, but also to the degradation of both organic and inorganic materials located in indoor environments as

in the case of the damage observed in the cultural heritage materials in several archaeological museums (Dahlin, 2000).

The role of biological organisms in the deterioration of monumental stones can occur through mechanical or chemical processes. For example, the roots of higher plants can grow within the stone, causing mechanical failure of the stone, Figure (I-13) (Mishra et al., 1995). Also, some lichens can produce organic acid which reacts with stone minerals, causing damage to stone by chemical weathering, (I-14).

The presence of organisms on the stone surface increases the duration of wetness in the stone due to the water retention by organisms (Miller et al., 2012). This in turn will enhance the other weathering processes; for example, the effectiveness of frost action usually increases for stone with a high residual water content. Again, an increased duration of wetness leads to further decay to the stone surface by various ways: increasing the amount of pollution captured by the stone, allowing further biocolonization of the stone by adding new organisms, and increasing the reaction times of dry deposition pollutants.

Fig. I-13. Roots of a tree growing on the monument, Ta Prohm-Angkor monument, Cambodia (Uchida et al., 1999).

Fig. I-14. Biological colonization at the Castle of Chambord, France (tuffeau limestone) (Janvier-Badosa, 2012).

2. Factors affecting the stone degradation

The natural stones used in the construction of historic monuments and cultural heritage buildings are exposed to different physical, chemical and biological weathering processes resulting in their degradation. However, the intensity of this degradation depends

on intrinsic factors which involve the properties of the stones themselves, and extrinsic factors represented by the surrounding environmental conditions.

2.1. Intrinsic factors (stone properties)

The intrinsic factors represent the properties of the stones themselves. These properties include: stone texture, grain size, mineral composition, pore space properties (porosity, pore size distribution, pore connectivity), water and thermal transfer properties. In the following, a summary of these properties and their effects on stone degradation will be presented.

2.1.1. Stone texture

Stones that have different textures show different degrees of resistance against weathering. For example, Yavuz and Topal (2007) carried out salt aging tests on six marble stones with different textures: grain size, grain size distribution and grain boundary. They concluded that the marbles with a small grain size, a limited range of dominant grain size, and an irregular grain boundary exhibited good interlocking between their components and they characterized these marbles as more durable against the accelerated weathering test. Again, the same stone type may have different textures. In this case the properties of the stone with different textures are different. Török and Vásárhelyi (2010) examined the following properties: density, ultrasonic wave velocity, effective porosity, and the uniaxial compressive strength of both air-dry and water saturated travertine with two different textures. They concluded that the massive travertine with a homogeneous micro-texture sustained weathering processes better than the less homogeneous laminated travertine.

2.1.2. Mineral composition

The minerals that are contained within the stone have a significant impact on its durability and resistance against degradation. Different minerals can be expected to show differing responses to weathering processes. For example, stone that contains clay minerals can expand on wetting and this can cause stone damage. Sebastián et al. (2008) confirmed that one of the factors that enhanced the damage to the sandstone of the church of San Mateo in Tarifa (Spain) was the presence of clay mineral. The clay minerals contained in

this sandstone generated local stress within the zone that experienced expansion after wetting. The stresses thus developed resulted in stone decay by flaking, Figure (I-15). Also, tuffeau, the main building material on the Castle of Chambord, contains about 10% of clay minerals (Dessandier, 1995). It is highly sensitive to the presence of moisture (Beck, et al., 2003). Tuffeau exposed to alternate wetting-drying cycles experiences contour scaling with plates a few millimeters thick (Beck, 2006), Figure (I-16).

Fig. I-15. Stone degradation by flaking, church of San Mateo, Spain (Sandstone) (Sebastián et al., 2008).

Fig. I-16. Stone degradation by contour scaling, Castle of Chambord, France (tuffeau limestone) (Beck, 2006).

2.1.3. Pore space properties

Pore space properties are the most important stone properties for identifying the severity of stone deterioration. The pore space properties are strongly related to all weathering processes: wetting-drying (Beck et al., 2003), freezing-thawing (Mutlutűk et al., 2004; Yavuz et al., 2006) and salt crystallization (Goudie, 1999; Van et al., 2007; Yu and Oguchi, 2010).

Contrary to the freezing of the water on the stone surface when the temperature drops down to 0 ºC, the freezing of pore water is strongly controlled by the size of the pores themselves: the water inside pores of different sizes freezes at different freezing temperatures. According to Kelvin's law, the freezing of pore water in the smaller pores is controlled by the curvature of the water meniscus. The pores with smaller radii have the lowest freezing point temperature. For each pore radius, there is a critical freezing temperature that can be calculated by Eq.1 (Camuffo, 1998):

$$T_{FP} = -273\frac{2\sigma_{sl}}{r.p_s.L_f} \qquad \text{Eq.1}$$

where:

σ_{sl}: Surface tension at the solid-liquid interface, 32.1 10^{-3} N/m.

p_s: Ice density, 0.917 g/cm^3.

L_f: Latent heat fusion, 333.55 N.m/g.

r: pore radius, μm

Pore size plays an important role in identifying the type of mechanism that degrades the stone by frost action. For example, the water inside the smaller pores needs very low temperatures in order to turn into ice. Here the degradation caused by increasing the volume of water will be limited. However, the presence of unfrozen water in the smaller pores can enhance degradation by water migration (Prick, 1995; Chen et al., 2004).

Again, the pore size can determine the degree of stone wetness by condensation of water vapor and the condensation phenomenon is governed by Kelvin's law (Camuffo, 1998):

$$RH_C = 100.e^{\frac{-2\sigma_W.V_m}{r.R.T}} \qquad \text{Eq.2}$$

where:

σ_w: Surface tension of water in air-liquid interaction, 0.072 N/m

V_m: Molar volume of water, 18 cm^3/mol

R :Gas constant, 8.3144621 N.m/mol/K

T: Temperature of thermodynamic system in equilibrium, K

r: pore radius, μm

Accordingly, the condensation inside pores of different diameters requires access to the critical relative humidity values and the condensation of water vapor inside the larger pores requires high relative humidity values (Ponziani et al. 2012; Al-Omari et al., 2014a).

Furthermore, increasing the degree of pore connectivity will improve the ability of water to move from/towards the stone. This in turn will enhance stone damage by water circulation and accelerate hydric expansion (Siegesmund and Dürrast, 2011). Moreover, the connectivity of the pores plays a significant role in damaging the stone by frost action. Well-connected pores make the stone more susceptible to damage as the unfrozen water can easily migrate during freezing, damaging the stone by ice crystal growth (i.e. ice crystallization pressure), whereas poorly connected pores mean that the freezing of water inside the finest pores requires a lower freezing temperature. This will reduce the risk of stone damage by frost action.

The porosity value affects the damage intensity to the stone. The experimental work by (Akin and Özsan, 2011) revealed that travertine limestone shows different degrees of damage intensity due to salt weathering. The greatest damage was observed for the low porosity travertine limestone (< 5%). The authors attributed these findings to the fact that the pressure exerted by salt weathering is more effective on stones with a lower porosity.

According to (Yu and Oguchi, 2010), the connected porosity was found to be a crucial factor that controls the degree of damage of porous stone subjected to a salt weathering test. The degree of damage, by salt weathering, of two stones having about the same total porosity can differ if their pore size distributions are different. For example, in the experimental work by Van et al. (2007) the two porous stones (with the same porosity of about 45%) showed different forms of weathering with imbibition/drying cycles with sodium chloride salt due to differences in their pore size distribution. The stone with coarser pores (and hence a higher permeability) presented a thick crust of salt due to efflorescence whereas the other stone with finer pores (and lower permeability) showed low efflorescence and more salt within the stone, and thus more damage.

2.1.4. Hydraulic conductivity and water retention characteristics

Stone with a low hydraulic conductivity shows low sensitivity to salt attack. Also, stone with a high water retention capacity reveals little damage by salt weathering because such stone is mostly in wet state and so no salt phase transitions occur.

The experimental work, both field observations and laboratory tests, performed by Kuchitsu et al. (1999) focused on bricks at the historic monuments in Ayutthaya, Thailand. They showed that salt efflorescence occurs in materials with a high hydraulic conductivity because the more water which passes through the material, the more ions are concentrated. They also confirmed that building materials with a high water retention show less evaporation during drying. This in turn will reduce the crystallization processes of salt solution, if any, in these materials. Contrary to salt weathering, frost action induces substantial degradation in stones that have a high residual water content (low hydraulic conductivity and high water retention characteristic).

2.1.5. Thermal stone properties

The main stone properties affecting stone temperature are thermal conductivity, albedo and the thermal expansion coefficient. Thermal conductivity is a measure of the rate at which temperature is transmitted inside the stone. Thus, in stone with a low thermal

conductivity, there is a big difference in the stone temperature at different depths and therefore the stone can be damaged by thermal gradient.

Albedo is defined as the stone property that controls the amount and speed of solar radiation absorbed by its surface. Stone with a high albedo is stone that can reflect most of the solar radiation falling on its surface due to the light color of the stone surface, whereas the opposite holds for stone with a low albedo.

The damage to stone due to differential thermal expansion is not restricted to stone containing different minerals. It can also affect monomineralic stones where the damage occurs due to mineral dilation in an anisotropic stone texture (Lion et al., 2005).

2.2. Extrinsic factors

In addition to weathering processes related to the properties of the stones themselves, other complications arise as a result of the external factors that impact the stone. Extrinsic factors are closely related to the climatic conditions surrounding the stones. Most of these factors produce different levels of degradation to the stone, ranging from little variation in the stones' physical properties (physical weathering processes) to very severe change represented by alteration in the stone texture and mineral composition (chemical weathering processes).

Variations in the climatic conditions such as relative humidity, temperature, wind, rainfall and solar radiation, are the main factors that affect the degradation of cultural heritage stones all over the world. Climate conditions are closely correlated to both physical and chemical weathering processes, in direct and indirect ways. For example, the variations in temperature and humidity resulting in moisture changes within the stone contribute to stone decay directly by means of freezing-thawing or dissolution of stone minerals, or indirectly by transporting soluble salts through the stone's pore space.

The role of climatic conditions in the degradation of building stones has been extensively investigated by several studies (Camuffo, 1998; Camuffo and Sturaro 2001; Viles, 2005; Bonazza et al. 2009a,b; Ponziani et al. 2012; Al-Omari et al., 2014a,c). The following is a discussion of the major climatic elements affecting stone weathering and how they influence specific stone weathering processes.

2.2.1. Relative humidity

The harmful effects of daily variation in the air relative humidity are almost invisible, but they have continuous cumulative effects over the long term, which cause significant damage to stone buildings.

One of the main sources of moisture within the stone is the physical condensation process which occurs frequently in highly humid climates. The role of condensation in promoting damage to monumental historic stone has been the topic of many previous studies (Watt and Colston, 2000; Camuffo and Sturaro 2001; Ponziani et al. 2012; Al-Omari et al., 2014a).

2.2.2. Temperature

Variation in air temperature is considered as the main factor that promotes physical weathering processes. Variation in air temperature leads to weathering as a result of the alternating warming and cooling of the stone surfaces under the direct influence of solar radiation or the indirect influence of a hot surrounding environment.

Arid and semi-arid regions experience significant diurnal temperature variations. This results in the stone surface expanding and contracting frequently. Consequently, breaking, fissuring and granular disintegration of the stone occurs when the strain generated by expansion and contraction exceeds the stone elastic limit. In cold regions, the seasonal variation of stone temperature around 0.0ºC contributes to damaging stone with a high water content, by frost action. Moreover, in wet-hot climates the fluctuation in stone temperature controls the presence of water within the stone through evaporation. This in turn can cause direct damage to the stone due to the dissolution of stone minerals or indirectly enhance stone damage by salt weathering.

The evaporation of salt solutions contained inside the stone's pores result in different salt crystals depending on the degree of heating responsible for the evaporation and the solubility of salt solutions. For example, the crystallization of sodium sulfate solution results in three types of crystalline salts depending on the amount of water in its composition: anhydrous thenardite Na_2SO_4, unstable heptahydrate $Na_2SO_4.7H_2O$, and dehydrated mirabilite $Na_2SO_4.10H_2O$. The crystallization of sodium sulfate in anhydrous

phase causes less damage compared with the other two phases (unstable heptahydrate and mirabilite). The critical temperature that represents the boundary between the salt crystals with little or a lot of damage is about 32.4°C (i.e. the temperature limit of mirabilite stability). Tsui et al., (2003) pointed that the greatest damage to stone occurs due to the crystallization of sodium sulphate solution below the temperature limit of mirabilite. These findings were confirmed by Angeli et al. (2010) during their experimental work including aging salt weathering tests on limestones under two parameters: temperature and concentration of sodium sulfate. Unfortunately, they were not able to identify which salt phase (mirabilite or heptahydrate) was responsible for causing damage to the stone, as both could take place at temperatures below 32.4°C.

The effect of variation in air temperature is not restricted to variation in the stone surface temperature; it also involves variation in the stone temperature at different depths. To estimate these variations, there is a need to study the physical and thermal stone properties and how they affect the reaction of a stone to surface heating or cooling. The other solution is to measure the stone temperature at different depths inside the stone by using, for example, special sensors. This was part of the *in situ* work conducted in this PhD study, where digital thermal-humidity sensors were inserted at different depths inside the stones on the east tower of the Castle of Chambord, France. The details of stone data analyses will further discussed in chapter 2 of this thesis.

2.2.3. Rainfall

Rainfall is one of the major sources of the presence of water within stone, and therefore, it enhances all the water-related weathering processes. However, rainfall is an effective factor for transferring pollutants from the atmosphere to the stone surface. Moreover, rain can strongly dissolve the stone material and cause significant degradation to the stone surface by erosion, Figures (I-17 and I-18).

In general, rainfall can participate in the degradation of natural stone through one of three ways:

- Rainfall is not affected by air pollution. In this case, the rainfall has a pH of about 5.6 and the effect of rainfall is restricted to the presence of water within the stone.

Fig. I-17. Effect of water flow in dissolving ground stone plate, Al-Nimrud monument, Iraq (marble).

Fig. I-18. Effect of water flow in dissolving the winged sculpture, Al-Nimrud monument, Iraq (marble).

- Rainfall reacts with the atmospheric pollutants SO_2 and NO_x. Here, acid rainfall causes severe damage to the stone such as generating a gypsum crust on the stone surface.
- Rainfall affects the stone surface previously polluted by dry deposits of different gases.

The degree of rainfall acidity is controlled by the characteristics of rainfall itself. Light rains with small drops result in high acidity rainfall. This is due to an increase in the reaction time between the rain and the pollutant atmosphere since small raindrops have a high surface area in contact with the pollutant atmosphere. Again, high intensity rainfall results in surface flow on the stone surface, minimizing the reaction time between the rains and the pollutant deposits on dry stone surfaces.

2.2.4. Wind

Wind can affect weathering processes by accelerating the evaporation of moisture at the stone surface and consequently enhancing associated weathering processes such as salt crystallization.

The effect of wind is not limited to increasing evaporation; it also contributes to transferring dust and air pollution. The deposition of these dry pollutions can enhance the degradation of monumental stone. This case was observed in the degradation of the Alhambra monument in Granada (Spain), where the wind is the agent causing the mobilization of dust coming from the deserts in North Africa (Horemans et al., 2011).

The prevailing wind makes it possible to identify different damage intensities to the same stone on the different faces of a building, Figure (I-19). Moreover, wind-blown particles contribute to causing considerable damage to building stones through their abrasive action. Wind also plays a crucial role in transferring aerosol species such as sea-salt particles and causing damage to historical stone by salt attack (Moropoulou et al., 1995).

Fig. I-19. biological colonization, at Paisley Town Hall, (Sandstone) (Welton, 2003).

3. Conclusion

The current interest in the preservation of stone cultural heritage monuments has led to the development of specialized studies to preserve building stones from degradation. The stones' characteristics and the surrounding environment are the main factors that determine the type and severity of the degradation.

Most weathering processes, physical, chemical and biological, are directly related to the presence of water and its circulation within the stone. The effect of physical weathering due to water transfer, hygrothermal stresses within the stone, freezing action and condensation in the degradation of porous stones were studied in this thesis. The risk of damage to the studied stone due to these weathering processes was evaluated.

Chapter 2

Thermo-hydro-mechanical stone decay

CHAPTER 2

Thermo-hydro-mechanical stone decay

Sedimentary limestones are the major building stones used for built cultural heritage. This widespread use of limestones is a consequence of their common occurrence on the earth crust, and also because of the relative easiness of their cutting, quarrying, and their perceived durability. The study of the decay of stone used in built heritage is a vital part of our scientific research. All the weathering processes that lead to the degradation of the stones depend to a large extent on the properties of these stones. This chapter examines the durability in the local natural environment of the two French limestones: tuffeau and Richemont stone. The aim is to characterize these two stones and to assess the damage risk to these stones due to cyclic variations in the climatic conditions.

1. Materials characterization

All the complementary analytical techniques used in this research work are briefly described; the two limestones, tuffeau and Richemont stone, are then characterized with respect to their petrographic, microstructural, water transfer, thermo-hydro-mechanical and elastic properties.

1.1. General description of the studied limestones

1.1.1. Tuffeau limestone

The French tuffeau limestone is of Turonian age (the Upper Cretaceous period, approximately 88-92 million years ago). Its Latin etymology, *tofus*, which means spongy, is due to its special characteristics: soft and highly porous limestone. It comes from the quarries close to the Loire River (NW France). It is a type of siliceous fine-grained limestone, white in color, Figure (II-1), with several mineral phases (calcite, quartz, opal, clayey minerals). Due to geological deposition, tuffeau stones may vary in their chemical composition, physical characteristics, and color, even if they come from the same quarry (Dessandier, 1995).

Tuffeau has been commonly exploited as a construction material due to its light weight and easiness in terms of labor, although its high porosity (~45%) limits its durability. This limestone has been well studied in a large number of research investigations (Dessandier, 1995; Rautureau, 2001; Beck et al., 2003; Beck, 2006; Beck and Al-Mukhtar 2010,2014; Janvier-Badosa, 2012; Al-Omari et al., 2013a,b,2014a,b,c; Janvier-Badosa et al., 2010,2013a,b). It was extensively used as traditional building material in the Architectural Heritage of France and particularly in the Loire Valley, for example in the castles of Chenonceau, Valençay, Blois, Chaumont-sur-Loire, and Chambord, Figure (II-2). Nowadays, tuffeau is mainly used for the restoration of ancient monuments previously built of tuffeau. In this work, the white tuffeau comes from the quarry of Usseau in Vienne, France, and has been characterized and used in different experiments carried out in this research.

Fig. II-1. Cylindrical sample (Ø 40 × 80 mm) of tuffeau limestone.

Fig. II-2. The royal entrance of the Castle of Chambord, (Loire-Valley, France).

1.1.2. Richemont limestone

Richemont stone is a fine-grained bio-pelmicrite limestone, a monomineralic calcitic limestone, dating back to the Turonian age, like tuffeau. It was obtained from a quarry in Charente-Maritime, France. In general, Richemont limestone is a mechanically resistant material, whitish-beige in color, Figure (II-3). It contains fine irregular short white

lines which are shell fragments. Recently, Richemont stone has been commonly used as ornamental and building material in modern architecture in France. In addition, it is used in the restoration work of historic buildings. It was used as an alternative stone in the Castle of Chambord in the mid-20th century, Figure (II-4) (Janvier-Badosa, 2013b).

Fig. II-3. Cylindrical sample (Ø 40 × 80 mm) of Richemont limestone.

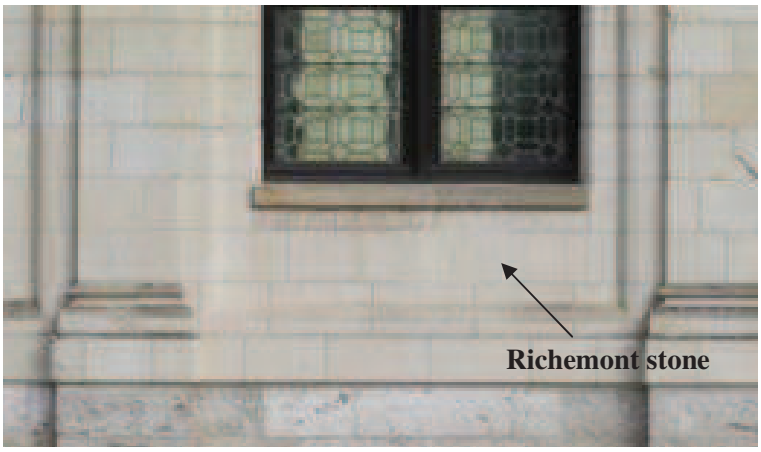

Fig. II-4. Richemont stone on the wall of the Castle of Chambord used in the restoration work in 1955, (Janvier-Badosa, 2012).

1.2. Petrographic studies

1.2.1. Mineral composition of the stones

The mineral composition of the two studied stones, tuffeau and Richemont stone, was determined by powder X-ray diffraction using a Philips PW-1830 diffractometer. The analysis conditions were: radiation Cu Kα (λ = 1.5406 Å), 40 kV voltage and 30 mA current intensity. The explored angle area was between 4º and 60º (2θ) with a step of 0.025º and a counting duration of six seconds at each step.

The diffraction patterns of the two limestones are presented in Figure (II-5). The mineralogical analyses show that Richemont stone is mainly composed of calcite with traces of quartz. Unlike Richemont stone, tuffeau contains other mineral phases in addition to calcite and quartz: opal (cristobalite-tridymite), mica (biotite and muscovite) and clay minerals (glauconite, illite and smectite), (Beck et al., 2003).

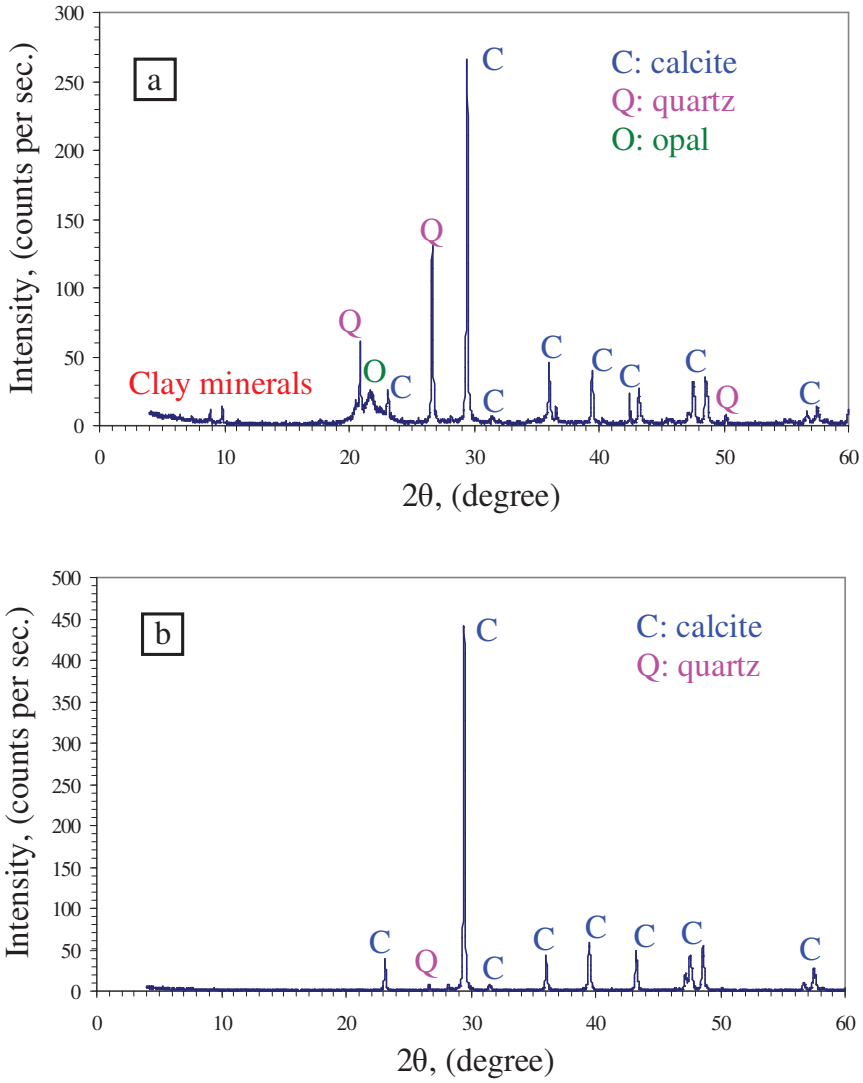

Fig. II-5. Diffraction patterns of the stones, (a) tuffeau; (b) Richemont stone.

Chemical analysis was carried out by the technique of Optical Emission Spectrometry with Induced Coupled Plasma (ICP-OES). The elemental concentrations in aqueous solution were determined using a Jobin-Yvon ULTIMA apparatus. Ultra high purity water was used for all dilutions. This technique was used to determine the elemental concentrations in the aqueous media from very low (ppm) to high concentrations. The overall chemical analyses for the two stones are presented in Table (II-1).

Table II-1. Chemical analysis of the studied stones obtained by ICP-OES test.

Oxide type	Proportion of oxide in the stones, %	
	Tuffeau	Richemont stone
SiO_2	41.78	2.16
CaO	27.74	52.84
Al_2O_3	1.99	0.40
Fe_2O_3	0.88	0.32
MgO	0.23	0.54
Na_2O	0.00	0.03
K_2O	0.54	0.11
TiO_2	0.14	0.03
P_2O_5	0.09	0.04
WL*	24.26	42.48
Total	97.66	98.94

* Weight loss at 1000°C

The results of ICP-OES analysis indicate that tuffeau contains high percentages of SiO_2 and CaO and the chemical elements of Al^{3+}, $Fe^{2+,3+}$, Mg^{2+}, K^+ were also observed, indicating the presence of clay minerals. These data confirm the results obtained by the X-ray diffraction test. In contrast, CaO was found to be the main chemical element present in Richemont stone. Richemont stone also contains the chemical elements related to clay minerals but in lower percentages compared to tuffeau. The proportion of the calcite mineral $CaCO_3$ present in the stones can be estimated from the elementary chemical composition of calcium oxide CaO obtained by ICP-OES, Table (II-2), and compared to results from thermogravimetric analysis (TGA) measurements.

Table II-2. The proportion of calcite obtained by two different techniques for tuffeau and Richemont stone.

	TGA analysis	ICP-OES analysis
% of calcite in tuffeau	48.8 ± 2.2	49.5
% of calcite in Richemont stone	94.92 ± 1.2	94.3

Thermogravimetric analysis (TGA) was adopted in this study in order to confirm the previous results obtained by X-ray diffraction and by ICP-OES analysis. This test was carried out on the powder samples using a Setaram (TG-DTA 92-18) apparatus. The powder samples were heated from room temperature to 1000°C at a constant rate of 2°C per minute while the weight loss due to the chemical reaction following the increase in temperature was measured.

The losses in weight of the powder samples during the test are presented in Figure (II-6). The blue curve shows the evolution of the loss in weight as percentage while the curve in pink color shows the differential loss in weight as milligram per centigrade. The curves of the thermogravimetric analysis of tuffeau show some weight loss between 200°C and 600°C resulting from the loss of the bonded water and dehydroxation of clay minerals. This is not the case for Richemont stone. These findings provide further evidence for the presence of a certain amount of clay minerals in tuffeau rather than in Richemont stone. Again, the two stones show a significant weight loss around 800°C which results from the decomposition of calcite ($CaCO_3$) to calcium oxide after the ignition of CO_2. Based on the measurement of this weight loss in the limestones, the proportion of calcite was estimated and is presented in Table (II-2). The results revealed that calcite is the main mineral phase for Richemont stone, accounting for about 95%, while for tuffeau the proportion of calcite was found to be about 50%. These calcite percentages matched the results obtained by the ICP-OES analysis, confirming the results obtained.

1.2.2. Fabric of the stones

The morphology of tuffeau and Richemont stone was observed using a PHILIPS XL40 high resolution scanning electron microscope (SEM). The size, shape and the arrangement of the grains present in tuffeau and Richemont stone are shown in Figure (II-7). These SEM images were taken from the rough surface samples.

The SEM images for the polished thin section samples prepared by using resin impregnation for tuffeau and Richemont stone are presented in Figure (II-8). In these images the stone texture can be described precisely, making it possible to distinguish the size of the minerals and the pores resulting from the mineral arrangement. Tuffeau has

different types of grains: quartz, calcite, clays such as glauconite and mica flakes. The sizes of these grains are varied, ranging from 10 µm for the spherical opal grains to 100 µm for the quartz grains present within the sparitic and micritic calcite (Beck, 2006).

The variations both in the types and the sizes of the grains give tuffeau an inhomogeneous micro-fabric with several sizes of pores. In contrast, Richemont stone is mainly composed of calcite with traces of quartz and clay minerals. The size of the calcite grains range from less than 5 µm to about 20 µm. The calcite crystals are micritic in nature, giving Richemont stone a porous micro-fabric with pore sizes mainly about 1 µm to 5 µm, while the bigger pores ranged between 10 µm and15 µm.

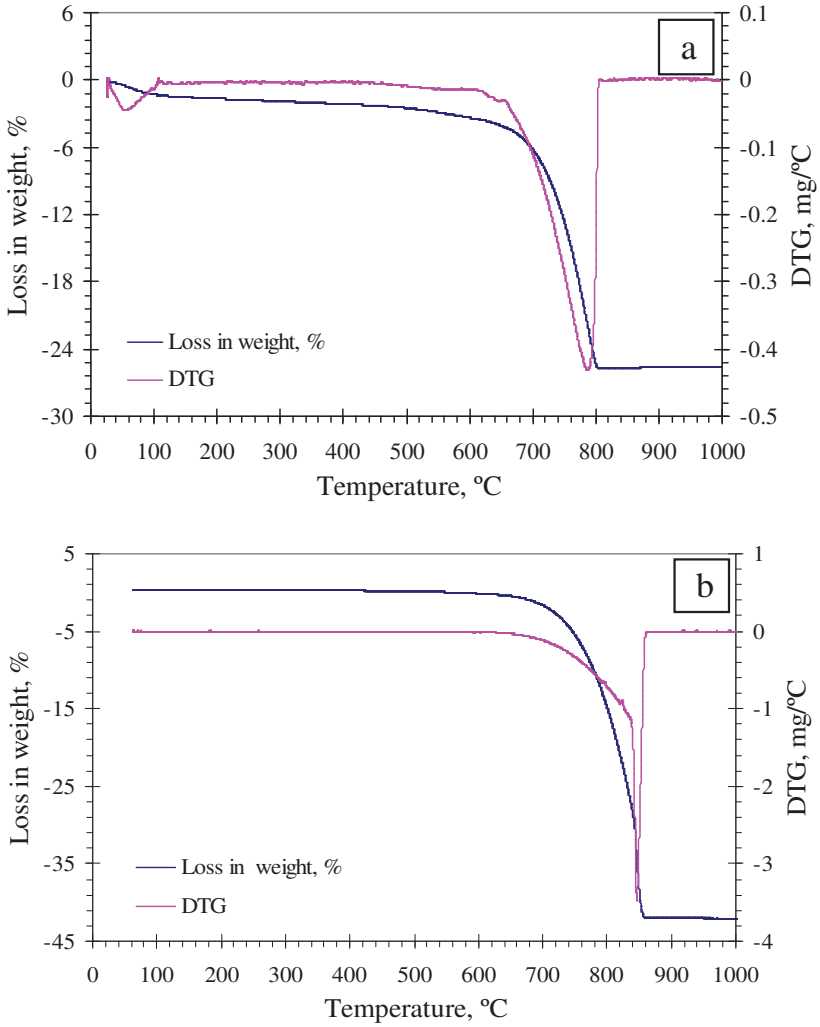

Fig. II-6. Thermo-gravimetric analysis of the limestones: (a) tuffeau; (b) Richemont stone.

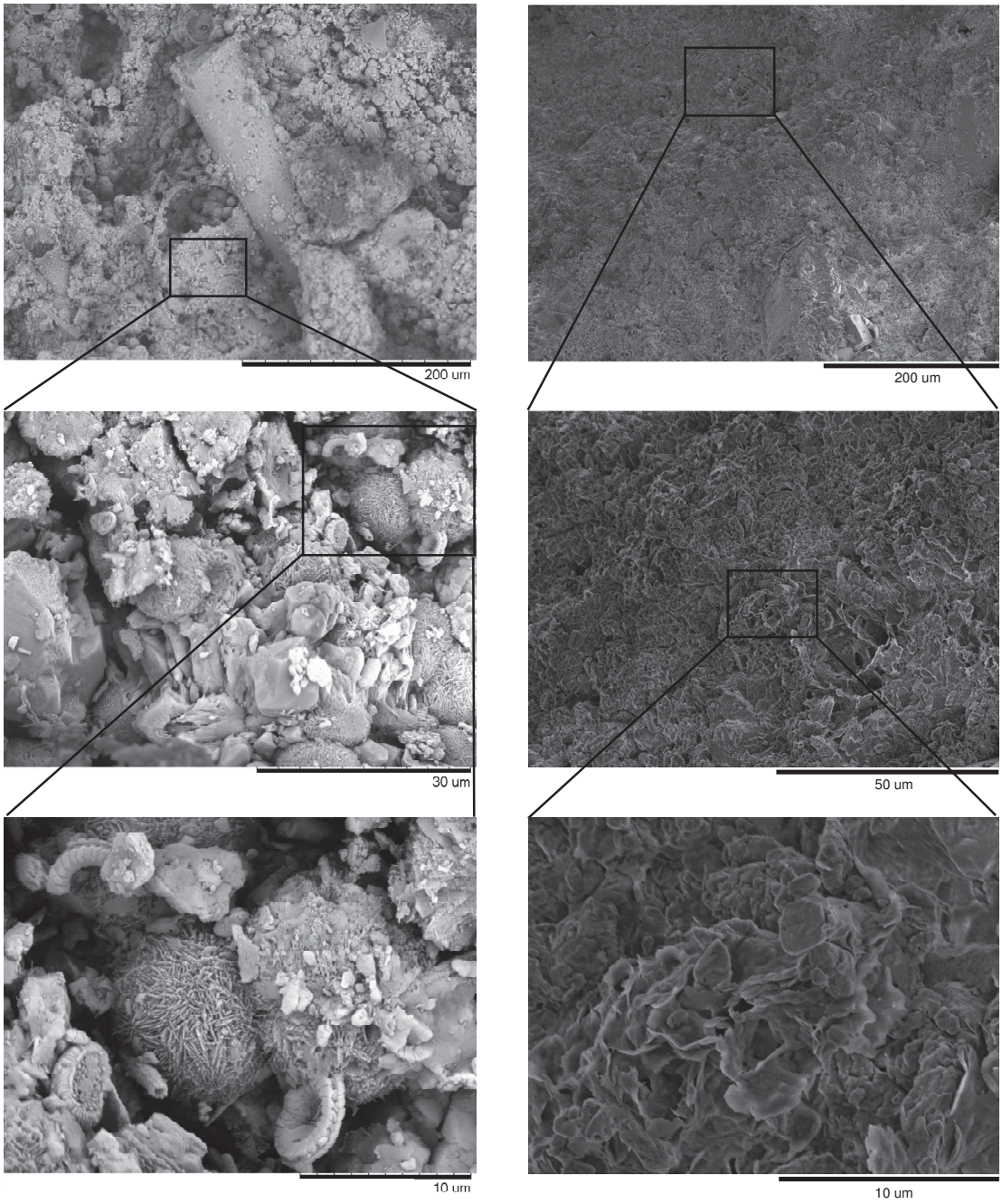

Fig. II-7. Rough surface SEM images showing the topography of the grains in the stones: (*left*) tuffeau: (*right*) Richemont stone.

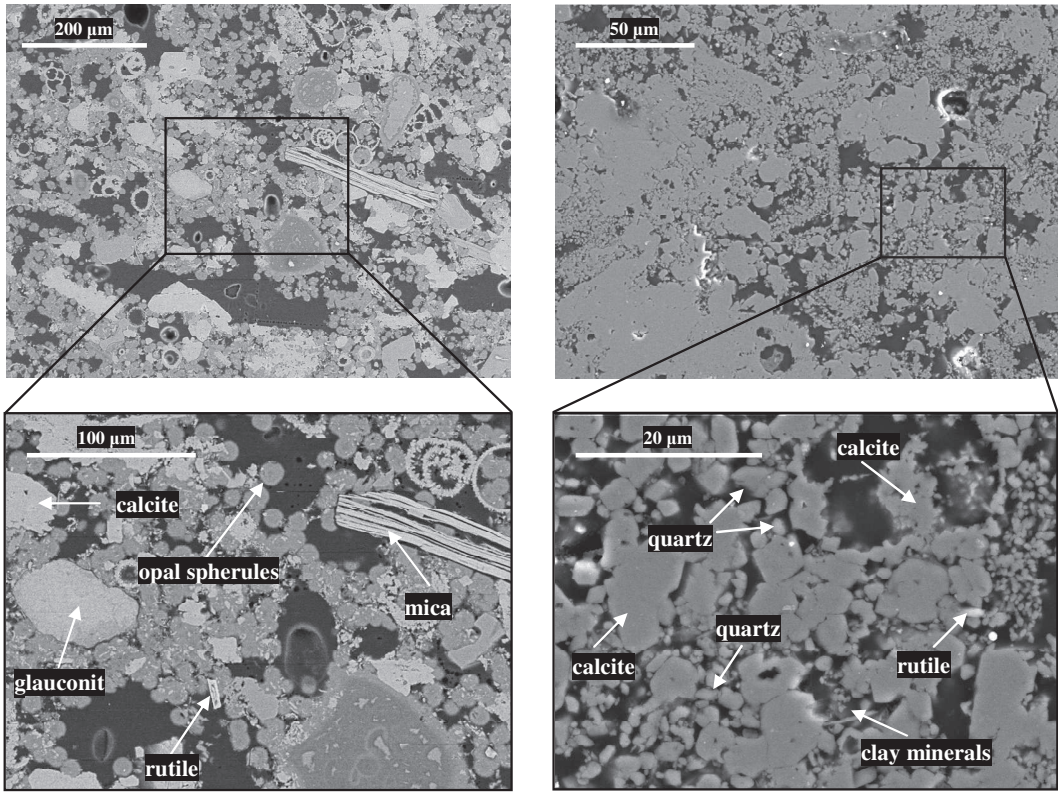

Fig. II-8. Scanning electron microscope images on polished sections of the two limestones: tuffeau (*left*), (Beck, 2006); Richemont stone (*right*).

On polished images it is also possible to define the full mapping of all the minerals present. In this study, the mapping of chemical elements was carried out by using the same scanning electron microscope but equipped with a FEG Hitachi S4500 - EDS OXFORD INCA Energy Dispersive Spectroscope (EDS). The observations of the full mapping for elements contained in tuffeau and Richemont stone are presented in Figures (II-9,10). The mapping was carried out on the same area observed previously by SEM. Concerning tuffeau stone, the signals of silicon and calcium are related to quartz and calcite, respectively, while the signals of silicon, aluminum and iron indicate the presence of clay minerals such as glauconite (iron potassium phyllosilicate group mineral). In addition, the grain of rutile is clearly distinguished by the signal of titanium. The analysis on Richemont stone revealed that calcium is the main element, indicating that this stone is mainly composed by calcite. The signals of silicon and aluminum observed on the same area (inside the red rectangles) indicate the presence of clay minerals near the pores. There are

some areas (inside the yellow rectangles) with a high concentration of silica minerals, indicating the presence of quartz grains. Finally, the titanium signal confirms the previous results of the chemical analysis obtained by ICP-OES showing the presence of titanium oxide TiO_2.

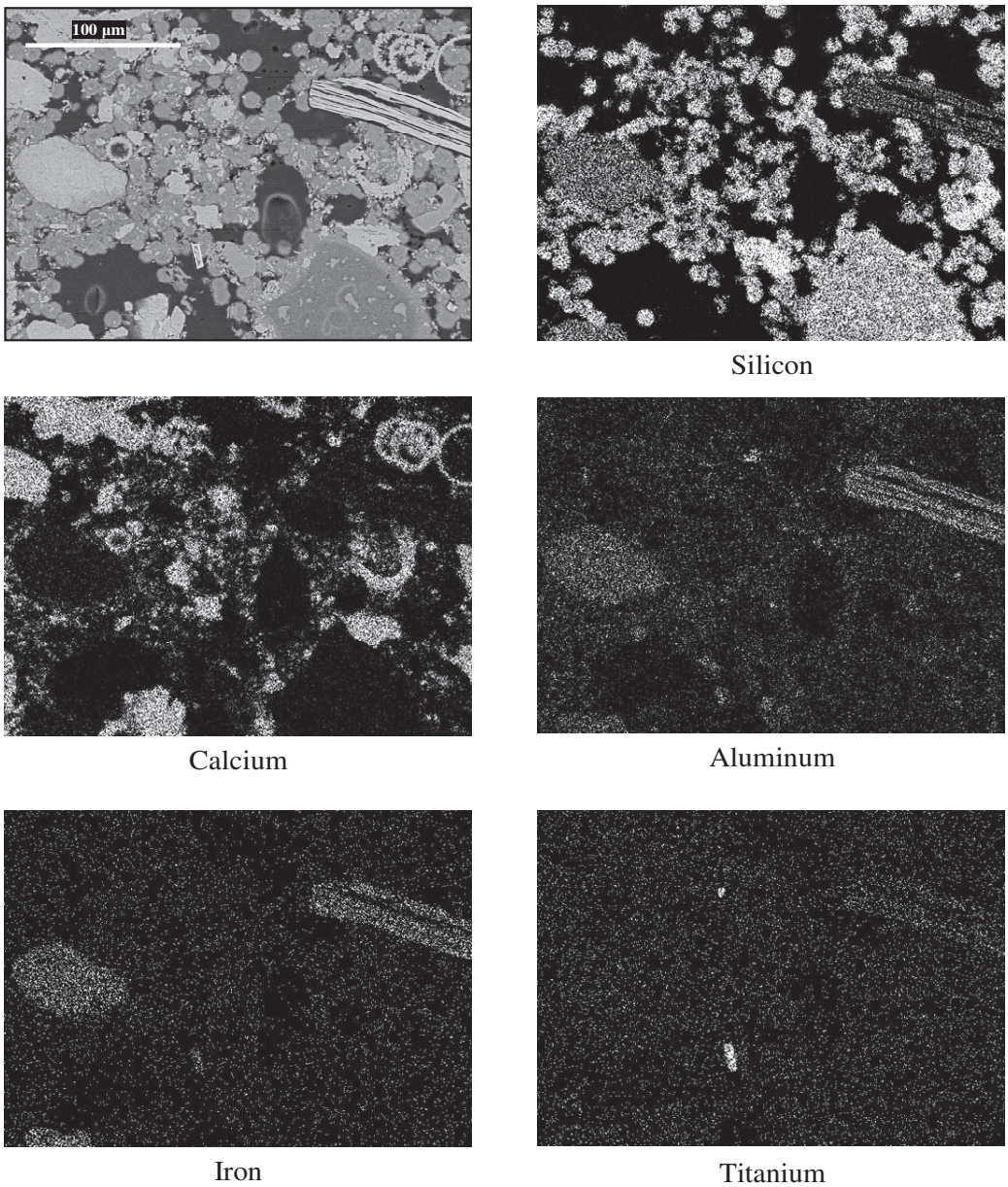

Fig. II-9. EDS maps showing the elemental compositions of Ca, Si, Al, Fe and Ti present in tuffeau limestone, (after Beck, 2006).

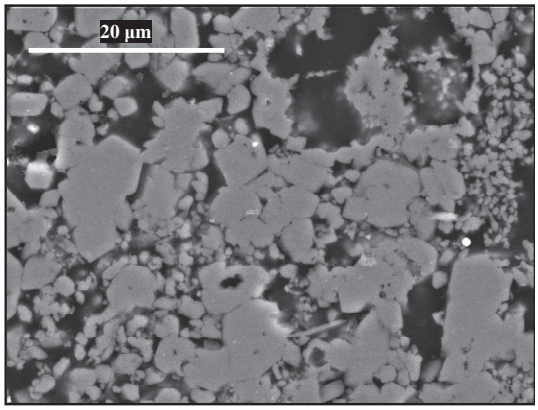

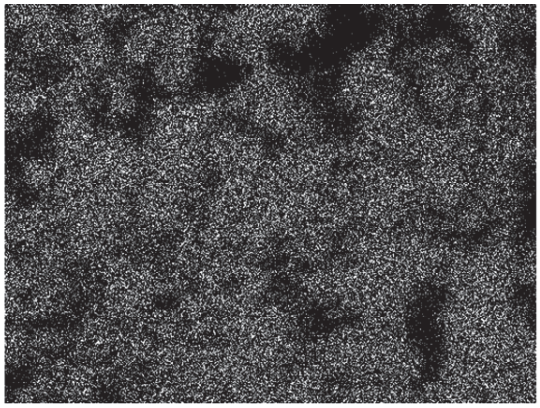

Calcium

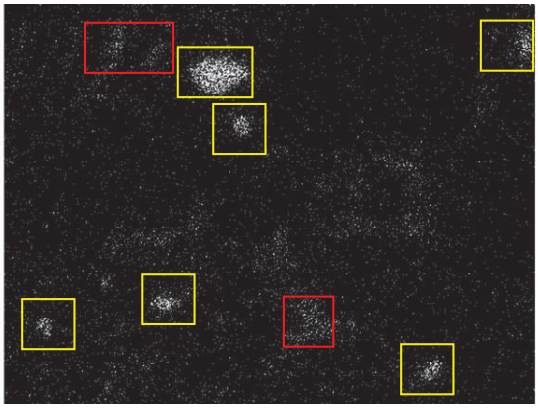

Silicon

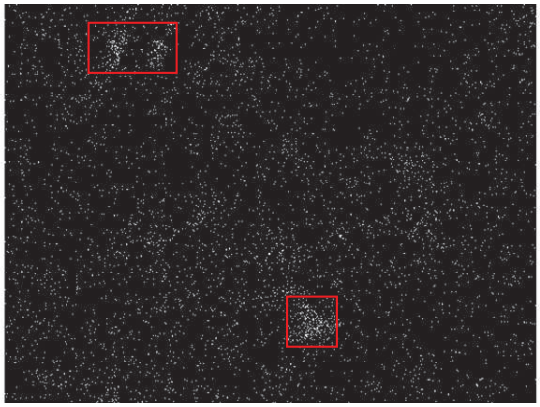

Aluminum

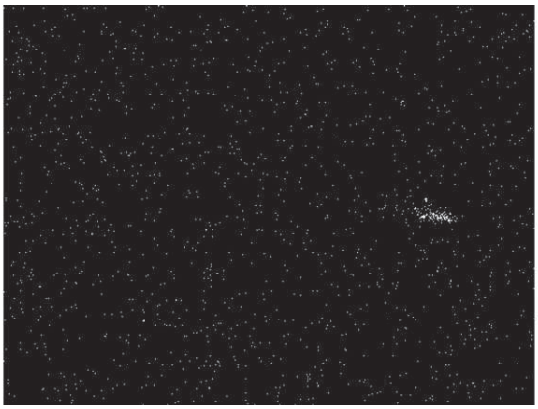

Titanium

Fig. II-10. EDS maps showing the elemental compositions of Ca, Si, Al and Ti present in Richemont limestone.

1.3. Density and pore space characterisation

1.3.1. Density and total porosity

The densities of a porous stone, i.e. apparent density (ρ_a) and skeletal density (ρ_s), are associated to the porosity of a stone. The apparent density can be defined as the ratio of stone mass to the total volume of a stone, while the skeletal density depends on the components contained in the stone regardless of the available porosity. In other words, the skeletal density represents the ratio between the mass of a stone and its solid volume. Therefore, it gives some indications about the mineral composition of a stone.

The total porosity of a stone is defined by the ratio of all pore volumes (pores, open cracks) to the total volume of the whole stone. According to the definition of the apparent and skeletal densities, the total porosity of a stone can be expressed by Eq.1:

$$\phi = (1 - \frac{\rho_a}{\rho_s}) \qquad \text{Eq.1}$$

The three aforementioned physical stone properties can be determined by following different methods, but the simplest and often the most accurate method is hydrostatic weighing, with the measurement based on the buoyancy affecting a stone sample immersed in water, the Archimedes method. In this method, three parameters can be used to determine the physical stone properties:

- The weight of the sample in dry state (M_{dry}).
- The weight of the sample in fully saturated state ($M_{sat.}$).
- The weight of the sample in fully saturated state but immersed in water ($M_{imm.}$).

The weight of the dry sample is determined by drying the sample in an oven at 105±5°C for at least 24 h. The fully saturated state of the stone sample can by obtained by extracting the entire pore air before saturation. To do that, the dry samples were placed in a chamber under vacuum pressure (0.1 kPa) maintained for 24 hours. Then distilled water was allowed to immerse the stone sample. Finally, the stone sample was left immersed in water for an additional 24 h. The weight of the fully saturated sample in air, ($M_{sat.}$), and the weight of the fully saturated sample immersed in water ($M_{imm.}$) were determined.

When ρ_w is the density of water in g/cm^3, then the volume of the pores filled with water and the total volume of the stone sample can be determined by Eqs.2 and 3:

$$V_{pore} = \frac{M_{sat.} - M_{dry}}{\rho_w} \qquad \text{Eq.2}$$

$$V_{total} = \frac{M_{sat.} - M_{imm.}}{\rho_w} \qquad \text{Eq.3}$$

The difference between the total volume of the stone sample and the pore volume will result in the volume of the solid material in the stone sample, Eq.4:

$$V_{solid} = \frac{M_{sat} - M_{imm} - (M_{sat} - M_{dry})}{\rho_w}, \qquad V_{solid} = \frac{M_{dry} - M_{imm}}{\rho_w} \qquad \text{Eq.4}$$

According to the definitions of the physical stone properties mentioned above, the apparent density, skeletal density and total porosity of the porous stone can be determined through Eqs.5, 6 and 7, respectively:

$$\rho_a = \frac{M_{dry}}{\frac{M_{sat} - M_{imm}}{\rho_w}} \qquad \text{Eq.5}$$

$$\rho_s = \frac{M_{dry}}{\frac{M_{dry} - M_{imm}}{\rho_w}} \qquad \text{Eq.6}$$

$$\phi = \frac{M_{sat} - M_{dry}}{M_{sat} - M_{imm}} \qquad \text{Eq.7}$$

This method does not consider the closed pore space that cannot be accessed during the saturation process. In general, most sedimentary stones have few or no closed pores (Vázquez et al., 2013). In this study, the porosity accessible to water under vacuum obtained by Eq.7 will be considered as the total porosity of the stone.

Table (II-3) lists the measured densities and the total porosity for the two limestones. The measurements were carried out on ten samples for each limestone. Tuffeau has a higher porosity (45%). The apparent density is related to the amount of pores contained in the stone, thus the more porous tuffeau stone has a lower apparent density. Tuffeau contains 30% of amorphous silica in the form of opal (cristobalite-tridymite), see

section 2.1, which has a low grain density. This reflects the lower skeletal density of tuffeau. Richemont stone is characterized as a highly porous stone with a total porosity of about 29%. This stone contains about 95% of calcite mineral, thus it has a skeletal density quite similar to the density of calcite (2.71 g/cm^3). Richemont stone has an apparent density of about 1.94 g/cm^3.

Table II-3. Physical properties: total porosity, apparent density and skeletal density obtained from the hydrostatic weighing method of the two studied stones, (average value and standard deviation)

Stone type	Apparent density g/cm^3	Skeletal density g/cm^3	Total porosity %
Tuffeau	1.40 0.02	2.56 0.01	45.2 0.58
Richemont stone	1.92 0.02	2.71 0.01	29.0 0.67

Each value results from the test of 15 samples

1.3.2. Pore size distribution

The size of the pores contained in porous stone can be determined by the pore radius, which is related to the radius of a cylinder representing the ideal form of a pore. This representation is not, however, the real shape of the pores in a natural porous stone. In fact, the pores in a sedimentary stone usually have different shapes and a more complex geometry than that of a cylinder. Therefore, the smallest diameter or radius of a pore can only be reflected by determining the pore size. This smallest pore radius is usually the throat (or entry) of a pore or crack, and can be defined as the pore throat radius.

The Young-Laplace equation, presented in Eq. 8, is considered as the reference method to determine the pore (throat) radius distribution:

$$r_p = \frac{-2\gamma.\cos\theta}{P} \qquad \text{Eq.8}$$

where:

r_p : the pore throat radius of a capillary pore

γ : the surface tension at the liquid interface

θ : the liquid-solid contact angle and P : the applied pressure

Equation 8 is based on the principle that there is a special pressure value that is responsible for pushing a non-wetting fluid into the capillary pore with a certain radius. However, the relationship between pressure and capillary pore radius presented in Eq.8 is applicable only when the pushed fluid is a non-wetting fluid, and thus has a contact angle θ greater than 90°, such as mercury which is non-wetting fluid with almost all materials. Therefore, most laboratory studies use the mercury intrusion porosimetry (MIP) technique to determine the pore size distribution of any porous material. Note, however, that the pressure-related mercury intrusion technique can measure the porosity and the pore size radii distribution in different ranges depending on the working conditions of the apparatus used.

In general, the MIP test is carried out in two stages: the low pressure stage, and the high pressure stage. The test starts with the low pressure stage in which the bigger pores are first filled with mercury, while the smaller pores are then filled with mercury during the high pressure stage. It should be mentioned that during the test the bigger pores may have small entries through which the mercury can flow. In this particular case, high pressure is required to fill these pores. However, according to the Young-Laplace equation, the bigger pores require a low pressure to be filled with mercury. This phenomenon, known as the "ink bottle effect", is the main disadvantage of using the MIP technique to determine the pore size distribution of a porous stone. The results from the MIP test should therefore be accompanied by SEM observations in order to examine the exact condition of the pores present within the porous stone tested.

The MIP test gives preliminary information about the pore size distribution. The measured porosity of the stone may not be representative of its porosity because some proportions of the pores are not observed in this test. So, from this test it is possible to obtain the value of the apparent density and the mean pore diameter, but skeletal density and porosity are underestimated.

In this study, the apparatus used was a Micromeritics Autopore IV 9520 porosimeter which is able to apply pressures in the range of 2.76 kPa up to 414 MPa and can measure pore diameter sizes from 0.003 μm up to 450 μm. In this test, the physical properties: apparent density, skeletal density and porosity, in addition to the mean pore

diameter and the pore size distribution of the two studied stones were determined and are presented in Table (II-4).

Table II-4. Results of MIP test for the two stones: (φ) connected porosity; (ρ_s) skeletal density; (ρ_a) apparent density; (D_m) mean pore diameter and pore size distribution.

Stone type	D_m	pore size distribution, %					ρ_a g/cm^3	ρ_s g/cm^3	φ %
		Small pores		Medium pores	Big pores				
		<0.01 µm	0.01-0.1 µm	0.1-1.0 µm	1.0 -10 µm	>10 µm			
Tuff.	1.8	6.22	12.55	20.29	52.02	8.92	1.35 0.02	2.47 0.07	45.03 0.78
Rich.	1.2	--	2.96	42.17	51.58	3.29	1.91 0.01	2.63 0.001	27.73 0.58

Tuffeau has a bimodal pore distribution, Figure (II-11). It includes a wide range of pore diameter sizes, from 20 µm to less than 0.01 µm, with a mean pore diameter of 1.8 µm. This is due to the homogeneous size of the main grains (opal in the form of spherules about 10 µm in diameter) and the micritic calcite present in this stone. The large pores with a diameter ranging from 1 µm to 10 µm represent more than half of the investigated pores, Table (II-4). The main peak is around the pore diameter of 8 µm. The second peak, about 0.01 µm, is due to the rough surface of spherules of opal, and to the clayey minerals. It should be noted that the larger pores observed by SEM were poorly detected in the MIP test, mainly due to the effect of the "ink bottle" phenomenon.

Richemont stone has a submodal distribution of pore size, with one main peak at the pore diameter of 2 µm and a shoulder at 0.6 µm of pore diameter, Figure (II-12). The proportion of large pores, between 1 µm and 10 µm, is quite similar to the proportion observed in tuffeau. However, the pore size distribution of Richemont stone indicates that more than 90% of the pores are in the range of 0.1-10 µm. With this distribution, Richemont stone has a medium pore diameter of about 1.2 µm.

The densities for the two studied stones measured by MIP are less or more than the densities obtained from the hydrostatic weighing method. This reflects the reliability of the

two test methods. However, all the porosities measured by MIP are underestimated compared to the porosities determined by the hydrostatic weighing method. This is related to the fact that not all the pores contained in porous stones are filled by mercury and consequently they are not all measured by the MIP test. Moreover, the heterogeneity of the tested samples can contribute to make some additional differences.

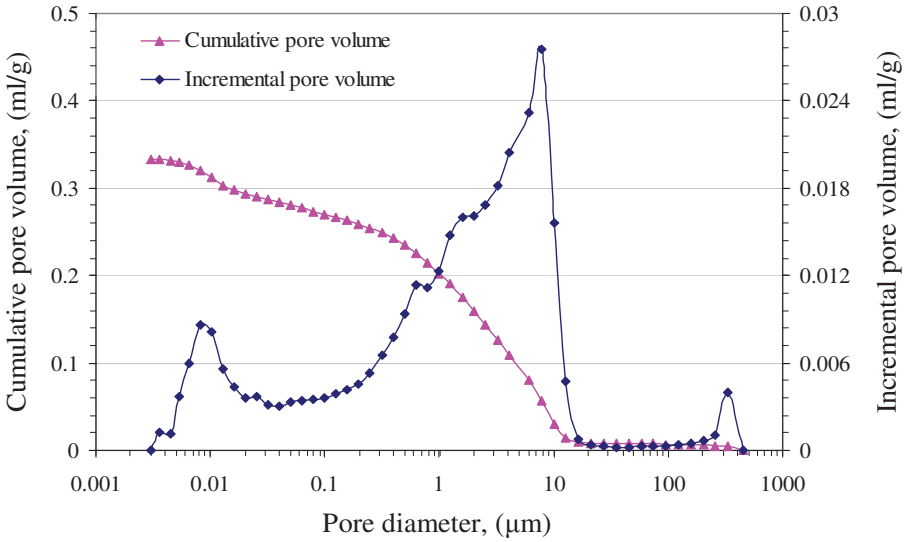

Fig. II-11. Pore size distribution of tuffeau limestone.

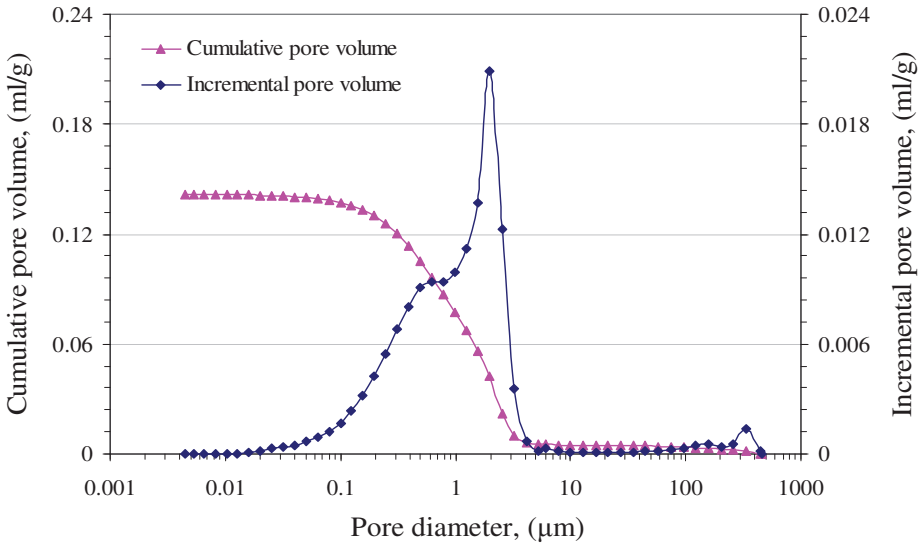

Fig. II-12. Pore size distribution of Richemont stone.

1.4. Water transfer properties

It is well known that the amount of moisture contained in stone, as well as the water movements from/towards the stone, is controlled by the pore space of the stone. The following sections present the main water transfer properties both for tuffeau and Richemont stone, and the main results are discussed.

1.4.1. Water retention capacity

The water retention capacity for each stone was determined by the water retention curve (WRC). The WRC represents the relationship between the water content (or degree of saturation) and the water-stone potential (or stone suction), which is related to the relative humidity of the environment. These relationships make it possible to predict the stone water storage. In this study three techniques were used to determine the WRC:

- *Saturated salt solution method*: according to Kelvin's law, the relative humidity of a closed system can be controlled by using different saturated salt solutions. The samples were placed inside a closed system with specific humidity (lower than 98%) in order to impose high values of stone suction (greater than 2.7 MPa).
- *Osmotic solution method:* this technique was employed to determine the part of the WRC in the range of stone suction between 0.1 MPa and 1.5 MPa. The stone samples were placed inside a semi permeable membrane and immersed in Poly Ethylene Glycol (PEG) solution. The concentration of the PEG solution controls the suction.
- *Tensometric plate method:* in this technique, low levels of suction, ranging between 0.001 MPa and 0.01 MPa, can be imposed on the stone sample in contact with a saturated high air entry ceramic disk under the height of a water column in equilibrium.

In the three aforementioned techniques, the stone samples can gain or lose moisture depending on the initial state of the stone in order to reach equilibrium. Due to the hysteresis effect between the filling and draining of the pores, two types of WRCs can be

distinguished: wetting curve (when the stone samples are initially in dry state) and drying curve (when the stone samples are initially in saturated state).

The WRC of tuffeau was already obtained by (Beck, 2006), Figure (II-13). In the present study, the WRC of Richemont stone was determined and is presented in Figure (II-14). These curves make it possible to determine the ability of the stone to capture (in the case of wetting curve) or retain (in the case of drying curve) water by the suction imposed by the external environment. Thus, the WRC can provide valuable information that can be used to explain the correlation of stone degradation to the variation in its moisture content.

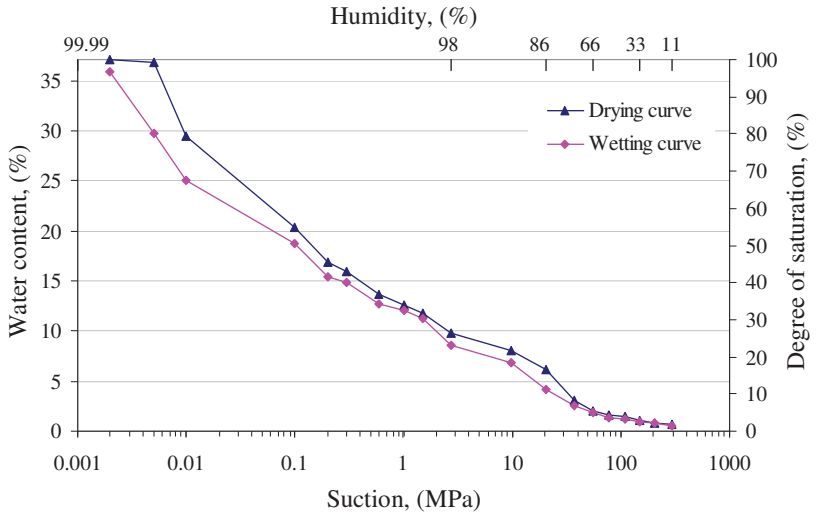

Fig. II-13. Water retention curve of tuffeau limestone (Beck, 2006).

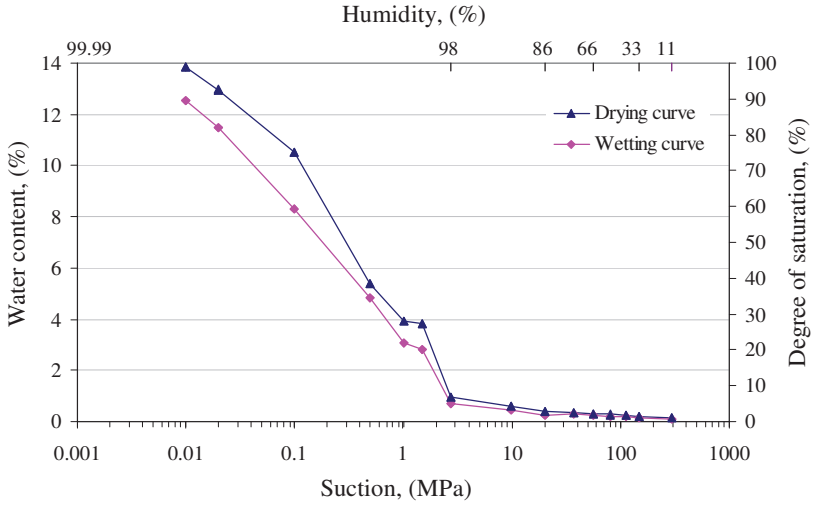

Fig. II-14. Water retention curve of Richemont stone.

The data in Figure (II-13) show that tuffeau has a high ability to capture moisture from the surrounding humid atmosphere. It can contain a considerable amount of water, about 9% of water content (or a degree of saturation about 25%), when located in an environment with 98% of relative humidity. This is not the case for Richemont stone. In fact, Richemont stone is almost dry even when it is in contact with a highly humid environment. For example, the water content of Richemont stone is limited to 1% (or a degree of saturation of 5%) in an environment with 98% of relative humidity.

The different behaviors of the two limestones are strongly influenced by both the microstructure and the mineralogical composition of the stone. Tuffeau has considerable microporosity and contains about 10% of clayey minerals. These features give tuffeau limestone a high ability to easily absorb moisture from a humid atmosphere. Tuffeau also has a wide range of pore size distributions, which enable moisture to be absorbed at a constant rate. In Richemont stone, in contrast, the microporosity is lower, thus it is characterized by two different moisture absorption rates. However, the sudden change in moisture absorption can be seen for humidity higher than 98%.

1.4.2. Free water absorption

The free water absorption property under atmospheric conditions provides information about how much water is absorbed by the stone over a period of time, usually 48 h, when the stone is immersed in water. In this test, three cylindrical stone samples (Ø 40 mm × 40 mm) for tuffeau and Richemont stone were dried at 105±5 °C for a period of 24 h. Once the stone samples had cooled, their dry weights (M_{dry}) were determined. Then the stone samples were immersed in distilled water at room temperature for a period of 48 h under atmospheric pressure. In this case the weight of the immersed stone samples (M_{sat48h}) was also determined. Then the free water absorption ($A_{atm.}$) under atmospheric pressure conditions can be determined through Eq.9:

$$A_{atm.} = \frac{M_{sat48h} - M_{dry}}{M_{dry}} \qquad \text{Eq.9}$$

During the free water absorption test, there is always trapped air in the pores which cannot be filled with water under atmospheric pressure conditions. Contrary to free water absorption, in the forced water absorption test under vacuum pressure ($A_{vac.}$), all the effective porosity is filled with water (i.e. no air trapped in the pores). Thus the forced water absorption is, of course, higher than the free one. The forced water absorption is determined by Eq.10:

$$A_{vac.} = \frac{M_{sat.} - M_{dry}}{M_{dry}} \qquad \text{Eq.10}$$

The symbol ($M_{sat.}$) represents the weight of the fully saturated sample under vacuum pressure. The ratio of the free water absorption to the forced water absorption determines the so-called degree or saturation coefficient (S_{48h}). The coefficient of saturation at 48h of a stone is indicative of the proportion of the pore space which is accessible to water absorption. Equation (11) was used to determine this saturation coefficient.

$$S_{48h} = \frac{A_{atm.}}{A_{vac.}} \qquad \text{Eq.11}$$

The values of the water absorption properties ($A_{atm.}$, $A_{vac.}$ *and* $S_{48h.}$) for the tuffeau and Richemont stone are listed in Table (II-5). Tuffeau and Richemont stone have nearly the same high values of coefficient of saturation at 48h, about 0.85 and 0.80, respectively. This is due to the fact that the two limestones have the same proportion of pores in the range of 1-10 μm, see Table (II-4).

Table II-5. Water absorption properties of the two studied stones, ($A_{atm.}$) free water absorption under atmospheric pressure; ($A_{vac.}$) forced water absorption under vacuum pressure; ($S_{48h.}$) coefficient of saturation at 48h.

Stone type	$A_{atm.}$ (%)	$A_{vac.}$ (%)	S_{48h}
Tuffeau	26.91 0.35	31.50 0.25	0.85 0.01
Richemont	11.79 0.33	14.69 0.43	0.80 0.01

1.4.3. Capillary water absorption

In general, porous stone can absorb the water in contact with it by capillarity. The rising of water inside the small diameter pores is related to the capillary force generated. This capillary force is created to equilibrate the surface tension of water and the adhesive force of the pores. Water with a polar surface represents an ideal wetting liquid characterized by a wetting angle that enables it to rise easily inside the capillary pores.

The capillary water absorption test was carried out by following the procedure described in the AFNOR B10-613 standard. The tests were performed on three cylindrical (Ø 40 mm × 80 mm) samples of the two studied stones. In this test, the cylindrical samples were placed inside a basin containing water so that only the bottom of the stone was in contact with water. The water height inside the basin should remain constant during the test. Both the capillary front height and the water uptake per surface area were measured periodically.

By applying the Washburn equation principle, when the unit area of a porous stone is in contact with water, both the rise of water height (h) and the water gained per unit surface area (W/S) can be directly proportioned to the square root of time (t):

$$h = H_{capillary} \times \sqrt{t} \qquad \text{Eq.12}$$

$$W / S = W_{capillary} \times \sqrt{t} \qquad \text{Eq.13}$$

where:

$H_{capillary}$: the capillary front height coefficient

$W_{capillary}$: the water uptake coefficient

Most porous stones show linear relationships both of the capillary front height and the water uptake per unit area versus the square root of time. The slopes of these linear curves represent, respectively, the two coefficients presented in Eqs.12 and 13. The capillary water absorption curves for tuffeau and Richemont limestones are, respectively, shown in Figures (II-15, 16).

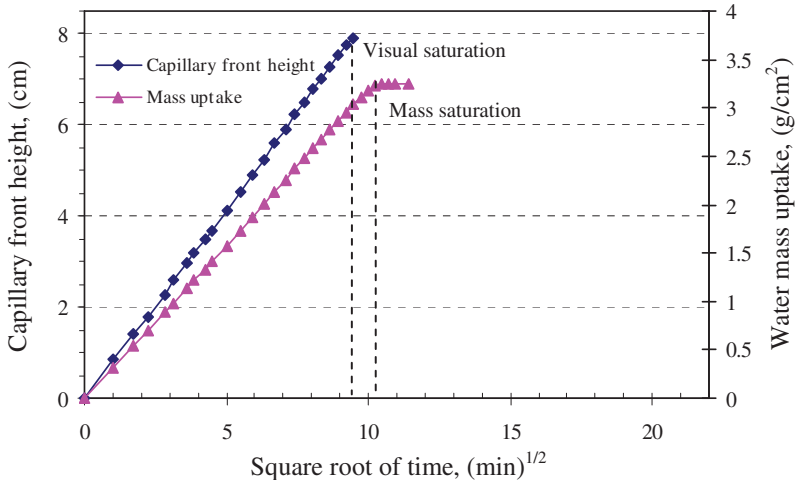

Fig. II-15. Curves of the capillary water absorption for tuffeau limestone.

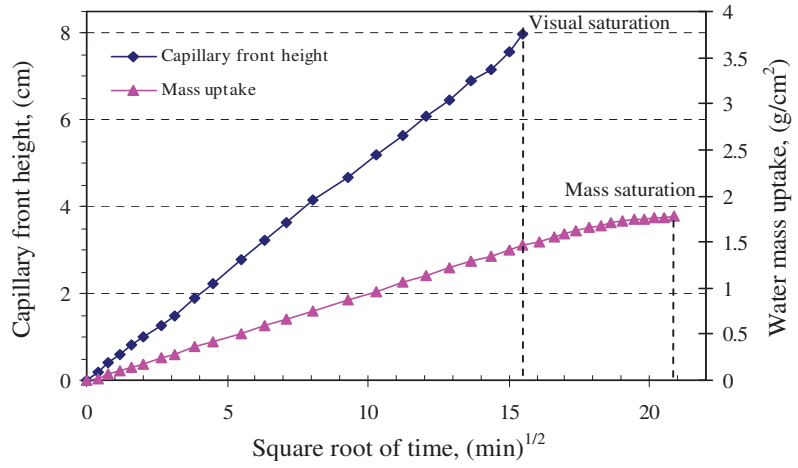

Fig. II-16. Curves of the capillary water absorption for Richemont stone.

These curves indicate that there are two distinct stages: a visual saturation stage (when the capillary front reaches the total height of the sample) and a mass saturation stage (when no further increase in the weight of the sample takes place). The linear slopes of these curves indicate the homogeneity of the porous networks for the two stones. Tuffeau has high capillary absorption coefficients ($H_{capillary}$: 0.96 ± 0.07 cm/min$^{1/2}$, $W_{capillary.}$: 0.36 ± 0.03 g/cm^2/min$^{1/2}$), as might be expected in view of the high porosity and wide pore diameter access size of tuffeau. When the sample reaches the visual saturation stage, the sample continues to gain water. However, at the end of the mass saturation stage, there are

some entrapped air bubbles which cannot be filled with water under atmospheric pressure conditions. Tuffeau has high porosity (45%) and pores with a wide range of pore access diameter distribution. Consequently, the absorption continues for a short period, until the sample reaches saturation.

Richemont stone has lower porosity (29%) compared with tuffeau, and thus lower water transfer properties ($H_{capillary}$: 0.48 ± 0.01 cm/min$^{1/2}$, $W_{capillary.}$: 0.09 ± 0.01 g/cm^2/min$^{1/2}$). In fact, Richemont stone took longer to go from the visual to the mass saturation stage (i.e. slower rate) compared with tuffeau. This difference is attributed to the geometry of the capillary pore network (the size and the shape of the pores), the connectivity and the tortuosity present in each limestone.

1.4.4. Water permeability

The permeability of the two limestones was examined in this test. Three cylindrical samples (Ø 40 mm × 40 mm) were prepared for each limestone. Prior to the test, the cylindrical samples were fully saturated under vacuum by following the procedure previously discussed in (section 2.2.1.).

Figure (II-17) shows the layout of the experimental set-up used in this test. The samples were subjected to constant head pressure by using an automatic hydraulic pressure system. The bottom-up water flow direction was adopted in this test in order to flush out any entrapped air bubbles and to ensure saturation of the samples during the test. The cylindrical samples were sealed on the lateral surface by a rubber sleeve, sandwiched between two porous disks, and subjected to sufficient confining pressure, slightly higher than the applied head pressure, by using another automatic hydraulic pressure system. The applied confining pressure is important to enforce the path of water flow in one direction. The flow of water that passed through the tested sample was collected by a container placed on a balance. The water flow can be determined through periodic measurements of the water mass collected. Great attention was paid to ensure that the applied head pressure was as low as possible so as to satisfy laminar flow conditions during the test. This is important for Darcy's law to be applicable, Eq.14:

$$Q = K.S.i \qquad \text{Eq.14}$$

where:

Q : the water flow, m^3/s

S: cross sectional area, m^2

K: hydraulic conductivity, m/s

i : the applied head pressure gradient

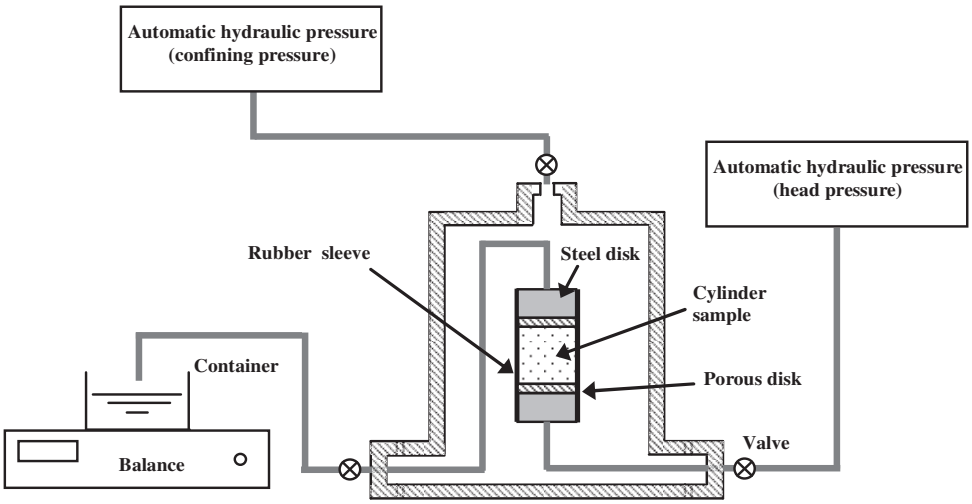

Fig. II-17. Scheme of the experimental set-up used in permeability test.

The results from the water permeability test were found to match the other results obtained from the capillary water absorption test: tuffeau limestone had a higher permeability coefficient, with $3.05\ 10^{-7} \pm 0.29\ 10^{-7}$ m/s, while the permeability coefficient value of Richemont stone was smaller, at $5.38\ 10^{-8} \pm 0.60\ 10^{-8}$ m/s. This is due to the high connectivity of the pore network, added to the high open porosity of tuffeau stone as well as the higher mean access pore diameter. It should be noted that highly porous stone is not always characterized by a higher permeability. In fact, two porous stones with the same porosity can differ in their permeability (Beck, 2006; Šperl and Trčková, 2008). The geometry of the pore network such as the pore diameter access, the degree of pore connectivity and the pore tortuosity are the main factors that control the permeability properties of a porous stone.

1.5. Mechanical properties

1.5.1. Stone strengths

The mechanical properties related to the stone strength both in compression by means of the Unconfined Compression Test (UCT) and in tension by the Indirect Tension Test (ITT), were obtained both for tuffeau and Richemont stone. In the UCT, the cylindrical samples (Ø 40 mm × 80 mm) were placed vertically and subjected to a compression force parallel to the vertical sample axis, Figure (II-18). The test was conducted according to the methodology described in (Norm AFNOR P94-420), using an Instron 4485 press machine at a loading rate of 0.05 mm/min, so that the sample failed within 10 to 15 minutes. The unconfined compressive strength of the sample is given by Eq.15. The ITT was carried out by means of the Brazilian test following the procedure listed in (Norm AFNOR P94-422). The tests were performed on cylindrical samples (Ø 40 mm × 40 mm) using the same press machine as in the UCT with the same loading rate. The cylindrical samples were loaded diametrically across the circular cross section as shown in Figure (II-19), where the samples failed due to fractures perpendicular to bedding plane. The indirect tensile strength was determined by Eq.16.

$$\sigma_c = \frac{4F}{(\pi.D^2)} \qquad \text{Eq.15}$$

where:

σ_c : the unconfined compressive strength, MPa

F: the applied load, N

D : diameter of the cylindrical sample, mm

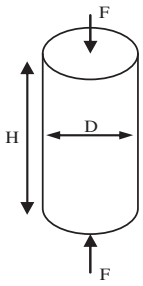

Fig. II-18. Scheme of samples in unconfined compression test.

$$\sigma_t = \frac{2F}{\pi.D.L} \qquad \text{Eq.16}$$

Where:

σ_t : the indirect tensile strength, MPa

F: the applied load, N

D : diameter of the cylindrical sample, mm

L : length of the cylindrical sample, mm

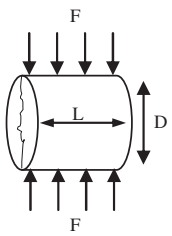

Fig. II-19. Scheme of samples in the Brazilian test.

It should be pointed out that in the Brazilian test, the tensional stress conditions within the sample are not homogenous. Thus, Brazilian test is a suggested procedure to determine the approximate value of the stone tensile strength. In the two mechanical tests mentioned above, the tests were carried out on the tuffeau and Richemont stone samples prepared in dry state (24 h in an oven at 105±5ºC) and in fully saturated state (saturation under vacuum pressure). Three samples were tested for each stone and for each test condition. The results of the mechanical properties are listed in Table (II-6).

Tuffeau has a different mineral composition and structural fabric to Richemont, thus as expected, it behaved differently in relation to strength properties. The values of the mechanical properties of tuffeau were lower than those of Richemont stone. In fact, both the compressive and tensile strength values of tuffeau were about less than half those of Richemont stone. This also reflects the influence of physical properties: high porosity, lower density and poorly cemented grains in tuffeau lead to lower strength values than Richemont stone.

The results in Table (II-6) show that there is a great decrease in the strength values measured for the saturated samples with respect to those measured for the dry samples. A similar reduction in strength with increasing water content was found by (Hawkins, 1998; Vásárhelyi, 2003). The presence of water plays an important role in the strength of the stone; it reduces the surface energy between the constituent grains and weakens the intergranular bonds within the stone matrix. One of the key findings is the significant reduction (58%) in the compressive strength, for example, of tuffeau against 35% for Richemont stone. This can be related to the presence of clay minerals in tuffeau which are extremely sensitive to water.

Table II-6. The mechanical properties of the two studied stones, (σ_c) unconfined compressive strength; (σ_t) indirect tensile strength

Mechanical property	Test condition	Tuffeau	Richemont stone
σ_c , (MPa)	Dry	11.67 ± 0.33	19.41 ± 1.03
	Saturation	4.83 ± 0.33	12.61 ± 1.17
σ_t , (MPa)	Dry	1.30 ± 0.11	2.01 ± 0.13
	Saturation	0.51 ± 0.06	0.85 ± 0.13

Each value results from the test of 15 samples

1.5.2. Ultrasonic wave velocity

The elastic parameter of the ultrasonic pulse velocity for the stone was investigated according to the (AFNOR P94-411) standard. The main advantage of this mechanical test is that it is non-destructive (Yasar and Erdogan, 2004). The test was carried out on cylindrical samples (Ø 40 mm × 80 mm) using a PUNDIT pulse apparatus with two transducers having a frequency of 83 kHz. In this test, the direct method proposed by (Kahraman, 2002) was applied to detect the ultrasonic pulse velocity of the tested stones, tuffeau and Richemont stone, in dry state (dried at 105°C for 24 h). Fifteen samples were tested, each one with four measurements. The tests were applied at room temperature under constant pressure to provide good contact between the stone samples and the transducers. The ultrasonic pulse velocity was determined from the ratio of the length of the sample to the transit time of the pulse.

The ultrasonic pulse velocity is directly related to the porosity and mineralogical composition of the stone. Samples of tuffeau limestone with high porosity and a clay content of about 10% will result in low ultrasonic wave velocity values. The mean and the standard deviation of the ultrasonic pulse velocity for tuffeau and Richemont stone are 1624±48 m/s and 2600±89 m/s, respectively. However, according to Anon (1979) the two stones can be classified as having low and very low ultrasonic pulse velocities.

2. The stone damage risk assessment in natural environment

The damage of natural stones is strongly related to the surrounding environment that is in direct contact with the stones. It is well known that the constant action of daily variations in climatic conditions results in damaging natural stones. This damage may remain invisible for limited periods but its cumulative effects in the long term are significantly destructive.

The degradation of natural stone used in historical sites due to variation in the climatic conditions has been intensively studied. The present research focuses on assessing the damage risk to the stones used in the castle of Chambord: tuffeau and Richemont stone, due to cyclic variations in the local climatic conditions. This damage risk was assessed through three weathering processes: condensation, freezing-thawing action, thermal and hygrothermal stress. Following a brief discussion about data collection and analysis, the methodologies adopted to assess the risk of damage to the stone are presented.

2.1. Brief description of the castle of Chambord

The Castle of Chambord is situated in the Centre region of France in a rural area about 150 km south-west of Paris, Figure (II-20), approximately 84 m above average sea level. This castle is one of the most famous castles in the world and the largest of the Loire Valley castles; its construction began in 1519 and was completed in 1547. It has been listed in the UNESCO world heritage site since 2000. The castle was mainly constructed using tuffeau stone. However, it experienced a lot of restoration work at different periods. In the early 20^{th} century, Richemont stone was selected as an alternative stone in order to replace the degraded ones.

This research focuses on a particular part of the castle: the east tower. The stones on the walls of this tower were selected in this study for three main reasons: firstly, most of the stones in the walls of the east tower are original tuffeau stones (about 72% of the total stones on the tower), Janvier-Badosa, (2012). Secondly, the east tower includes many highly degraded stones, with two main patterns of degradation: biological colonization (different types of lichens and mosses) and stone detachment in the form of stone spalling

and exfoliation (Janvier-Badosa et al., 2013b). Lastly, the semi-circular shape of the east tower makes it possible to study both north and south wall orientations.

In order to assess the risk of damage to the stones on the wall of the castle of Chambord, both weather data (air temperature, air relative humidity and rainfall) and stone data (stone temperature and stone humidity) were monitored and analyzed.

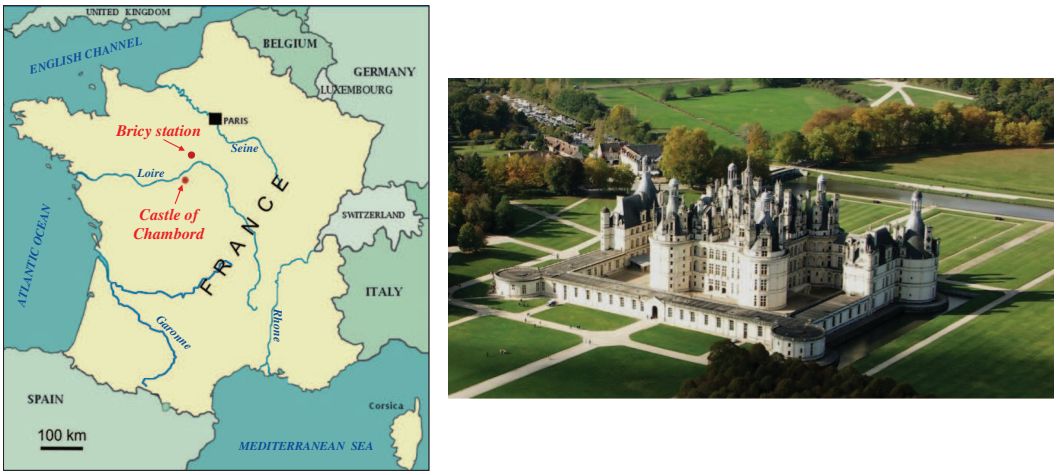

Fig. II-20. Geographical setting of the Castle of Chambord (*right*); the Castle of Chambord- aerial view; copyright: Domaine national de Chambord (*left*).

2.1.1. Weather data

The weather data at the castle of Chambord were intensively monitored by using a local meteorological station installed on the roof of the east tower of the castle, Figure (II-21). These data, comprising air temperature, air relative humidity and rainfall, were recorded every five minutes for a short period of about seventeen months (between April/2010 and August/2011). The statistical analysis of the recorded weather data is presented in Table (II-7). The recorded data revealed that the extreme annual average air temperatures varied, respectively, between 15.9±6.9 °C and 5.9±4.5 °C for maximum and minimum temperature, with a summer maximum of 33.3 °C in July and a winter minimum of -10 °C in November. The mean annual precipitation is 530 mm with maxima of 157 mm in summer in July.

Fig. II-21. General view of the east tower of the castle of Chambord showing the thermal-humidity sensors (*left*), and the meteorological station (*right).*

Table II-7. Statistical analysis of the weather data measured by the local station placed on the east tower of the castle of Chambord, during 2010/2011.

Year: 2010-2011	T_{max} / average T_{max} (ºC)	T_{min} / average T_{min} (ºC)	Mean RH (%)	Mean rainfall (mm)
Jan.	14.5 / 7.1	-6.2 / 1.3	87	16.4
Feb.	17.3 / 10.3	-3.0 / 1.6	86	22.6
March	22.8 / 14.6	-2.6 / 3.3	72	7.0
April	26.8 / 17.3	0.3 / 4.9	66	20.8
May	29.9 / 17.8	1.0 / 6.9	70	29.7
June	31.2 / 22.8	6 / 11.8	74	33.4
July	33.3 / 26.6	8.7 / 13.8	70	157.1
Aug.	31.8 / 24.0	6.5 / 11.9	71	37.1
Sep.	27.7 / 21.1	1.8 / 8.1	77	80.6
Oct.	24.5 / 16.1	-3.7 / 5.8	81	37.5
Nov.	17.9 / 9.74	-10.0 / 3.2	89	37.9
Dec.	9.3 / 3.9	-7.6 / -1.4	89	56.6

These weather data were analyzed and compared with the meteorological data, namely air temperature and air relative humidity, for a long period (1973-2012), obtained from Bricy weather station, the station nearest to the castle of Chambord (about 45 km NE). Figure (II-22) shows the monthly variations in mean maximum and mean minimum, both

of air temperature and air relative humidity for the two periods (2010–2011) and (1973–2012). In this figure, the month #1 is for January. As the min and max values of data from short period lies within the range of the standard deviation of the climate data from long period, we can assume both weather data are statistically similar. Therefore, the data acquired *in situ* during the period (2010–2011) can be considered as representative of the local climatic conditions in the studied area.

In this study, the short period weather data were employed to assess the risk of damage to the stones through two physical weathering processes: condensation and freezing–thawing action.

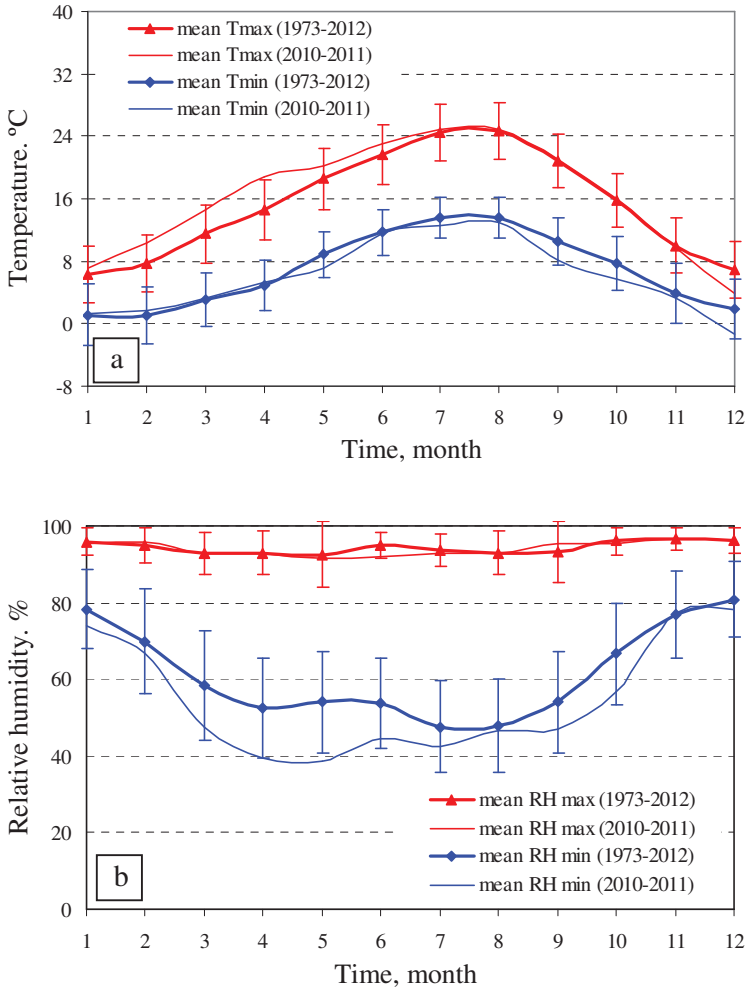

Fig. II-22. Monthly variations in the extreme values of mean air temperature (a) and mean air relative humidity (b) for the two periods: 2010–2011 & 1973–2012.

2.1.2. Stone data

The stone temperature and the stone humidity were recorded more extensively by using FHAD–46x digital thermal-humidity sensors linked to a special microstation data-logger. The sensor's accuracy is 1.3% for a temperature range from -20°C to 80°C, and 1.8% for humidity between 0%–90%. The stone data were measured to observe the conditions of the stones on the castle of Chambord and to study, intensively, the effects both of temperature and relative humidity on the degradation of these stones. To achieve this goal, different conditions in the measurements of the stone data were adopted in this study. The stones on the walls, with an average thickness of about 80 cm, of the east tower were selected in this study. Altogether, 16 thermal-humidity sensors were inserted into the walls of the east tower in two directions (north-facing and south-facing walls) at three different levels (top, middle and bottom of the wall), on the surface and at different depths inside the stones (15, 30, 50 and 250 mm), Figure (II-21). The stone data were measured every 30 minutes for three years, from June/2009 to June/2012, and provide comprehensive information on the changes in temperature and moisture both on the surface and inside the stone.

Table (II-8) lists a statistical analysis for the measured values both of stone surface temperature and stone surface humidity in the case of the stone on the south wall of the east tower for the period of one year (June/2009 to June/2010). It can be clearly seen that the stone temperature can reach high values, up to 35 ºC in summer and that it falls to about -8 ºC in winter. In the case of the measured stone relative humidity, the data in Table (II-8) indicate that the stones are humid most days of the year. These extreme, but realistic, stone data prompted us to study the role of local climatic conditions in enhancing the observed degradation for the stone on the walls of the castle of Chambord.

It is interesting to present the stone data at different depths inside the stone for the purpose of examining the variety of stones' responses to the prevailing environmental conditions.

Figure (II-23) shows an example of stone data measured at 15 mm and 250 mm depth inside the stones located on the south wall, during one year. The stone data are presented as the daily maximum and minimum both in temperature and in relative

humidity. It can be clearly observed that the highest temperature and humidity variations occur at a depth of 15 mm inside the stone. At this depth, the daily difference between the extreme values of temperature and humidity can exceed 20 °C and 30%, respectively, whereas at a depth of 250 mm, low or negligible variations were observed for both temperature and humidity (i.e. below 3 °C for temperature and below 0.5% for humidity). For more details concerning the analysis of climate data please see appendix (1) and (3). These observations support the idea of studying the stresses generated in the stones due to the daily variation both in the stone temperature and in stone humidity, as discussed below in Section 2.5: *Assessment of the stone damage risk due to thermal and hygrothermal stresses*.

Table II-8. Statistical analysis of surface temperature and relative humidity measured for the stones located on the south wall of the east tower of the castle of Chambord, from June 2009 to June 2010.

Year: 2009-2010	T_{max} / average T_{max} (ºC)	T_{min} / average T_{min} (ºC)	RH_{max} / average RH_{max} (%)	RH_{min} / average RH_{min} (%)
Jan.	16.7 / 7.1	-8.4 / -0.9	95 / 87	81 / 85
Feb.	18.1 / 9.6	-8.3 / 1.1	86 / 83	77 / 81
March	24.8 / 15.9	-3.2 / 3.5	81 / 72	55 / 67
April	29.7 / 21.9	1.1 / 6.7	77 / 63	41 / 56
May	33.1 / 21.8	4.3 / 9.4	71 / 61	41 / 54
June	34.9 / 27.3	9.0 / 13.9	77 / 67	50 / 60
July	35.2 / 27.5	11.5 / 15.2	97 / 71	48 / 62
Aug.	37.8 / 31.1	9.1 / 15.6	71 / 62	38 / 52
Sep.	35.3 / 27.0	7.1 / 12.0	75 / 63	42 / 54
Oct.	28.9 / 21.5	0.3 / 8.1	81 / 68	50 / 63
Nov.	21.0 / 15.2	2.1 / 7.3	93 / 83	73 / 81
Dec.	19.8 / 10.3	-7.1 / 1.9	90 / 84	76 / 82

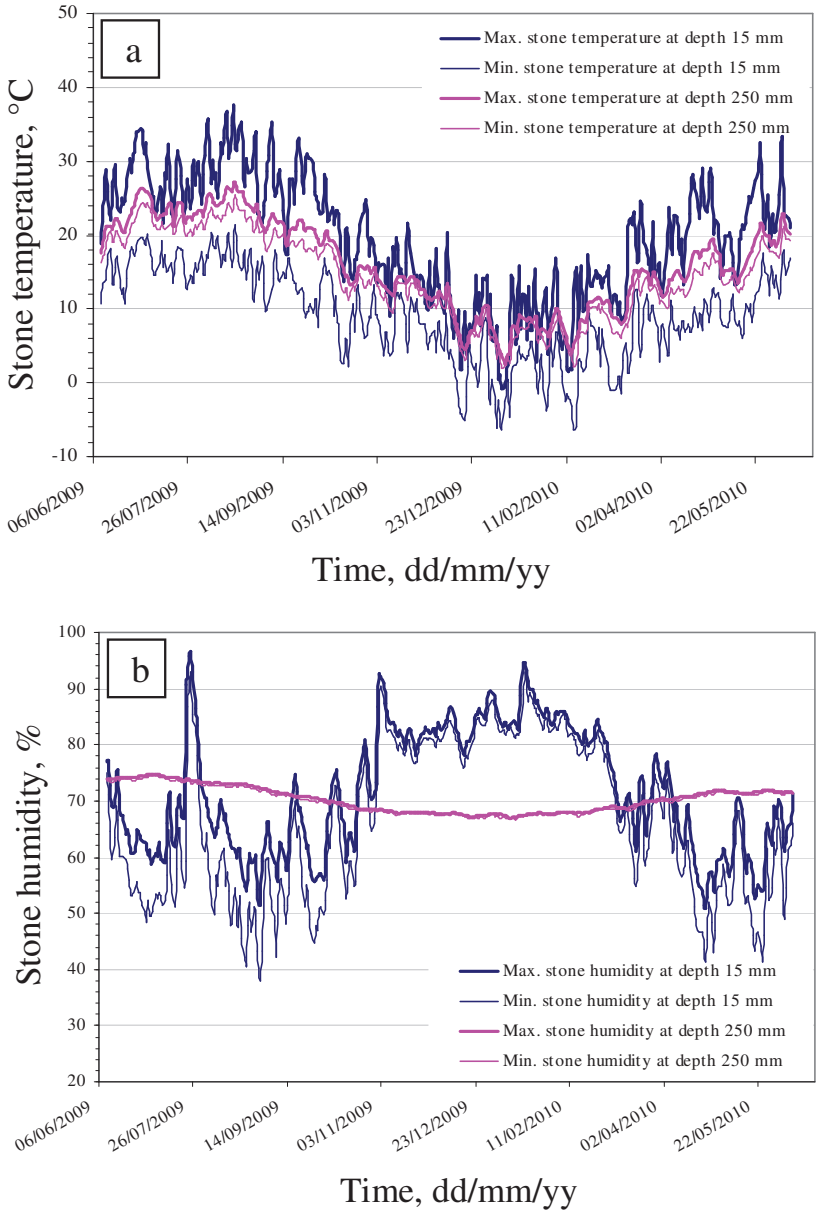

Fig. II-23. Daily maximum and minimum values of temperature (a) and relative humidity (b) at 15 and 250 mm depth, on the south wall for the period from June/2009 to June/2010.

2.2. Assessment of the stone damage risk due to condensation

The damage risk to the stone by the action of condensation was assessed by two different methods: first, through condensation on the external stone surfaces; and second,

through condensation within the porous structure of the stones. The following sections present these two approaches.

2.2.1. Condensation on stone surface

Condensation is a physical process defined as when free water vapor, in humid air at constant barometric pressure, turns from a gaseous to a liquid state and finally accumulates on cold material surfaces. It is the main source of moisture at the surface and within stone building materials. Thus, in this study the risk of damage to the stone by the physical weathering process of condensation was observed. In this observation, two types of data were analyzed: air data (temperature and relative humidity) obtained from the local meteorological station, and stone data represented by stone surface temperature measured by the sensor.

The air data recorded during the short period, from April/2010 to August/2011, were used to calculate the dew point temperature. Dew point temperature is the temperature that promotes condensation at the given relative humidity. Condensation is assumed to occur when the stone surface temperature is colder than the calculated dew temperature.

The results of analysis showed that condensation events on stone surfaces, on both the north and south walls of the east tower, occur throughout the year with annual frequencies exceeding 29% and 33% for the north and south façade walls, respectively, Figure (II-24). They are more frequent in the months characterized by high humidity, i.e. September to February. The condensation frequencies for the south wall are slightly higher than those of the north walls. This can be attributed to the fact that stones in the south wall experience higher variations in daily surface temperature, thus enhancing the probability of the dew point temperature being greater than the stone surface temperature.

2.2.2. Condensation within the stone porous structure

The condensation within the porous structure of the stone was observed by analyzing two sets of data: the stone data (temperature and relative humidity) at different depths inside the stones, and the data from the mercury intrusion porosimetry test involving the pore size distribution of the stones.

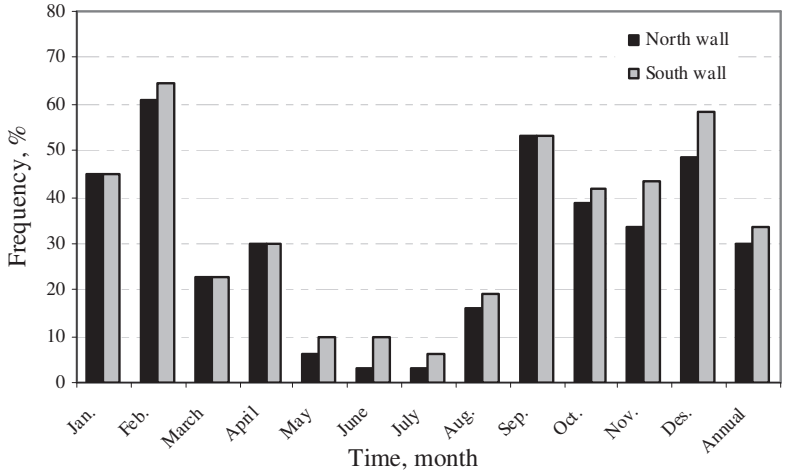

Fig. II-24. Frequency of condensation events on stone surfaces of the north and south walls.

The condensation within the stone pore space is assumed to occur when the relative humidity inside the pore exceeds the critical relative humidity, which is mainly controlled by the pore radius. The critical relative humidity can be calculated through Eq.17, (Camuffo, 1998):

$$RH_c = 100.e^{\frac{-2\sigma_w.V_m.}{r.R.T}} \qquad \text{Eq.17}$$

where:

σ_w: Surface tension of water in air-liquid interaction, 0.072 N/m

V_m: Molar volume of water, 18 cm^3/mol

R :Gas constant, 8.31 N.m/mol/K

T: Temperature of thermodynamic system in equilibrium, K

r: pore radius, μm

Table (II-9) lists the calculated values of the critical relative humidity for the different pore radius sizes. It is obvious that the lowest values of the critical relative humidity are associated to the smallest pores. This is due to the effect of the meniscus curvature of the pore water (Camuffo, 1998). The stone humidity measured at different depths inside the stones at different heights on both the north and the south wall was

analyzed and compared with the critical relative humidity. Then the annual frequencies of condensation events (i.e. values of stone humidity higher than the critical one) were determined by using percentile format. Table (II-9) presents examples of these annual frequencies of condensation events that occur at different depths inside the stone at the bottom level of the north wall, as a function of the pore radius. The term percentile can, statistically, be defined as the value of a variable (e.g. condensation events) below which a certain percentage of occurrences of observations are equal or smaller. For example, in the case of 15 mm depth inside the stone with pore radius of 0.01 μm, there are 81.4% of days per years with relative humidity less than or equal to 89.666%. Thus, the annual frequency of condensation events at this particular case is 18.6%, i.e. (100-81.4)%. The results show that the frequencies of condensation mainly depend on the depth inside the stone. The condensation occurrences always decreased with depth. There are no condensation events at 250 mm depth.

Table II-9. Annual frequencies of condensation events with values of RH_c as a function of pore radius at different depths inside the stone at the bottom part of the north wall.

Pore radius (μm)	RH_c (%)	Depth inside the stone			
		15 mm	30 mm	50 mm	250 mm
1	99.981	0.1	-	-	-
0.1	98.915	5.4	0.3	-	-
0.09	98.795	4.2	0.9	-	-
0.07	98.454	4.8	1.9	-	-
0.05	97.842	5.6	2.7	-	-
0.03	96.430	7.2	3.9	-	-
0.01	89.666	18.6	14.5	4.9	-
0.009	88.586	21.8	17.7	7.2	-
0.007	85.571	36.7	35.4	14.4	-
0.006	83.378	48.2	48.5	26.5	-
0.005	80.401	62.4	61.1	42.9	-

In order to assess the damage risk to the stone due to the occurrence of condensation within the porous structure of the stone, the results presented in Table (II-9) were correlated to the results obtained from the mercury intrusion porosimetry test both for tuffeau and Richemont stone, Figure (II-11, 12). The porosimetry analysis indicated that the Richemont

stone has a pore size distribution restricted to the range between 0.01 μm and 2 μm. In accordance with the smaller pores observed in Richemont stone, the higher annual frequencies of condensation events can reach up to 18.6% at 15 mm depth inside the stone at the bottom part of the north wall. Tuffeau is characterized by a wide range of pore networks, with pore radii ranging from 0.003 μm to 10 μm. Thus, the annual frequencies of condensation events at the smallest pore radius of 0.005 μm are always higher, by at least three times, compared with Richemont stone. Since the stone weathering processes (freezing action, salt weathering, biological colonization …) are strongly related to the presence of water within the stone, the risk of damage by the physical process of condensation is more significant for tuffeau than for Richemont stone.

2.3. Assessment of the stone damage risk due to freezing

When the stone contains a sufficient amount of water (due to condensation and/or rainfall) and undergoes variations in temperature around the freezing point, it may be subjected to damage by freezing. Freezing is one of the main factors that cause damage to stone in cold regions. As for condensation, the damage risk to the stone by the action of freezing was assessed using two different base methods: first, through freezing on the external stone surfaces; and second, through freezing within the porous structure of the stones.

2.3.1. Freezing on stone surface

The risk of damage to the stone surface by the physical weathering process of freezing was examined. In this examination, two data sets were analyzed: stone data involving the stone surface temperature measured by the sensor, and the meteorological data (air temperature, air relative humidity, and rainfall) obtained from the local weather station.

In order to estimate the frequencies of freezing events on the stone surface, the minimum stone temperature and the freezing point temperature were compared. Freezing is assumed to occur when the minimum stone temperature is below the freezing point temperature.

On the stone surface, the freezing point temperature is assumed to be 0.0°C, and the analysis of the minimum stone temperature for three years, from June/2009 to June/2012, indicated that the annual frequencies of freezing events were 9.7% and 10.5% for the south and north walls, respectively. However, the real damage to the stone surface by freezing requires the presence of water on these stone surfaces. Thus, it is necessary to establish a relation between the freezing events and the presence of water on the stone surface either by rainfall or by condensation. To this end, the rainy days and the days with condensation just before freezing events were identified by analyzing the meteorological data. Figure (II-25) presents the frequencies of freezing events for each month in the case of the north wall, with and without taking into account the presence of water on the stone surfaces. The results showed that the freezing events only occur during the period November-March and are more concentrated in December and January.

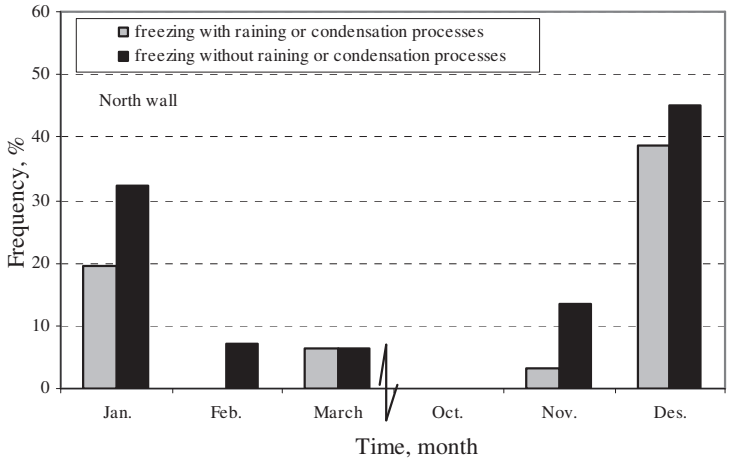

Fig. II-25. Frequency of freezing events with or without effects of rain and condensation processes.

A comparison between both types of analysis was made to assess the interest of taking into account the presence of water on the stone surface. The result indicates that considering the presence of water significantly reduces the calculated frequencies of freezing. Hence, the first analysis focuses on estimating the risk of damage due to freezing, while the frequencies of this weathering process are actually measured in the second analysis. However, to estimate the freezing damage risk within the stone, it is necessary not

only to verify the presence of water within the stone, but also to identify the amount of this water, i.e. the critical degree of saturation at which the damage to the stone starts when freezing. This issue will be further discussed in Section 2.4: *Freezing action and the critical degree of saturation.*

2.3.2. Freezing within the stone porous structure

The frequencies of freezing events within the porous structure of the stone over the period of 3 years were estimated by analyzing two data sets: the stone temperature, measured by the sensor, at different depths inside the stone and at different heights on both the north and south walls, and the data from the mercury intrusion porosimetry test involving the pore size distribution.

The freezing events within the stone pore space are assumed to occur when the minimum stone temperature inside the pore drops below the freezing point temperature inside the pore. The freezing point temperature inside the pore depends on the radius of the pore. This is due to the effect of the meniscus curvature of the pore water that leads to lowering the freezing point temperature for smaller pores (Camuffo 1998). The freezing point temperature can be calculated using Eq.18:

$$T_{FP} = -273\frac{2\sigma_{sl}}{r.P_s.L_f} \qquad \text{Eq.18}$$

where:

σ_{sl}: Surface tension at solid-liquid interface, 32.110^{-3} N/m

p_s: Ice density, 0.917 g/cm^3

L_f: Latent heat fusion, 333.55 N.m/g

Table (II-10) presents the calculated values of the freezing point temperature for different pore radius sizes. It can be clearly seen that the freezing point temperature drops for the pores with smaller radii. The damage risk to the stone due to freezing action was

estimated by analyzing the minimum stone temperature, and the annual frequencies of freezing events inside the stones were determined by using the same percentile format used in the analysis of the annual frequency of condensation events (section 2.2.2.). Table (II-10) lists examples of these annual frequencies of freezing events, as a function of the pore radius, occurring at different depths inside the stone at the bottom level of the north wall.

From the results of the mercury porosimetry test for the two limestones, tuffeau and Richemont, in combination with the results presented in Table (II-10), it is evident that the two limestones can be considered as exposed to similar magnitudes of freezing events. The freezing events are slightly higher at 15 and 30 mm compared to 50 mm depths, and negligible or nil at 250 mm.

Table II-10. Annual frequencies of freezing events with values of T_{FP} as a function of pore radius at different depths inside the stone at the bottom part of the north wall.

Pore radius (μm)	T_{FP} (ºC)	Depth inside the stone			
		15 mm	30 mm	50 mm	250 mm
1	-0.03	5.8	5.7	3.8	0.2
0.1	-0.29	5.2	5.1	3.5	0.1
0.09	-0.32	5.1	5.1	3.5	0.1
0.07	-0.41	4.9	5.0	3.3	0.1
0.05	-0.58	4.8	4.7	3.1	0.1
0.03	-0.97	3.9	3.7	2.8	-
0.01	-2.90	1.9	1.8	1.2	-
0.009	-3.22	1.7	1.7	1.1	-
0.007	-4.14	1.3	1.2	0.8	-
0.006	-4.83	1.0	1.0	0.4	-
0.005	-5.80	0.7	0.6	0.2	-

2.4. Freezing action and the critical degree of saturation

As discussed in (section 2.3.1), the damage by freezing on the stone surfaces requires the presence of water on these surfaces. Likewise, the presence of a sufficient amount of water within the porous structure of the stone is necessary to promote damage by freezing. On this point, determining the freezing damage risk within the stone still requires identifying the amount of water in the stone which could induce damage when freezing. To achieve this goal, a series of laboratory tests were carried out on the two limestones, tuffeau and Richemont stone. These tests aimed to investigate the petrophysical and mechanical properties of the two stones both for fresh and aged samples after having been subjected to freeze-thaw tests of up to 50 cycles with eight different degrees of water saturation. In the following, a brief discussion of the performance of the freezing test is given and the main results obtained are presented.

2.4.1. Freezing-thawing test

The cylindrical samples (Ø 40 × 40 mm) of tuffeau and Richemont stone were prepared with eight different degrees of saturation: 20, 40, 70, 80, 85, 90, 95 and 100%, and subjected to different cycles: 2, 4, 10, 16, 20, 30 and 50 freezing-thawing test cycles by following the procedure given in ASTM (D5312-04). A Vötsch-VT 4011 climate chamber was used for the freezing-thawing tests. All the stone samples were frozen to -18°C and kept there for 12 h. This was followed by a thawing phase with a temperature of 32°C for another 12 h. The change in chamber temperature from/to the freezing-thawing conditions took place within a few minutes and thus one freezing-thawing cycle lasted 24 h. Figure (II-26) shows the scheme for the freezing-thawing test and the general setting of the stone during the test.

The total porosity and the mechanical properties (indirect tensile strength and ultrasonic pulse velocity) for the fresh samples and the aged samples with freezing-thawing test were determined and compared in an attempt to identify the critical degree of saturation responsible for damaging the stones by freezing.

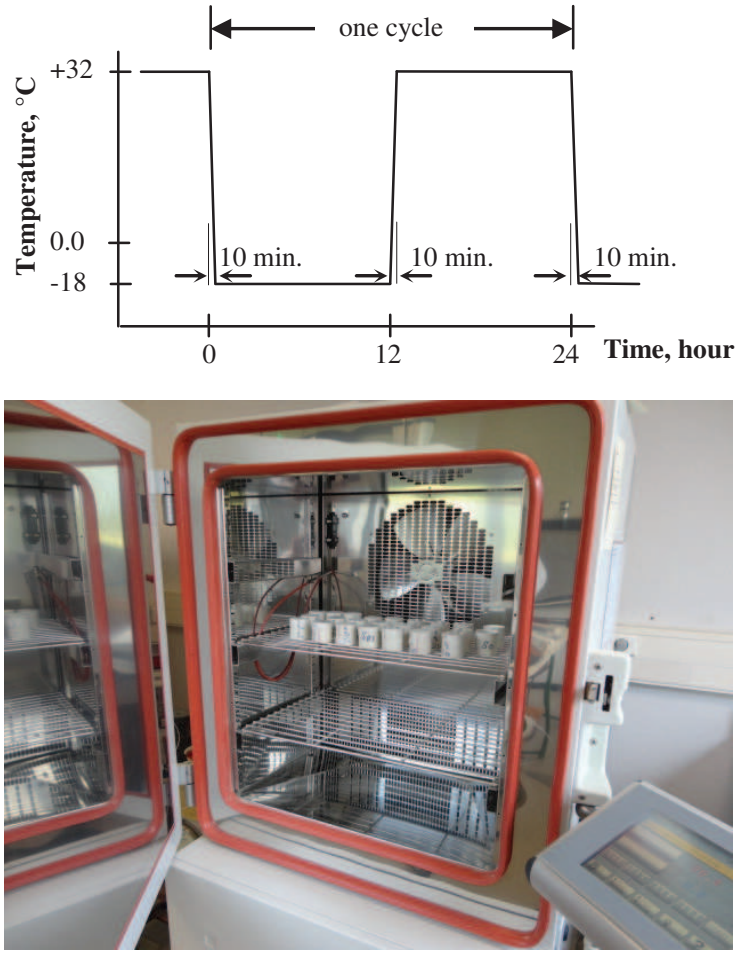

Fig. II-26. Schematic for one freezing-thawing cycle (*top*), general setting of the tested samples inside the freezing chamber (*bottom*).

2.4.2. Identification of the critical degree of saturation

The results of the total porosity of the aged samples were normalized to their initial total porosity values of the same samples but in fresh state. Then the normalized values were related to the initial degree of water saturation of the stone samples as shown in Figure (II-27). The results indicate that the normalized porosity values differ for the samples prepared with low water saturation and the ones with high water saturation. Considerable changes in the normalized values were found for the samples with a water saturation higher than 85%.

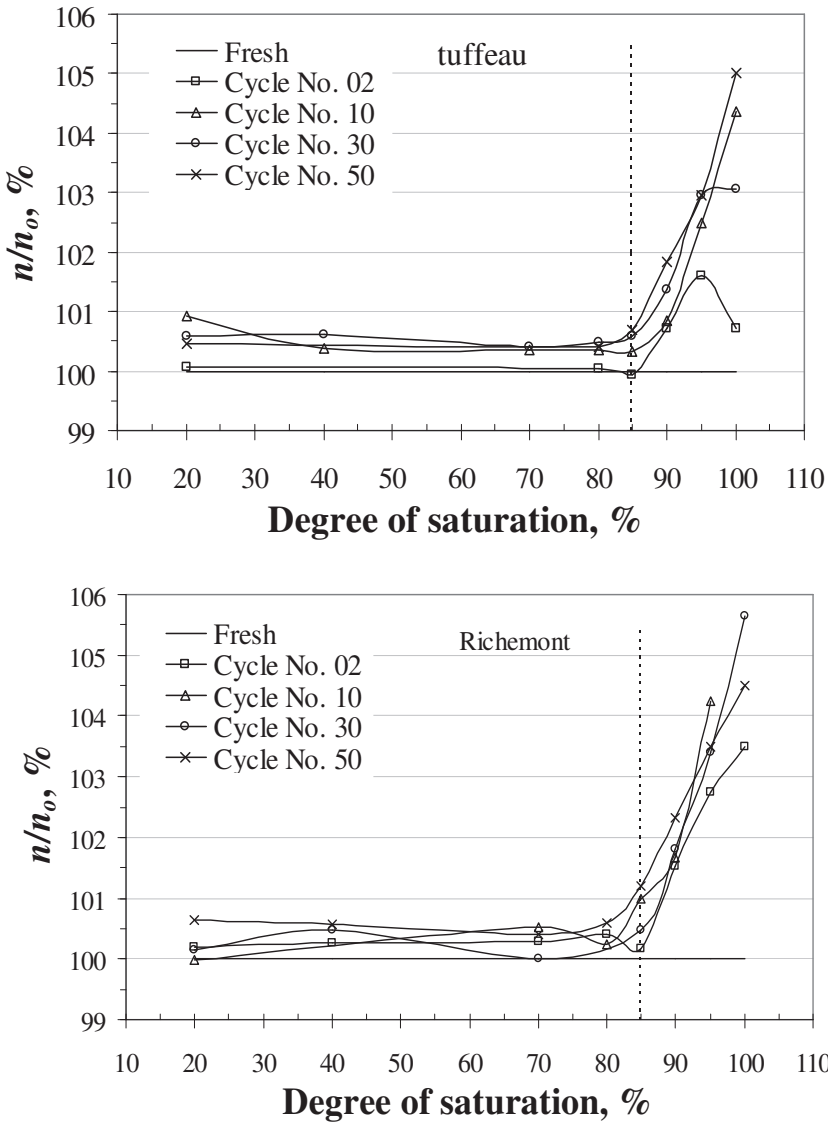

Fig. II-27. Normalized total porosity after freeze-thaw test of tuffeau and Richemont stone.

Figure (II-28) presents the values of the ultrasonic pulse velocity of the fresh samples and the aged ones with different cycles of the freezing-thawing test. The stone samples with an initial degree of water saturation below 85% show minor and almost negligible changes in the ultrasonic pulse velocity values. In contrast, significant decreases in these velocity values were obtained for the other samples with a higher initial degree of water saturation. These findings were the same for both tuffeau and Richemont stone samples.

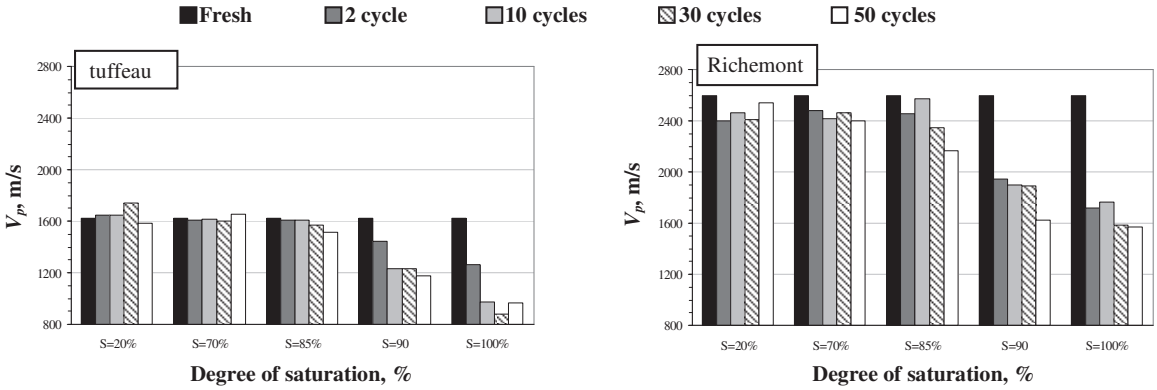

Fig. II-28. Ultrasonic pulse velocity for fresh and aged samples at different degrees of saturation, tuffeau and Richemont stone.

The values of the indirect tensile strength both of the fresh samples and of the samples prepared at different degrees of water saturation and subjected to different numbers of freezing-thawing cycles are presented in Figure (II-29). The results indicate that the tensile strength of both fresh samples and samples subjected to freezing-thawing is higher when the samples have a low water saturation, while samples with a high water saturation level that are subjected to freezing-thawing have a lower tensile strength. The best fits for the two groups of the low and the high tensile strength values are shown by the red and blue dotted lines, respectively. It is obvious that the slopes of these dotted lines differ. The blue ones, which represent the more weathered samples, have a steeper slope. The nick-point between the two slopes is located at about 85% of water saturation.

In conclusion, by comparing the results of the physical and mechanical properties for the fresh and the aged samples, presented above, it is can be observed that there appears to be a threshold degree of water saturation at which the stone samples start to deteriorate when subjected to freeze-thaw cycles, and show a sudden decrease both in the pulse velocities and the tensile strength and an increase in the total porosity with respect to fresh samples. This level of saturation, at which major changes took place, is called a critical degree of saturation, and was found to be around 85% for both tuffeau and Richemont stone.

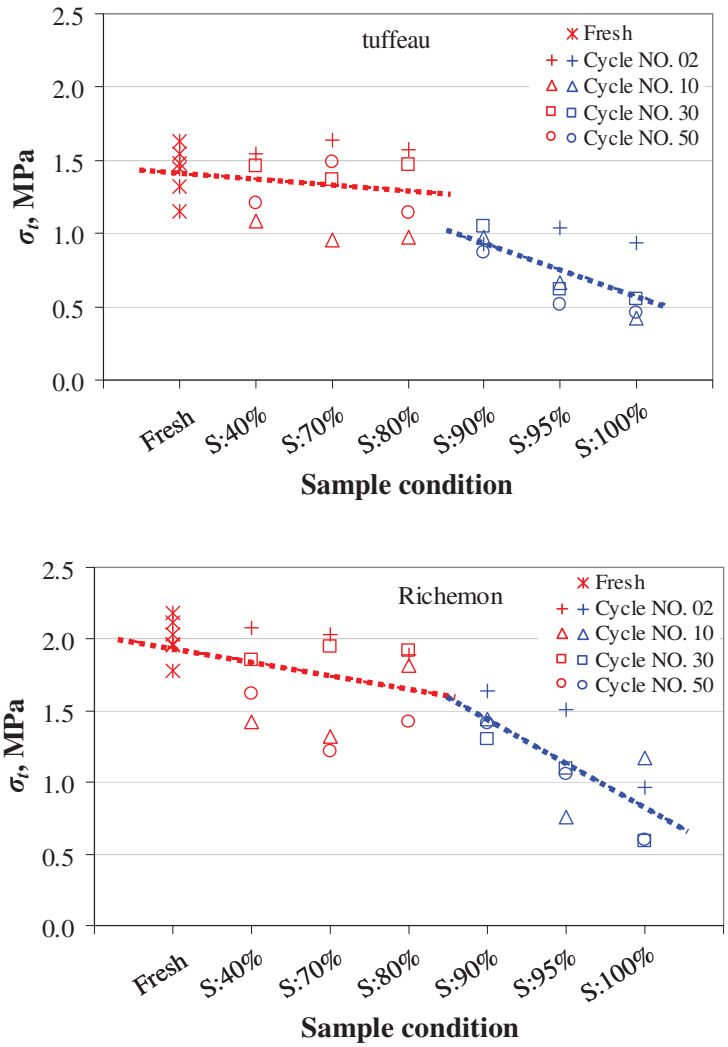

Fig. II-29. Indirect tensile strength for fresh and aged samples of tuffeau and Richemont stone.

2.4.3. Degree of saturation: an intrinsic stone property

A total of 50 freezing-thawing cycles were performed and samples were continuously monitored. The obtained data set, Figures (II-27, 28 and 29), provided evidence that an increase in the number of freeze-thaw cycles had no effect on the minimum degree of saturation at which frost damage occurred, i.e., the number of freeze-thaw cycles had a fairly limited effect on the fatigue of the stone. In other words, the critical degree of saturation can be defined as an intrinsic property of the stone. In fact, this

intrinsic stone property can be linked to the measurements both of the stone data and of the weather data that were used to define the frequencies of condensation and rainfall events during the freezing period, and finally to identify the warning level of moisture that damages the stone of the castle of Chambord when freezing.

2.5. Assessment of the stone damage risk due to thermal & hygrothermal stresses

When the stone building materials are located in an area that experiences daily variations in the climatic conditions, they will suffer daily variations in their temperature and moisture content. In some cases, these variations are sufficiently high to damage the stone by generating both thermal and/or hygrothermal stresses within the stones. The damage risk to tuffeau and Richemont stone, due to thermal and hygrothermal stresses, was assessed and is presented in the following sections.

2.5.1. Thermal stress

According to the theory of elasticity, daily variations in the stone surface temperature create a restrained thermal dilation (i.e. thermal stress). The thermal stress generated can be calculated through Eq.19, (Bonazza et al., 2009b; Ponziani et al., 2012; Al-Omari et al., 2014a):

$$\sigma_T = \frac{E.\alpha.\Delta T}{1-\upsilon} \qquad \text{Eq.19}$$

where:

σ_T: Maximum thermal stress, MPa

E: Young's modulus, MPa

α: Thermal expansion coefficient, K^{-1}

ΔT: Daily variation in stone surface temperature, K

υ: Poisson's ratio, %

It should be mentioned that the daily variation in stone surface temperature can be obtained from the previous stone data measurements using the digital thermal-humidity sensors. Therefore, calculating the thermal stress generated within the stones of the castle of Chambord requires defining the three parameters (α, E and υ) of the stones. The following paragraphs deal with the determination of these three parameters.

2.5.1.1. Linear thermal expansion coefficient

The linear thermal expansion coefficient (LTEC) represents the change in length of the material per degree of temperature change. The increasing recognition of the potential magnitudes of thermal movements and stresses induced within the structure of stone that is exposed to daily variations in ambient temperature, suggest the need for a realistic determination of this coefficient rather than an assumed value for use in further calculations.

The determination of the LTECs in laboratory experiments consists in measuring the dilation of a stone due to the increase in the exposed temperature. To this end, three cylindrical samples (Ø 40 mm × 80 mm) of tuffeau and three samples of Richemont stone were dried for 24 h at 105ºC till they reached a constant weight. Then the samples were cooled to room temperature. During cooling, the change in their height was measured using a digital dial gauge with 0.001 mm accuracy. The LTEC was calculated as the ratio between the change in length of the samples ΔL and the original sample length L multiplied by the temperature interval ΔT in Kelvin, Eq.20:

$$LTEC = \frac{\Delta L}{L.\Delta T} \qquad \text{Eq.20}$$

The results of tests showed that tuffeau had an average LTEC of $(8.41\pm0.12)10^{-6}$ K^{-1}, and Richemont stone of $(5.84\pm0.04)10^{-6}$ K^{-1}.

2.5.1.2. Elastic properties

Two elastic properties, elastic modulus and Poisson's ratio, were determined both for tuffeau and Richemont stone. These properties were measured for cylindrical samples (Ø 40 mm × 80 mm) in dry condition (oven at 105ºC for 24 h). The measurements of the elastic properties consist of compressing the cylindrical samples using a special cell which works with a hydraulic pressure system. The applied pressure, in the elastic range, was controlled by the hydraulic pressure controller unit with a precision of 0.001 MPa. During loading, the measurements of stone strain were made by using the strain gauge. A 5mm-long triaxial foil strain gauge, type KFG-5-120-D17 manufactured by KYOWA Measuring Instruments, Japan, was glued onto a smooth surface at the middle height of the sample. The wires of the strain gauge were connected to the National Instruments device (model NI9219-4Ch 24-Bit Universal Analog Input 60 VDC) via the 'data receiver box'. Data were recorded by the National Instruments software. The principle of the experimental layout is presented in Figure (II-30).

From the test, the resulting stress-strain relationships were used to calculate both the elastic modulus and Poisson's ratio of the stone samples. Three measurements were carried out on three samples for each stone, tuffeau and Richemont. The lowest dry elastic modulus values were measured for tuffeau samples with an average value of 3482±20 MPa. Richemont stone had higher dry elastic modulus values than tuffeau, and the average value of 14962±233 MPa was obtained. The average values of the dry Poisson's ratio were 0.204±0.005 for tuffeau and 0.231±0.004 for Richemont stone.

2.5.1.3. Calculation of thermal stress

Through the analysis of the stone surface temperature, measured for the period of three years by using digital thermal–humidity sensors installed on the north and south walls of the east tower in the castle of Chambord, and in combination with the stone thermo-mechanical properties, the values of the thermal stresses generated both in tuffeau and Richemont stone were calculated. As for condensation, the annual percentile values of the calculated thermal stresses were determined.

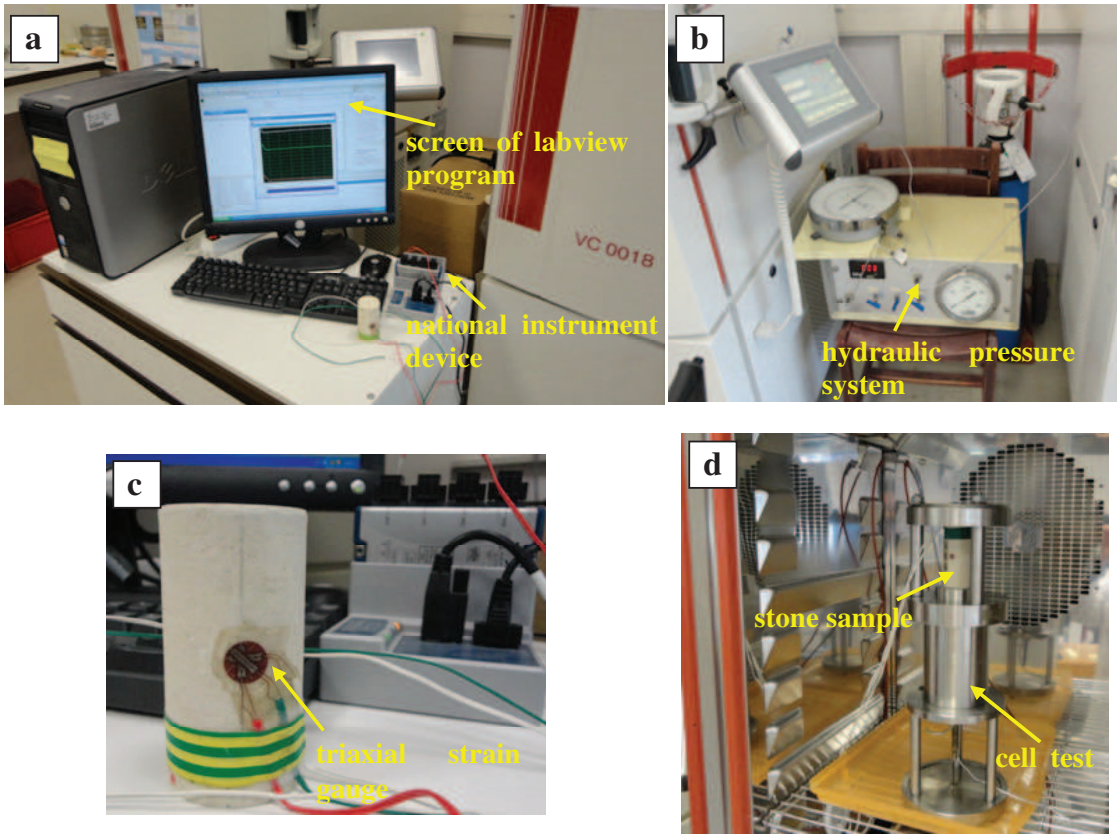

Fig. II-30. Photo showing the layout of the experimental set-up with the tools used: (a) data logger; (b) hydraulic pressure system; (c) strain gauge on the stone sample; (d) setting of the cell inside the climate chamber.

Table II-11. Annual percentile values of thermal stress calculated for tuffeau and Richemont stone located on the south wall of the east tower.

Percentile (%)	Thermal stress (MPa)	
	Tuffeau	Richemont
0	0.04	0.12
1	0.07	0.20
5	0.11	0.35
25	0.26	0.80
50	0.42	1.29
75	0.58	1.80
95	0.78	2.39
99	0.86	2.64
100	0.91	2.79

Table (II-11) presents the main annual percentile values of the calculated thermal stresses generated in tuffeau and Richemont stone located on the south wall. It is clearly shown that all the calculated values of thermal stress for Richemont stone are three times higher than those calculated for tuffeau. This behavior can be attributed to the different values of the thermo-mechanical properties (Young's modulus, Poisson's ratio and the thermal expansion coefficient) of the two stones.

2.5.1.4. Assessment of the stone damage risk due to thermal stress

The risk of damage to the stone due to thermal stress was assessed by comparing the calculated thermal stress with the stone maximum sustainable load. The stone shows damage when the generated thermal stress exceeds the maximum sustainable load of a stone (Bonazza et al., 2009b; Ponziani et al., 2012; Al-Omari et al., 2014a). The stone maximum sustainable load was obtained by dividing the unconfined compressive strength of a stone by the safety factor of three. According to the unconfined compressive strength of the two stones, the maximum sustainable loads are 3.89 MPa and 6.47 MPa for tuffeau and Richemont stone, respectively. Returning to Table (II-11), the maximum values of thermal stresses were found never to exceed the maximum sustainable loads either for tuffeau or Richemont stone. Thus, the risk of damage by thermal stress is probably negligible both for tuffeau and Richemont stone located on the castle of Chambord.

2.5.2. Hygrothermal stress

The description of the two stones indicates that tuffeau, with low mechanical and high water transfer properties, is more sensitive to humidity (i.e. its mechanical properties are strongly dependent on water content). Hygrothermal data are available for tuffeau as they have been measured on the surface and at different depths of the stones of the "Tower of Chaudron". Thus, the risk of damage by hygrothermal stress was investigated only for tuffeau and not for Richemont stone.

The hygrothermal stresses ($\sigma_{T\text{-}H}$) generated inside the tuffeau stone due to the variation in temperature and humidity were calculated by modifying Eq.19 to take the form below:

$$\sigma_{T-H} = \frac{E_{T-H} \cdot \varepsilon_{T-H}}{1 - \upsilon_{T-H}} \qquad \text{Eq.21}$$

Where the three elastic parameters: elastic modulus ($E_{T\text{-}H}$), Poisson's ratio ($\upsilon_{T\text{-}H}$) and strain ($\varepsilon_{T\text{-}H}$), are functions of stone temperature and stone saturation.

In fact, the determination of these hygrothermal elastic properties consists of two stages: firstly, identifying, experimentally, the elastic properties in different conditions of temperature and water saturation. Secondly, modeling these identified hygrothermal elastic properties using the suitable tool available in the literature. These two stages are presented below.

2.5.2.1. Elastic properties at different conditions of water saturation and temperature

Great attention was paid to experimentally examine the effect of the variations in both temperature and water saturation on the elastic properties and strain of a soft tuffeau limestone. To achieve this goal, laboratory tests were carried out on cylindrical samples (Ø 40 mm × 80 mm) prepared with different conditions so as to cover wide ranges both of water saturation (between 0% and 100%) and of temperature (between -8°C and 40°C). These ranges were selected in an attempt to represent the extreme, but realistic, range of stone data conditions measured *in situ*, see Table (II-8).

The experimental work consisted in measuring the elastic modulus and Poisson's ratio of the tuffeau samples prepared at five different water saturations (0, 7, 23, 80 and 100%) and exposed to four temperature levels (40, 20, 2 and -8 °C). These measurements were achieved by adopting the same procedure followed to measure the elastic properties for the samples in dry state, discussed above in section (2.6.1.), with the exception that the cell used to apply the load was placed inside the climatic chamber during the test.

In the beginning, the sample was put inside the temperature-controlled chamber at 20 ºC and the strains of the sample were recorded every 10 seconds. Then the temperature was increased to 40 ºC. Once the sample had reached equilibrium at the new temperature (i.e. stabilization of the recorded strain data), the strain variation of the sample was calculated as the difference between the strain data recorded at 20 ºC and at 40 ºC. The

sample at 40 ºC was loaded in the elastic range, and the resulting stress-strain curve was used to measure the elastic modulus and Poisson's ratio of the tested sample. The same protocol was followed to measure the strain, elastic modulus, and Poisson's ratio of the sample when the temperature changed from 20ºC to 2ºC and from 20ºC to -8ºC. Figure (II-31) presents the experimental plan followed during the test. The following section gives a brief discussion of the results obtained.

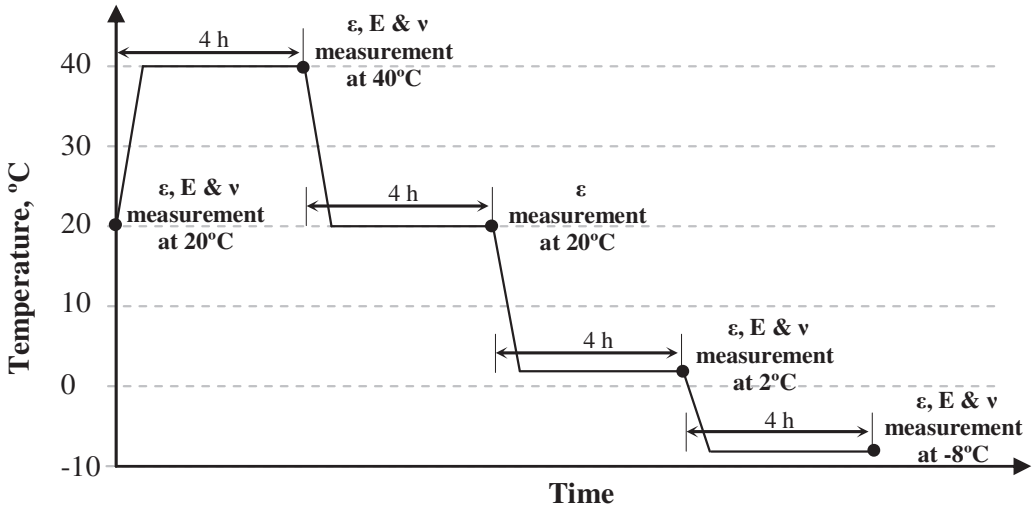

Fig.II-31. Outline showing the stages followed for the elastic properties measurements for the samples with different temperature conditions.

2.5.2.1.a. Strain of sample

The stone strain data measurements are presented in Figure (II-32). Each value is the average of the axial, lateral and diagonal strain measurements. Zero strain, i.e. the stone sample in dry state at room temperature, was selected as the reference state. It is obvious that the rise in temperature from 20 °C to 40 °C results in increasing the strain. The opposite is the case when the temperature falls from 20 ºC to 2 ºC. This occurs as a result of the well-known and expected thermal dilation of the mineral components of the sample. Similarly, increasing the water saturation of the sample from 0 to 100%, or at any intermediate step, results in increasing the strain. This is due to hygric dilation.

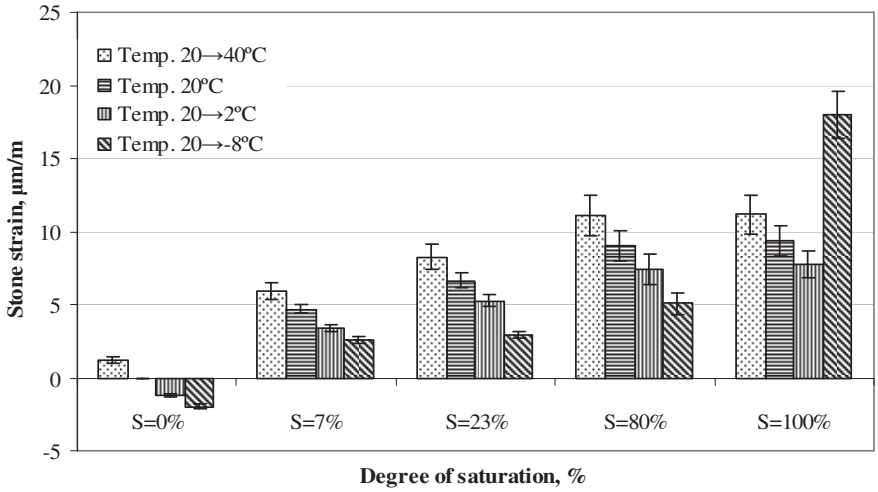

Fig. II-32. Effect of water saturation and temperature on stone strain values.

Concerning the case when the temperature was reduced from 20ºC to -8ºC, three observations can be drawn:

- The fully saturated sample showed significant increases in strain. This behavior relates to the increases in volume of the sample resulting from ice growth.

- For the dry sample there was no frozen water. Thus, a decrease in the sample strain was observed due to shrinkage of the minerals at -8 ºC.

- The partially saturated sample prepared with water saturation of 7%, 23% and 80%, showed contraction when exposed to sub-zero temperatures, although the sample contained water. Here, the ice crystallization pressure caused by ice growth was probably dissipated in the air-filled pores. Indeed, the three partially saturated tests did not result in cracking the sample after freezing, even at 80% of water saturation. This indicates that these levels of water saturation were below the critical one at which the sample starts to degrade during freezing (Chen et al., 2004; Al-Omari et al., 2013b). Added to the thermal dilation effect, the observed contraction can be attributed to the effect of the migration of unfrozen pore water from the smallest pores toward the larger ones during freezing (Prick, 1995).

2.5.2.1.b. Elastic modulus

The average value of three measurements of the elastic modulus is shown in Figure (II-33). The samples containing 80% and 100% of water saturation showed decreases in their elastic modulus when the temperature increased from 20 ºC to 40 ºC, while noticeable increases were found when the temperature decreased from 20 ºC to -8 ºC. This can be attributed to the growth of ice within the stone pore space that strengthens the sample. Again, in the dry sample or samples with a low level of water saturation, i.e. degree of saturation of 7% or 23%, the elastic modulus was weakly affected by the changes in temperature. This behavior is attributed to the small amount of water in the pores.

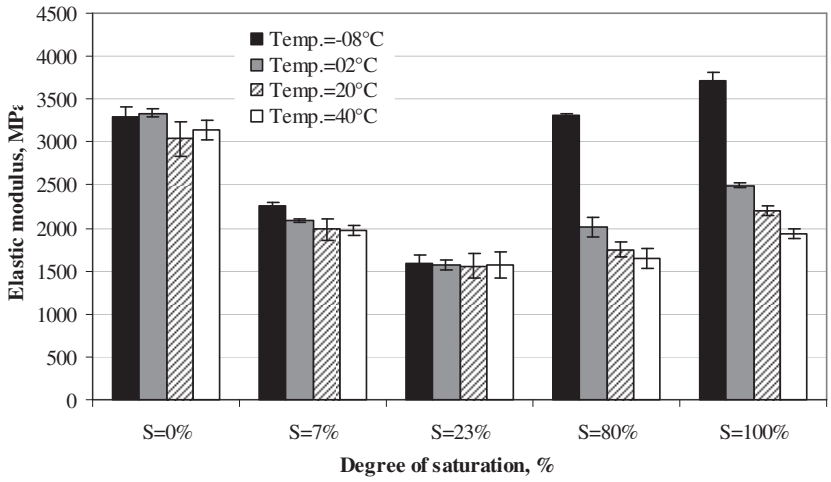

Fig. II-33. Effect of water saturation and temperature on values of elastic modulus.

2.5.2.1.c. Poisson's ratio.

The measurements of Poisson's ratio were carried out three times for each test condition. The average of the three measurements is presented in Figure (II-34). All the measurements but one were in the range 0.201–0.334. There is an unexpected measurement for the particular condition relative to full saturation and -8 °C with a value over 0.5. This may be attributed to the damage of the stone resulting from freezing prior to loading. In this case, a significant amount of unfrozen water may migrate to the cracks during loading, generating an anisotropic expansion and thus an artifact measurement of Poisson's ratio.

However, the results in Figure (II-34) show negligible effects of temperature on the Poisson's ratio measured. Again, Poisson's ratio seemed to increase slightly when increasing the water saturation.

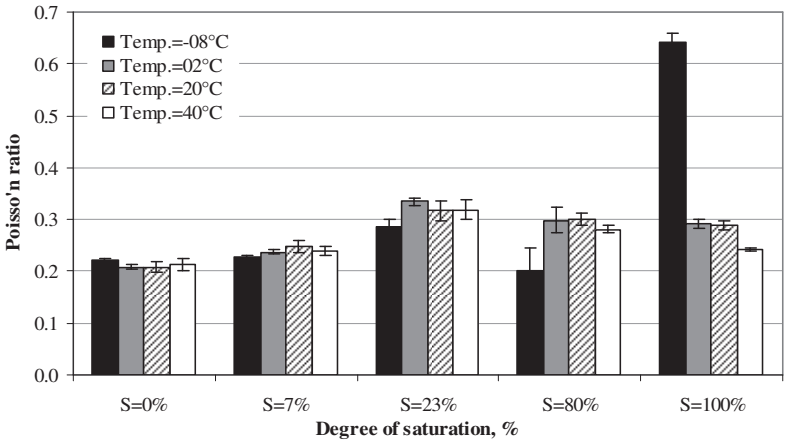

Fig. II-34. Effect of water saturation and temperature on the values of Poisson's ratio.

2.5.2.2. Modeling the elastic properties as a function of water saturation and temperature

The main objective for the determination of the elastic and strain properties of tuffeau stone, at different temperatures and degrees of water saturation, is to develop a mathematical relationship that correlates the elastic properties of the stone with both the water saturation and temperature of the stone. The models developed can be used to estimate the elastic modulus, Poisson's ratio and strain of the stone in a wide range of temperature (-8 ºC to 40 ºC) and water saturation (0% to 100%) in order to simulate the extreme, but realistic, range of stone temperature and humidities measured in the field.

The design of experiment (DOE) methodology was used to process the experimental results of the elastic and strain properties, obtained at different parameter levels of temperature and of water saturation, and finally to generate the proposed models. The DOE is a tool that ensures the quantification of interactions between parameters (here: temperature and water saturation) and allows statistical analysis of the relevance of the resulting model. The DOE consists of five consecutive stages to determine the final form of

the required models (for more details see appendix 2: paper No.2). Equations 22, 23 and 24 represent the final forms of the models used, respectively, for estimating the strain, elastic modulus and Poisson's ratio of the stone.

$$\text{Strain}_{(t,s)} = [\,61.898 + 5.202t + 18.854s - 4.09t^2 + 1.519s^2 - 0.489ts - 3.944t^2s + 1.584ts^2 + 8.16t^3 + 0.565s^3 + 4.54t^3s + 0.965ts^3 + 5.53t^2s^2 - 2.36s^4 - 4.08t^3s^2 + 3.26t^2s^3 - 2.7t^3s^3\,] \cdot (10)^{-5} \quad \text{Eq.22}$$

$$\text{Elastic modulus}_{(t,s)} = 1570.775 + 17.303t + 19.098s + 6.02t^2 + 248.808s^2 - 94.496st + 11.67t^3 + 61.634st^2 - 92.936s^2t - 100.175s^3 - 19.486st^3 + 58.033s^3t + 191.29s^2t^2 - 127.7s^2t^3 + 80.14s^3t^2 + 21.89s^4t - 75.66s^3t^3 \quad \text{Eq.23}$$

$$\text{Poisson's ratio}_{(t,s)} = 0.325 - 0.021t + 0.033s - 0.011st - 0.53s^2 + 0.021s^2t - 0.017st^2 + 0.016t^3 - 0.003s^3 + 0.012st^3 - 0.009s^2t^2 + 0.003s^3t + 0.008s^4 - 0.008s^2t^3 + 0.005s^3t^2 - 0.004s^4t - 0.005s^3t^3 + 0.004s^4t^2 \quad \text{Eq.24}$$

The symbols *s* and *t* represent the coded values used in the design of experiment which are related to the temperature and water saturation of the stone. These three mathematical models can be displayed as a surface plot. Figure (II-35) shows the three surface plots of the stone's property / temperature-water saturation relationship as presented in Eqs.22, 23 and 24, respectively.

It is clear that all the curves of the mathematical models show coupling effects between the estimated stone property (strain, elastic modulus or Poisson's ratio) and both the two studied parameters (temperature and water saturation). For more details on the description of these surface plots, see appendix 2. The models developed are able to estimate, precisely, the strain and elastic properties of the stone due to the variations both in temperature and water saturation. This means that the proposed models represent an essential contribution to the determination of the hygrothermal stresses generated within the stone due to the variation in the temperature and water saturation of the stone.

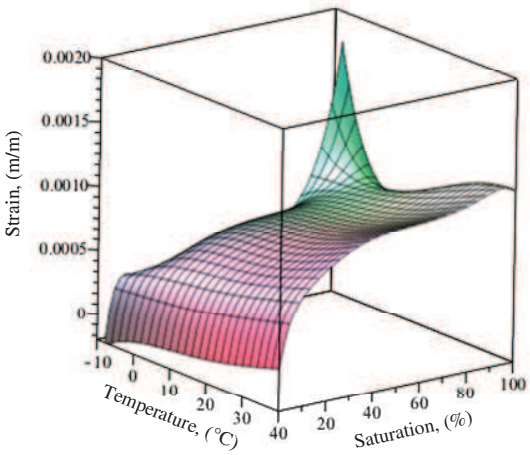

a) Strain

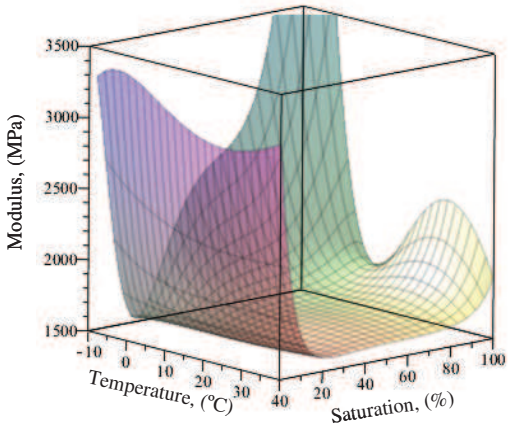

b) Elastic modulus

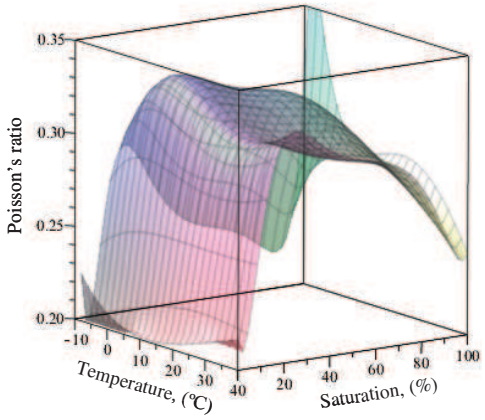

c) Poisson's ratio

Fig. II-35. 3-D Graphical representations of the models of (a) strain; (b) elastic modulus; (c) Poisson's ratio as a function of water saturation and temperature.

2.5.2.3. Assessment of the stone damage risk due to hygrothermal stress

The hygrothermal stresses were calculated using Eq.21. These stresses were calculated 48 times per day for each value of temperature and humidity collected (i.e. every 30 min) during three years at different depths inside the stone both on the north and south wall of the east tower in the castle of Chambord.

The stone damage risk was assessed through analyzing the calculated hygrothermal stresses with two methods: *daily variation in hygrothermal stresses*, and *maximum and minimum differential hygrothermal stresses*. In the following, a description of these methods is given

2.5.2.3.a. Daily variation in hygrothermal stresses

For each day, the maximum and minimum values of the calculated hygrothermal stresses were identified, and then the daily variations in the hygrothermal stresses were determined as the difference between the maximum and minimum hygrothermal stresses. Figure (II-36) shows an example of the daily variation in the hygrothermal stresses at different depths inside the stone on the south wall, over a one-year period (from June/2009 to June/2010).

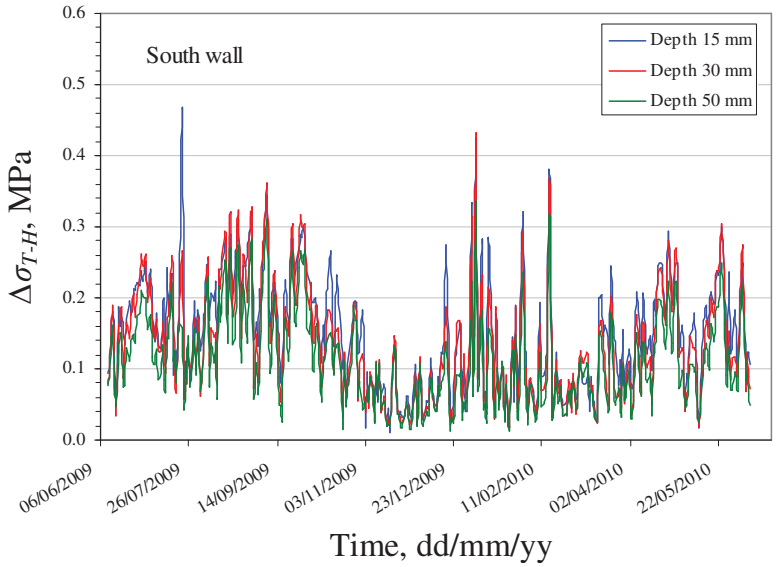

Fig. II-36. Daily variations in hygrothermal stresses at different depths inside the stone on the south wall for the period from June 2009 to June 2010.

In order to assess the risk of damage to the stones located on the castle of Chambord, the daily variations in the hygrothermal stresses were compared with the daily stone sustainable load. Damage to the stone is assumed to occur when the daily variation in the hygrothermal stress exceeds the stone sustainable load. The daily stone sustainable loads were obtained by dividing the daily unconfined compressive strength by a safety factor. As for condensation, the percentile format was use in the analysis. Table (II-12) lists the annual percentages of days with a daily variation of hygrothermal stresses exceeding the stone sustainable loads at different safety factors, over the period of three years for the stones located on the south wall of the east tower in the castle of Chambord. The results show that hygrothermal stresses exceed the stone sustainable load during a non-significant percentage of days, even at high values of the safety factor. It is concluded that the stone damage risk due to daily variations in the hygrothermal stresses is negligible.

Table II-12. Annual percentage of days with daily variation in hygrothermal stresses exceeding the stone sustainable load over the 3-year period (June 2009 to June/2012) for south walls, at different safety factor.

Safety factor	South		
	15 mm	30 mm	50 mm
1	--	--	--
2	--	--	--
4	--	--	--
8	--	--	--
12	0.1	--	0.1
16	0.3	0.1	0.2
20	0.7	0.6	0.5

2.5.2.3.b. Maximum and minimum differential hygrothermal stresses

This method attempted to determine both the compression and tension stresses which could be generated inside the stone due to variations in the temperature and water saturation of the stone. This method required comparing the extreme values of the calculated daily hygrothermal stresses generated in the stone close to the stone surface (i.e. 15, 30 and 50 mm) with the reference stone stress at 250 mm depth inside the stone. In this method, the hypothesis is based on the fact that hygrothermal stresses vary significantly near the stone surface compared with the stable level of hygrothermal stress.

The maximum and minimum differential hygrothermal stresses were calculated as the difference between the daily maximum and minimum hygrothermal stresses at depths near the stone surface and the reference hygrothermal stresses at 250 mm depth inside the stone. When this differential stress was positive, it was compression, and tension when negative. Figure (II-37) shows an example of the calculated maximum and minimum differential stresses at different depths inside the stone located on the south wall of the east tower in the castle of Chambord, over a one-year period (from June/2009 to June/2010).

The stone damage risks due to the maximum and minimum differential hygrothermal stresses were assessed by comparing the calculated hygrothermal stress in compression and in tension with the compressive and tensile sustainable load. Again, damage to the stone is assumed to occur when the calculated compression and tension stresses exceed the compressive and tensile sustainable load, respectively. The compressive and tensile sustainable load can be determined by dividing the compressive and tensile stone strength by a suitable safety factor. Table (II-13) lists the annual percentages of days with damage risk to the stone when compression and tension hygrothermal stresses exceed the sustainable loads both in compression and in tension conditions at different safety factors over the period of three years for the stones located on the south wall of the east tower in the castle of Chambord.

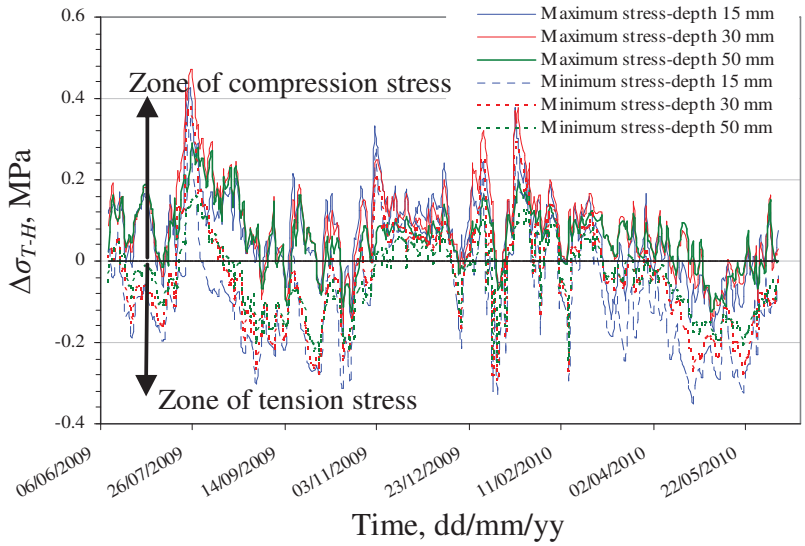

Fig. II-37. Maximum and minimum differential hygrothermal stresses at different depths inside the stone on the south wall for the period from June 2009 to June 2010.

The data in Table (II-13) clearly show that the damage to the stone is more significant in the case of tension stress than in compression stress. It is well known that the tensile strength of a stone is much lower than its compressive strength. Thus, the calculation of the tension stress may be more critical.

It is evident that, in the case of the compression stress, the risk of damage from differential hygrothermal stresses is more effective than the risk of damage from the daily variation in the hygrothermal stress, see Tables (II-12 and 13). The data showed that in case of the hygrothermal tension stresses, the safety factor is 2, while as for hygrothermal compression stresses, the safety factor is 12. Thus, the calculation of the differential hygrothermal stresses seems to be more important, since they give the stone damage risk not only in the case of compression stresses but also in the case of tension stresses.

Table II-13. Annual percentage of the damage risk when the compression, tension hygrothermal stresses exceed the stone compressive, tensile strength over the 3-year period for south walls.

Safety factor	Case of tension stress			Case of compression stress		
	15 mm	30 mm	50 mm	15 mm	30 mm	50 mm
1	--	--	--	--	--	--
2	--	0.1	0.2	--	--	--
4	16.8	8.5	2.2	--	--	--
8	54.6	43.0	30.9	--	--	--
12	68.4	60.2	46.9	0.4	--	--
16	76.3	69.9	58.9	0.8	1.0	--
20	82.1	75.8	66.2	1.7	3.1	--

3. Conclusion

Different complementary techniques were used to characterize the petrographic properties at microscopic level of the two limestones: tuffeau and Richemont stone. Tuffeau is a soft porous stone composed of different mineral phases: calcite, silica, clay mineral and mica. The silica minerals were observed in two forms: well-crystallized (quartz) and more or less amorphous (opal cristobalite/trydimite). It is characterized by very high total porosity (≈46%), giving the stone a low apparent density of 1.40 g/cm^3 and a skeletal density of 2.56 g/cm^3. Tuffeau has a wide range of pore size distribution (pore diameter from 0.006-20 μm). Richemont stone is a fine-grained limestone mainly composed of calcite (95%) with a low proportion of quartz and clay minerals. It is characterized by high total porosity (≈29%). Its skeletal density is quite equivalent to the density of calcite (2.71 g/cm^3) because the stone is mainly composed of calcite. The pore size distribution of Richemont stone is more restricted than that of tuffeau, ranging from 0.02 to 4 μm. It seems that there is a significant difference in the morphology properties of the two stones. This is mainly due to the difference in the mineralogical composition of the two stones. The morphology of the stones can help us to find explanations for the differences in the other stone properties investigated such as water transfer properties, thermal and mechanical properties.

Water transfer property measurements (capillary absorption, free water absorption and permeability) for the two stones show that the values of the measured property are higher for tuffeau than for Richemont stone. This is due to the differences in the features of the pore space system between the two stones. Also, the values of the measured mechanical properties (unconfined compressive and tensile strength and ultrasonic pulse velocity) are consistent with the measurements of the physical properties, in terms of density and porosity. The higher mechanical properties belong to the highly dense and less porous stone, i.e. Richemont stone.

The description of the two stones indicates that tuffeau, with low mechanical and high water transfer properties, is more sensitive to weathering processes than Richemont stone. This prompted further study that focused on investigating the elastic properties

(stone dilation, elastic modulus and Poisson's ratio) of tuffeau in relation to the variation in temperature and water saturation. This study highlights the following points:

- The variations both in the water saturation and in the temperature are accompanied with significant changes in the elastic properties of tuffeau.
- The design of experiment methodology is a good tool that was successfully applied to obtain mathematical relationships between the elastic properties of tuffeau stone and the two parameters of temperature and water saturation.
- The proposed mathematical relationships give an accurate estimation of the elastic properties of tuffeau stone in a wide range of environmental conditions (outdoor state of buildings).

The daily variations in the climatic conditions have a significant influence on the performance and, of course, the degradation of historic stones. In relation to the two stones used in the castle of Chambord and through the analyses of three sets of data, weather data (rainfall and temperature and relative humidity of air), stone data (temperature and humidity of stone), and intrinsic stone properties (pore size distribution and hygrothermal elastic properties), it was possible to assess the damage risk to the stone with respect to three weathering processes: condensation, freezing action and thermal and hygrothermal stresses.

The castle of Chambord is located in an area that experiences a highly to moderately humid climate, thus the role of the weathering process of condensation in the degradation of the stone is vital and can be considered to be the major damaging process. The analysis of meteorological data shows that the freezing events could be encountered on the castle of Chambord. However, the damage to the stone by freezing action requires the presence of a sufficient amount of water within the pore space of the stone. The results of the experimental tests indicate that damage to the stone by freezing is restricted to the stones that have a water saturation higher than the threshold water saturation, or so-called critical degree of saturation. This level of saturation was found to be 85% and identical both for tuffeau and Richemont stone. Different values of the critical degree of saturation were found for other stones (Chen et al., 2004; Prick, 1997). The same critical degree of saturation for the two stones is attributed to the presence of the same proportion of pores in

the range of 1-10 μm in both stones. However, the critical degree of saturation is not affected by the number of freezing-thawing cycles, suggesting that this critical degree of saturation is an intrinsic stone property.

The third weathering process analyzed in this work is thermal and hygrothermal stresses within the stone due to daily variations in the climatic conditions. Mathematical equations, available in the literature (Eq.19) or newly developed (Eq.21) based on the restrained dilation, were used to calculate these stresses. However, in all previous studies (Bonazza et al., 2009b; Ponziani et al., 2012; Al-Omari et al., 2014a) the calculation of this stress was only related to the elastic properties of the stone in dry state. In the new calculation of hygrothermal stress presented here, the actual state of the stone is considered. These hygrothermal stresses were calculated for tuffeau only because this stone is assumed to be more sensitive to the change in water saturation. In fact the analysis of hygrothermal stresses could be done for any porous material (i.e. here also for Richemont stone). However, the hygrothermal characterization of elastic properties of the related stone has to be performed because the hygrothermal characterization of tuffeau cannot be extended to any other stones. The results of analysis showed a significant daily variation in the calculated hygrothermal stresses for the stone near the surface. Taking into account the steady state of the stresses deep inside the stone, the calculated hygrothermal stresses at the surface can be in tension or in compression. Results highlighted the significant role of hygrothermal stresses in inducing damage to the stone through the development of joint cracks in the case of tension stress or surface buckling in the case of compression stress.

Chapter 3

The ancient Iraqi monuments in Al-Nimrud city

Chapter three

The ancient Iraqi monuments in Al-Nimrud city

This study was carried out on monuments in Al-Nimrud, an ancient Iraqi city (the second millennium BCE) located in the north of Iraq. The present chapter comprises three main sections:

1. Presentation of Al-Nimrud city.

This section presents Al-Nimrud city from a variety of perspectives: a brief history and the geological setting of the city, listing the main ruins discovered; the building materials used in the construction of the monuments and the main forms of the degradation observed on these building materials.

2. Stone damage risk assessments due to natural environmental conditions.

This section examines the response of limestone in Al-Nimrud city in relation to its damage, and to variations in the local climatic conditions. The estimation of stone damage is analyzed through the effect of thermal stress, condensation and freezing-thawing action.

3. Health record of Al-Ziggurat monument in Al-Nimrud city.

This section attempts to establish the health record of Al-Ziggurat monument through two starting points: firstly, characterization of the weathered limestone and of a fresh quarried stone to be used in future restoration work, by different complementary techniques at the macroscopic level; secondly, creating a 3D model of Al-Ziggurat wall that can be used in the digital health record of this monument.

1. Presentation of Al-Nimrud city

Al-Nimrud is the modern name of the ancient Assyrian city, Kalhu. This city is located in the northern part of Iraq, on the eastern bank of the River Tigris, about 30 km southeast of Mosul, Figure (III-1). The city was built during the Middle Assyrian Empire by the Assyrian King Shalmaneser I (1280-1260 BCE), but did not flourish only in the era of King Ashurnasirpal II (884-859 BCE) and of his son Shalmaneser III (859-824 BCE) since it became the capital of the Assyrian Empire.

The ruins of Al-Nimrud are in the form of a large asymmetrical rectangle, Figure (III-1). The city covers an area of about 4 km^2. Three-quarters of the area is a flat plain, but its south-west part rises vertically from the surrounding plain: the citadel mound.

Austin Henry Layard was the first archaeologist to undertake exploration work at Al-Nimrud city, on behalf of the British government, during the mid-nineteenth century (Layard, 1849). These explorations were followed in 1949 by the British Archaeological Institute mission headed by Max Mallowan (Mallowan, 1966). After these explorations, many of the precious antiques, decorative ivories, slabs of carved stone and the winged bulls were transferred to the British Museum.

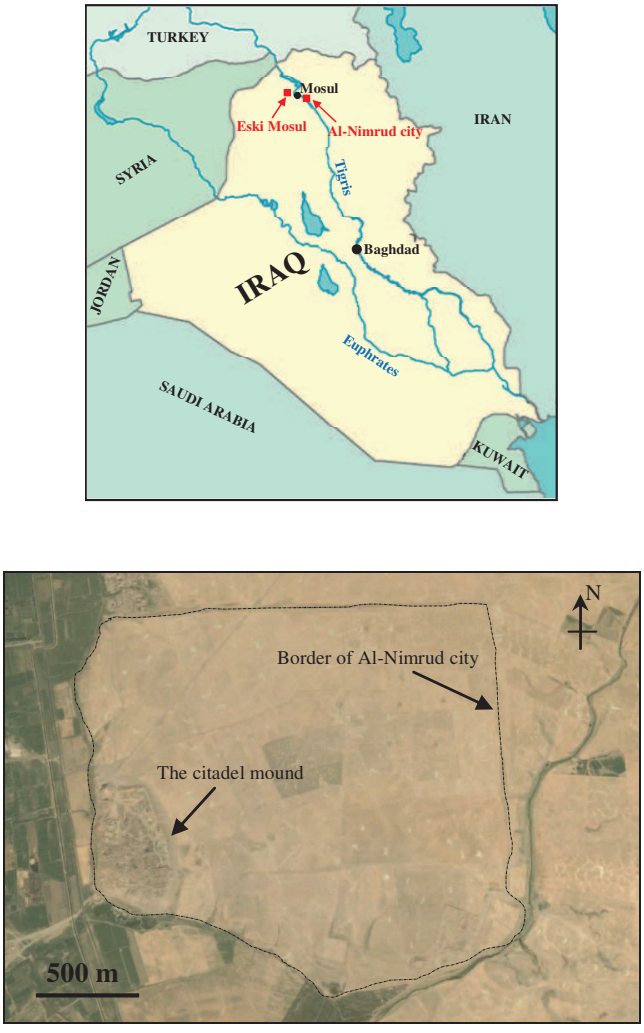

Fig. III-1. Map of Iraq showing the general setting of Al-Nimrud city (*top*); Google satellite image of Al-Nimrud city (*bottom*).

1.1. Geology and climate of Al-Nimrud city

The studied site is located in the foothill tectonic zone which forms part of the unstable-folded zone of the overall structural framework of Iraq (Jassim and Goff, 2006). The extensive geological study conducted by Al-Juboury and McCann in 2005 identified the lithology of the Hamam Al-Alil area, about 25 km south-east of Al-Nimrud. The authors showed that the studied area is an early Miocene evaporite formation (Fatha), with various lithofacies and lithotypes: sandstone, gypsum layer, marl, dolomitic limestone, and mudstone.

The site of Al-Nimrud has an average elevation of 205 m above sea level; GPS coordinates are 36°05′57″ N, 43°19′39″ E. This area experiences a continental-subtropical climate: summer is very hot and dry, while winter is cold with occasional snow falls. The meteorological records of Mosul station, the nearest station to Al-Nimrud, for the period from 1953 to 1962 were obtained from the National Oceanographic Data Center: Iraq climatological data, http://docs.lib.noaa.gov/rescue/data_rescue_iraq.html. These records revealed that the studied area is subjected to low rainfall with a mean annual rainfall of 370 mm. In summer, the maximum mean daily temperature exceeds 45°C, while in winter, the minimum mean daily temperature falls below 0°C. The mean annual relative humidity is 57% and sun exposure is high, with over 3192 hours per year, equivalent to 266 days per year. Preliminary analysis of the recorded meteorological data showed that the city of Al-Nimrud is subjected to a high atmospheric temperature range with daily variation often in excess of 20 °C. Exposure to such a harsh climate for a period of over three thousand years has enhanced the weathering processes of Al-Nimrud monuments (Al-Omari et al., 2012), especially in the absence of appropriate conservation and preservation measures.

1.2. The building materials in Al-Nimrud city

Most of the monuments in Al-Nimrud city were constructed with three main building materials: clay brick elements, green gypsum stone and white limestone, Figure (III-2). Most of the walls of Al-Nimrud monuments were constructed of clay brick elements about 0.8-1.0 m in width. Large plates 15-20 cm thick of green gypsum were used to cover most of the walls of the monuments. Square plates measuring

50×50×5 cm were used to cover large parts of the ground and the stairs of the tombs. In addition, large blocks (100×60×50 cm^3) of limestone were used in the construction of the wall of Al-Ziggurat. According to archival documents, both the green gypsum and the white limestone were quarried from Eski Mosul (about 60 NW from Al-Nimrud), which is the area on the right bank of the Tigris, Figure (III-1). The river was used to facilitate the transportation of the quarried stones to Al-Nimrud (Oates and Oates, 2001).

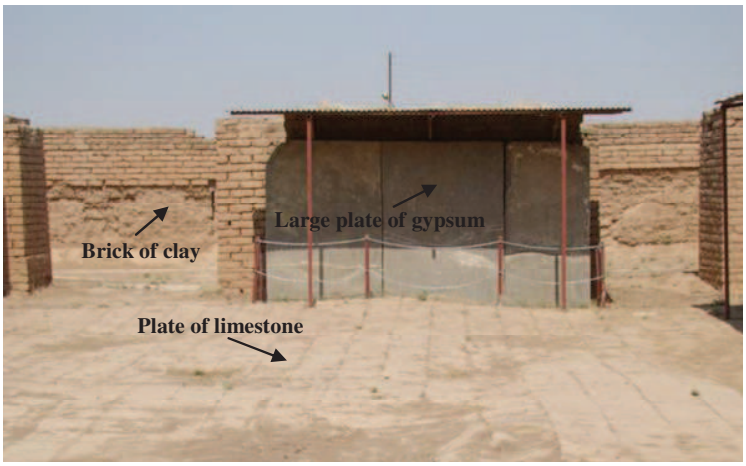

Fig. III-2. Setting of the building materials used in Al-Nimrud monuments.

1.3. The main ruins of Al-Nimrud city

Most of the ruins of Al-Nimrud are located in the citadel mound in the south-west part of the city. The most important monuments discovered in this mound are, respectively, from north to south and from west to east, Figure (III-3): Al-Ziggurat, Ninurta Temple, Ishtar Temple, north-west Palace (Ashurnasirpal II Palace), Adad-Nirari Palace, Central Palace (Shalmaneser III), Governor Palace, south-west Palace, Burnt Palace (Sergon II) and Nabu Temple, (Mallowan, 1966). This study focuses on Al-Ziggurat, the most famous monument in Al-Nimrud city. More information about Al-Ziggurat, including localization, dates of interest, and degradations, is available in section 3.2 dedicated to data for the creation of the health record.

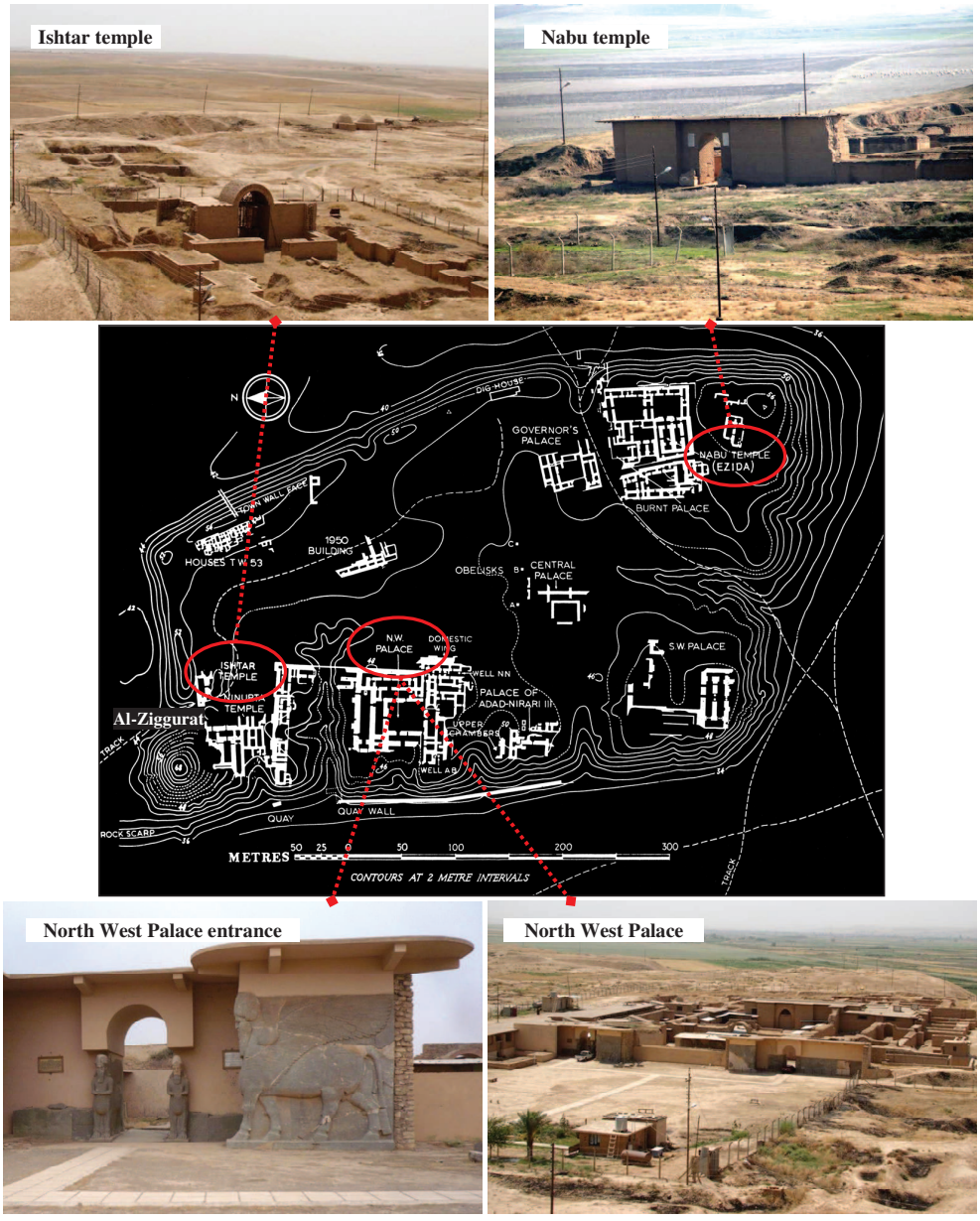

Fig. III-3. Map of the citadel mound in the center, (Mallowan, 1966) and the general view of the main ruins in Al-Nimrud city.

1.4. Degradation of limestone in Al-Nimrud city

Reade (2002) mentioned that Al-Nimrud was buried underground before the first excavation work carried out in the mid-nineteenth century, Figure (III-4). In fact, there is no evidence that confirms for how long the city was buried underground; burial may

have lasted several hundreds of years. The building materials of Al-Nimrud monuments were exposed to weathering mechanisms even if they were buried (Kaplan et al., 2013). In this case, the weathering of the buried monuments is controlled by the organic materials and the soluble salt contained in the soil; fluctuations in the water table can also play an important role in this weathering. Since their excavation, Al-Nimrud monuments have been exposed to the harsh elements of the surrounding climate: high daily variation in air temperature, intensive wind-blown sand and seasonal rains. Consequently, the post-excavated monuments are vulnerable to different forms of weathering processes.

Fig. III-4. Excavations in Al-Nimrud city in 1878 (Reade, 2002).

After the fall of the Assyrian Empire, the stones of Al-Nimrud monuments were subjected to two different conditions: buried for a long time and then exposed to the natural environment following the excavations. During this thesis, *in situ* observations carried out in 2012 revealed that the stones of Al-Nimrud monuments show different decay patterns. These decay patterns were defined according to the international glossary classification published by the International Council on Monuments and Sites - International Scientific Committee for stone, (ICOMOS-ISCS, 2008). The most common forms of stone decay were: stone detachment by granular disintegration in the form of powdering and sanding and by scaling in the form of spalling, formation of patina and discoloration, cracks, missing parts and differential erosion. Figure (III-5) shows the common decay patterns observed on the stones in Al-Nimrud monuments.

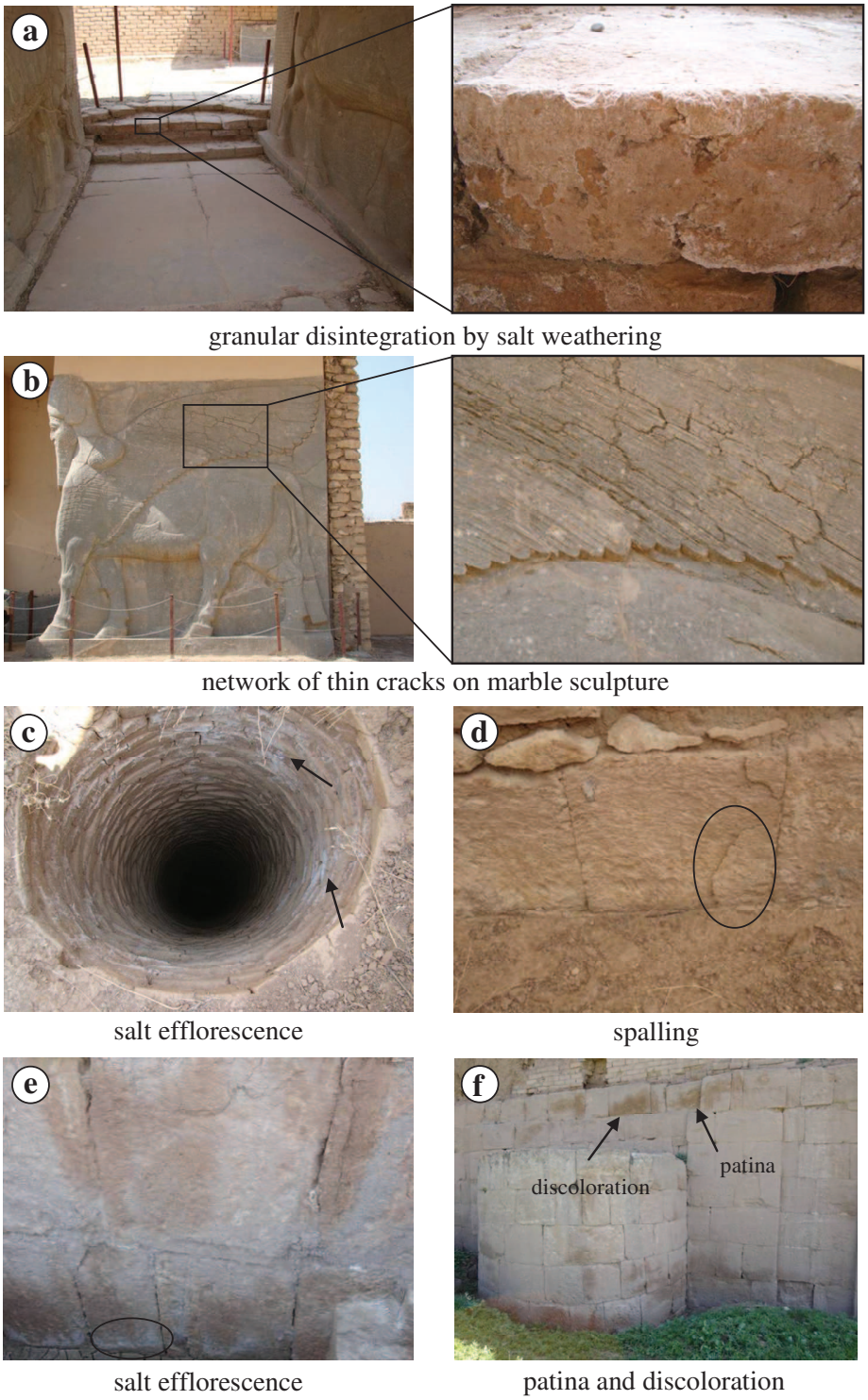

Fig. III-5. Patterns of stone decay in Al-Nimrud monuments: (a) limestone pavements at the NW Palace; (b) marble sculpture at the entrance of the NW Palace; (c) well made from brick at the NW Palace; (d) limestone block at Nabu temple; (e) and (f) limestone block on Al-Ziggurat wall.

2. Stone damage risk assessments due to natural environmental conditions

In this section the role of climatic conditions in the degradation of stone in Al-Nimrud monuments was investigated. It is assumed that the stone degradation is related to long-term cyclic environmental conditions. Hence, the damage risk to the stone was assessed through three weathering processes: thermal stress, condensation and freezing-thawing action. The methodology consisted in analyzing both the meteorological data and the stone data together with the stone properties, following the same procedure as that presented in chapter two for the risk assessment of tuffeau and Richemont stone.

The main climate elements considered in this study are: maximum, minimum and mean daily air temperature, mean daily relative humidity and minimum daily grass temperature (the minimum grass temperature is the grass temperature recorded in open air ground on short turf, using the thermometer just in contact with the tip of the grass blade, Crucifix (2009)). These climate elements were collected from the meteorological station near Al-Nimrud city. The minimum and the maximum daily air temperatures were analyzed in order to assess the effect of thermal stress, while the mean air temperature and mean relative humidity were used to estimate the action of condensation. Because of the lack of *in situ* direct measurements of stone data (temperature and relative humidity), the minimum grass temperature was assumed to be equivalent to the minimum stone temperature in order to predict freezing events (Al-Omari et al., 2012). The following section gives a brief presentation of the meteorological data used in the analyses.

2.1 Weather data

Ponziani et al. (2012) and Al-Omari et al. (2014a) indicated that a period of three continuous years is sufficient to measure the stone data used in the analysis of the risk assessment to stone through three weathering processes: thermal stress, condensation and freezing-thawing action. In this study the damage risk to the stone through these three weathering processes was assessed by analyzing the weather data recorded at Mosul station, the nearest station to Al-Nimrud city, for the three-year period 1963 to 1965. In fact, some of the data required in the analysis (such as minimum grass temperature) during these three years are missing, thus the analysis in this study was completed by analyzing the weather data for the period 1969-1970. These two sets of weather data were compared with the weather data from Mosul station for a long

period, 1953-1965, and are presented in Figures (III-6,7). The analyses show that the evolution of the monthly variations in mean maximum and mean minimum air temperature and in the mean air relative humidity for the two periods are quite similar. Therefore, the weather data for the short periods can be considered representative of the weather of the studied area.

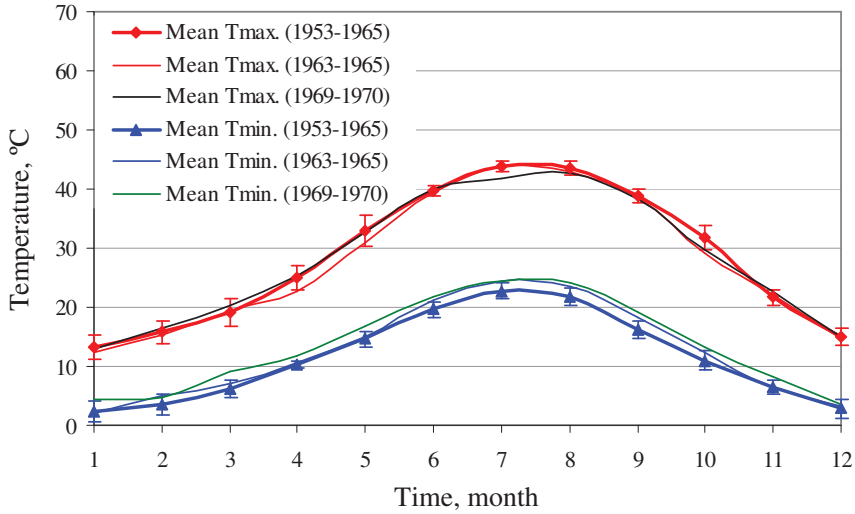

Fig. III-6. Monthly variations in the extreme values of mean air temperature for the periods 1953-1965, 1963-1965 and 1969-1970.

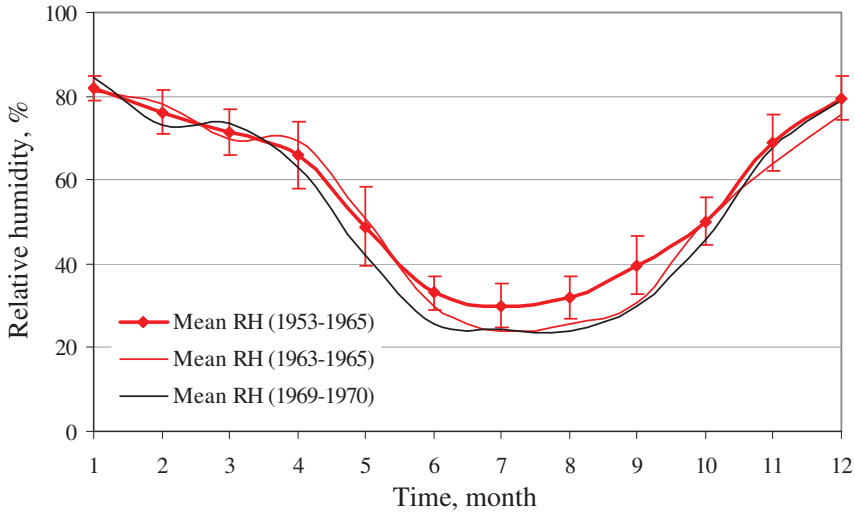

Fig. III-7. Monthly variations in the mean air humidity values for the periods 1953-1965, 1963-1965 and 1969-1970.

2.2. Damage risk to stone due to condensation

The damage risk to the historic stone in Al-Nimrud city by the action of condensation was assessed following the procedure described in (Ch 2: section 2.2.) through two types of measurements: condensation on the stone surface and condensation within the pore network of the stone structure.

2.2.1. Condensation on the stone surface

In this study the risk of damage to the stone by the physical weathering process of condensation was investigated through analyzing the air data (temperature and relative humidity) obtained from the local meteorological station at Mosul for the period 1969-1970, and the stone data (minimum stone surface temperature).

The site under study is located in a region characterized by a low humidity climate. The preliminary analysis of the relative humidity data collected from Mosul meteorological station in the period 1963-1965 is presented in Table (III-1). The results indicate that the mean air relative humidity reaches high limits, ranging between 91-97% in winter, while it falls to between 13% and 19% in summer. There are no days with a mean air relative humidity higher than 98%, while for about half of the year, the daily mean air relative humidity is less than 45%.

Table III-1. Absolute values of air relative humidity for the period 1963-1965, data from Mosul station.

Year	Three highest values of mean air RH, %	Three lowest values of mean air RH, %	No. of days with mean air RH > 98%	No. of days with mean air RH < 45%
1963	97 (04/01) 94 (11/04) 95 (12/02)	17 (19/07) 19 (30/07) 19 (20/08)	-- -- --	148
1964	91 (16/01) 94 (12/02) 91 (25/11)	18 (15/07) 16 (16/07) 13 (20/07)	-- -- --	174
1965	93 (08/01) 95 (29/12) 96 (30/12)	19 (25/07) 16 (22/08) 18 (23/08)	-- -- --	141

Table (III-2) lists the statistical analysis of the minimum grass temperature collected form Mosul station for the period 1969-1970. It shows that the mean values of the minimum grass temperature never fall below 0 ºC except in the cold winter months, November – February.

Table III-2. Statistical analysis of the minimum grass temperature value, data obtained from Mosul station for the period 1969-1970.

Month	Mean values of min. grass temp. ºC	Highest values of min. grass temp. ºC	Lowest values of min. grass temp. ºC	No. of days with min. grass temp. < 0 ºC
Jan.	1.9 ± 1.6	5.5 (03/01/1969)	-1.8 (13/01/1970)	4
Feb.	2.3 ± 2.0	8.4 (12/02/1970)	-1.2 (14/02/1969)	4
Mar.	5.9 ± 2.2	12.5 (30/03/1969)	1.5 (12/03/1969)	--
April	9.0 ± 3.3	19.6 (15/04/1970)	1.2 (03/04/1969)	--
May	13.3 ± 2.3	17.9 (14/05/1970)	9.2 (09/05/1969)	--
June	17.7 ± 1.8	23.2 (28/06/1970)	12.4 (01/06/1969)	--
July	20.1 ± 2.4	27.6 (09/07/1970)	13.2 (21/07/1969)	--
Aug.	20.7 ± 2.7	26.0 (12/08/1969)	16.3 (05/08/1969)	--
Sep.	13.1 ± 3.1	20.5 (29/09/1970)	5.8 (20/09/1970)	--
Oct.	8.2 ± 4.1	17.0 (05/10/1969)	0.5 (31/10/1970)	--
Nov.	4.6 ± 2.5	11.4 (14/11/1970)	-2.0 (19/11/1969)	2
Dec.	-0.1 ± 3.3	8.0 (06/12/1970)	-7.2 (22/12/1970)	13

In this study the minimum stone temperature is assumed to be equal to the minimum grass temperature (Al-Omari et al., 2012). This minimum stone temperature was compared with the dew temperature calculated from the air data obtained from Mosul station for the period 1969-1970. As mentioned in (Ch 2: section 2.2.1.), the condensation process occurs when the stone temperature is colder than the calculated dew temperature. As for the calculation of the annual frequency of condensation events presented in (Ch 2: section 2.2.2.), the percentile format was used in this analysis. Results presented in Figure (III-8) show that the high condensation events are associated to the winter months (January-April, November and December), and that the overall annual frequency of condensation events reaches up to 28%.

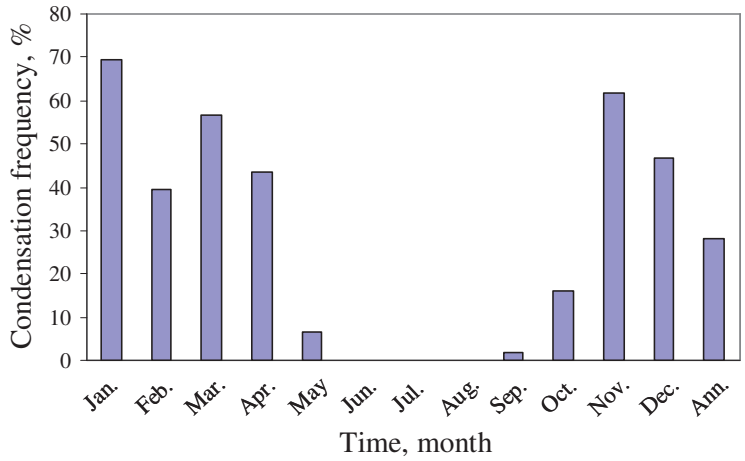

Fig. III-8. Frequency of condensation events on the stone surface.

2.2.2. Condensation within the stone porous structure

Condensation within the porous structure of the stone was observed by analyzing two data sets: the air relative humidity data from the Mosul meteorological station for the period 1963-1965, and the data from the mercury intrusion porosimetry test involving the pore size distribution.

The stone humidity values were assumed to be equal to the values of the air humidity recorded in the period 1963-1965, and were compared with the calculated critical relative humidity at different pore radii within the pore space of the stone. The critical relative humidity was calculated using Eq.17 presented in (Ch 2: section 2.2.2.).

Again, the percentile format was used to calculate the annual frequencies of condensation events as a function of the pore radius. Figure (III-9) shows that the annual frequencies of condensation events increased inside the pore spaces with a smaller radius. This is due to the meniscus curvature of pore water (Camuffo, 1998). Based on the pore size distribution of the fresh Al-Nimrud limestone (see section 3.3, Figure (III-24), and Table (III-9)), the results in Figure (III-9) indicate that when the pore radius exceeds 0.03 μm, condensation never occurs. It can also be clearly seen that the annual frequency of condensation events reaches only 3.5% for the limited proportion of pores in the range 0.01-1.0 μm. Thus, we can conclude that the risk of damage due to condensation is limited in Al-Nimrud monuments.

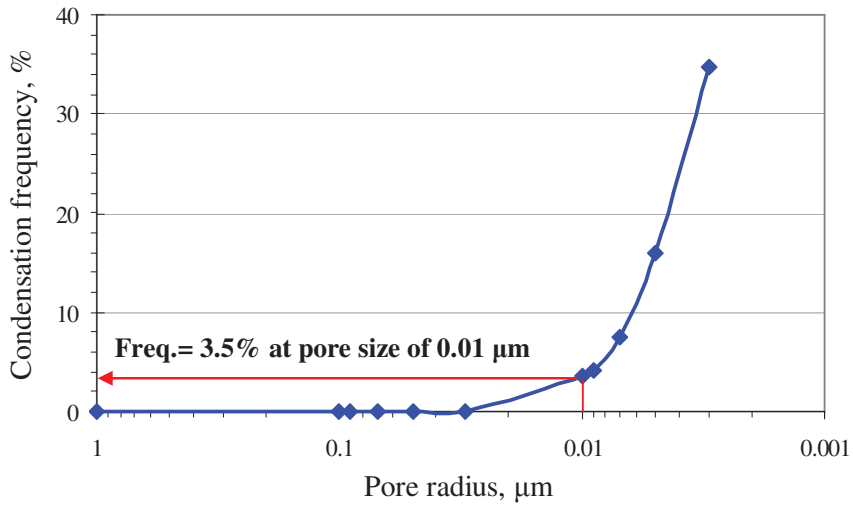

Fig. III-9. Annual frequencies of condensation events as a function of the pore radius.

2.3. Damage risk to stone due to freezing action

The frequencies of freezing events were estimated in order to assess the risk of damage to the stones in Al-Nimrud monuments. As for condensation, the damage to the stone by freezing was investigated through two sets of measurements: freezing on the stone surface and freezing within the pore network of the stone structure.

2.3.1. Freezing on the stone surface

The risk of damage to the stone by freezing was investigated by analyzing the minimum stone temperature which is assumed to be equivalent to the minimum grass temperature obtained from the local meteorological station in Mosul for the period 1969-1970.

Freezing of the stone surface is assumed to occur when the minimum stone temperature is lower than the freezing point temperature. The zero temperature was considered as the freezing point temperature on the stone surface. Figure (III-10) presents the results of the analysis. It is evident that freezing events on the stone surface are concentrated in the months November-February, with annual frequencies of about 6.12%. These annual frequencies of freezing events were calculated using the percentile format applied in the calculation of condensation frequency presented above.

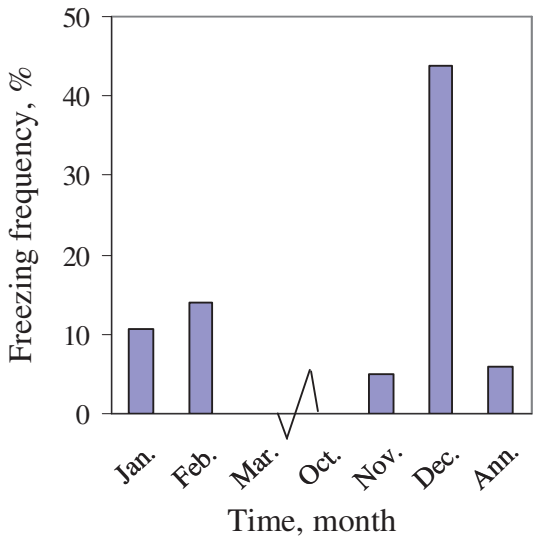

Fig. III-10. Frequency of freezing events on the stone surface.

2.3.2. Freezing within the stone porous structure

Freezing within the porous structure of the stone was examined by analyzing the minimum stone temperature and the pore size distribution of the stone. The freezing point temperature inside the pore space of the stone is controlled by the pore radius. The smaller the pores are, the lower the freezing point temperature is. This is due to the effect of the meniscus curvature of pore water (Camuffo, 1998). The freezing point temperature at different pore sizes can be calculated through Eq.18 presented in (Ch 2: section 2.3.2.).

As for freezing on the stone surface, the minimum stone temperature is assumed to be equal to the minimum grass temperature and the minimum stone temperature and the freezing point temperature at different pore sizes were compared in order to estimate the frequencies of freezing events. As for condensation, the percentile format was used in the analysis. Based on the pore size distribution the fresh Al-Nimrud limestone (Figure III-24), the results indicate that nearly all the pores in the stone are influenced by freezing. However, the annual frequencies of this action are rather low, reaching only 6.0% even for the larger pores, Figure (III-11).

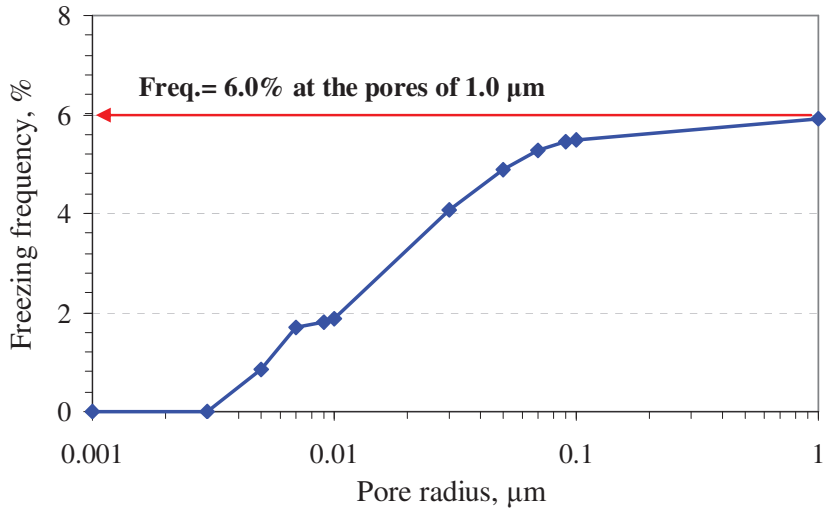

Fig. III-11. Annual frequencies of freezing events as a function of the pore radius.

2.4. Damage risk to stone due to thermal stress

In the calculation of the thermal stress, the daily variation in stone surface temperature was correlated to the daily variation in air temperature calculated from the meteorological data from Mosul station recorded for the three-year period 1963-1965. This correlation was made based on the field measurements, see section 2.4.1. these measurements include both the stone temperature and the air temperature that are measured for the period 2012-2013. The following section presents the details of these measurements.

2.4.1. Measurements of stone and air temperature

The extreme values of air temperature for Mosul city were measured using the commercial digital Thermo-Hygrometer type TFA Kat.Nr 30.5015 which is designed to measure the air temperature between -1 ºC to 70 ºC with an accuracy of ±1 ºC. These data were measured two days per week for the period from November/2012 to October/2013. Table (III-3) lists the statistical analysis of the measured air temperature.

Figure (III-12) shows the extreme and mean daily variation in the measured air temperature. There is a high daily variation in air temperature in excess of 25 ºC. This

high daily variation in air temperature induces high daily variations in the stone temperature, enhancing the stone damage by thermal stress.

Table III-3. Statistical analysis of air temperature measurements for the period from November 2012 to October 2013.

Year 2012-2013	T_{max} / ave. T_{max} (ºC)	T_{min} / ave. T_{min} (ºC)
Jan.	20.7 / 15.4	3.3 / 6.3
Feb.	26.4 / 23.6	7.8 / 10.1
Mar.	36.0 / 26.1	7.2 / 10.2
April	36.8 / 31.7	13.7 / 16.4
May	34.1 / 30.5	19.6 / 21.8
June	34.6 / 33.5	24.7 / 26.2
July	40.9 / 36.7	27.0 / 28.3
Aug.	40.7 / 39.5	26.8 / 28.9
Sep.	40.1 / 34.7	21.7 / 26.9
Oct.	28.4 / 28.4	17.9 / 18.9
Nov.	22.6 / 22.6	19.4 / 19.4
Dec.	26.6 / 19.0	5.8 / 9.3

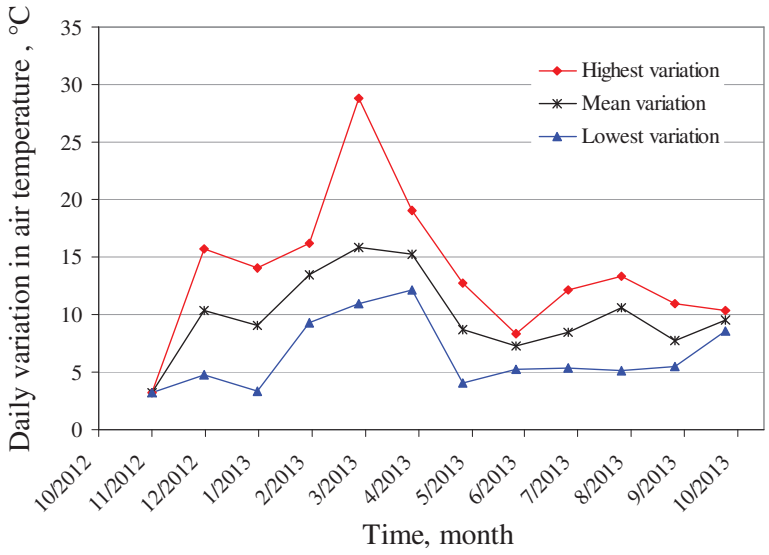

Fig. III-12. Highest, mean and lowest daily variations in air temperature for the period 2012-2013.

The stone temperature data were measured on a large block of historic limestone (80×50×30 cm^3) taken from Al-Nimrud city. This block was placed on the roof in contact with the environmental conditions of Mosul city, Figure (III-13). These data were measured along with the air temperature for the period from November/2012 to

October/2013. The stone temperatures of both the south and the north orientation of the block of limestone were measured, using the digital Thermometer probe type VOLTCRAFT DET1R. The thermometer operating conditions are: -10 to 200 ºC temperature range, 5% accuracy and 0.1 ºC resolution.

Fig. III-13. General setting showing the measurements of temperature for the large block of historic limestone for the period November/2012 - October/2013.

Table (III-4) lists the statistical analysis for the measured values of stone temperature. It can be clearly seen that the stone temperature can reach high values, up to 56 ºC in summer and down to about 3ºC in winter.

Figure (III-14) presents the preliminary analysis of the daily variations in stone temperature. The analysis indicates that the daily variation of the south-facing stone is greater than that of the north-facing stone. This is due to the direct effect of insolation on the south-facing stone. There is a wide range in these daily variations, up to 23ºC and 27ºC and down to 0.8ºC and 0.7ºC over the year, for the stone in north and south orientation, respectively.

The measurements of the stone and the air temperature presented above were further analyzed in order to determine the difference between their daily variations (ΔT_{stone} - ΔT_{air}). Table (III-5) lists the ten highest values of the differences between the daily variation of the stone and the air temperature. The analysis shows that the highest differences in the two daily variations occur in the dry-hot seasons, and the extreme

values of these differences ranged between 10 ºC and 20 ºC. Accordingly, in this study the calculation of the thermal stress was achieved by setting the daily variation in stone temperature equivalent to the daily variation in air temperature plus 10, 15 and 20 ºC (Bonazza et al., 2009b). This was done in order to cover the whole range of daily variations in stone surface temperature that the stone may encounter *in situ*.

Table III-4. Statistical analysis of stone temperature measurements in both north and south orientation for the period November/2012 - October 2013.

Year 2012-2013	North		South	
	T_{max} / ave. T_{max} (ºC)	T_{min} / ave. T_{min} (ºC)	T_{max} / ave. T_{max} (ºC)	T_{min} / ave. T_{min} (ºC)
Jan.	20.0 / 14.7	3.5 / 6.5	24.5 /18.4	3.4 /5.7
Feb.	24.6 /20.6	7.9 / 10.6	28.9 / 24.8	7.1 /9.9
March	34.7 / 26.8	8.2 / 11.2	37.9 / 30.6	8.4 / 11.3
April	41.8 / 35.6	13.8 / 16.6	43.5 / 37.6	13.4 /16.1
May	40.4 / 35.9	19.4 / 22.9	48.4 / 39.8	19.6 / 21.9
June	45.7 / 43.0	21.7 / 26.3	52.5 / 49.2	21.2 / 25.9
July	48.0 / 44.9	25.7 / 29.4	55.6 / 52.2	26.1 / 30.2
Aug.	48.1 / 46.5	28.9 / 30.3	55.7 / 51.3	28.5 / 29.8
Sep.	46.0 / 42.6	22.1 / 26.2	52.0 / 48.1	21.9 / 25.7
Oct.	38.0 / 35.7	20.1 / 20.2	45.9 / 41.1	19.7 / 19.9
Nov.	29.2 / 22.8	11.5 / 15.7	33.0 / 25.8	11.5 / 15.7
Dec.	22.3 / 17.7	7.4 / 9.3	29.7 / 21.5	5.8 / 7.8

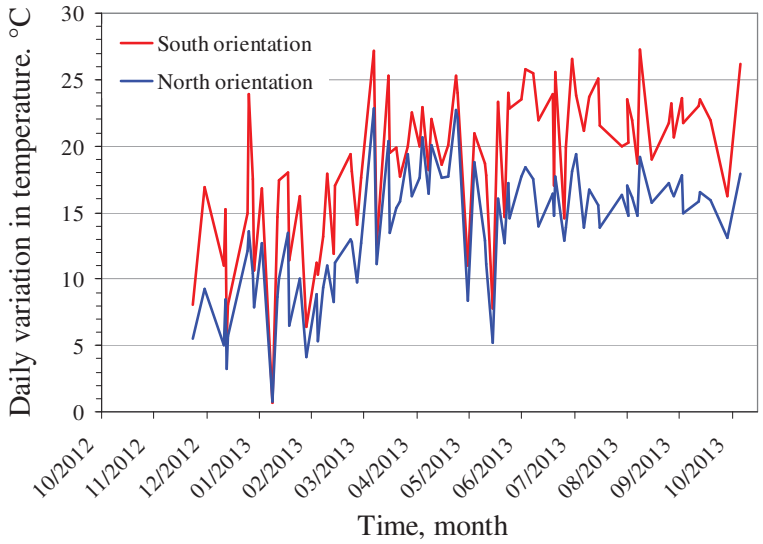

Fig. III-14. Daily variation in stone temperature both at north and south orientation for the period 2012-2013.

Table III-5. Highest values of the differences between the daily variation in stone temperature and in air temperature for the period November/2012 – October/2013.

Date	Stone surface temperature ºC				Air temperature ºC		ΔT_{stone} - ΔT_{air}*	
	North		South					
	max.	min.	max.	min.	max.	min.	North	South
06/06/2013	42.2	24.5	47.8	24.3	32.6	25.6	10.7	16.5
08/06/2013	40.1	21.7	47.0	21.2	33.3	25.0	10.1	17.5
13/06/2013	43.6	26.1	51.0	25.5	33.7	25.5	9.3	17.3
24/06/2013	45.0	28.6	52.5	28.6	34.2	27.4	9.6	17.1
26/06/2013	45.7	28.0	52.0	26.4	34.6	26.6	9.7	17.6
06/07/2013	45.6	27.5	53.3	26.7	36.3	28.2	10..0	18.5
08/07/2013	48.0	28.6	52.0	28.2	34.0	28.0	13.4	17.8
15/08/2013	48.1	28.9	55.7	28.5	38.4	28.2	9.0	17.0
08/09/2013	39.9	22.1	45.5	21.9	33.5	26.9	11.2	17.0
18/09/2013	42.5	26.7	48.4	25.4	32.9	27.0	9.9	17.1

* ΔT_{stone} - ΔT_{air} = [max. stone temp.- min. stone temp.] – [max. air temp.- min. air temp.]

2.4.2. Calculation of thermal stress

The thermal stress generated in the stone due to the high daily variation in stone surface temperature can be calculated by Eq.19 presented in (Ch 2: section 2.5.1.). The two elastic properties for fresh Al-Nimrud limestone included in Eq.3 are: elastic modulus, E=17040 MPa and Poisson's ratio, υ= 0.38, (Ali, 2011), while the measured linear thermal expansion coefficient is: α= 5.18E-6 K^{-1}. As for condensation, the percentile format was used in the calculation of the annual percentile values of thermal stress. Table (III-6) lists the values of the calculated thermal stress at different conditions of the daily variation in stone temperature.

The calculated thermal stress can be compared with the maximum sustainable load in order to assess the damage risk to the stone (Bonazza et al., 2009b; Ponziani et al., 2012 ; Al-Omari et al., 2014a). As discussed in chapter two, the determination of the maximum sustainable load is based on the unconfined compressive strength divided by a safety factor of three. Accordingly, the maximum sustainable load for the fresh Al-Nimrud limestone was found to be 5.3 MPa. Based on the results presented in Table (III-4), and assuming that the daily variation in stone temperature exceeded the daily variation in air temperature by 10 ºC, the analysis showed that the risk of damage to the

stone from thermal stress is probably negligible, since none of the thermal stress values exceed the maximum sustainable load of the stone. When the difference between the two variations in daily stone temperature and in daily air temperature is 20 ºC, there are about 25% of the days per year when the thermal stress is higher than the maximum sustainable load. In other words, the risk of damage due to thermal stress is significant during about one-quarter of the year. The risk of damage increases if the daily variations in stone temperature increase. Therefore, the results of analysis indicate that the major source of stone damage in Al-Nimrud monuments can be considered to be related to the significant role of thermal stress.

Table III-6. Annual percentile values of the calculated thermal stress for the period of three years 1963-1965.

Percentile	Thermal stress, MPa in case $\Delta T_{stone} = \Delta T_{air}$ + 10, 15, 20 ^{o}C		
%	10^{o}C	15^{o}C	20^{o}C
0	1.643	2.353	3.063
1	1.905	2.615	3.325
5	2.262	2.972	3.683
25	3.101	3.811	4.521
50	3.653	4.363	5.073
75	4.170	4.880	**5.590**
95	4.587	**5.297**	**6.007**
99	4.787	**5.497**	**6.208**
100	4.952	**5.662**	**6.373**

3. Health record of limestone in Al-Nimrud city

3.1. Introduction to the digital health record of historic monuments

The health record of a historic monument is an important research task which considers different approaches in order to centralize and store all the heterogeneous data related to the monument. It is a complex process that typically involves the processing and visualization of heterogeneous data sets such as: archive documents, survey data, *in situ* stone alteration recording and sampling, sets of data from laboratory tests, 3D modeling from digital data (laser scanning or photographs), restoration reports, other useful data such as meteorological and geological data, etc.

The digital health record represents a wide range of workflows concerning the historic building that requires high visual and metric accuracy. This is the consequence of the now widespread use of laser scanning and high resolution photogrammetric techniques. By using these techniques it is possible to accurately record the complex structures remotely, which was previously an intractable problem. Therefore, the use of the digital health record technology is considered a modern tool to provide new perspectives in the field of historic monument documentation. Thus, this documentation has moved toward intelligent data for the analysis, representation, maintenance and long-term management and monitoring of historic monuments. A detailed example concerning the digital health record of the castle of Chambord is provided in Janvier-Badosa (2012), Brunetaud et al. (2012a,b), Janvier-Badosa et al. (2013c) and Stefani et al. (2014).

In fact, the application of the digital health record requires the use of a 3D database to represent, document and analyze the collected features and results. The database should be web-based and open source to ensure its effectiveness and its distribution to all participants in the restoration process. This in turn allows the remote reviewing of the monument, allowing study of the monument at different times, as well as the online access and management of restoration and preservation works of historic buildings.

The essential characteristics of a digital health record are that it uses a 3D constructive solid geometry of the studied case that is able to store and spatially organize meaningful information about its objects. The complete digital health record program of a historic monument requires multidimensional processes, but the starting

point is to build the 3D model of the studied monument. The work in this thesis aims to satisfy the first steps of the digital health record concerning Al-Ziggurat monument in Al-Nimrud city: diagnosis *in situ* of stone decay; characterization of both weathered and unweathered historic stone; identification of a suitable stone for restoration work; building the 3D model of the monument, and finally conducting a preliminary data comparison by the use of different mappings.

3.2. Brief description of Al-Ziggurat monument and its degradations

The construction of Al-Ziggurat dates back to the era of the Assyrian king Ashurnasirpal II 884-859 BCE, but he died before completion of the work which was then finished by his son Shalmaneser III 859-824 BCE. Al-Ziggurat is the most prominent sign of Al-Nimrud city which can be seen from a distance. It is located in the north-west corner of the citadel mound, Figure (III-1). Nowadays, Al-Ziggurat appears as conical frame of completely eroded mud-brick, with a square base 50 m per side and a height of 17 m.

The earliest excavation work at Al-Ziggurat was carried out in the mid-nineteenth century by the British School of Archaeology in Iraq, led by Layard. At that time, no information was available about the origin of Al-Ziggurat and it was concluded that Al-Ziggurat was a pyramid with a mud-brick core containing the tombs of Assyrian kings. In the beginning of 1971, the Iraqi Department of Antiquities focused on the excavation in Al-Ziggurat, and its northern and western sides were detected. These sides were found to be enclosed by walls made from large brick masses of limestone and clay bricks inscribed in Cuneiform script relating to Shalmaneser III, Figure (III-15).

Fig. III-15. General view of Al-Ziggurat showing the north, the west walls and the brick-clay layer above the wall (*right*); the Cuneiform script on the clay-brick (*left*).

Field photographs of the stones on Al-Ziggurat walls reveal the different decay patterns. According to the illustrated glossary published by (ICOMOS-ISCS, 2008), salt efflorescence and stone detachment, by granular disintegration in the form of powdering and sanding and by scaling in the form of spalling, are the main decay patterns associated to salt weathering observed on the stone surface of Al-Ziggurat walls, Figure (III-16).

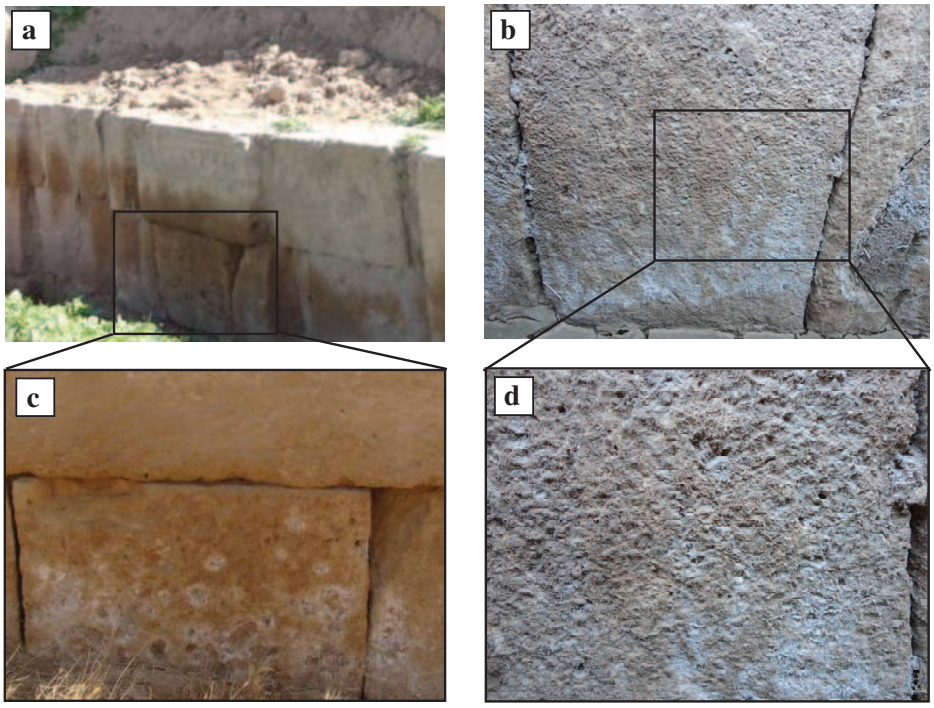

Fig. III-16. Field photographs showing: (a) and (b) the degraded stones on Al-Ziggurat wall; (c) and (d) details of salt weathering showing the decay patterns: granular disintegration, powdering and sanding.

3.3. Characterization of the limestone of Al-Ziggurat

This study aimed to characterise the weathered limestone on the walls of Al-Ziggurat in an attempt to investigate the mechanisms responsible for this weathering and to evaluate the weathering state of the stones for the purpose of their conservation. The study also aimed to identify an appropriate stone that could be used in future restoration work. To this end, the unweathered samples from the core of the historic limestone on the wall of Al-Ziggurat were characterised and compared with fresh samples from the quarry cited as the origin of the stone that was used in the construction

of Al-Nimrud city. A brief description of Al-Ziggurat is given below, followed by the stone characterization.

3.3.1. Weathered historic stone

The weathered stones were characterized through laboratory tests carried out on samples taken at the surface of the north and west façade walls of Al-Ziggurat, Figure (III-17): two powder samples (PS-N and PS-W) and two block samples (BS-N and BS-W). Laboratory tests were also performed on one soil sample taken near Al-Ziggurat walls, and one water sample from the well close to Al-Ziggurat.

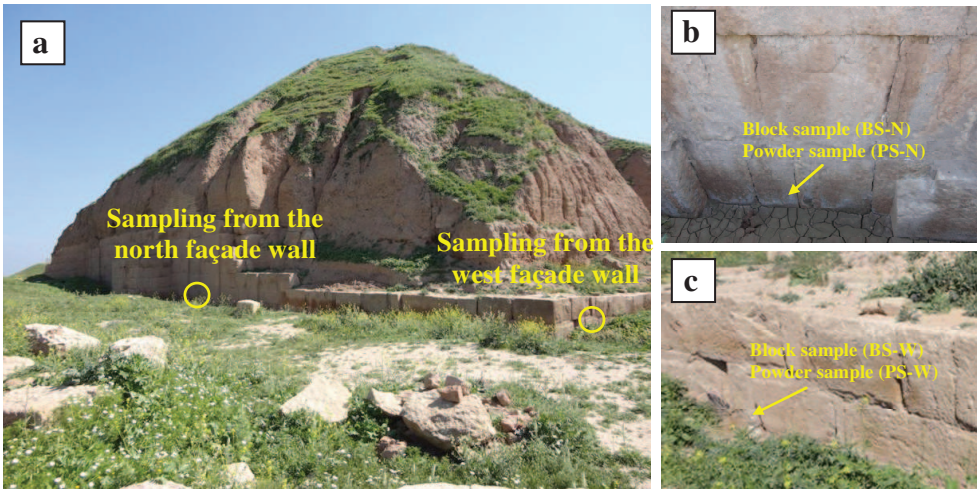

Fig. III-17. (a) General view of Al-Ziggurat; (b) sampling on the north façade wall; (c) sampling on the west façade wall.

The mineralogical composition of the two powder samples was determined by X-ray diffraction (XRD). The ion contents related to the main soluble salts present in the powder samples were determined by Ion Chromatography (IC), following the Italian standard (NORMAL 13/83 Dosaggio dei sali solubili). For this purpose, a solution was prepared by diluting 200 mg of powder in de-ionized water to a concentration of 0.01 g/ml. Then the solutions were stirred for 72 h at room temperature. The sample was filtered to 0.45 μm and the anions were determined by using a Dionex ICS 900 equipped with an AS17 (4×250 mm) and AG17 (4×50 mm) separator column. The eluent was 50 μL EGC-KOH Gradient 10 min with a speed injection of 1.0 ml/min and a pressure of about 1700 psi.

The fabric and the chemical composition of the two stone block samples and the soil sample were identified by using a PHILIPS XL40 high resolution Environmental Scanning Electron Microscope (ESEM) equipped with a FEG Hitachi S4500 EDS OXFORD INCA Energy Dispersive Spectroscope (EDS). These microanalyses enabled all the elements in the samples to be mapped.

The analyses of XRD tests carried out on the powder samples are presented in Figure (III-18). The tested samples are mainly composed of calcite with traces of quartz. The analysis shows that the soluble salts at the stone surface are gypsum $CaSO_4$, $2H_2O$ and thenardite Na_2SO_4. These exogenous minerals are due to external pollution in the limestone.

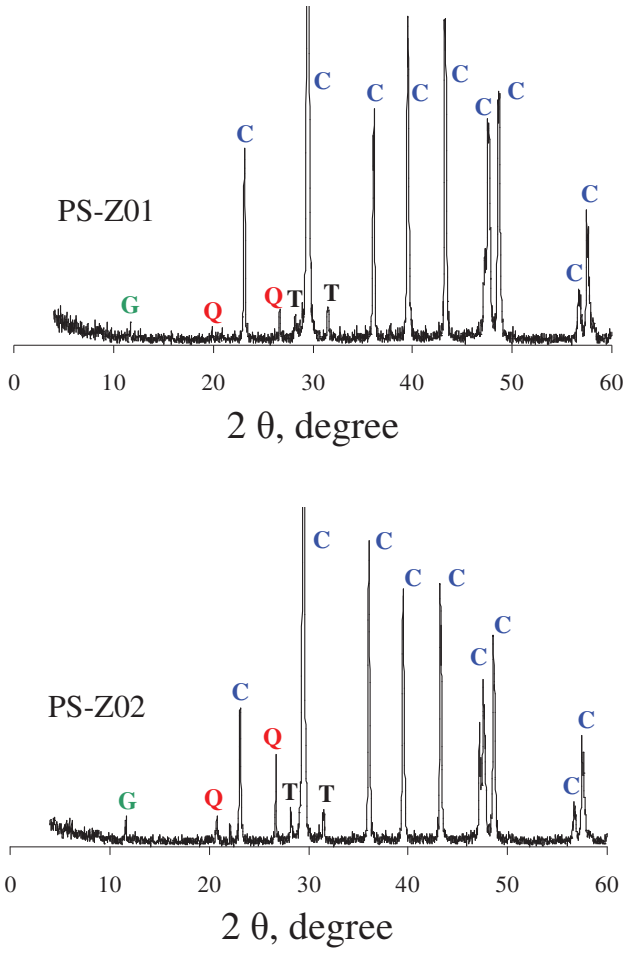

G: Gypsum; Q: quartz; C: calcite; T: thenardite

Fig. III-18. XRD patterns for the powder samples at the surface of the degraded stone.

Table (III-7) lists the results of the IC test performed on the powder samples (PS-N and PS-W) and on the soil and well-water samples. The Microequivalent per liter shows an approximate balance between SO_4^{2-} anion and Ca^{2+} cation, suggesting the presence of gypsum. In fact there are some increases in the molarity of calcium which could result from the dissolution of calcite $CaCO_3$ during the preparation of the tested solution. Results show the presence of: Cl^-, NO^{3-}, K^+, Mg^{2+} and Na^+, suggesting the presence of other minor salts such as sodium chloride, sodium nitrate, potassium chloride and magnesium nitrate.

Table III-7. Ion chromatography analysis for the soil sample and the two powdered samples taken from the stone surface on Al-Ziggurat walls.

Sampling	Concentration of ions, mg/l						
	SO_4^{2-}	Cl^-	NO_3^-	Ca^{2+}	Na^+	K^+	Mg^{2+}
PS-N	10.13	0.65	0.37	18.45	2.96	2.02	0.73
PS-W	102.24	4.14	3.84	56.19	3.80	3.22	0.90
Soil	187.97	0.49	1.24	106.09	0.47	2.92	2.09
Wellwater	2870.8	415.31	291.92	432.7	714.3	117.87	303.9
	Microequivalent molarity per liter, 10^{-6} mol/l						
	SO_4^{2-}	Cl^-	NO_3^-	Ca^{2+}	Na^+	K^+	Mg^{2+}
PS-N	105	18	6	460	128	51	30
PS-W	1064	116	62	1420	165	82	37
Soil	1957	13.8	20	2647	20	75	86
Wellwater	29885	11715	4708	10796	31083	3014	12503

The data analysis provides information about the proportion of the soluble salts, such as gypsum and thenardite. Concerning the powder sample (PS-W), and based on the assumption that both the soluble salts, gypsum and thenardite, are responsible for the liberation of sulfur and sodium ions, the calculation revealed that the percentages of gypsum and thenardite were 1.55% and 0.17%, respectively. The low amount of SO_4^{2-} ions in the powder sample (PS-N) could be related to the low percentage of gypsum (0.18%). On the other hand, the high amount of SO_4^{2-} contained in the soil sample is associated to a high gypsum content of 3.39%, while the water sample from the well

was found to be significantly polluted with gypsum, with a saturation level exceeding the solubility of gypsum in distilled water.

The images obtained by the ESEM-EDS from the block sample BS-N are presented in Figure (III-19). The microanalysis in SEM 1 shows that the chemical composition of the scanned block sample is not homogeneous. There are variations in the chemical elements observed on the inside and outside of the tested sample. The analysis clearly shows two parts in these mapped images, with abundant clayey minerals and the presence of aluminum, silica and magnesium in the upper part of the image, whereas the lower part of the image is mainly composed of calcium. These observations show that the upper part of the image, marked in white, is a thin clayey crust, and that the lower part corresponds to carbonate stone, as it is a calcium rich region. This clayey crust is due to the stone having been previously buried underground before the excavation conducted in 2011, and/or due to the dust from soil carried by the wind. The microanalysis carried out on zone (A) located at the thin clayey layer in image SEM 1 shows the presence of sulfur, indicating that gypsum crystals are associated in this zone. The images SEM 2 and SEM 3 show an enlargement of zone (A), where the morphology of a gypsum crystal, about 40 μm in length, can be recognized. However, the elemental maps from the image SEM 1 showed that there are some pores within the stone which contain sulfur, suggesting the presence of gypsum. These results matched observations obtained from previous studies indicating that dissolved gypsum is always found at the surface of the stone and that the migration of such salts into the pore spaces of the stone is very difficult (Janvier-Badosa et al., 2013a).

From the ESEM-EDS microanalysis carried out on the second block sample BS-W, different mineral phases were identified based on the elemental microanalysis realized on the stone surface, Figure (III-20). Spectrum 1 revealed the presence of sulfur and calcium, while sulfur and sodium were observed on spectrum 2. In this case, both gypsum and thenardite crystals are associated in these two spectra. These results support field observations showing that degradation, in the form of powdering, sanding and granular disintegration, of the stones on Al-Ziggurat walls is due to salt weathering.

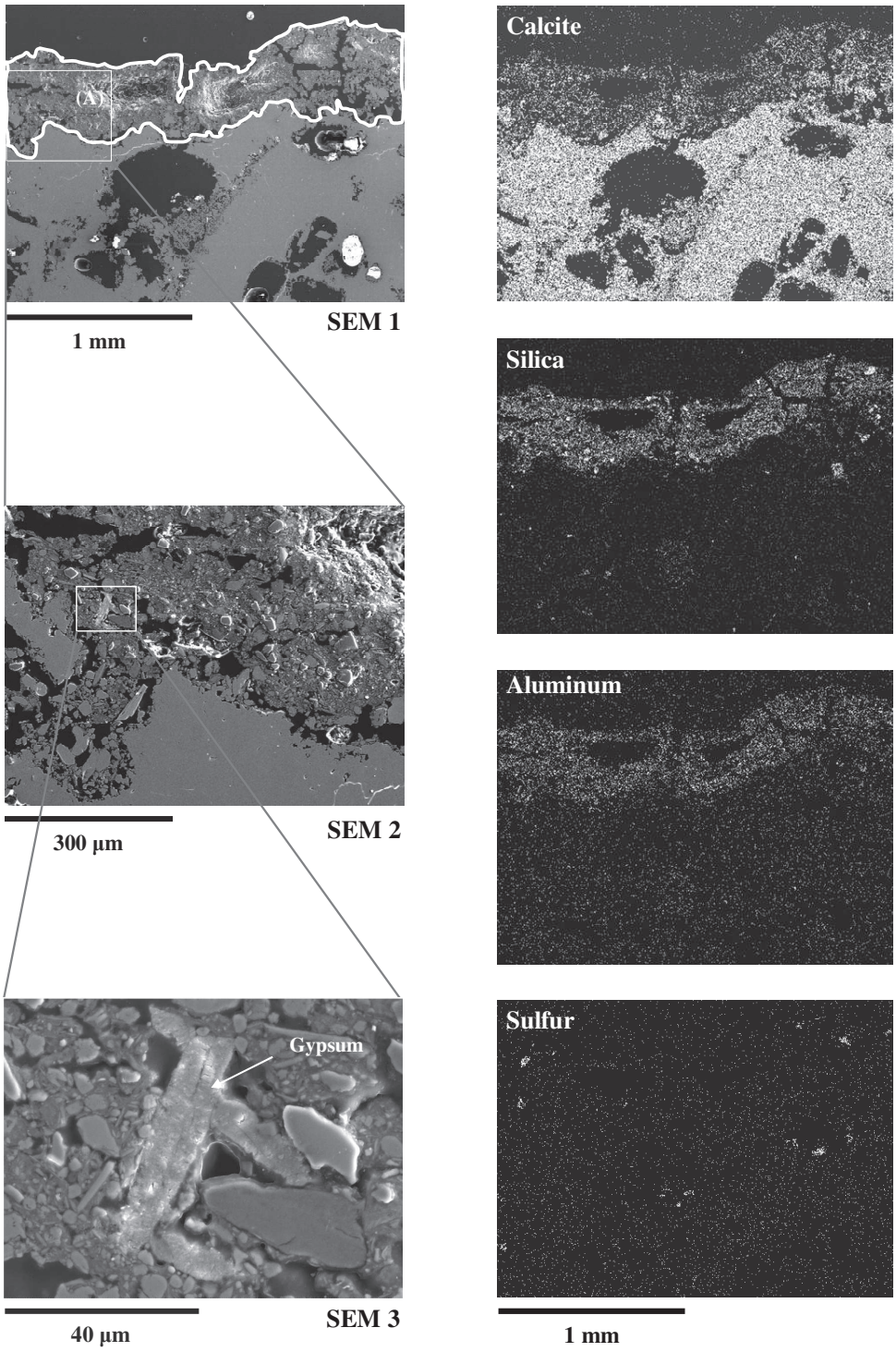

Fig. III-19. SEM images at different magnifications (SEM 1: ×50, SEM 2: ×150, SEM 3: ×1300) obtained from the sample BS-N (*left*); the elemental maps from the image SEM 1 (*right*).

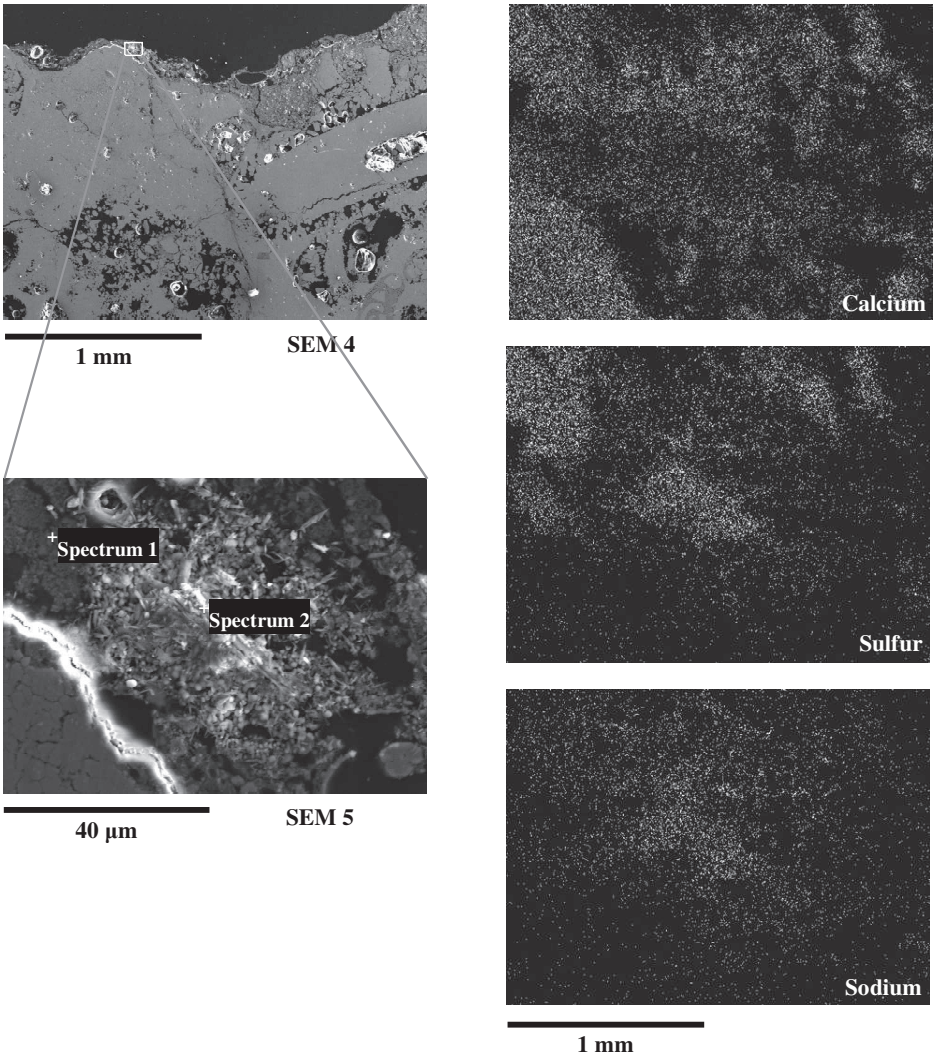

Fig. III-20. SEM images at different magnifications (SEM 4: ×50, SEM 5: ×1300) obtained from the sample BS-W (*left*); the elemental maps from the image SEM 5 (*right*).

To account for the presence of gypsum observed on Al Ziggurat walls, three hypotheses can be put forward:

1. The least likely hypothesis is that the presence of gypsum within the stone is due to the transfer of dissolved gypsum by wetting-drying alternation. During evaporation, gypsum may have migrated and precipitated as efflorescence on the stone surfaces.

2. A more realistic hypothesis is that the stone was degraded by gypsum due to contact between the soil and the stone during burial. When the present study was conducted,

the excavated stones had been buried underground for a long period. In fact, it is impossible to ascertain exactly how long the stones were buried underground, but it may well be several hundreds of years before the excavations undertaken in the last two centuries by Layard in 1845 (Layard, 1849), and Mallowan in 1952 (Mallowan, 1966). In this study sampling was carried out during the campaign done in March 2013, just after the latest excavations carried out by the Iraqi Department of Antiquities in an attempt to remove the soil covering large parts of Al-Ziggurat walls. It should be pointed out here that the weathering mechanisms of the degraded stones differ from those of the stones exposed to environmental conditions and from the buried stones (Kaplan et al., 2013). In fact, the SEM-EDS microanalysis of the block samples from the degraded stones indicated that gypsum is mainly found in the thin clayey layer at the stone surface. To check this hypothesis, the soil sample taken near Al-Ziggurat monument was examined by IC and ESEM-EDS. The IC test showed that there is a good balance in the Microequivalent per liter between SO_4^{2-} anion and Ca^{2+} cation, indicating the presence of gypsum. Also, the microanalyses in SEM 6 and SEM 7, presented in Figure (III-21), indicate the presence of gypsum crystals within the matrix of the tested soil sample. However, the source of gypsum in the soil can be attributed to dissolution of the gypsum bedrock during water table fluctuations (Blyth, 1971). After evaporation the salt deposits in the soil near the ground surface. Moreover, the presence of gypsum in the water table was confirmed through analysis of the water sample taken from the well in the studied area, Table (III-7).

3. The third hypothesis for the presence of gypsum on the stone surface is related to the combined effects of pollution and wind. In fact, although the studied area is located in a rural area, it is close to the Badush cement factory (45 km NW) and sulfur quarries in Al-Mishraq (10 km SW). Thus, wind could play a significant role in the deposition of air pollution and the magnitude of the factory waste near the studied area can provide a source of gypsum.

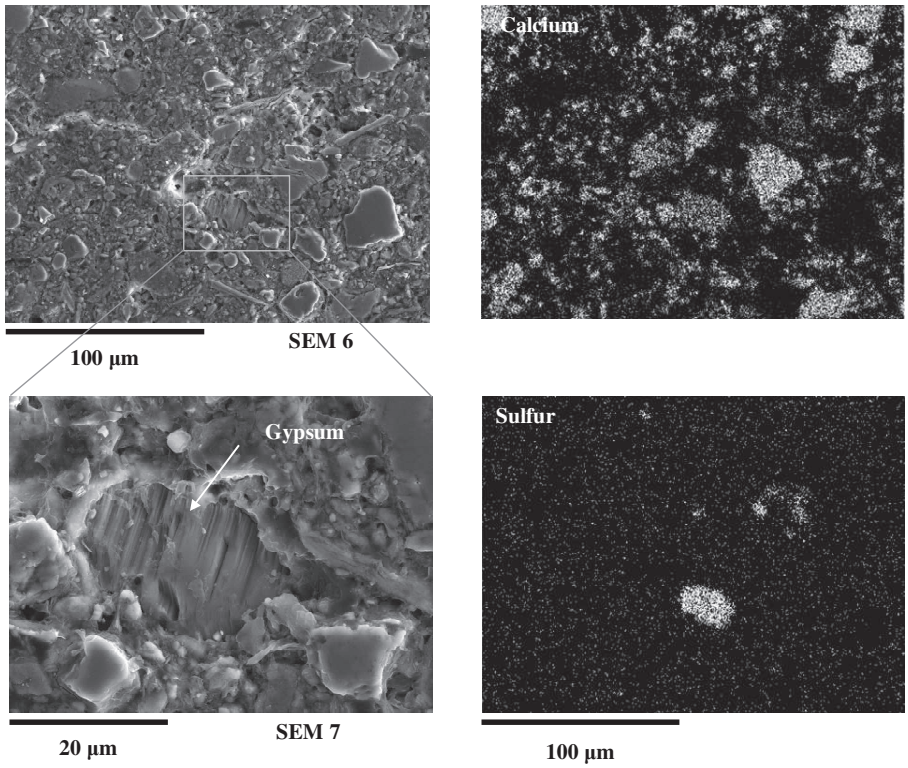

Fig. III-21. SEM images at different magnifications (SEM 6: ×500, SEM 7: ×2000) obtained from the soil sample (*left*); the elemental maps from the image SEM 6 (*right*).

3.3.2. Unweathered stones: fresh and historic stones

According to the archive text introduced by Oates and Oates (2001), the original stones used in the construction of Al-Nimrud monuments came from the quarry at Al-Mur hill district located in Eski Mosul (45 km NW of Mosul, Iraq). Experimental work by Ali (2011) also indicated that the limestone from Al-Mur hill could be the original stone used in Al-Nimrud monuments. In the present study both the unweathered part of the *in situ* historic stone and the fresh stone taken from Al-Mur hill were characterized. This was done in an attempt to determine the compatibility between these two stones so that the fresh stone could be used, if necessary, in future restoration work to replace the degraded stones on Al-Ziggurat walls.

The laboratory analyses were carried out on the samples extracted from the core at 15 cm depth inside the historic stone, measuring 80 × 70 × 50 cm^3 taken from Al-Ziggurat walls, as well as on the samples of fresh stone. The porosity, apparent density and skeletal density of the two stone samples were determined by the hydrostatic

weighing method described by (RILEM, 1984). The stone fabric was identified by testing thin slices using polarizing optical microscopy. The pore size distributions of the historic and the fresh stones were obtained by mercury intrusion porosimetry (MIP). The mineralogical composition was determined by XRD, while the elemental analysis was carried out by Optical Emission Spectrometry with Induced Coupled Plasma (ICP-OES) using a Jobin-Yvon ULTIMA apparatus. The proportion of calcite mineral in the two studied limestones was determined by thermo-gravimetric analyses (TGA-DTG).

The fresh stone is a limestone of Miocene age (Al-Naqib and Aghwan, 1993). It is whitish-gray in color and contains many fossils, resulting in a high macroporosity that gives the stone a heterogeneous texture. Thin slices of the two stones were observed by polarizing optical microscopy, Figure (III-22). The stone is bioclastic limestone containing bivalves and gastropods. The grains of stone are biosparite or bioclasts and the spaces within the stone texture are filled with sparite cement.

The unweathered historic stone is an oolitic limestone cemented with sparitic calcite and its grains are oosparite or oolitic. These results confirm that while the facies of the two stones are different, their constituted matters belonged to the same shallow marine carbonate platform. Thus the two stones can be considered to be of the same origin and to come from the same quarry but at different sedimentation levels.

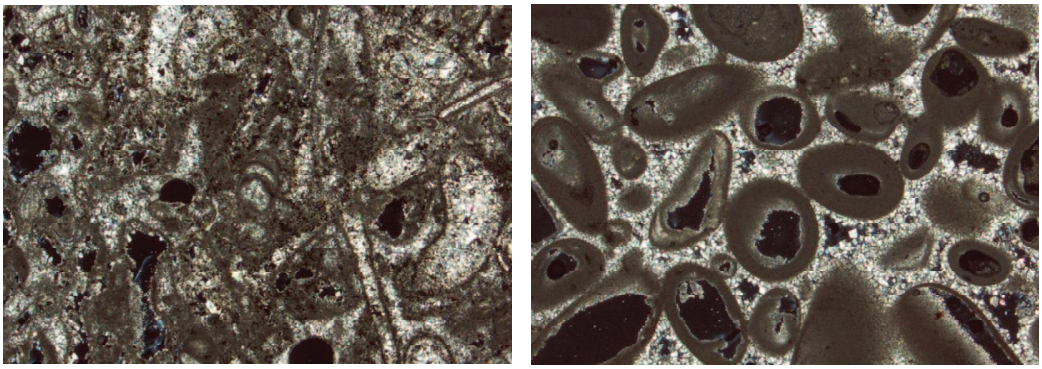

Fig. III-22. Microscopic images (POM, magnification ×2.5), (*left*) fresh stone; (*right*) unweathered historic stone.

The XRD results revealed that the two stones are dominated by calcite mineral and traces of quartz, Figure (III-23). The proportion of calcite in the two stones was

obtained through thermo-gravimetric analysis (TGA). The analysis shows that the proportions of calcite are quite similar, with 96.3% and 95.4% for fresh and historic stones, respectively.

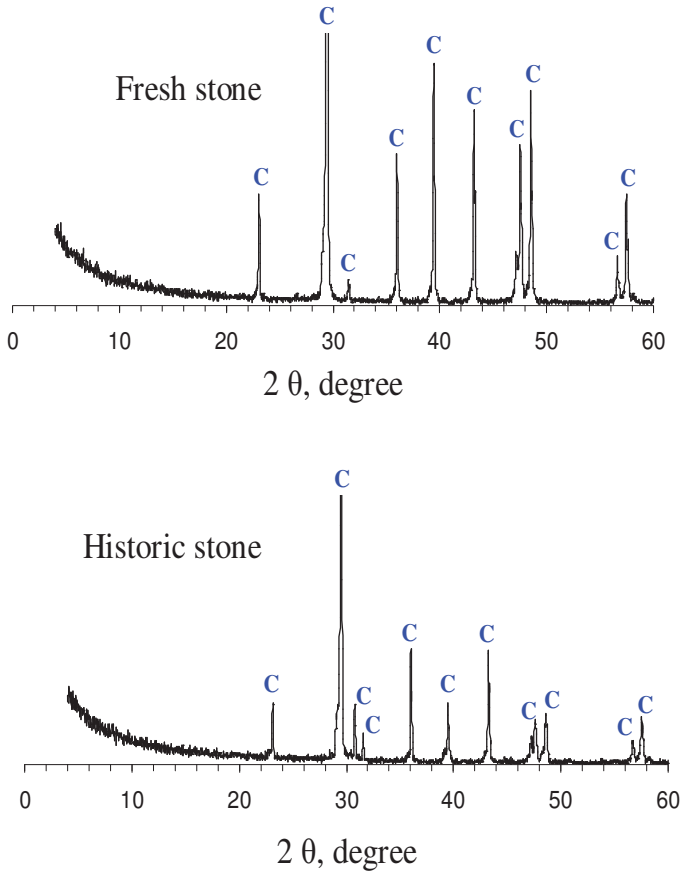

Fig. III-23. XRD patterns for the powder samples from the fresh and unweathered historic stone.

The chemical compositions from the ICP-OES test for the two stones are listed in Table (III-8). The results show that the two stones are composed mainly of calcium oxide (CaO) with minor elements of silicon dioxide (SiO_2), aluminum oxide (Al_2O_3), iron oxide (Fe_2O_3) and magnesium oxide (MgO). The silicon content indicates the presence of quartz, while the minor elements of Al_2O_3, Fe_2O_3 and MgO evidence the presence of clay minerals within the mineralogical composition of the stones. Clay minerals are in too low amounts to be detected by XRD analysis.

Table III-8. Elemental composition of fresh and unweathered historic stones, obtained from the ICP-OES test.

Tested stone	CaO %	SiO_2 %	Fe_2O_3 %	MnO %	MgO %	Al_2O_3 %	Na_2O %	K_2O %	TiO_2 %	P_2O_5 %	wl* %	Tot. %
Fresh	54.26	0.73	0.10	0.03	0.32	0.22	0.03	0.05	<l.d.	0.03	43.03	98.80
historic	52.83	1.84	0.48	0.04	0.67	0.57	0.03	0.11	0.04	0.04	42.20	98.85

Wl*: weight loss at 1000 °C

The apparent and skeletal densities and the total porosity values of the fresh and historic stones obtained by two different techniques (hydrostatic weighing method and MIP) are presented in Table (III-9). Results show that the values of the physical properties for the two stones are quite similar. The porosity values obtained by the hydrostatic method are higher than the porosity from MIP. These differences were found both for the fresh and the historic stones. This can be attributed to the limited sizes of pores that can be measured by MIP, mainly pores with a diameter greater than 450 µm. The pore size distributions of the fresh and unweathered historic stones are presented in Figure (III-24), and the proportion of micro-meso-macro pores in the unweathered historic stone compared to the fresh stone is given in Table (III-9), with a measurement accuracy of ±3%. The MIP results show that the fresh stone has nearly the same pore size distribution as the unweathered historic stone. The predominant pores present in these two stones are on the macro scale (larger than 1 µm), but they also contain meso and micro pores in smaller proportions.

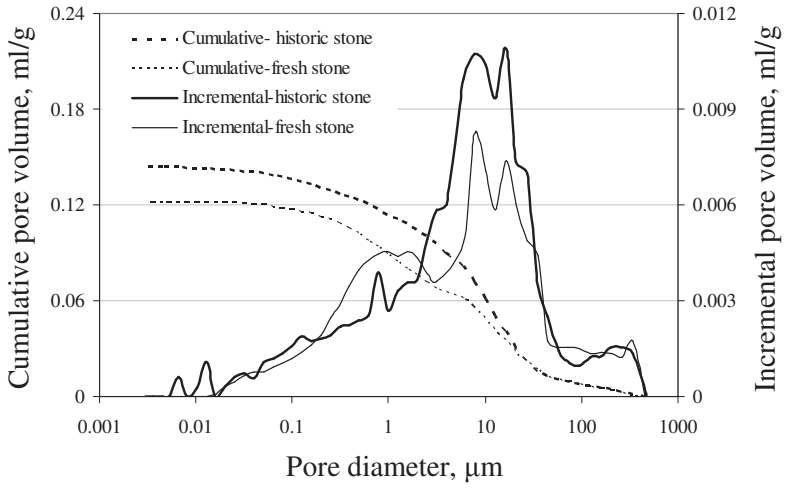

Fig. III-24. Analysis of mercury intrusion porosimetry test, pore size distribution for the two stones.

Table III-9. Physical properties and results of MIP test for fresh and historic stones: (φ_c) connected porosity; (φ) total porosity; (ρ_s) skeletal density; (ρ_d) apparent density; and pore size distribution.

Stone type	Results from MIP						Physical properties		
		Proportion of pores, %							
	φ_c %	Micro pores		Meso pores	Macro pores		φ %	ρ_s g/cm^3	ρ_d g/cm^3
		<0.01 µm	0.01-0.1 µm	0.1-1.0 µm	1.0 -10 µm	>10 µm			
Fresh	24	--	4	22	33	40	27.70 ± 1.80	2.69 ± 0.01	1.95 ± 0.05
Historic	27	--	5	15	36	42	28.52 ± 1.83	2.71 ± 0.01	1.94 ± 0.02

From the presentation above we can conclude that the characteristics of the two stones are quite similar, demonstrating that the quarry at Al-Mur hill district located in Eski Mosul was certainly the source of the construction material for Al-Ziggurat. Thus the fresh stone is a suitable choice that can be used to replace the fully degraded stone in restoration work.

3.4. 3D modeling

Usually the description of objects through a 2D view (e.g. orthophotos) provides only limited information about the state of the surfaces that are orthogonal to the direction of projection. In this case, there are probably numbers of hidden surfaces located behind the obstacles which cannot be identified. Thus, this conventional method for data processing and representation has now been replaced by modern methods of 3D modeling which provides various new possibilities that are necessary when dealing with monuments. For example, the damage area on a monument can be fully structured, analyzed and mapped. 3D modeling is now intensively used to study archaeological monuments for the purposes of their management, monitoring, preservation and restoration (Al-kheder et al., 2009; Cabrelles et al., 2010; Alsadik et al., 2013; Stefani et al., 2014).

3.4.1. Method for creating the 3D model

In the field of the monitoring and conservation of our cultural heritage, many techniques have been developed to build a 3D model (Pavlidis et al., 2007). Laser scanning and photogrammetry are two common techniques that generate a scatterplot from the survey points and the photographs. In some archaeological sites and monuments, the use of heavy, large and expensive devices is impossible. Thus, a simple middle-end digital camera, which is extremely portable and not ostentatious, should be preferred for 3D acquisition. The photogrammetric technique is easy to apply, fast and low cost. This method can be performed through the use of different software packages to create the 3D model of the monument with tolerable accuracy. In this study, photogrammetric techniques were adopted to create the 3D model of Al-Ziggurat walls.

3.4.2. 3D modeling of Al-Ziggurat wall

The principle of the photogrammetric technique is based on the acquisition of photographs. In the present study, photographs were acquired with a high-resolution digital camera (16 million pixels). Altogether, 21 photographs of Al-Ziggurat walls were taken at different orientations and distances from the walls, in orange in Figure (III-25). These photographs covered the whole of the north wall, and some parts of the west and the east walls. These photographs were processed using Autodesk ImageModeler 2009. Processing involved three main stages in order to complete the 3D modeling of Al-Ziggurat walls:

3.4.2.a. Stage of camera calibration

In this stage, the user needs to choose and locate many calibration points (i.e. locators used for calibration) on the captured photographs. During this stage, each chosen point is manually located on as many photographs as possible, simultaneously. During this calibration stage, the program computes both the extrinsic (camera position and orientation) and intrinsic (focal length and distortion) parameters. Then, by inverse calculation, the positions of the calibration points are computed.

The greater the number of the chosen points, the more accurate the resulting calibration. Figure (III-25) shows the positions of the calibration points (in blue) at the end of the calibration stage. Two distances were measured *in situ* in very distant locations in Al-Ziggurat walls. The first one was used to set the scale of the model by

fixing the reference distance. The other one was used to assess the uncertainty by comparing the value of the model's distance to the real one. The resulting relative uncertainty was about 1.5 %.

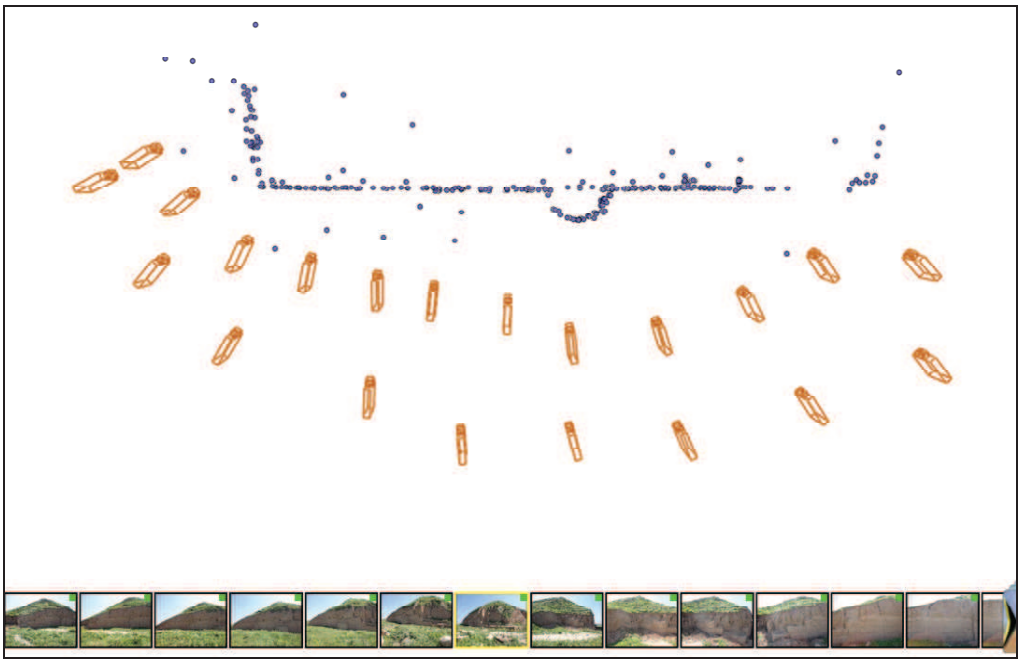

Fig. III-25. Orientation of camera, position of calibration points at the end of the calibration stage (top view).

3.4.2.b. Stage of 3D modeling

In this stage, the 3D model is completed by the addition of extra locators representing the positions of critical points required to define the essential shapes of the monument. Based on all the locators and on the user's interpretation, the surfaces of the walls can be defined by creating faces between locators, or by adjusting primitive shapes to the dimensions of the monuments, Figure (III-26). These surfaces must be developed to describe as far as possible all the details of the structure. However, these surfaces must be simple enough to be easily handled during the subsequent mapping process. It should be mentioned that the surfaces created must be perfectly joined to the others, i.e. no overlap nor space between surfaces (i.e. manifold). This last issue is the main requirement for effective texture extraction and subsequent mapping.

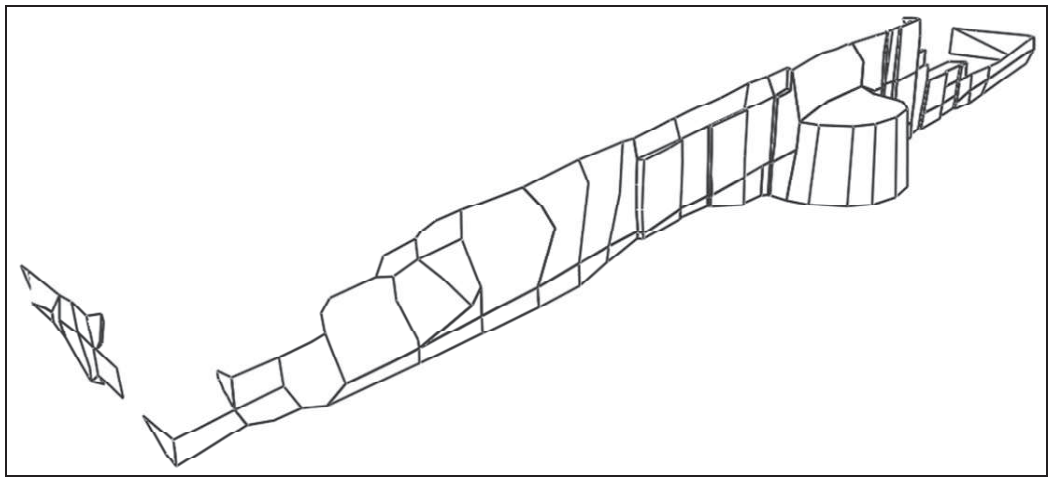

Fig. III-26. 3D wireframe model of Al-Ziggurat walls with its surfaces.

3.4.2c. Stage of texture extraction

This is the final stage in order to obtain the 3D model of Al-Ziggurat walls. During this stage, the photographs used to obtain locators and the model's surface are now projected onto the model's surface to create textures. For this purpose, each surface is associated to a specific UV projection (i.e. 2D map of texture projection). At the end of this stage, the general appearance of the real structure can be obtained. Figure (III-27) shows the final model of Al-Ziggurat walls with textures applied on its surfaces.

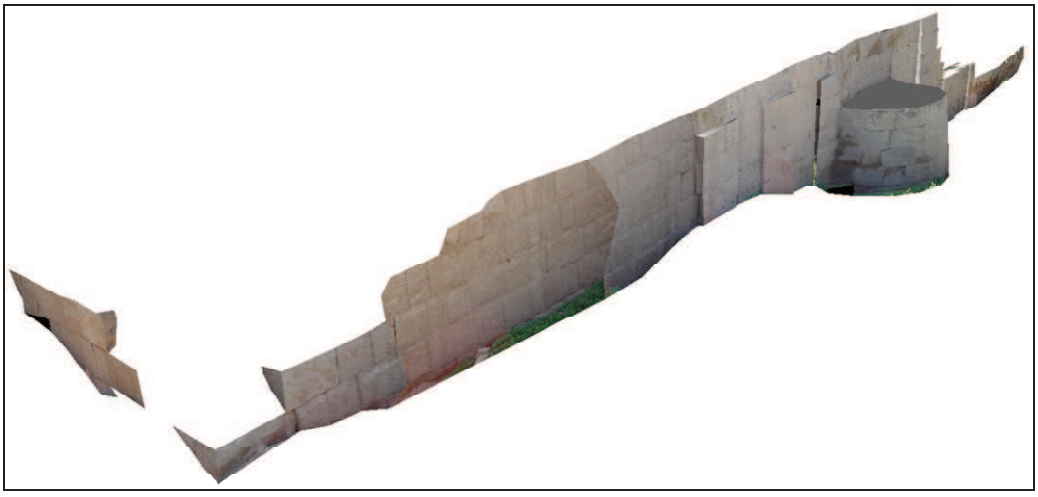

Fig. III-27. General view of the 3D construction of Al-Ziggurat walls.

3.5. Application of the health record

This section presents an example of application of the digital health record. Based on the 3D model, this digital application aims to highlight the methodology to be used to associate data to the model and the analysis required to establish the monument's diagnosis. This partial application does not claim to represent a full study: such a study would require the comprehensive collection of all available historical and scientific data, and the use of a 3D database to organize and analyze all the data. Here, a very simple process was performed to show the main technical stages that can be accomplished with very limited software resources.

3.5.1. Added documentation: successive states of burial

In the nineteenth and twentieth centuries, while Al-Nimrud city was completely buried under the ground, the city experienced several excavation campaigns aiming to discover the archaeological treasures of the city. Among the most prominent of these campaigns were those accomplished in 1845 by Layard under the supervision of the British School of Archaeology in Iraq (Layard, 1849), and a second series carried out in the period (1949-1958) by Max Mallowan (Mallowan, 1966), followed by David Oates (1960-1963) (Oates, 1968). Figure (III-28) shows that the walls of Al-Ziggurat were previously totally buried. After the above-mentioned explorations, large parts of Al-Ziggurat walls were discovered, and other parts were still buried. Excavations have continued until very recently. Figure (III-29) displays nearly the same part of the northern façade of Al-Ziggurat wall in 2011 and 2013, showing the part of the buried walls that was explored between the two dates by the Iraqi Department of Antiquities.

The current study proposes to clarify the limits of the buried stones on the walls of Al-Ziggurat just before the last exploration performed in 2011. Based on the comparison between several pictures taken in 2011 and 2013, Figure (III-30) shows the mapping of the previous state of burial in 2011 projected on the 3D model relative to the state in 2013. This mapping was obtained with ImageModeler by creating new face boundaries in the model at the limit between the two states of burial, and by assigning a specific color to the previously buried part instead of its texture.

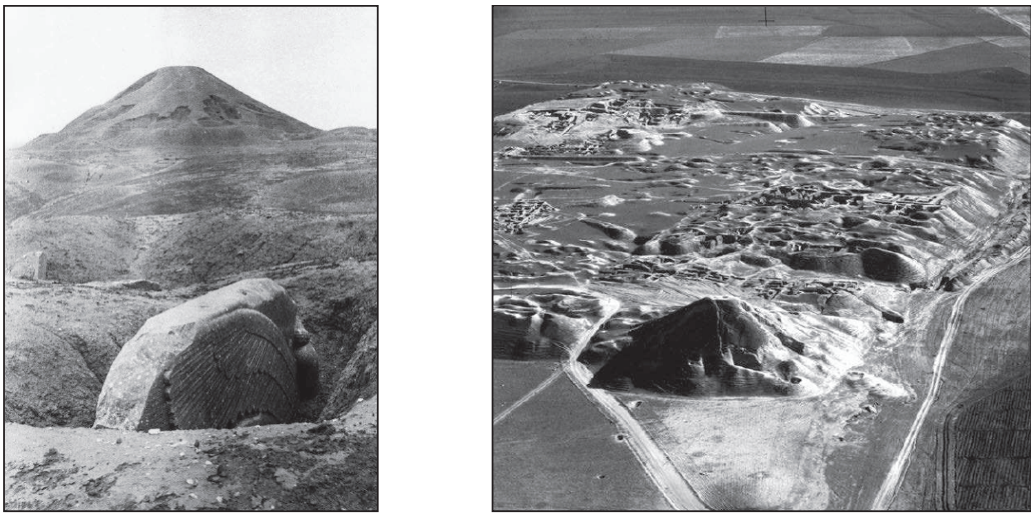

Fig. III-28. The ruins of Al-Nimrud city in 1906, part of the winged lion and Al-Ziggurat beyond (Reade, 2002), (*left*); aerial view of the citadel mound with the main ruins of Al-Nimrud city, (Oates, 2002), (*right*).

Fig. III-29. Photos showing part of Al-Ziggurat wall on its northern façade at two different periods: 27 June 2011 (*left*), and 23 March 2013 (*right*).

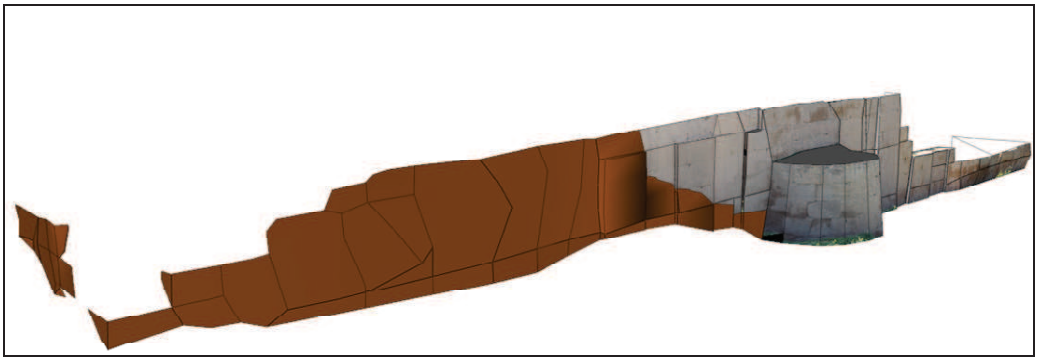

Fig. III-30. Mapping of the state of burial in 2011 projected on the model of 2013.

3.5.2. Mappings of degradations

Thanks to the use of a real 3D model able to represent all the parts without any hidden surfaces, the stone degradation can be mapped with a high degree of accuracy and metric value.

The mapping of stone degradation was achieved by following the ICOMOS classification glossaries. *In situ* observations showed that discoloration and detachment in the form of disintegration and scaling are the most frequent decay patterns in the limestones of Al-Ziggurat walls. Some of the degraded stones were also found to be affected by mechanical weathering, resulting in missing parts. Two forms of biological effects represented by plant life and lichen were observed. Moreover, stones suffered deterioration by patina formation. The above observations can be used to map the degradation of the stones on the walls of Al-Ziggurat and can be integrated into the 3D model. The different types of stone degradation observed *in situ* were directly outlined and colored on the 3D construction of Al-Ziggurat walls, Figure (III-31b), as for the previous mapping. This partial view of the mapping can be used to highlight the main characteristics of the state of degradation. For example, discoloration by moisture mainly affects the lower part of the wall due to the presence of water near the ground as the stone is not protected against rising damp. Patina is observed on higher levels of the wall where water accumulates due to rain on the roof of the walls as the stones are not protected by any type of sealing. Some mappings appear in dark color; this is due to the effect of lighting rendering on steeply inclined faces of the model.

Due to the relatively low resolution of the 3D modeling obtained by this photogrammetric technique, some very small decay patterns such as cracks or fissures could not be represented. For a finer result, it is recommended to use the laser scanning technique or a very high resolution camera associated to the latest dense correlation algorithms.

3.5.3. Discussion about monument diagnosis

The monument diagnosis typically stems from the analysis and the synthesis of all available data. 3D model makes it possible to handle several complementary mappings, and is a valuable tool in combining these mappings. This can be helpful to observe, for example, correlations between the spatial distribution of degradations and

other layers of mapping. By comparing the mapping of the previous state of burial and the mapping of degradation, Figure (III-31), some general conclusions can be drawn. Firstly, both parts (recently uncovered, and uncovered during the nineteen sixties) are affected by missing parts, in similar proportions. This mechanical-related degradation could be the consequence of the excavation process or ancient ageing before progressive burial, as both parts were previously buried before the 20th century. Secondly, the part that was uncovered during the 1960s is now submitted to severe degradation related to physical processes such as flaking and disintegration whereas the recently uncovered part is not affected by these types of degradation. Moreover, the different samples cored in the stones of Al- Ziggurat, both in buried stones and uncovered stones, revealed the presence of gypsum, which can be involved in triggering or at least enhancing flaking and disintegration. The current healthy state of the recently uncovered part can be explained by two complementary hypotheses: (a) This part was recently buried and up to this date was protected against the combined effect of climate variation and probably recent gypsum pollution; (b) This part is covered by a layer of clayey dust that can act as an intermediate medium that lowers humidity variations in the stone, and thus delays the salt crystallization processes. However, this clayey dust can also act as a vector for pollution as it may contain gypsum.

The combined hypothesis leads to the conclusion that the recently uncovered part is temporarily in a healthy state. As climate variation will continue to affect the stones, and as the layer of clayey dust will be leached by rain, this part will certainly suffer from the same degradation patterns as the other part. Two complementary solutions could be applied to protect both parts from further damage: (a) Protecting the surface from rain by sealing the roof and the bedrock and by providing a watershed. (b) Carrying out a desalination campaign to avoid any effect of salt crystallization. However, the waterproofing of the walls would be difficult as they are bonded to soil. Moreover, desalination of gypsum is known to be virtually impossible as this salt is particularly difficult to extract.

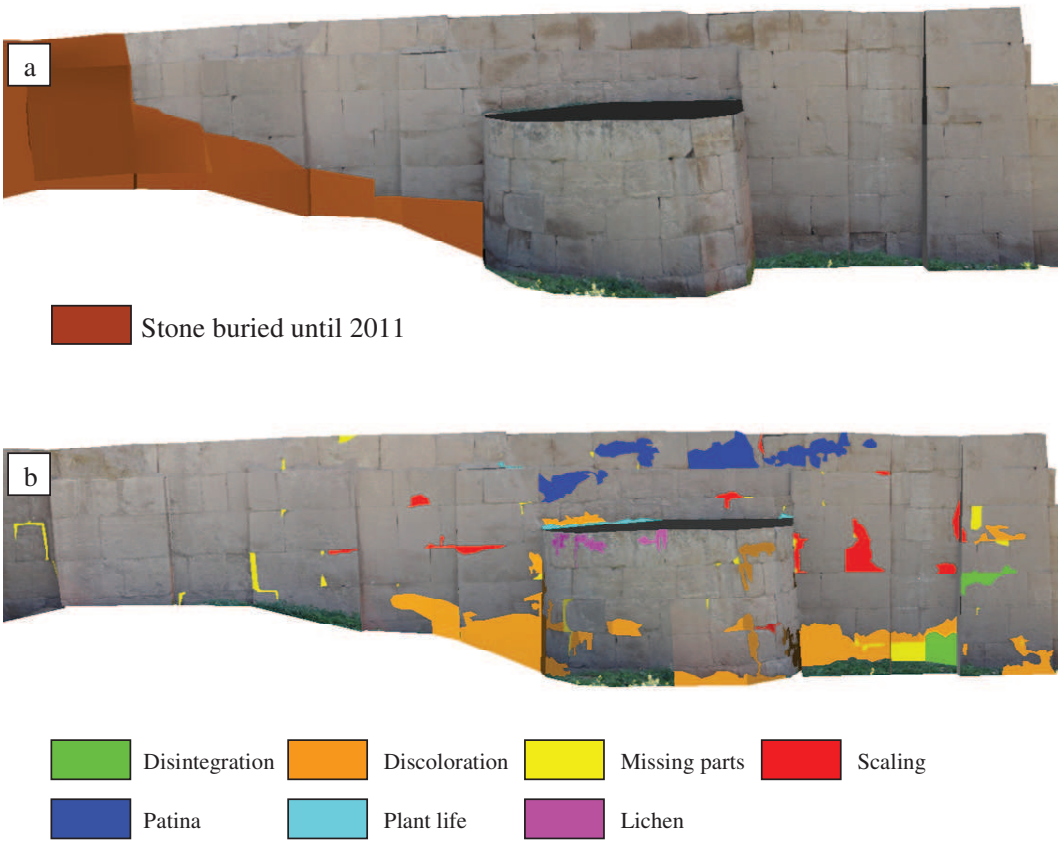

Fig. III-31. Part of Al-Ziggurat wall showing: (a) the state of the burial in 2011; (b) the state both of the recently uncovered and the degraded stones that projected on the created 3D model.

4. Conclusion

The second millennium monuments in Al-Nimrud city have never been restored. These constructions reveal numerous decay patterns: efflorescence, granular disintegration (sanding and powdering), spalling, missing parts, discoloration and differential erosion. Different weathering processes are responsible for the degradation of stones.

The risk of damage to the stones in Al-Nimrud monuments was assessed through three physical weathering processes: condensation, freezing-thawing action and thermal stress. These weathering processes are directly related to the climatic conditions, and the daily, or even seasonal, variation in the climatic conditions enhances the degradation of the stones. Data from the meteorological station (air temperature and relative humidity and grass temperature) and the data from laboratory tests (pore size distribution and thermo-mechanical properties of limestone from Al-Nimrud) were analyzed. In these analyses all the data related to the stone temperature and relative humidity were predicted from the meteorological station. The results of analysis clearly highlighted the significant role of climatic conditions in causing damage to the stones of Al-Nimrud monuments. The effects due to condensation and freezing action are limited. However, as these weathering processes have continued over a long period (since 850 BCE), they contribute to the degradation of the stones. Weathering by thermal stress is assumed to be the major process that causes damage to the stone and its effects increase if the daily stone temperature variation increases.

The characterization of the unweathered historic stone was compared to that of the fresh stone from Al-Mur quarry to assess the relevance of its selection for the restoration of Al-Nimrud city. The main properties and characteristics of the two stones are quite similar, demonstrating that the quarry at Al-Mur hill district located in Eski Mosul was certainly the source of the construction material for Al-Ziggurat. Thus the fresh stone is a suitable and sustainable choice that can be used to replace the fully degraded stone in restoration work.

In this research, different approaches were considered in an attempt to provide scientific documentation for the health record of monuments in Al-Nimrud city. Concerning the stones on the walls of Al-Ziggurat, the laboratory tests indicate that the degradation of stones is related to the action of salt weathering, and gypsum was the

main salt observed in the weathered stones. In order to explain the origin and the source of gypsum that is responsible for the stone degradation, the most reliable hypothesis, which is confirmed by a number of results in particular microanalyses, is that the thin clayey layer covering the stone surface and the source of gypsum is related to the soil in contact with the stone during burial.

The historic stones in Al-Nimrud city are threatened with further deterioration. The lack of appropriate prevention enhances the degradation for many of the ancient wall reliefs that have to face harsh weather conditions such as wind-blown sand and heavy seasonal rains. Thus restoration work in Al-Nimrud city is an urgent issue. The fresh stone from the quarry at Al-Mur hill district, located in Eski Mosul, was found to be a suitable choice for this purpose.

Finally, the 3D modeling of Al-Ziggurat wall was successfully achieved with good accuracy by using the photogrammetric technique. This model can be linked to both the field observations and the laboratory investigations in order to build the first steps for the digital health record of Al-Ziggurat monument. The comparison between the mappings of degradation and the mapping of the previous state of burial leads to the conclusion that excavation can damage stones by direct mechanical action and by exposing the stones to climate fluctuations. This climate action, added to the presence of gypsum pollution, is thought to enhance or trigger physical processes of degradation such as flaking and disintegration. To limit further damage, the protection of the stone of Al-Ziggurat is an urgent necessity. This example of the use of a health record, including the realization of the 3D model and the collection of historical and scientific data, can be extended to all the monuments in Al-Nimrud city.

General conclusions and perspectives

General conclusions

The study presented in this thesis deals with the ageing of limestone structures. The degradations experienced by these stones result from interaction with their environment. Hence, studying the in situ ageing of stone requires both the characterization of the material and of the local climatic conditions. Among the different degradation processes, physical processes (freezing-thawing, condensation and hygro-thermal dilations) are notably difficult to assess. This is due to the fact that their cyclic effect over long periods can generate fatigue of the mechanical properties of stone. From a general point of view, even if the description of the different physical weathering processes is based on recognised theoretical bases, the estimation of the weight of these processes, and their precise role in the actual degradation of stones still needs scientific evidence and discussion. The objective of this thesis was to study the role of climatic conditions in enhancing the evolution of the stone properties by a quantitative estimation of the weight of the different physical weathering processes.

Two major historic sites were selected to constitute the experimental field of investigation and of application of this study: the Château of Chambord in France and the archaeological site of Al-Nimrud City in Iraq. In the case of Chambord, the materials studied are tuffeau, which was intensively used for wall facings, and Richemont limestone, widely used as a substitute for tuffeau during restoration, even if this solution was applied only during part of the 20th century. In the case of Al-Nimrud, three types of stone were selected. The first one is represented by samples cored in situ in stones assumed to be original, and visibly weathered. The second one is the same lithotype, but in its healthy state. The last one is the stone that could be used as a substitute for the restoration of in situ limestone due to its geological and geographical proximity with in situ stones. All these stones are porous fine limestones used for wall facings, and directly subjected to climate fluctuations.

The approach chosen for damage risk assessment for stones exposed to climate was as follows:

1. A literature review on the quantification of the impact of the different degradation processes involved in stone weathering, highlighting the main stone properties and the main meteorological factors affecting stone durability.

2. Realization of a multiphysics and multiscale experimental characterization campaign of the limestone used at Chambord, focusing on the main properties involved in weathering processes.

3. Collection of meteorological data at Chambord thanks to a weather station placed next to the site added to in situ measurements.

4. Realization of an experimental campaign to estimate the specific weight of identified parameters (here: freezing-thawing) to supplement the database used for damage risk assessment.

5. Damage risk assessment by the combined use of climate data and material characterization, through the calculation of the impact of the different physical weathering processes; methodological development of the calculation when required.

6. Application of the damage risk assessment methodology to Al-Nimrud site: stone characterization and diagnosis, collection of climate data, damage risk assessment.

7. Development of the bases of the digital health record of Al-Ziggurat with a view to diagnosing its durability.

The steps relative to the characterization of stone properties, climate data collection, and damage risk assessment are iterative since climate data may prove to be initially insufficient, a further characterization of properties can be required for relevant risk assessment, and their application in calculation of the damage risk can require additional scientific development.

The first chapter of this thesis is dedicated to a review of the literature. It provides a description and illustration of the main degradation processes (physical, biological, chemical) proposed in the literature that explain the degradation patterns observed on stones subjected to climate effects. The description is supplemented by the stones' properties and the environmental factors involved in these processes. This documentation focuses specifically on physical processes, because the damage risk assessment explored in the following chapters is based on these processes. Physical processes are involved when the climate conditions generate stresses without chemical or biological interaction with the stone matrix. It includes stress from hygric or thermal

restrained dilation due to temperature and relative humidity variation, freezing-thawing, and crystallization of exogenous salts. Chemical processes are characterized by changes in the mineralogical composition of the stone, or its distribution, resulting from chemical reactions such as oxidation, hydration, and hydrolysis. Biological processes deal with the growth of biological organisms such as mosses, algae, and lichens. These organisms can induce the degradation of stone through physical and chemical processes. The different factors affecting stone durability comprise the stone properties (internal factors) and external vectors (external factors). Internal factors are the stone properties governing stone durability such as the stone texture, its grain size, its mineral composition, and the characteristics of its porosity (total porosity, pore size distribution, pore connectivity). A recurrent factor in degradation processes is water movement; hence, any property enhancing water movement and its accumulation tends to weaken the stone behavior as a response to environmental assaults. External factors are relative humidity, temperature, wind, precipitation and solar radiation. Based on this synthesis, condensation, freezing-thawing and the effect of restrained hygro-thermal dilation were chosen as the key physical processes to be assessed in this study.

The second chapter deals with studies relative to the limestone used in the facing of the Château of Chambord: tuffeau and Richemont stone. It includes the definition of all the procedures performed to characterize the physical-chemical and textural properties, the characterization of water transport and retention properties, mechanical strength, hygro-thermal elastic properties and the analysis of the results. The core of this chapter concerns the damage risk assessment due to stone being exposed to climate fluctuations. This assessment involves calculation of the frequency of events such as condensation and freezing-thawing both on the surface and within the porosity of stones, added to the calculation of hygro-thermal stress variations relative to the associated compressive and tensile strength of the stones. Finally, the notion of critical degree of water saturation was studied to provide the value of the minimal degree of water saturation required to trigger damage by freezing.

The mineralogical characterization of tuffeau and of the Richemont stone was performed by the use of XRD, ICP OES, TGA/DTA. Tuffeau is mainly calcareous (49 %) with a high silica content, and with a significant clay content, whereas Richemont stone is almost purely calcareous (96 %) without clay. The microtexture of both stones observed by SEM equipped with EDX showed that tuffeau is composed of a wide range

of grain sizes and morphologies compared to Richemont stone, which is altogether finer and more homogeneous. Hydrostatic weighing showed that the total porosity of tuffeau (45 %) is significantly higher than that of Richemont stone (29 %). Thanks to the mercury intrusion porosimetry test, tuffeau showed a rather bimodal pore size distribution: a first peak at 8 µm with another one at 0.01 µm. Richemont stone is rather monomodal with a peak at 2 µm and a shoulder at 0.6 µm. The water retention capacity of tuffeau is much higher than that of Richemont stone. The atmospheric absorption at 48h reached 27 % for tuffeau, which is twice the value of that of Richemont stone (12 %). At the end of capillary imbibitions, the weight gain was 60 % higher for tuffeau within half the time. The water permeability of tuffeau (3.1E-7 $m.s^{-1}$) proved to be much higher than that of Richemont stone (5.4E-8 $m.s^{-1}$). The strength of tuffeau reached 12 MPa in compression at dry state, and 10 % of this value in tension. In both cases, the fall in strength at saturated state is 60 %. For Richemont stone, the strength is 20 MPa in compression and also 10 % of this value in tension. The fall in strength at saturated state is the same as tuffeau in tension whereas it is only 35 % in compression. The speed of propagation of compression waves reached 1600 $m.s^{-1}$ for tuffeau against 2600 $m.s^{-1}$ for Richemont stone.

The damage risk assessment of stones exposed to their environment required the collection of climatic data through different sources: a weather station placed in situ, sensors inserted into the stones, and the weather station located 45 Km from Chambord. A statistical analysis established that the meteorological data extracted from the in situ weather station were representative of the climate; this data set was then used for damage risk assessment despite its relatively short duration (17 months). All the combined climate data tend to emphasize that the local climate at Chambord is rather mild and humid. The sensors inserted into the stones showed that temperature and relative humidity variations decreased with depth; core data were notably stable. Data from both the sensors and the in situ weather station were used to quantify the effect of climate conditions for the damage risk assessment. The annual frequency of days with at least one occurrence of condensation reaches 31 % at Chambord, which means that this process is of major importance. Within porosity, the frequency of condensation decreases with depth, and increases for low pore radii. Hence, the porosity of Richemont stone is three times less subject to condensation (30 %) than tuffeau (90 %). At the stone surface, the annual frequency of days with at least one occurrence of

freezing with the simultaneous presence of water is between 5 and 10 %. Within the porosity of stones, only the biggest pores near the surface experience freezing. For the damage risk assessment relative to the occurrence of freezing, an experimental campaign based on freezing and thawing cycles (-18 to 32°C cycles within 24h) was performed in the laboratory. At the end of monitoring, all the indicators (total porosity, speed of sound, residual tensile strength) confirmed that the minimal degree of saturation for freezing to damage stone is 85 % for both stones. This conclusion does not depend on the number of cycles, suggesting that it is an intrinsic stone property. The last risk studied concerned the development of stress generated by restrained hygro-thermal dilations. The work first focused on the calculation of thermal stresses in both stones. The results showed that stresses were higher in Richemont stone compared to tuffeau although stresses remain well below the sustainable load of both stones. In order to refine this calculation, the effect of restrained hygric dilations was added. To achieve this, it was necessary to investigate the elastic properties of tuffeau (elastic modulus, Poisson's ratio and free dilations) as a function of the temperature and degree of water saturation. This experimental work consisted in measuring the response of a 3-axis strain gauge glued on the samples inserted into a hydraulic loading cell at controlled temperature and relative humidity thanks to the use of a climate chamber. The free dilation, the axial strain due to loading and its resulting transversal strain were measured to calculate the selected elastic properties. A Design of Experiments methodology was then applied to obtain and statistically validate, for each elastic property, a mathematical model able to represent every result. These models giving the variation of the elastic properties as a function of temperature and degree of water saturation were used, combined with climate data, to calculate the stress induced by restrained hygro-thermal dilations according to two schemes. The first scheme relative to the calculation of the daily variation in stress showed that the damage risk is low, even next to the surface, because the safety factor is about 12. The second, more realistic, scheme is relative to the calculation of the differential stress between surface and core (250 mm depth into the stone), based on the assumption that stone plasticity and creep effect should enhance a stable state at the core. This differential stress, once compared with the associated tensile or compressive strength depending on its sign, showed that the compression damage risk is similar to that of the first scheme. However, the tensile damage risk becomes critical since the factor of safety is only 2, which can be considered as low due

to fatigue effect. Hence, the mild humid climate of Chambord promotes condensation at the surface and within the porosity of stones. The risk of freezing is low, as is damage by freezing due to the high critical degree of water saturation. By assuming the core state as a reference mechanical state, the variation of hygro-thermal stresses generates sustainable compressive stresses while the resulting tensile stresses come dangerously close to the stone's limits, highlighting the major role of this process in the degradation of stones at Chambord.

The third chapter deals with studies relative to the historic limestone, in its weathered and healthy state, used in the facing of the Al-Ziggurat monument in Al-Nimrud city, and to the stone applicable for restoration. The stones of this three-thousand-year-old monument have never been restored and exhibit various degradation patterns: efflorescence, stone detachment by granular disintegration in the form of powdering and sanding and by scaling in the form of spalling, formation of patina and discoloration, cracks, missing parts and differential erosion. Applying the methodology developed for the damage risk assessment of stones in Chambord, the risks of condensation, freezing-thawing and thermal stresses were assessed for the Al-Nimrud Ziggurat. The frequency of condensation and freezing are low but non-nil. Hence, the very long period of exposure to climate fluctuations could nonetheless make these processes relevant through fatigue effect. The effect of thermal stresses seems particularly significant and is probably the main damaging process. The fresh stone extracted from Al-Mur quarry was characterized and compared to the healthy historic stone. The properties of the two stones proved to be close enough to conclude that they are compatible, and that Al-Mur quarry was certainly the source of stones for the construction of Al-Ziggurat walls. Hence, this stone, which is still available, constitutes a relevant and sustainable choice for the substitution of severely damaged stones. Finally, the first step of the creation of the digital health record for Al-Ziggurat is presented. It consists in the realization of a 3D photomodel of the stone walls supplemented by the definition of two mappings: the previous state of burial of the stones, and the distribution of degradation. The comparison of the two mappings, added to data from the characterization of the weathered stones, indicates that the recent excavation of the stones could enhance their accelerated ageing if no precautionary measures are quickly undertaken.

Perspectives

This research has revealed gray areas in knowledge. Among those that seem relevant to explore to refine the present results are the following proposals:

1. For condensation, results could be refined by analyzing the specific effect of rain, drizzle, fog, hail, and snow in combination with the speed and the direction of wind.

2. The critical degree of water saturation for freezing-related damage is 85 % for the tested stones, which corresponds to a relative humidity very close to 100 %. However, the thermal-humidity sensors used in the present study are not accurate for high humidity. Hence, there is a need to develop in situ techniques for monitoring stone humidity for high values to provide a better assessment of freezing-related damage risk.

3. The analysis of the effect of restrained dilations is based on the notion of safety factor. This notion includes the effect of fatigue. To refine the value of the safety factor to be used as a threshold, there is a need to quantify hygro-thermal fatigue laws.

4. Although potentially major damage processes have been highlighted, up to now, it has not been possible to demonstrate which process or which combination of processes is enough to trigger scaling. Even if some assumptions are provided, the question is still open.

5. The characterizations of Al-Ziggurat stones and their degradation diagnosis are based on a small number of in situ samples. An additional coring campaign would be necessary to supplement and/or consolidate the present conclusions.

6. The first step in the creation of the digital health record proposed in this manuscript should be pursued to constitute a real database of the site to be used for a durability diagnosis on the monument scale. A comprehensive database requires the collection of further historic data and scientific results. Moreover, the use of a documentation platform able to spatially organize and analyze the database, such as NUBES, would also be necessary

References

References

Akin M. Özsan A. (2011): Evaluation of the long-term durability of yellow travertine using accelerated weathering tests. Bulletin of Engineering Geology and the Environment, 70(1), pp 101–114.

Ali H. E. (2011): Study the Mechanism of Deterioration on the Rocks Used in the Historical Building, Ph.D. thesis, University of Mosul, Mosul, Iraq.

Al-Juboury A. I., McCann T. (2005): The Middle Miocene Fatha (Lower Fars) Formation, Iraq. GeoArabia 12 (3), pp 141–174.

Al-kheder S., Al-Shawabkeh Y., Haala N. (2009): Developing a documentation system for desert palaces in Jordan using 3D laser scanning and digital photogrammetry. Journal of Archaeological Science, 36, 537‑546.

Al-Naqib S. Q., Aghwan T. A. (1993): Sedimentelogical study of the calstic Units of the Lower Fars formation. Iraqi Geological Journal, 26 (3), pp 108–121.

Al-Omari A., Brunetaud X., Beck K., Al-Mukhtar M. (2012): Climatic condition and limestone decay in Al-Namrud monuments: Review and Discussion. IEEE conference publication, Engineering Sciences (FNCES), 2012 First National Conference for Engineering Sciences, 7-8 November, Baghdad, Iraq, DOI: 10.1109/NCES.2012.6740455.

Al-Omari A., Brunetaud X., Beck K., Al-Mukhtar M. (2013a): Effect of environmental conditions on the degradation of stones in the Castle of Chambord. 31èmes Rencontres de l'AUGC, E.N.S. Cachan, 29–31 May.

Al-Omari A., Brunetaud X., Beck K., and Al-Mukhtar M. (2013b): Experimental study on the role of freezing–thawing in the degradation of stones in the Castle of Chambord. Proceedings of International Conference on Built heritage, Milano, Italy, pp 1352–1358.

Al-Omari A., Brunetaud X., Beck K., and Al-Mukhtar M. (2014a): Effect of thermal stress, condensation and freezing–thawing action on the degradation of stones on the Castle of Chambord, France. Environmental earth science, 71(9), pp 3977–3989.

Al-Omari A., Brunetaud, X., Beck K., and Al-Mukhtar M. (2014b): Coupled thermal-hygric characterisation of elastic behaviour for soft and porous limestone. Construction and Building Materials, 62, pp 28–37.

Al-Omari A., Brunetaud, X., Beck K., and Al-Mukhtar M. (2014c): Hygrothermal stress and damage risk in the stones of the Castle of Chambord-France. International Journal of Civil and Structural Engineering, 4(3), 402–418.

Alsadik B., Gerke M., Vosselman G. (2013): Automated camera network design for 3D modeling of cultural heritage objects. Journal of Cultural Heritage, 14, 515–526.

Amoroso G. G., Fassina V. (1983): Stone decay and conservation. Materials Science Monograph. vol. II. Elsevier, Amsterdam.

Angeli M. (2007): Multiscale study of stone decay by salt crystallization in porous networks. PhD thesis, University of Cergy-Pontoise, France.

Angeli M., Hébert R., Menéndez B., David C., Bigas J.-P. (2010): Influence of temperature and salt concentration on the salt weathering of a sedimentary stone with sodium sulphate. Engineering geology, 115, pp 193–199.

Anon. (1979): Classification of rocks and soils for engineering geological mapping. Part 1-Rock and soil materials. Bull Int. Assoc. Geo., vol. 19, pp. 364-371.

ASTM, (2004): Standard Test Method for Evaluation of Durability of Rock for Erosion Control Under Freezing and Thawing Conditions. Standard D5312-04.

Baptista Neto J. A., Smith B. J., McAlister J. J., Silva M. A. M., Silva A. L. C. (2011): Salt weathering of historic building stones in Rio de Janeiro central area: a case study of the São Francisco de Paula Church. Salt Weathering on Buildings and Stone Sculptures (SWBSS), 19-22 October, Limassol, Cyprus, 113–120.

Bayram F., (2012): Predicting mechanical strength loss of natural stones after freeze–thaw in cold regions. Cold Regions Science and Technology, 83-84, pp 98–102.

Beck K. (2006): Etude des propriétés hydriques et des mécanismes d'altération de pierres calcaires à forte porosité. Ph.D. Thesis. University of Orleans, France.

Beck K., Al-Mukhtar M. (2010): Weathering effects in an urban environment: a case study of tuffeau, a French porous limestone. Geological Sociality London, Special Publication, 331, pp 103–111.

Beck K., Al-Mukhtar M. (2014): Cyclic wetting-drying ageing test and patina formation on tuffeau limestone. Environmental Earth Science, 71 (5), pp 2361–2372.

Beck K., Al-Mukhtar M., Rozenbaum O., Rautureau M. (2003): Characterisation, water transfer properties and deterioration in tuffeau: Building material in the Loire Valley, France. International Journal of Building and Environment, 38 (9), pp1151–1162.

Benavente D., Cultrone G., Gomez-Heras M. (2008): The combined influence of mineralogical, hygric and thermal properties on the durability of porous building stones. European Journal Mineral, 20, pp 673–685.

Blyth F. G. H. (1971): A Geology for Engineers, Fifth Edition, Edulard Arnold, Ltd London.

Bonazza A., Messina P., Sabbioni C., Grossi C. M., Brimblecombe P. (2009a): Mapping the impact of climate change on surface recession of carbonate buildings in Europe. Science of the Total Environ, 407, pp 2039–2050.

Bonazza A., Sabbioni C., Messina P., Guaraldi C., De Nuntiis P. (2009b): Climate change impact: mapping thermal stress on Carrara marble in Europe. Science of the Total Environ, 407, pp 4506–4512.

Brunetaud X, Stefani C, Janvier-Badosa S, Beck K, Al-Mukhtar M. (2012a): Comparison between photomodeling and laser scanning to create a 3D model for a digital health record. European Journal of Environmental and Civil Engineering, 16(sup1), pp s48–s63.

Brunetaud X., De Luca L., Janvier-Badosa S., Beck K., Al-Mukhtar M. (2012b): Application of digital techniques in monument preservation. European Journal of Environmental and Civil Engineering, 16(5), pp 543–56.

Cabrelles M., Seguí A. E., Navarro S., Galcerá S., Portalés C., Lerma J. L. (2010): 3D photorealistic modeling of stone monuments by dense image matching. International Archives of Photogrammetry, Remote Sensing and Spatial Information Sciences, vol. XXXVIII, Part 5 Commission V Symposium, Newcastle upon Tyne, UK, pp 121–124.

Camuffo D. (1998): Microclimate for cultural heritage. Elsevier, Amsterdam.

Camuffo D., Sturaro G. (2001): The climate of Rome and its action on monument decay. Climate Research, 16, pp145–155.

Chen T. C., Yeung M. R., Mori N. (2004): Effect of water saturation on deterioration of welded tuff due to freeze-thaw action. Cold Regions Science and Technology, 38, pp 127–136.

Colas E., Mertz J. D., Thomachot-Schneider C., Barbin V., Rassineux F. (2011): Influence of the clay coating properties on the dilation behavior of sandstones. Applied Clay Science, 52(3), pp 245–252.

Connors K. A. (1990): Chemical Kinetics: The Study of Reaction Rates in Solution. John Wiley and Sons, VCH.

Crucifix M. (2009): Vegetation and Climate Variability: A Couple Model Study. Richard and Cox: London, U.K. 5-6.

Dahlin E. (2000): Preventive Conservation Strategies for Organic Objects in Museums, Historic Buildings, and Archives, Damage assessment–causes-mechanisms and measurements, pp 57–60.

Dessandier D. (1995): Etude du milieu poreux et des propriétés de transfert des fluides du tuffeau blanc de Touraine. Application à la durabilité des pierres en oeuvre. PhD thesis, University of Tours, France.

Docampo S., Trigo M. M., Recio M., Melgar M., García-Sánchez J., Cabezudo B. (2011): Fungal spore content of the atmosphere of the Cave of Nerja (southern Spain): Diversity and origin. Science of the Total Environment, 409, pp 835–843.

Duthie L. J. (2011): The impact of climate change on blond sandstone decay in Glasgow. PhD thesis, University of Glasgow, United Kingdom.

Fagerlund G. (1977a): The critical degree of saturation method of assessing the freeze-thaw resistance of concrete. Materials And Structures, 10 (58), pp 217–229.

Fagerlund G. (1977b): The international cooperative test of the critical degree of saturation method of assessing the freeze/thaw resistance of concrete. Materials and Structures, 10(58), pp 231–253.

Gómez-Bolea A., Llop E., Ariñob X., Saiz-Jimenezc C., Bonazzad A., Messinad P., Sabbionid C. (2012): Mapping the impact of climate change on biomass accumulation on stone. Journal of cultural heritage, 13, pp 254–258.

Goudie A. S. (1999): A comparison of the relative resistance of limestones to frost and salt weathering. Permafrost and Periglacial Processes, 10, pp 309–316.

Hawkins A. B. (1998): Aspects of rock strength. Bulletin of Engineering Geology and the Environment. 57(1), 17–30.

Horemans B., Cardell C., Bencs L., Kontozova-Deutsch V., De Wael K., Van Grieken R. (2011): Evaluation of airborne particles at the Alhambra monument in Granada, Spain. Microchemical Journal, 99, pp 429–438.

Hosono T., Uchida E., Suda C., Ueno A., Nakagawa T. (2006): Salt weathering of sandstone at the Angkor monuments, Cambodia: identification of the origins of salts using sulfur and strontium isotopes. Journal of Archaeological Science, 33, pp 1541–1551.

ICOMOS–ISCS (2008): Illustrated glossary on stone deterioration patterns. Available on line:http://international.icomos.org/publications/monuments_and_sites/15/pdf/Monuments_and_Sites_15_ISCS_Glossary_Stone.pdf.

Jamshidi A., Nikudel M. R., Khamehchiyan M. (2013): Predicting the long-term durability of building stones against freeze–thaw using a decay function model. Cold region science and technology, 92, pp 29–36.

Janvier-Badosa S, Beck K., Brunetaud X., Al-Mukhtar M. (2013a): The occurrence of gypsum in the scaling of stones at the Castle of Chambord (France). Journal of Environmental Earth Sciences, DOI: 10.1007/s12665-013-2865-2.

Janvier-Badosa S. (2012): Le carnet de sante´ d'un monument, application au château de Chambord, French Ph-D thesis, University of Orléans, France.

Janvier-Badosa S., Beck K., Brunetaud X., Al-Mukhtar M. (2010): Characterization of stone weathering: A case study for Chambord Castle, France. In: 8th international symposium on the conservation of monuments in the Mediterranean Basin, Patras.

Janvier-Badosa S., Beck K., Brunetaud X., Al-Mukhtar M. (2013b): Historical study of Chambord castle: basis for establishing the monument health record. International Journal of Architectural Heritage, 7, pp 247–260.

Janvier-Badosa S., Stefani C., Brunetaud X., Beck K., De Luca L., Al-Mukhtar M. (2013c): Documentation and analysis of 3D mappings for monument diagnosis. Proceedings of International Conference on Built heritage, Milano, Italy, pp 710–718.

Jassim S. Z., Goff J. C. (2006): Geology of Iraq. Dolin, Prague and Moravian Museum, Czech Republic, Brno.

Kahraman S. (2002): Estimating the direct P-wave velocity value of intact rock from indirect laboratory measurements. International journal of rock mechanics and mining sciences, 39, pp 101–104.

Kaplan Ç. D., Murtezaoğlu F., İpekoğlu B., Böke H. (2013): Weathering of andesite monuments in archaeological sites. Journal of Cultural Heritage, 145, pp e77-e83.

Koch A., Siegesmund S. (2004): The combined effect of moisture and temperature on the anomalous expansion behaviour of marble. Environmental Geology, 46(3-4), pp 350–363.

Kuchitsu N., Ishizaki T., Nishiura T. (1999): Salt weathering of the brick monuments in Ayutthaya, Thailand. Engineering Geology, 55, pp 91–99.

La Iglesia A., Garcia del Cura M. A., Ordoñez S. (1994): The physicochemical weathering of monumental dolostones, granites and limestones; dimension stones of the Cathedral of Toledo (Spain). Science of the Total Environment, 152, pp 179–188.

Layard A. H. (1849): Nineveh and Its Remains, 2 Vols, London, John Murray.

Li W., Pour-Ghaz M., Castro J., Weiss J. (2012): Water absorption and critical degree of saturation relating to freeze-thaw damage in concrete pavement joints. Journal of Materials in Civil Engineering, 24, pp 299–307.

Lion M., Skoczylas F., Ledesert B. (2005): Effects of heating on the hydraulic and poroelastic properties of bourgogne limestone. International Journal of Rock Mechanics and Mining Sciences, 42, pp 805–520.

Lopez-Arce P., Doehne E., Martin W., Pinchin S. (2008): Magnesium sulfate salts and historic building materials: experimental simulation of limestone flaking by relative humidity cycling and crystallization of salts. Materiales de Construcción, 58, pp 125–142.

Lopez-Arce P., Garcia-Guinea J. (2005): Weathering traces in ancient bricks from historic buildings. Building and Environment, 40, pp 929–941.

López-Arce P., Garcia-Guinea J., Benavente D., Tormo L., Doehne E. (2009): Deterioration of dolostone by magnesium sulphate salt: an example of incompatible building materials at Bonaval Monastery, Spain. Construction and Building Materials, 23(2), pp 846–855.

Ludovico-Marques M., Chastre C. (2012): Effect of salt crystallization ageing on the compressive behavior of sandstone blocks in historical buildings. Engineering Failure Analysis, 26, pp 247–257.

Mallowan M. E. L. (1966): Nimrud and its Remains. 3 Vols, British School of Archaeology in Iraq.

Maravelaki-Kalaitzaki P., Biscontin G. (1999): Origin, characteristics and morphology of weathering crusts on Istria stone in Venice. Atmospheric Environment, 33, pp 1699–1709.

McMahon D. J., Sandberg P., Folliard K., Mehta P. K. (1992): Deterioration mechanisms of sodium sulfate, in JD Rodrigues, F Henriques, FT Jeremisas (eds), International Congress on Deterioration and Conservation of Stone, 705–714. Lisbon: Laboratorio Nacional de Engenharia Civil.

Miller A.Z., Sanmartin P., Pereira-Pardo L., Dionísio A., Saiz-Jimenez C., Macedo M. F., Prieto B. (2012): Bioreceptivity of building stones: A review. Science of the Total Environment, 426, pp 1–12.

Mishra A. K., Jain K. K., Garg K. L. (1995): Role of higher plants in the deterioration of historic buildings. Science of the Total Environment, 167, pp 375–392.

Moropoulou A., Theoulakis P., Chrysophakis T. (1995): Correlation between stone weathering and environmental factors in marine atmosphere. Atmospheric Engineering, 29, 895–903.

Mutlutűk M., Altindag R., Tűrk G. (2004): A decay function model for the integrity loss of rock when subjected to recurrent cycles of freezing–thawing and heating– cooling. International Journal of Rock Mechanics and Mining Science, 41 (2), pp 237–244.

Nakamura Y. (1996): Experimental study of rock deterioration and weathering. Tsuchi To Kiso, JSSMFE, 44 (9), pp 55– 60.

National Oceanographic Data Center: Iraq climatological data, http://docs.lib.noaa.gov/rescue/data_rescue_iraq.html.

Norme AFNOR (2002): Référence NF P94-411. Roches - Détermination de la vitesse de propagation des ondes ultrasonores en laboratoire. 7 p.

Norme AFNOR. (2000): Référence NF P94-420. Détermination de la résistance à la compression uniaxiale. 7 p.

Norme AFNOR. (2001): Référence NF P94-422. Détermination de la résistance à la traction. Méthode indirecte – Essai brésilien. 7 p.

Oates D. (1968): Studies in the Ancient History of Northern Iraq. London, Oxford University Press.

Oates J., Oates D. (2001): Nimrud an Assyrian imperial city revealed. British School of Archaeology in Iraq.

Pavlidis G., Koutsoudis A., Arnaoutoglou F., Tsioukas F., Chamzas C. (2007): Methods for 3D digitization of cultural heritage. Journal of Cultural Heritage, 8, pp 93–98.

Ponziani D, Ferrero E, Appolonia L, Migliorini S. (2012): Effects of temperature and humidity excursions and wind exposure on the arch of Augustus in Aosta. Journal of Cultural Heritage, 13, pp 462–468.

Powers T. C. (1945): A working hypothesis for further studies of frost resistance of concrete. ACI journal Proceedings, 41(3), pp 245–272.

Price C., Brimblecombe P., (1994): Preventing salt damage in porous materials. In: ROY, A. & SMITH, P. (eds) Preprints of the Contributions to the Ottawa Congress, Preventive Conservation – Practice, Theory and Research. IIC, London, pp 90–93.

Prick A. (1995): Dilatometrical behaviour of porous calcareous rock samples subjected to freeze-thaw cycles. Catena, (25), pp 7–20.

Prick A., (1997): Critical degree of saturation as a threshold moisture level in frost weathering of limestones. Permafrost and Periglacial Processes, 8, pp 91–99.

Rautureau M. (2001): Tendre comme la pierre, collective book, directed by Michel Rautureau. ed Conseil Re´gional Centre and University of Orleans.

Reads J. (2002): Nineteenth-century Nimrud: motivation, orientation, conservation. In New Lights on Nimrud, (Eds.) John E. Curtis, Henrietta McCall, Dominique Collon and Lamia al- Gailani Werr, Proceedings of the Nimrud Conference, 11th–13th March 2002, London: British Museum Press.

RILEM Recommendations (1984): Absorption of Water by Immersion under Vacuum. Materials and Structures, RILEM CPC 11.3, 101, pp 393–394.

Sebastián E., Cultrone G., Benavente D., Fernandez L. L., Elert K., Rodriguez-Navarro C. (2008): Swelling damage in clay-rich sandstones used in the church of San Mateo in Tarifa (Spain). Journal of Cultural Heritage, 9, pp 66–76.

Selby M. J. (1993): Hillslope materials and processes, Oxford, UK, Oxford University Press.

Siegesmund S., Dürrast H. (2011): Physical and Mechanical Properties of Rocks, [in:] S. Siegesmund, R. Snethlage (eds.), Stone in Architecture, Properties, Durability, 4th ed., Springer-Verlag, Berlin–Heidelberg, Germany, pp 97–225.

Šperl J., Trčková J. (2008): Permeability and porosity of rocks and their relationship based on laboratory testing. Acta Geodyn. Geomater., 5(1), pp 41–47.

Stefani C., Brunetaudb X., Janvier-Badosab S., Beckc K., De Luca L., Al-Mukhtar M. (2014): Developing a toolkit for mapping and displaying stone alteration on a web-based documentation platform. Journal of Cultural Heritage, 15, pp 1–9.

Sterflinger K. (2010): Fungi: Their role in deterioration of cultural heritage, Fungal Biology Reviews, 24, pp 47–55.

Thomachot, C. & Matsuoka, N. (2007): Dilation of building materials submitted to frost action. In: PI~IKRYL, R. & SMITH, B. J. (eds) Building Stone Decay: From Diagnosis to Conservation. Geological Society, London, Special Publications, 271, pp 167–178.

Torfs K., Van Grieken R. (1997): chemical relations between atmospheric aerosols, deposition and stone decay layers on historic buildings at the Mediterranean coast. Atmospheric Environment, 31(15), pp 2179–2192.

Török A., Vásárhelyi B. (2010): The influence of fabric and water content on selected rock mechanical parameters of travertine, examples from Hungary. Engineering Geology, 115, pp 237–245.

Tsui N., Flatt R. J., Scherer G. W. (2003): Crystallization damage by sodium sulfate. Journal of Cultural Heritage, 4, pp 109–115.

Uchida E., Ogawa Y., Maeda N., Nakagawa T. (1999): Deterioration of stone materials in the Angkor monuments, Cambodia. Engineering Geology, 55, pp 101–112.

Van T. T., Beck K., AL-Mukhtar M. (2007): Accelerated weathering tests on two highly porous limestones. Environmental Geology, pp 52: 283–292.

Vásárhelyi B. (2003): Some observation regarding the strength and deformability of sandstones in case of dry and saturated conditions. Bulletin of Engineering Geology and the Environment. 62, pp 245–249.

Vázquez M. A., Galán E., Guerrero M. A., Ortiz P. (2011): Digital image processing of weathered stone caused by efflorescences: A tool for mapping and evaluation of stone decay. Construction and Building Materials, 25, pp 1603–1611.

Vázquez P., Alonso F. J., Carrizo L., Molina E., Cultrone G., Blanco M., Zamora I. (2013): Evaluation of the petrophysical properties of sedimentary building stones in order to establish quality criteria. Construction and Building Materials, 41 pp 868–878.

Viles H. A. (2005): Microclimate and weathering in the central Namib Desert, Namibia. Geomorphology, 67, pp 189–209.

Warke P. A., McKinley J., Smith B. J. (2006): Variable weathering response in sandstone: factors controlling decay sequences. Earth Surface Processes and Landforms, 31, pp 715–735.

Warke P. A., Smith B. J. (1994): Short-term rock temperature fluctuations under simulated hot desert conditions: Some preliminary data. IN ROBINSON, D. and WILLIAMS, R. (Eds.) Rock Weathering and Landform Evolution. J. Wiley & Sons, Chichester, pp 57–70.

Warke P. A., Smith B. J. (1998): Effects of direct and indirect heating on the validity of rock weathering simulation studies and durability tests. Geomorphology, 22, pp 347–357.

Watt D., Colston B. (2000): Investigating the effects of humidity and salt crystallisation on medieval masonry. Building and Environment, 35, pp 737–749.

Weiss G. (1992): Die Eis-und Salzkristallisation im Porenraum von Sandsteinen und ihre Auswirkungen auf das Gefüge unter besonderer Berücksichtigung gesteinsspezifischer Parameter. Münchner Geowiss Abh, 9, pp 1–118..

Weiss T., Siegesmund S., Kirchner D., Sippel J. (2004): Insolation weathering and hygric dilatation: two competitive factors in stone degradation. Environmental Geology, 46(3-4), pp 402–413.

Welton R. G. (2003): Algal degradation of natural stone masonry: implication for conservation and construction, PhD thesis, University of Paisley, United Kingdom.

William A. C. (1967): Freezing and Thawing of Concrete: Mechanisms and Control. American Concrete Institute, pp. 29– 30.

Yasar E., Erdogan Y. (2004): Correlating sound velocity with the density, compressive strength and Young's modulus of carbonate rocks. International Journal of Rock & Mining Sciences, 41, pp 871–875.

Yavuz A. B., Topal T. (2007): Thermal and salt crystallization effects on marble deterioration: Examples from Western Anatolia, Turkey. Engineering Geology, 90, pp 30–40.

Yavuz H., Altindag R., Sarac S., Ugur I., Sengun N. (2006): Estimating the index properties of deteriorated carbonate rocks due to freeze–thaw and thermal shock weathering. International Journal of Rock Mechanics & Mining Sciences, 43, pp 767–775.

Yu S., Oguchi C. T. (2010): Role of pore size distribution in salt uptake, damage, and predicting salt susceptibility of eight types of Japanese building stones. Engineering Geology, 115, pp 226–236.

Zeisig A., Siegesmund S., Weiss T. (2002): Thermal expansion and its control on the durability of marbles. Geological Society, London, Special Publications, 205, pp 65–80.

Zucconi L., Gagliardi M., Isola D., Onofri S., Andaloro M. C., Pelosi C., Pogliani P., Selbmann L. (2012): Biodeterioration agents dwelling in or on the wall paintings of the Holy Saviour's cave (Vallerano, Italy). International Biodeterioration & Biodegradation, 70, pp 40–46.

List of publications resulting from this PhD research

List of publication resulting from this PhD research

International Journal

1. Al-Omari A., Brunetaud X., Beck K., Al-Mukhtar M. (2014): Effect of thermal stress, condensation and freezing–thawing action on the degradation of stones on the Castle of Chambord, France. Environmental earth science, 71(9), pp 3977–3989.
2. Al-Omari A., Brunetaud, X., Beck K., Al-Mukhtar M. (2014): Coupled thermal-hygric characterisation of elastic behaviour for soft and porous limestone. Construction and Building Materials, 62, pp 28–37.
3. Al-Omari A., Brunetaud, X., Beck K., Al-Mukhtar M. (2014): Hygrothermal stress and damage risk in the stones of the Castle of Chambord-France. International Journal of Civil and Structural Engineering, 4(3), 402–418.
4. Al-Omari A., Brunetaud, X., Beck K., Török Á., Al-Mukhtar M. Critical degree of saturation: A control factor of freeze-thaw damage of porous limestones at Castle of Chambord, France. Engineering Geology (Accepted with minor revision).
5. Al-Omari A., Beck K., Brunetaud, X., and Al-Mukhtar M. Weathering of limestone on Al-Ziggurat walls in the ancient Al-Nimrud city (Iraq). Submitted to International Journal Environmental earth science. (Submitted in April 2014).
6. Al-Omari A., Brunetaud, X., Beck K., Al-Mukhtar M. Preliminary digital health record of limestone in Al-Ziggurat, Al-Nimrud city, Iraq. Submitted to International Journal of Cultural Heritage. (Submitted in May 2014)

International conferences

1. Al-Omari A., Brunetaud X., Beck K., Al-Mukhtar M. (2013): Experimental study on the role of freezing–thawing in the degradation of stones in the Castle of Chambord. Proceedings of International Conference on Built heritage, Monitoring Conservation Management, 18-20 November, Milan, Italy, pp 1352–1358.
2. Al-Omari A., Beck K., Brunetaud, X., Al-Mukhtar M. (2014): Evaluation of durability/compatibility of two building stones based on their petrophysical and mechanical properties. International Civil Engineering and Architecture Symposium for Academicians, 17-20 May, Antalya, Turkey.
3. Al-Omari A., Beck K., Brunetaud, X., Khattab S., Ali H., Al-Mukhtar M. (2014): Characterisation of the decayed stones of Al-Ziggurat wall in Al-Nimrud city. 9th International Symposium on the Conservation of Monuments in the Mediterranean Basin, IMPROVEMENTS IN CONSERVATION AND REHABILITATION – INTEGRATED METHODOLOGIES, 3-5 June, Ankara, Turkey.

National conferences

1. Al-Omari A., Brunetaud X., Beck K., Al-Mukhtar M. (2012): Climatic condition and limestone decay in Al-Namrud monuments: Review and Discussion. IEEE conference publication, Engineering Sciences (FNCES), 2012 First National Conference for Engineering Sciences, 7-8 November, Baghdad, Iraq, DOI: 10.1109/NCES.2012.6740455.
2. Al-Omari A., Brunetaud X., Beck K., Al-Mukhtar M. (2013): Effect of environmental conditions on the degradation of stones in the Castle of Chambord. 31èmes Rencontres de l'AUGC, E.N.S., 29-31 May, Cachan, Paris, France.
3. Al-Omari A., Brunetaud X., Beck K., Al-Mukhtar M. Coupled thermal-hydraulic characterisation of strain variation for soft and porous limestone, 32èmes Rencontres de l'AUGC, E.N.S., 4-6 June, Orleans, France.
4. Al-Omari A., Beck K., Brunetaud X., Al-Mukhtar M. Caractérisation de la dégradation des pierres de la ziggurat du site archéologique de la cité Al-Nimrud en Irak, 32èmes Rencontres de l'AUGC, E.N.S., 4-6 June, Orleans, France.

Appendixes

Appendix 1

Paper No. 1: Published in International Journal of Environmental Earth Science

"Effect of thermal stress, condensation and freezing–thawing action n the degradation of stones on the Castle of Chambord, France"

Appendix 2

Paper No. 2: Published in International Journal of Construction and Building Materials

"Coupled thermal–hygric characterisation of elastic behaviour for soft and porous limestone"

Appendix 3

Paper No. 3: - Published in International Journal of Civil and Structural Engineering

"Hygrothermal stress and damage risk in the stones of the Castle of Chambord-France"

Appendix 4

Paper No. 4: Accepted with minor revision in International Journal of Engineering Geology

"Critical degree of saturation: A control factor of freeze-thaw damage of porous limestones at Castle of Chambord, France"

Appendix 1

Environ Earth Sci (2014) 71:3977–3989
DOI 10.1007/s12665-013-2782-4

ORIGINAL ARTICLE

Effect of thermal stress, condensation and freezing–thawing action on the degradation of stones on the Castle of Chambord, France

Asaad Al-Omari · Xavier Brunetaud · Kevin Beck · Muzahim Al-Mukhtar

Received: 21 April 2013 / Accepted: 28 August 2013 / Published online: 13 September 2013

Abstract This work consists in estimating the role of climatic conditions in the degradation of two French limestones, tuffeau and Richemont stone, used in the construction and the restoration of the Castle of Chambord, the largest castle in the Loire Valley, France. Meteorological data, air temperature, air relative humidity and rainfall were statistically analysed in combination with stone data from thermal–humidity sensors inserted into the walls. The climatic conditions of the surrounding area were described to assess their role in enhancing the degradation of the stones through three weathering processes: thermal stress, condensation and freezing–thawing. The damage risks due to the weathering processes were taken into account not only through the bulk effects on the stone surfaces, but also their effects were extended to investigate the damage that occurs within the porous structure of the stone. Field observations showed that the main patterns of degradation affecting the stones of the castle are biological colonization and stone detachment in the form of stone spalling and exfoliation. The results of the analysis show that there is no risk of damage to the stones due to thermal stress. Moreover, the two stones experience similar overall trends against freezing–thawing processes. Finally, this study clearly highlights the important role of condensation in the degradation of the stones of the castle.

A. Al-Omari · X. Brunetaud · K. Beck · M. Al-Mukhtar (✉)
Universite d'Orléans, CNRS, CRMD FRE 3520, 1b rue de la Férollerie, 45071 Orleans Cedex 2, France
e-mail: muzahim.al-mukhtar@univ-orleans.fr

A. Al-Omari
Department of Civil Engineering, College of Engineering, Mosul University, Al-Majmooah Street, Mosul, Iraq

Keywords Thermal stress · Condensation · Freezing–thawing · Weathering processes · Climatic conditions · Stonework

Introduction

The main construction units for cultural-historic buildings, temples and monuments are stones. Moreover, stones have been used as an architectural feature, trim, ornament or facing for buildings or other structures. Pope et al. (2002) used the term cultural stones for "the stone that has been physically altered by humans—abraded, engraved, quarried, chipped or chiselled, or dressed".

The preservation of historical monuments is not only considered as a cultural requirement, but also a scientific challenge; that is why, in the last few decades, considerable attention has been paid to studying the mechanisms that lead to the decay of built heritage and, therefore, to the stones used for construction. The weathering processes that cause monument degradation involve physical weathering due to mechanical stresses, such as stresses induced by freezing, thermal stress, salt crystallization and pollution. Moreover, chemical weathering results from changes in chemical and mineralogical composition. Finally, biological weathering, once triggered by the appropriate outdoor environment, including humid air and mild temperatures, promotes the growth of simple living organisms (e.g. fungi, lichen, bacteria and algae) on the outer surfaces of stones.

These weathering processes are related to the surrounding climatic conditions. In polar or hot desert environments, physical weathering processes may be considered to be the most common factors that control stone deterioration; in contrast, in the warm and wet regions, the effects of chemical and biological weathering processes are expected

to be dominant. The effect of climatic and environmental conditions on the decay processes of stone building materials has already been the object of previous studies (Bonazza et al. 2009a, b; Camuffo and Sturaro 2001; Eklund 2008; Hoxha et al. 2010; Moropoulou et al. 1995; Ponziani et al. 2012; Van et al. 2007; Viles 2005).

The seasonal, daily and even hourly variations in climatic conditions, air temperature and air humidity play an important role in the decay of stone and could generate damage by fatigue. The estimation of damage risk related to the degradation of stones in the Castle of Chambord, due to the variation in climatic conditions through the weathering process of thermal stress, condensation and freezing–thawing action, has never before been studied. This paper aims to provide quantitative information that will help in understanding the degradation of two types of limestones, tuffeau and Richemont stone, used in the Castle of Chambord. The present work involves analysing meteorological elements together with the measured stone temperature and stone relative humidity in an attempt to assess the role of climatic conditions in the stones' degradation. Climatic conditions were analysed using data collected over more than 40 years from the meteorological station nearest to the castle and from a meteorological station installed on the roof of the east tower of the castle. The second set of data includes the measured stone temperature and relative humidity using thermal–humidity sensors inserted into the walls of the same tower. The study consists of not only observing the effects of weathering processes on the external surfaces of stone walls, but also in taking into account those processes that happen within the porous structure of the stone.

The Castle of Chambord: site, stones and degradation of stones

The Castle of Chambord, built in 1519, is the largest castle in the Loire Valley, France, and has been part of the UNESCO World Heritage list since 2000. It is located in a rural area at a distance of about 50 km to the south-west of Orleans, at latitude 47°36′N, longitude 1°31′E, with an average elevation of about 84 m above sea level. This study is focused on the behaviour of stones located in the east tower, which has been only slightly restored and monitored for several years using thermal–humidity sensors and a weather station.

Tuffeau was the main building material used in the construction of not only the Castle of Chambord, but also many other French ancient buildings, including the famous castles of the Loire Valley. This soft limestone is very fragile and has low compressive strength. That is why a harder stone "Beauce limestone" was used for the construction of the foundations of the castle (Janvier-Badosa et al. 2013). However, the particular properties of tuffeau, including its fine grain and its homogeneous white colour, meant it was commonly used for superstructures, including ornamented walls. During limited periods of the early twentieth century, the limestone named "Richemont stone" was used in the restoration of the tuffeau walls, where the degraded stones had to be replaced. For the east tower of the Castle of Chambord, tuffeau represents 80 % of the stones, whereas Richemont stone is limited to only 20 % (Janvier-Badosa et al. 2013). Neither tuffeau nor Richemont stone have a specific location on the walls of the castle.

The characterization of the studied stone was achieved using complementary laboratory techniques: X-ray diffraction tests (XRD), chemical analysis and thermo-gravimetric analysis (ATG), together with scanning electron microscopy (SEM). The pore size distribution was obtained by mercury intrusion porosimetry (MIP) testing. The engineering properties, Young's modulus, Poisson's ratio and unconfined compressive strength of the two stones in a dry state were measured using an Instron 4485 press machine. The thermal expansion of the stones was measured using a digital dial gauge. Moreover, the vacuum saturation method was used to measure the stones' physical properties; total porosity, dry density and skeleton density.

Table 1 Main physical and thermo-hydro-mechanical properties of the two studied stones

Stone property	Stone type	
	Tuffeau	Richemont stone
Mineralogical composition	Calcite ≈ 50 % Quartz ≈ 10 % Opal CT ≈ 30 % Clays and micas ≈ 10 %	Calcite ≈ 95 % Quartz ≈ 5 %
Skeleton density (g/cm^3)	2.57 ± 0.01	2.71 ± 0.01
Bulk dry density (g/cm^3)	1.30 ± 0.02	1.94 ± 0.01
Total porosity (%)	45.0 ± 0.52	29.5 ± 0.54
Unconfined compressive strength (MPa)	11.67 ± 0.33	19.41 ± 1.03
Young modulus (MPa)	3482 ± 20	14962 ± 233
Poisson's ratio (%)	0.207 ± 0.005	0.231 ± 0.004
Linear thermal expansion coefficient (K^{-1})	(8.41 ± 0.12)E−06	(5.84 ± 0.04)E−06
Water retention as a degree of saturation (%) at:		
33 % RH	2.63	0.42
56 % RH	3.62	0.68
76 % RH	6.81	1.55
98 % RH	22.89	3.94

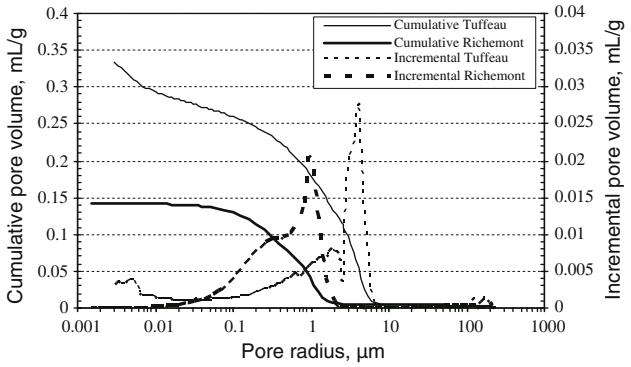

Fig. 1 Pore size distribution for the two studied stones

Table 1 summarizes all the measured physical and thermo-hydro-mechanical properties of the two stones.

In the present work, the two porous limestones, tuffeau and Richemont stone, used in the construction and conservation of the Castle of Chambord are considered. Tuffeau is composed of calcite, quartz, opal (cristobalite/tridymite) and clay–mica minerals, while the Richemont stone is mainly composed of calcite with a low percentage of quartz. Figure 1 shows the results of porosimetry: the tuffeau matrix is composed of a wide range of pore access radii, between 0.003 µm and 10 µm, while they are between 0.01 and 2 µm for Richemont stone. Tuffeau, white-light beige in colour, and Richemont stone, light beige, are greenish and reddish in colour, respectively, after wetting. Tuffeau is a lightweight material with high total porosity compared with Richemont stone.

The two stones differ in terms of the clay mineral content and the fineness of the pores, explaining the different amounts of moisture absorbed by the stones when exposed to high humidity conditions. The degrees of saturation of tuffeau and Richemont stone resulting from exposure at different relative humidities are given in Table 1. The water retention capacity of tuffeau is always much higher than that of Richemont stone. This suggests that tuffeau may be more subjected to degradation due to water transport than Richemont stone.

Several studies concerning the Castle of Chambord were carried out: either from the perspective of historical study (Janvier-Badosa et al. 2013), to identify the types of stone degradation (Beck and Al-Mukhtar 2005; Janvier-Badosa et al. 2010) or for the scientific monitoring and planning of restoration works using new digital techniques (Brunetaud et al. 2012a, b). However, field observations (Fig. 2) indicated that there were two main patterns of alteration including the stones of the Castle of Chambord; biological colonization (different types of lichens and mosses) and stone detachment in the form of stone spalling and exfoliation.

The Castle of Chambord: climatic conditions, temperature and relative humidity data

The Castle of Chambord is located in an area that experiences a mild humid temperate climate with moderately warm summers and no dry season. According to meteorological data, for the period 1997–2012, gathered from Bricy Air Base weather station (Orléans, France), the nearest station to the Castle of Chambord, the temperature typically varies from 0 to 26 °C and is rarely below −5 °C or above 31 °C. The relative humidity typically ranges from 45 to 98 %, rarely dropping below 30 % and reaching as high as 100 %. Precipitation is most likely around December, occurring on 48 % of days, while it is least likely around August, occurring on 28 % of days. Typical wind speeds vary from 1 to 7 m/s, rarely exceeding 11 m/s.

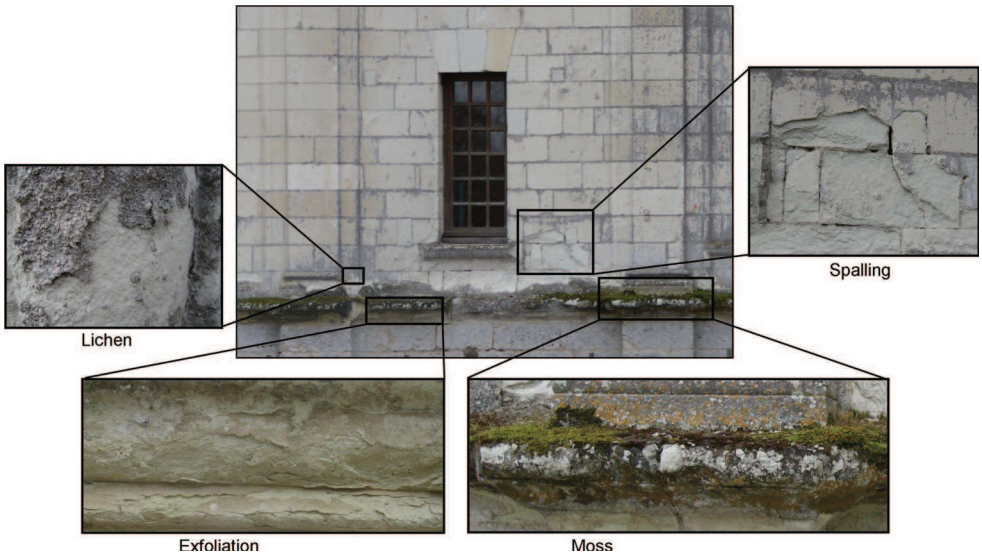

Fig. 2 Types of degradation of stones observed in the north wall of the east tower

The possibility of snow falling is highest around February, occurring on 7 % of days. This climate represents a typical environment that promotes physico-chemical weathering processes.

To estimate the risk of damage to the stones due to the variations in climatic conditions, two sets of data were acquired and analysed. The first relates to meteorological data: air temperature, air relative humidity and rainfall were recorded every 5 min for about 17 months, from April 2010 to August 2011, using the meteorological station installed on the roof of the east tower of the castle. The second set of data includes the stone temperature and relative humidity. They were measured using thermal–humidity sensors inserted into the walls of the same tower. A total of 16 sensors were set up in two directions (north and south) at three different levels (top, middle and bottom, i.e. 2 m; 5 and 8 m), on the surface and at different depths inside the stones (15, 30, 50 and 250 mm). These data were measured every 30 min for 3 years, from June 2009 to June 2012, and provide comprehensive information on the changes in temperature and moisture both on the surface and inside the stones. Figure 3 shows the east tower with a meteorological station on its roof and the sensors installed at different positions on the walls. The east tower is much damaged by weathering and has been only slightly restored (Janvier-Badosa et al. 2013). Thus, this tower represents an interesting case for the study of the relationship between climate data and stone weathering.

Data analysis and discussion

The meteorological data, air temperature and air relative humidity, for the period 1973–2012 obtained from Bricy weather station, were analysed and compared with meteorological data obtained from the local weather station placed on the roof of the east tower of the castle. Figure 4 presents the monthly variations in mean maximum and mean minimum, both of air temperature and air relative humidity for the two periods 2010–2011 and 1973–2012. These evolutions for the two different periods are similar. Therefore, the data acquired in situ during the period 2010–2011 can be considered as representative of the local climatic conditions in the studied area.

In the present work, the methodologies followed to assess the risk of damage to the stones due to weathering can be summarized as follows:

- Analysis of the daily variation in stone surface temperature was used to assess the role of thermal stress.
- Analysis of air temperature and relative humidity was linked with analysis of stone surface temperature in an attempt to estimate the risk of physical weathering damage due to freezing and condensation on the stone surface.
- The measured values of temperature and relative humidity at different depths inside the stones together with the characterization of the pore size distribution of the studied stones were analysed to investigate the frequencies of freezing and of condensation events within the porous structure of the stones.

Daily variation in stone/air temperature and thermal stress

The stone surface temperature (SST) of the two wall directions, north and south, of the east tower is characterized with seasonal variations over the year. Table 2 presents the extreme values of SST over 3 years, from June 2009 to June 2012. In the hot summer months, June, July and August, the SST exceeds 27 °C for the north wall, and in the case of the south wall it exceeds 34 °C. In the cold months, November to February, the temperature falls

Fig. 3 The meteorological station above the east tower and the sensors positioned on the south wall

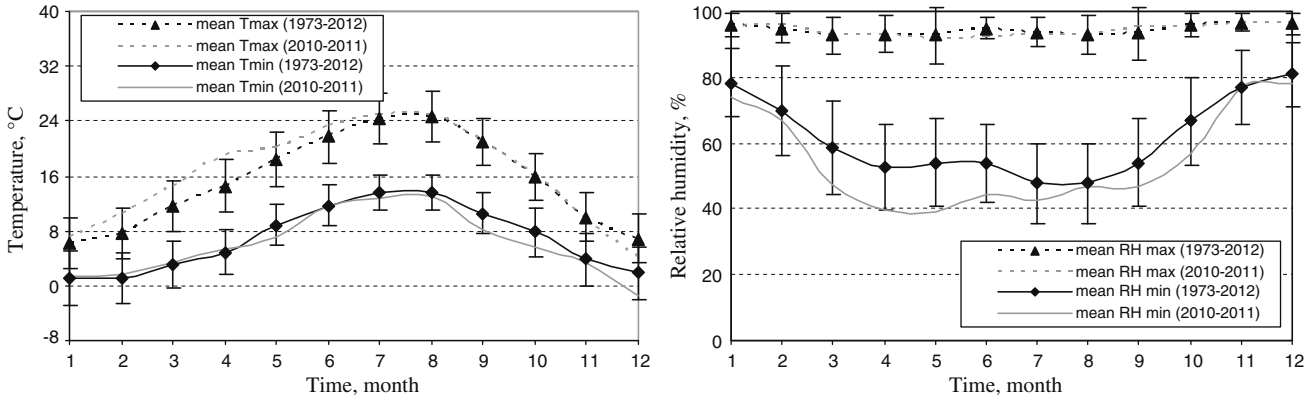

Fig. 4 Monthly variations in the extremes values of mean air temperature (on the *left*) and mean air relative humidity (on the *right*) for the two periods: 2010–2011 and 1973–2012

Table 2 Summary of the extreme stone surface temperature values over 3 years

Year	Highest three values of SST (°C)		Lowest three values of SST (°C)		No. of days with SST >30 °C		No. of days with SST <0 °C	
	North wall	South wall	North wall	South wall	North wall	South wall	North wall	South wall
2009/2010	28.3 (02/07)	35.9 (06/08)	−7.6 (08/01)	−8.2 (05/01)	0	47	47	46
	29.4 (21/07)	36.7 (16/08)	−7.3 (15/02)	−8.4 (08/01)				
	29.0 (19/08)	37.8 (19/08)	−7.5 (16/02)	−8.3 (15/02)				
2010/2011	29.3 (01/07)	35.3 (27/06)	−6.1 (30/11)	−6.5 (30/11)	1	37	36	41
	30.6 (02/07)	35.0 (01/07)	−3.9 (15/12)	−5.7 (14/12)				
	29.0 (09/07)	34.5 (21/08)	−4.8 (26/12)	−5.8 (26/12)				
2011/2012	27.8 (26/06)	37.4 (27/06)	−12.6 (07/02)	−14.2 (07/02)	2	29	26	25
	31.1 (27/06)	35.9 (28/06)	−11.4 (09/02)	−11.0 (06/02)				
	30.5 (28/06)	35.7 (22/08)	−10.9 (12/02)	−12.3 (09/02)				

below freezing point, with −12.6 and −14.2 °C, respectively, as the lowest SSTs for the north and south walls.

The number of days with SST higher than 30 °C ranges between 0 and 2 and 29 and 47 for the north and south walls, respectively. There are between 25 and 47 days with sub-zero temperatures for the north and south walls, respectively. Figure 5 presents the preliminary analysis of the daily variations in SST. There is a wide range of daily variations in SST, up to 13, 24 °C and down to 0.25, 0.2 °C over the year, for the north and south walls, respectively.

To provide more detailed analysis for the daily variations in SST, the maximum and minimum air temperatures for the days characterized with the highest values of SST are listed in Table 3 and compared with maximum and minimum values of SST, for the north and south walls, respectively. For the north wall the analysis shows that the maximum air temperature exceeded the maximum SST by a range of 1.56–6.5 °C. In contrast, in the case of the south wall, the maximum SST exceeded the maximum air temperature by up to 5.5 °C. Concerning the minimum temperature values, in general, the SST was slightly higher than the minimum air temperature for both wall directions. Consequently, for the stone located in the north wall, the daily variations in air temperature are higher than the daily variations in SST by up to 3.4–9.2 °C, while in the south wall these two variations are quite similar. These findings are attributed to the effect of direct exposure to sun radiation in the case of the stones located in the south wall. This can explain why the SST after midday is higher than the surrounding air temperature, while generally, at other times, it is equal to or slightly below the air temperature.

To assess the effect of direct insolation on the heating of the stone surface, it is important to take into account the albedo. Albedo is defined as the thermal rock property that controls the amount and speed of heat absorbed by its surface due to radiation (Warke and Smith 1998). In the experimental work of Viles (2005), albedo was examined precisely for two stones: granite and marble. Resulting from the absorption of sun radiation, the granite was found to have a higher surface temperature due to its darker colour, that is, low albedo, compared with marble.

When the stones are subjected to cyclic temperature variations, the constituent minerals expand/contract in different intensities depending on their thermal expansion

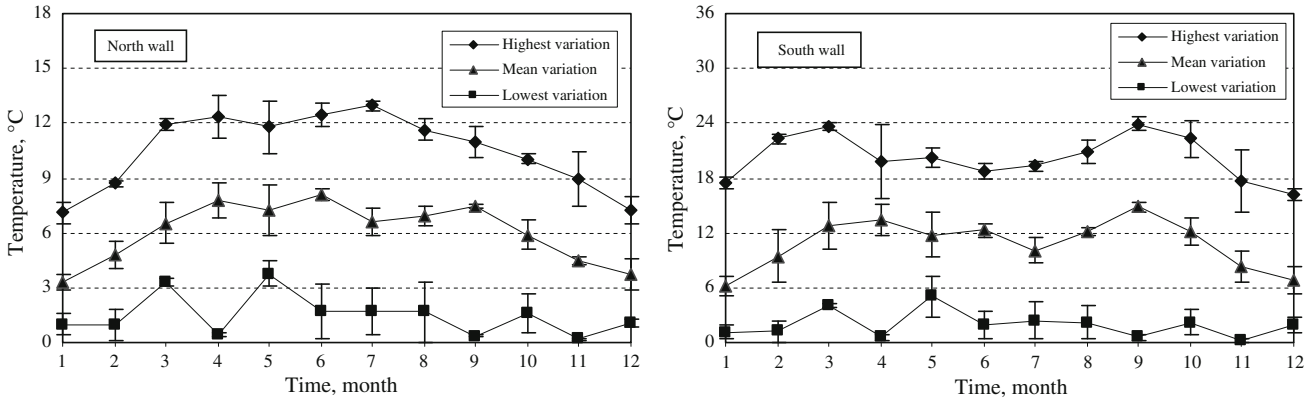

Fig. 5 Highest, mean and lowest daily variation in stone surface temperature for the period June 2009–June 2012

Table 3 Values of SST and air temperature at some specific days

Date (dd/mm/yy)	Max T_{air} (°C)	Min T_{air} (°C)	ΔT_{air} (°C)	North façade wall			South façade wall		
				Max SST (°C)	Min SST (°C)	ΔSST (°C)	Max SST (°C)	Min SST (°C)	ΔSST (°C)
27/06/2010	31.2	13.9	17.3	28.3	16.8	11.5	35.3	16.2	19.1
01/07/2010	32.5	15.1	17.4	29.3	18.2	11.1	35.0	17.9	17.1
02/07/2010	32.2	17.5	14.7	30.6	20.2	10.4	34.5	19.8	14.7
09/07/2010	33.0	19.1	13.9	29.0	21.0	8.0	31.8	20.4	11.4
26/06/2011	32.4	12.8	19.6	27.8	14.9	12.9	33.0	14.6	18.4
27/06/2011	37.0	15.6	21.4	31.1	18.0	13.1	37.4	17.8	19.6
28/06/2011	33.0	18.1	14.9	30.5	22.2	8.3	35.9	21.7	14.2
21/08/2011	31.8	13.0	18.8	25.3	15.7	9.5	34.5	15.5	19.0
22/08/2011	30.3	19.5	10.8	27.6	20.2	7.4	35.7	20.7	15.0

coefficient values; consequently, the induced internal pressure within the stones can lead to changes in the micro-structures of the stones by creating new cracks or the development of the pre-existing micro-cracks (Mutlutürk et al. 2004; Yavuz et al. 2006, 2010). Temperature variation is not the only factor influencing the micro-structure of stones, but its effects are extended to induce damage to the stones on a macro scale, that is, the damage induced by thermal stress. Referring to the work of Bonazza et al. (2009b) the risk of damage due to thermal stress on Carrara marble was predicted using Eq. (1):

$$\sigma_T = \frac{E \cdot \alpha \cdot \Delta T}{1 - \nu} \quad (1)$$

where σT is the maximum thermal stress, MPa; E is the Young's modulus, MPa; a is the thermal expansion coefficient, K^{-1}; ΔT is the daily variation in SST, K; Y is the Poisson's ratio, %.

The thermo-mechanical properties of the studied stones, tuffeau and Richemont stone, were measured and are presented in Table 1. The daily variation in SST is calculated as the difference between the daily maximum and minimum stone surface temperatures.

Table 4 presents the main annual percentile values of σ_T calculated using Eq. (1) for the data analysed over a period of 3 years, both for the north and south walls. The term percentile can, statistically, be defined as the value of a variable (e.g. thermal stress) below which a certain percentage of occurrences of observations are equal or smaller. For example, in the case of tuffeau located in the north wall, the 50th percentile of the calculated thermal stresses is ≤0.23 MPa. Again, the 100th percentile corresponds to the maximum value of the thermal stress and the 0th percentile corresponds to the minimum. To estimate the risk of damage to the stones located in the Castle of Chambord due to the effect of thermal stress, we compared the calculated thermal stress, σ_T, with the maximum sustainable load. The maximum sustainable loads for tuffeau and Richemont stone were obtained by adopting the same procedure used in the literature (Bonazza et al. 2009b; Ponziani et al. 2012). In this analysis, the unconfined compressive strength (UCS) value of the two stones was

Table 4 Annual percentile values of thermal stress calculated at two façade walls of the east tower

Percentage (%)	Thermal stress (MPa)			
	Tuffeau		Richemont stone	
	North wall	South wall	North wall	South wall
0	0.04	0.04	0.11	0.12
1	0.05	0.07	0.16	0.20
5	0.09	0.11	0.26	0.35
25	0.17	0.26	0.51	0.80
50	0.23	0.42	0.71	1.29
75	0.30	0.58	0.94	1.80
82	0.34	0.65	1.05	1.98
95	0.41	0.78	1.26	2.39
99	0.46	0.86	1.42	2.64
100	0.49	0.91	1.52	2.79

divided by a safety factor of three. The values of the UCS of the studied stones are presented in Table 1. The maximum sustainable loads are 3.89 MPa for tuffeau and 6.47 MPa for Richemont stone.

The results presented in Table 4 illustrate that all the calculated values of thermal stress for Richemont stone are three times higher than those calculated for tuffeau. Such behaviour can be attributed to the different values of the thermo-mechanical properties (Young's modulus, Poisson's ratio and the thermal expansion coefficient) of the two stones. Also, the values of the thermal stresses are always higher for the south wall compared to the north wall, for both types of stone. These findings can be attributed to the fact that the south wall is more exposed to direct sunlight. Moreover, tuffeau located in the south wall have a maximum thermal stress of 0.91 MPa compared with 0.49 MPa for the same type of stones in the north wall, while in the case of Richemont stone, these stresses are 2.79 and 1.52 MPa for the south and north walls, respectively. On the other hand, the results show that the risk of damage to the two studied stones, located in the walls of the north façade or the south façade, from thermal stress is probably negligible, where all values of thermal stress never exceed the maximum sustainable load of the stone.

Condensation

Water movement can induce severe damage due to the dissolution of stone minerals, reduction of the free energy of grain material weakening the resistance, transport of the air pollutants into porous media, and so on. The most common sources of moisture are rainfall, capillary water and condensation. The role of condensation in the wetting of stones and its effects on the degradation of stones as a microclimate process have been studied in the literature (Camuffo and Sturaro 2001; De Freitas and Schmekal 2003; Ponziani et al. 2012).

The dew point temperature (T_d) is the temperature at which the free water vapour, in humid air at constant barometric pressure, turns from a gaseous to a liquid state and finally accumulates on the cold material surfaces. At 100 % relative humidity, the T_d is equivalent to air temperature. The T_d can be calculated using Eq. (2) based on the August–Roche–Magnus approximation for the saturation vapour pressure of water in air as a function of temperature.

$$T_d = \frac{b\gamma(T, \mathrm{RH})}{a - \gamma(T, \mathrm{RH})} \quad (2)$$

with

$$\gamma(T, \mathrm{RH}) = \frac{aT}{b+T} + \mathrm{In}\left(\mathrm{RH}/100\right)$$

where *RH* relative humidity; $100 > \mathrm{RH} > 1$, %; *T* air temperature, $60 > \mathrm{T} > 0$, °C; *a* 17.271; *b* 237.7 °C.

Air relative humidity plays a significant role in promoting the process of condensation. To assess the occurrence of condensation on the surface of the studied walls, the first step was to analyse precisely the relative humidity of the air surrounding the Castle of Chambord. The data analysis of mean air relative humidity, obtained from the meteorological station installed on the roof of the east tower of the Castle of Chambord, for the period April 2010 to August 2011 shows that the values of mean air relative humidity are, mostly, between 60 and 90 %. They reach values exceeding 95 % in the winter months and rarely fall below 50 %. Again, the analysis shows that the mean air relative humidity reaches up to 96–98 % in the high humidity months, October–January, while it falls down to 48–53 % in the less humid months, April, June and July. A considerable number of days are characterized with high

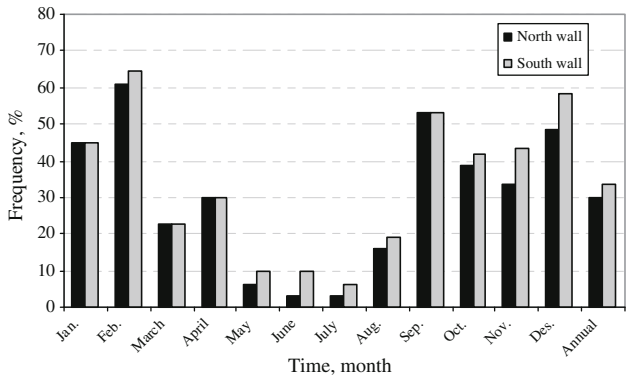

Fig. 6 Frequency of condensation events on stone surfaces of north and south walls

humidity: 14.2 % of days per year experience air relative humidity of over 90 %, and only 2.5 % of days per year to air relative humidity of <55 %. We can conclude that the Castle of Chambord is located in an area that experiences a high to moderate humid climate which can enhance the availability of moisture within the stones. As tuffeau is characterized with high water holding capacity (Table 1), we can raise the hypothesis: in situ, the observed degradation of tuffeau in the Castle of Chambord may be related, strongly, to characteristics of the humid climate.

The work presented in this study focused on examining the action of condensation in the degradation of the stones from two different base methods: first, through condensation on the external stone surfaces; and second, through condensation within the porous structure of the stones (i.e. taking into consideration the meniscus curvature of the pore water). The following paragraphs present these two approaches.

Condensation on the stone's surface

The procedure followed to assess the condensation occurrence on the stone's surface consists of comparing the calculated T_d with SST. When T_d is higher than SST, the water vapour condenses on the stone's surface. The frequencies of condensation events on stone surfaces, both on north and south walls of the east tower, were calculated and are presented in Fig. 6. These events occur throughout the year with annual frequencies exceeding 29 and 33 % for the north and south façade walls, respectively. They are more frequent in September–February. On the other hand, the frequencies for the south wall are slightly higher compared with the north walls; this can be attributed, as mentioned in "Daily variation in stone/air temperature and thermal stress", to the fact that stones in the south wall experience higher variations in daily surface temperature, thus enhancing the probability of T_d being greater than the SST.

Condensation within the stone porous structure

In the case of the porous material and within the micropore system, the condensation phenomenon is governed by Kelvin's law, where for each pore radius (r) there is a critical relative humidity, RH_c (Camuffo 1998). Condensation occurs when the measured relative humidity inside

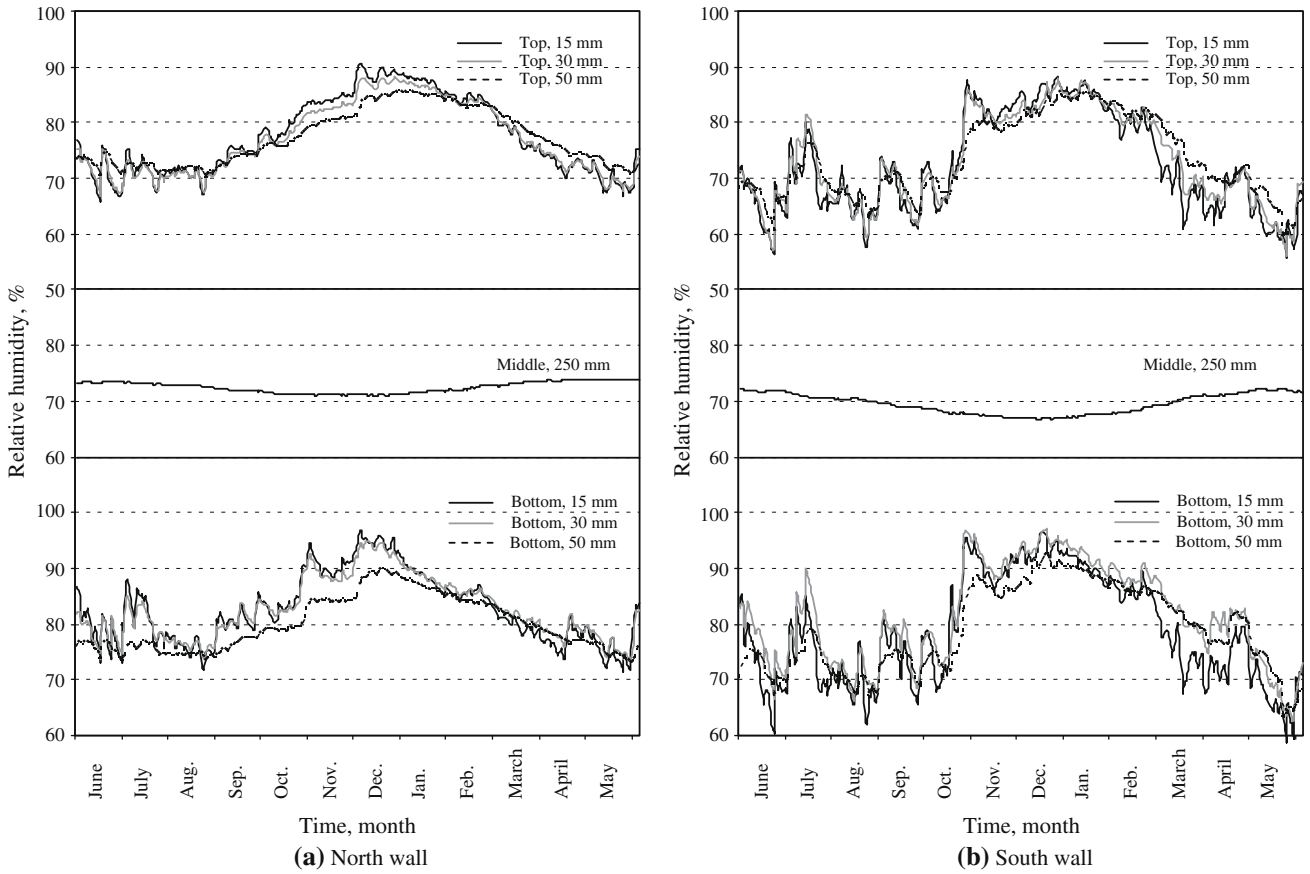

Fig. 7 Evolution of mean maximum relative humidity at different depths inside the stone for the period of 3 years: **a** north wall, and **b** south wall

the stone (RH_s) is higher than the calculated RH_c. The RH_c can be calculated using Eq. (3):

$$RH_c = 100 \cdot e^{\frac{-2\sigma_w \cdot V_m}{r \cdot RT}} \quad (3)$$

where σ_w surface tension of water in air–liquid interaction, 0.072 N/m; V_m molar volume of water, 18 cm^3/mol; R gas constant, 8.3144621 N m/mol/K; T temperature of thermodynamic system in equilibrium, K.

Figure 7 presents the evolution of the mean maximum RH_s measured for a period of 3 years using thermal–humidity sensors inserted into the walls of the east tower in different directions (north and south), at different levels (top, middle and bottom) and at different depths inside the stones (15, 30, 50 and 250 mm). Both for the north and south walls, the mean maximum RH_s inside the bottom stones is higher than the mean maximum RH_s inside the top stone. The measured mean maximum RH_s inside the bottom stones ranges between 70 and 95 %, compared with 60 and 90 % for the top stones. There is a slight fluctuation in depth with the mean maximum RH_s values measured near the surface (i.e. 15, 30 and 50 mm). At 250 mm depth, the mean maximum RH_s is more stable with values between 65 and 75 % both for the north and south walls. Finally, because the stones in the south wall are more subjected to sun radiation, the measured humidity inside these stones experiences fluctuations of greater amplitude compared to stones in the north wall.

The calculated values of RH_c are listed in Table 5. These values mainly depend on the pore size radius, with a limited effect of temperature. Indeed, for a full range of SST experienced in the field, there is no significant variation in the calculated values of RH_c. The resulting variation is small enough to be ignored compared to sensor accuracy. Hence, in this analysis, a constant mean value of the temperature of the stones in each case was used to calculate the RH_c. The effect of meniscus curvature of the pore water in micro-pores can be observed through the reductions in the RH_c values for smaller pore radii. In this study, the measured RH_s were analysed and compared with RH_c. As for thermal stress, the frequency of condensation events was estimated using a percentile format, and the annual frequencies of days with condensation occurrences (i.e. values of RH_s higher than the RH_c) are presented in Table 5 as a function of pore radius.

The results show that the frequencies of condensation depend on the height of the stone in the wall (top or bottom), the depth within the stone (15, 30, 50 and 250 mm) and the orientation of the wall façade (north or south). Stones located at the bottom are always subjected to more frequent condensation events than those at the top. The annual frequencies of condensation events mainly depend on the depth inside the stone. For stones located on the

Table 5 Annual frequencies of condensation events with values of RH_c as a function of pore radius at different locations on the north and on the south walls

Pore radius, r (μm)	RH_c (%)	North wall						South wall					
		Bottom of the wall			Middle	Top of the wall			Bottom of the wall		Middle	Top of the wall	
		15 mm depth	30 mm depth	50 mm depth	250 mm depth	15 mm depth	30 mm depth	50 mm depth	15 mm depth	30 mm depth	50 mm depth	250 mm depth	15 mm depth	30 mm depth	50 mm depth
1	99.891	0.1	–	–	–	–	–	–	0.2	–	–	–	–	–	–
0.1	98.915	3.4	0.3	–	–	–	–	–	2.5	3.1	–	–	0.1	–	–
0.09	98.795	4.2	0.9	–	–	–	–	–	2.6	3.8	–	–	0.1	–	–
0.07	98.454	4.8	1.9	–	–	–	–	–	3.2	4.9	–	–	0.1	–	–
0.05	97.842	5.6	2.7	–	–	–	–	–	4.0	6.7	0.1	–	0.2	–	–
0.03	96.430	7.2	3.9	–	–	0.6	–	–	5.7	9.0	0.6	–	0.3	0.4	–
0.01	89.666	18.6	14.5	4.9	–	4.5	4.3	0.7	23.1	30.6	10.6	–	2.3	3.1	–
0.009	88.586	21.8	17.7	7.2	–	5.7	4.8	2.6	26.9	36.0	13.7	–	3.9	4.1	0.1
0.007	85.571	36.7	35.4	14.4	–	16.3	12.1	7.4	37.4	47.5	31.3	–	11.3	8.4	3.4
0.006	83.378	48.2	48.5	26.5	–	29.8	20.4	13.1	44.3	54.8	40.8	–	20.5	15.7	10.4
0.005	80.401	62.4	61.1	42.9	–	40.6	39.2	34.0	50.8	62.6	51.2	–	31.5	31.9	27.2
0.003	69.636	93.9	97.6	98.8	95.4	82.6	83.2	88.3	74.6	81.9	79.2	44.8	58.9	61.2	62.8

north wall, the condensation occurrences always decrease with depth. In contrast, for the south wall, the percentages of condensation events are maximal at 30 mm depth. This could be attributed to the impact of direct sunlight on the humidity of the stones near the surface. However, there is no condensation at 250 mm depth, even for the shortest pore radii. For 30 and 50 mm depths inside the stones, the condensation events for the bottom part of the south wall face are more frequent compared with north at the same height. On the other hand, for the top part of the north wall face, these occurrences are equal or slightly higher compared with the south.

The annual frequencies of condensation events inside the porous structures of the stones have been correlated to the results obtained from the mercury porosimetry test. The porosimetry analysis indicated that Richemont stone has a pores size distribution restricted to the range 0.01–2 μm of the pore radius with the main peak of incremental pore volume at 1 μm with a shouldering at 0.3 μm (see Fig. 2). Taking into account Table 5, only in a few days per year the Richemont stone is submitted to condensation. In accordance with the observed smallest pores in Richemont stone, the higher frequencies of condensation events reach up to 18.6 and 30.6 % for the bottom part of the north and south walls, respectively. These occurrences are much lower or nil for the same pore sizes at other levels or at different depths within the stones. On the other hand, the pore network of tuffeau is characterized by a typically bimodal distribution with a large mean peak at 4 μm (from pore radius of 0.003–10 μm) and the second one at 0.005 μm. The smallest pores are notably subjected to condensation. The frequencies of condensation for the pore radius of 0.003 μm range, respectively, between 93.9–98.8 and 74.6–81.9 % at the bottom part of the north and south walls at different depths within the stones Therefore, as tuffeau in the Castle of Chambord is subjected to a high occurrence of condensation, this physical process may be considered to be one of the main causes for the degradation of this stone.

Freezing–thawing action

When stone is in a moist state and undergoes variations in temperature around freezing point, it may be subjected to freezing. Several experimental works conducted on different stone types have shown that their physical and

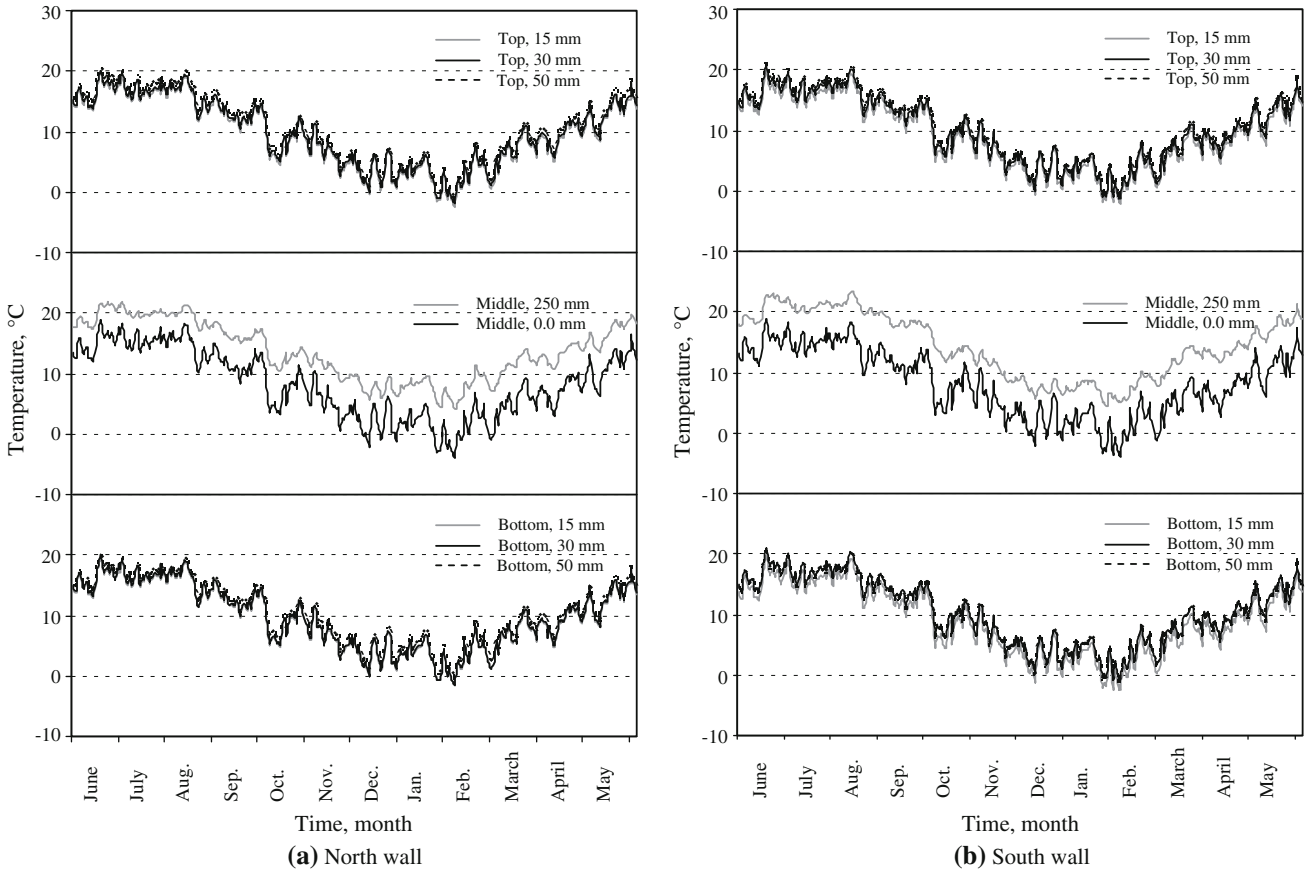

Fig. 8 Evolution of mean minimum temperature at stone surface and at different depths inside the stone for a period of 3 years: **a** north wall, and **b** south wall

engineering properties are widely influenced by the recurrent action of freezing–thawing (Altindag et al. 2004; Mutlutürk et al. 2004; Tan et al. 2011; Yavuz et al. 2006).

To assess the risk of freezing damaging the stones in the Castle of Chambord, the frequencies of days with freezing–thawing events were evaluated. As for condensation, the freezing events both on the stone surface and within the pore network of the stone were included in the analysis. The effect of the meniscus curvature of the pore water leads to the lowering of the freezing point temperature, T_{FP}, for smaller pores (Camuffo 1998). The T_{FP} can be calculated using the expression below:

$$T_{FP} = -273\frac{2\sigma_{sl}}{r \cdot P_s L_f} \quad (4)$$

where σ_{sl} surface tension at solid–liquid interface, 32.1E−03 N/m; p_s ice density, 0.917 g/cm^3; L_f latent heat fusion, 333.55 N m/g.

Figure 8 presents the evolution of the mean minimum temperature on the stone surface and at different depths inside the stone for the period of 3 years, both for the north and south walls. The mean minimum temperatures measured on the stone surface and at different depths inside the stone (15, 30 and 50 mm) are quite similar and range between 0.0 and 20 °C. They fall below 0.0 °C in the months of January and February. These observations are independent of the orientation and the height of the stones. However, in the case of the 250 mm depth, the mean minimum temperatures never drop below 0.0 °C.

To estimate the frequencies of days with freezing–thawing events, we refer to the comparison between the calculated T_{FP} with the measured minimum stone temperature. Freezing is assumed to happen when the minimum stone temperature is below the T_{FP}.

Freezing action on the stone surface

On the stone surface, T_{FP} was assumed to be 0.0 °C, and the freezing events were observed in two ways: the first by analysing the minimum SST measured using thermal–humidity sensors for the period of 3 years (from June 2009 to June 2012). The data analysis showed that the annual frequencies of freezing events were 9.7 and 10.5 % for the south and north walls, respectively (see Table 6). It should be noted that freezing events were assumed to happen when the SST was just below the T_{FP}, regardless of the presence of water on the stone surfaces. The second analysis was conducted over only a short period, from 1 April 2010 to 25 August 2011, (i.e. the period of the meteorological data acquisition using the local weather station). The objective of this second analysis was to identify the conjunction between freezing events and the presence of water on the stone surface due to rain or condensation.

Table 6 Annual frequencies of freezing events with values of T_{FP} as a function of pore radius at different locations on the north and on the south walls

Pore radius, r (μm)	T_{FP}, (°C)	North wall				South wall			
		Bottom of the wall			Middle	Top of the wall			
		15 mm depth	30 mm depth	50 mm depth	250 mm depth	15 mm depth	30 mm depth	50 mm depth	
1	−0.03	5.8	5.7	3.8	0.2	6.2	5.7	4.7	
0.1	−0.29	5.2	5.1	3.5	0.1	5.8	5.5	4.4	
0.09	−0.32	5.1	5.1	3.5	0.1	5.7	5.4	4.4	
0.07	−0.41	4.9	5.0	3.3	0.1	5.6	5.2	4.1	
0.05	−0.58	4.8	4.7	3.1	0.1	5.5	4.8	3.8	
0.03	−0.97	3.9	3.7	2.8	–	4.7	4.2	2.8	
0.01	−2.90	1.9	1.8	1.2	–	2.1	1.7	1.4	
0.009	−3.22	1.7	1.7	1.1	–	1.8	1.5	1.2	
0.007	−4.14	1.3	1.2	0.8	–	1.4	1.2	0.7	
0.006	−4.83	1.0	1.0	0.4	–	1.0	0.7	0.7	
0.005	−5.80	0.7	0.6	0.2	–	0.7	0.6	0.5	
0.003	−9.40	–	–	–	–	0.1	0.1	–	

Pore radius, r (μm)	T_{FP}, (°C)	South wall							
		Bottom of the wall			Middle	Top of the wall			
		15 mm depth	30 mm depth	50 mm depth	250 mm depth	15 mm depth	30 mm depth	50 mm depth	
1	−0.03	7.7	5.4	4.7	0.1	6.7	5.5	5.1	
0.1	−0.29	7.2	4.9	4.6	0.1	6.1	5.2	4.5	
0.09	−0.32	7.1	4.8	4.5	0.1	6.0	5.1	4.4	
0.07	−0.41	6.9	4.7	4.5	–	5.8	5.0	4.3	
0.05	−0.58	6.3	4.5	4.1	–	5.7	4.5	3.9	
0.03	−0.97	5.8	3.8	3.4	–	5.2	3.8	3.3	
0.01	−2.90	4.6	2.1	1.7	–	2.6	1.9	1.5	
0.009	−3.22	2.6	1.8	1.3	–	2.3	1.6	1.4	
0.007	−4.14	2.1	1.1	0.9	–	1.7	1.1	1.0	
0.006	−4.83	1.6	0.9	0.7	–	1.2	0.9	0.8	
0.005	−5.80	1.0	0.5	0.4	–	1.0	0.5	0.5	
0.003	−9.40	0.2	–	–	–	0.1	0.1	–	

At stone surfaces the T_{FP} is zero and the corresponding annual freezing events are 9.74 and 10.49 % for the north and south walls, respectively

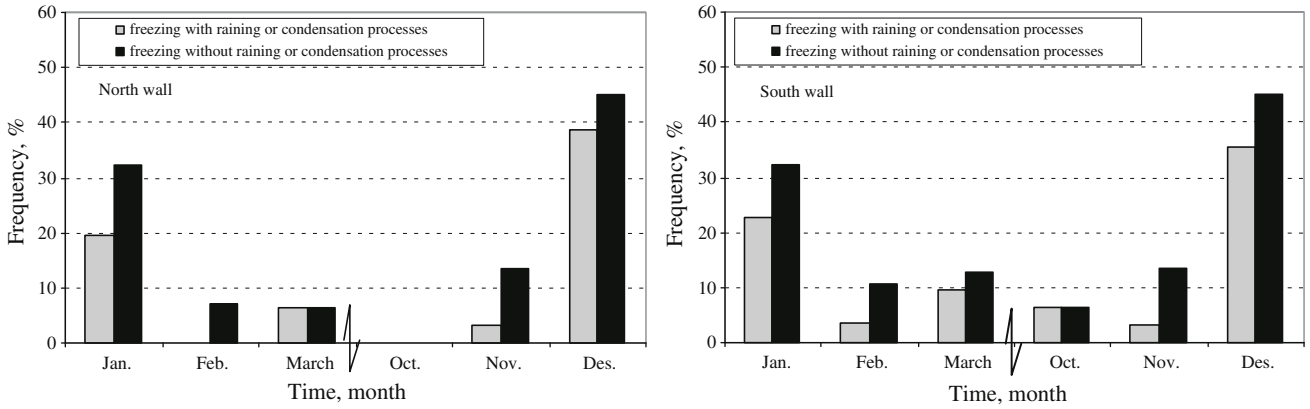

Fig. 9 Frequency of freezing events with or without effects of raining and condensation processes

Figure 9 presents the frequencies for each month. Freezing events only occur during the period November–March and are more concentrated in December and January. Freezing occurrences are more frequent for the south wall compared to the north. A comparison between both types of analysis was made to assess the interest of taking into account the presence of condensed water on the stone surface. The result indicates that considering the presence of water significantly reduces the calculated frequencies of freezing (see Fig. 9). Hence, the first analysis focuses on estimating the risk of damage due to freezing, while the frequencies of this weathering process are actually measured in the second analysis.

Freezing action within the stone's porous structure

Concerning the freezing action within the porous structure of the stone, the frequencies of freezing events over the period of 3 years were estimated by analysing the values of the minimum stone temperatures measured at different depths inside the stone, at different levels (top, middle and bottom) on the south and north walls. Again, the percentile format was used to present the results of the analysis, and the annual frequencies of freezing events are presented in Table 6. As described in Eq. (4), the values of the freezing point temperature, within the porous structure of the stone, depend on pore radius; consequently, the T_{FP} drops for the pores with smaller radii.

From the results of the mercury porosimetry test, in combination with the results presented in Table 6, it is evident that the two limestones, tuffeau and Richemont stone, can be considered as exposed to similar magnitudes of freezing–thawing. The results revealed that the location of the stones (on the top or at the bottom of the walls) has a limited effect on the annual frequencies of freezing events. However, freezing occurrences are slightly higher at 15 and 30 mm compared to 50 mm depths, and nil at 250 mm. In general, the south wall is a bit more exposed to freezing events compared to the north wall.

Conclusion and outlook

In this study, statistical analysis concerning the temperature and humidity of stones located in the walls of the east tower of the Castle of Chambord, together with meteorological data of the weather experienced at the castle, was taken into consideration to estimate the role of climatic conditions in the development of degradation of two French limestones, tuffeau and Richemont stone, used in the construction and restoration of the castle. The study focused on the estimation of the stones' behaviour with respect to three weathering processes: thermal stress, condensation and freezing–thawing.

The SST analysis shows that the daily variations in stone temperature can reach 20 °C. However, the daily variation depends on the orientation of the stone in the studied tower: higher variation is detected in the south wall, which is exposed to the sun, compared to the north wall. The effects of thermal stress generated by daily variations in temperature are more significant in the Richemont stones than in tuffeau. Indeed, even if the mechanical strength of Richemont stone is higher compared with tuffeau, tuffeau is less stiff (lower Young's modulus) and can experience higher deformation due to thermal dilation without damage. However, all calculated values of thermal stress remain lower than the maximum sustainable load for both stones. As a consequence, daily variations in temperature may not be considered to be a significant source of degradation. However, cyclic fluctuations in temperature over time may generate stone damage by fatigue, but this last aspect was not investigated in this study.

Relative humidity data show that the Castle of Chambord is located in an area that experiences a high to

moderate humid climate, which can enhance the continuous availability of moisture within the stones. The presence of biological colonization (more than 43 % of all identified alterations) on the east tower of the Castle of Chambord confirms the humid climate that reigns in situ. Condensation events occur on stone surfaces throughout the year, with annual frequencies exceeding 29 and 33 % for the north and south façade walls, respectively. The frequencies of condensation events analysed with sensor measurements in the walls of the east tower show that stones located at the bottom are subjected to more frequent condensation events than those at the top. The occurrence of condensation decreases with depth inside the stone. At the 250 mm depth, no condensation occurs. This is due to fluctuations in relative humidity decreasing with depth until 250 mm, where the relative humidity is almost constant. The frequency of condensation for Richemont stone hardly reaches 30 %, while it reaches even higher than 90 % for tuffeau. This is due to the effect of pore size distribution, much finer for tuffeau compared to Richemont stone.

No freezing is experienced at the 250 mm depth. Freezing occurrence is maximal near the surface (at 30 and 15 mm depths) and slightly lower at the 50 mm depth. The height and the orientation of the stones have no significant effects. However, freezing frequency is low and concerns only the porosity limited to the finest pores.

As a conclusion, the analysis of the Chambord data indicated that neither Richemont stone nor tuffeau is affected by thermal stress, while condensation events are more frequent in tuffeau. The risk of freezing for both stones is similar, but is not considered to be the main damaging process. In this study, the measured stone temperature and stone humidity were analysed by a simplified approach. Thus, it is recommended that more attention be given to water saturation when assessing freezing action, and to investigate the role of rainfall, drizzle, fog, hail and snow, in combination with wind direction. Finally, cyclic effects must be studied to assess the damage generated by fatigue.

References

Altindag R, Alyildiz IS, Onargan T (2004) Mechanical property degradation of ignimbrite subjected to recurrent freeze–thaw cycles. Int J Rock Mech Min Sci 41:1023–1028

Beck K, Al-Mukhtar M (2005) Multi-scale characterization of two French limestones used in historic constructions. Int J Restor Build Monum 11(4):219–226

Bonazza A, Messina P, Sabbioni C, Grossi CM, Brimblecombe P (2009a) Mapping the impact of climate change on surface recession of carbonate buildings in Europe. Sci Total Environ 407:2039–2050

Bonazza A, Sabbioni C, Messina P, Guaraldi C, De Nuntiis P (2009b) Climate change impact: mapping thermal stress on Carrara marble in Europe. Sci Total Environ 407:4506–4512

Brunetaud X, De Luca L, Janvier-Badosa S, Beck K, Al-Mukhtar M (2012a) Application of digital techniques in monument preservation. Eur J Environ Civil Eng 16(5):543–556

Brunetaud X, Stefani C, Janvier-Badosa S, Beck K, Al-Mukhtar M (2012b) Comparison between photomodelling and laser scanning to create a 3D model for a digital health record. Eur J Environ Civil Eng 16(sup1):s48–s63

Camuffo D (1998) Microclimate for cultural heritage. Elsevier, Amsterdam

Camuffo D, Sturaro G (2001) The climate of Rome and its action on monument decay. Climate Res 16:145–155

De Freitas CR, Schmekal A (2003) Condensation as a microclimate process: measurement, numerical simulation and prediction in the Glowworm cave, New Zealand. Int J Climatol 23:557–575

Eklund S (2008) Stone weathering in the monastic building complex on Mountain of St Aaron in Petra, Jordan. M.Sc Thesis, University of Helsinki-Finland

Hoxha D, Do D, Belayachi N (2010) A fully coupled thermo-hydro mechanical analysis of the impact of temperature and humidity variation on the state of historical stone buildings. In: 8th international symposium on the conservation of monuments in the Mediterranean Basin, Patras

Janvier-Badosa S, Beck K, Brunetaud X, Al-Mukhtar M (2010) Characterization of stone weathering: A case study for Chambord Castle, France. In: 8th international symposium on the conservation of monuments in the Mediterranean Basin, Patras

Janvier-Badosa S, Beck K, Brunetaud X, Al-Mukhtar M (2013) Historical study of Chambord Castle: basis for establishing the monument health record. Int J Archit Herit 7:247–260

Moropoulou A, Theoulakis P, Chrysophakis T (1995) Correlation between stone weathering and environmental factors in marine atmosphere. Atmos Eng 29:895–903

Mutlutürk M, Altindag R, Türkc G (2004) A decay function model for the integrity loss of rock when subjected to recurrent cycles of freezing–thawing and heating–cooling. Int J Rock Mech Min Sci 41:237–244

Ponziani D, Ferrero E, Appolonia L, Migliorini S (2012) Effects of temperature and humidity excursions and wind exposure on the arch of Augustus in Aosta. J Cult Herit 13:462–468

Pope GA, Meierding TC, Paradise TR (2002) Geomorphology's role in the study of weathering of cultural stone. Geomorphology 47:211–225

Tan X, Chen W, Yang J, Cao J (2011) Laboratory investigation on the mechanical properties degradation of granite under freeze–thaw action. Cold Reg Sci Technol 68:130–138

Van TT, Beck K, Al-Mukhtar M (2007) Accelerated weathering tests on two highly porous limestones. Environ Geol 52(2):283–292

Viles HA (2005) Microclimate and weathering in the central Namib Desert, Namibia. Geomorphology 67:189–209

Warke PA, Smith BJ (1998) Effect of direct and indirect heating on the validity of rock weathering simulation studies and durability tests. Geomorphology 22:347–357

Yavuz H, Altindag R, Sarac S, Ugur I, Sengun N (2006) Estimating the index properties of deteriorated carbonate rocks due to freeze–thaw and thermal shock weathering. Int J Rock Mech Min Sci 43:767–775

Yavuz H, Demirdag S, Caran S (2010) Thermal effect on the physical properties of carbonate rocks. Int J Rock Mech Min Sci 47:94–103

Appendix 2

Construction and Building Materials 62 (2014) 28–37

Contents lists available at ScienceDirect

Construction and Building Materials

journal homepage: www.elsevier.com/locate/conbuildmat

Coupled thermal–hygric characterisation of elastic behaviour for soft and porous limestone

Asaad Al-Omari [a,b], Xavier Brunetaud [a], Kevin Beck [a], Muzahim Al-Mukhtar [a,*]

[a] Universite d'Orléans, CNRS – CRMD FRE 3520, Orleans, France
[b] Department of Civil Engineering, College of Engineering, Mosul University, Al-Majmooah Street, Mosul, Iraq

HIGHLIGHTS

- Soft limestone was exposed to −8 °C to 40 °C and 0–100% relative humidity.
- The measurements include strain, elastic modulus and Poisson's ratio.
- The DOE methodology was successfully applied to obtain mathematical relationships.
- Determined elastic properties were compared with elastic properties at dry state.
- Dry state elastic properties are inaccurate to simulate field conditions.

ARTICLE INFO

Article history:
Received 11 October 2013
Received in revised form 2 March 2014
Accepted 19 March 2014

Keywords:
Thermal–hygric characterisation
Tuffeau
Strain
Poisson's ratio
Elastic modulus
Design of experiments

ABSTRACT

The experimental work presented in this study was focused on examining the effect of the variation of two parameters: temperature and water saturation, on the elastic modulus, Poisson's ratio, and dilation properties of a limestone used widely in French construction called tuffeau. Experimental results were treated using a design of experiment to assess the coupling effects of the studied parameters, and to create mathematical models used to estimate the measured elastic properties in the range of −8 °C to 40 °C for temperature and 0–100% for water saturation. The elastic properties, generally characterised in the dry state or without real coupling with water saturation, proved to be inaccurate for most environmental conditions, suggesting that the proposed models represent an essential contribution to any further research involving the simulation of outdoor conditions in soft limestone construction.

1. Introduction

Soft and porous limestones have been used in the construction of individual houses, official buildings, churches, cathedrals and castles in France. This stone continues to be used in the replacement and reparation of stone construction. Moreover, the aesthetic aspect and low density of porous limestone promotes its use today in wall cladding in order to provide a prestigious exterior wall area for buildings [1]. However, these interesting properties make soft limestone very sensitive to weathering when exposed to outdoor environmental conditions. Different weathering processes can occur such as thermal stress, condensation, freezing, salt crystallisation, and biological colonisation. Accelerated ageing laboratory tests, like salt crystallisation tests and freeze–thaw tests, can be used as quality standards to enable selection of the appropriate stone as a building material [2]. Moreover, a recent study managed to estimate some stone mechanical properties based on non-destructive testing, thanks to the use of artificial neural networks [3].

Even if the accumulation of temperature and humidity cycles is frequently quoted as a major source of stone degradation in the literature, there is still a need for improving the assessment of the consequences of this weathering process. Recent studies [4–7] focused on investigating the role of the daily variation of temperature in the development of thermal stresses within the stones, considering that the thermal stress depends only on the thermal dilation. Furthermore, the calculation of these stresses was carried out on the assumption that the linear thermal expansion coefficient (α) and the mechanical properties of the stone, elastic modulus (E) and Poisson's ratio (ν) were considered constant. However, these mechanical properties depend on both the temperature and the degree of water saturation of the stone. Moreover, the constant

* Corresponding author. Tel.: +33 238494992.
E-mail addresses: muzahim@cnrs-orleans.fr, muzahim.al-mukhtar@univ-orleans.fr (M. Al-Mukhtar).

http://dx.doi.org/10.1016/j.conbuildmat.2014.03.029
0950-0618/

values used in the simplified approach stem from standard characterisation, usually in the dry state, whereas the actual state of soft stones in the field may be very different. Therefore, the accurate calculation of the thermal stresses of stones requires the knowledge of the effect of temperature and degree of water saturation on the stone's mechanical properties (E and ν).

Stone used in buildings suffers stress for restraining thermal dilation, but there is another significant source of dilation: hygric dilation, due to variation in water content. Hence, the calculation of the stress induced by the daily variation in environmental conditions must take into account not only the effect of the restrained thermal dilation, but also the dilation induced by the coupled effects of the daily variation in temperature and degree of water saturation. The resulting thermal–hygric stress depends on the mechanical properties, E and ν as a function of the temperature and relative humidity of the stone, while the strain results from the free thermal–hygric dilation (liner thermal–hygric expansion coefficient).

Most stones show thermal dilation or/and hygric expansion when subjected to variation in temperature and humidity. These two behaviours strongly depend on the origin of the stone (sedimentary, metamorphic, magmatic), its texture (grain shape, grain size distribution, degree of grain interlocking), and its mineral composition [8,9]. Degradation by thermal dilation is not restricted to the dry stones; on the contrary this degradation can be more severe for wet stones. For example, Koch and Siegesmund [10] pointed out that saturated marbles are more sensitive to thermal dilation degradation than the dry ones. Moreover, the presence of clay minerals is another factor that increase the degradation by thermal dilation or/and hygric expansion.

This research stems from a more global approach concerning the conservation and monitoring of the construction stones at the Chateau of Chambord, France, built in tuffeau, a soft and porous limestone. To date, there is no experimental study concerning the mechanical properties of stone under the coupled effect of temperature and humidity variation. Therefore, to estimate the stresses within the stone there is a need to obtain a mathematical relationship to link the mechanical properties of the stone to both temperature and water saturation.

The objective of this paper is to experimentally examine the effect of variations in both temperature and water saturation on the mechanical and dilation properties of a soft limestone. An experimental plan was designed, and the results were analyzed, statistically tested and finally modelled thanks to the use of a design of experiments (DOE). DOE is a methodology that ensures the quantification of interactions between parameters (here: temperature and water saturation) and allows statistical analysis of the relevance of the resulting model. The methodology of the design of experiments (DOE) was used to rigorously assess the coupling effects and to develop mathematical relationships that can be used to estimate any value of elastic modulus, Poisson's ratio and strain based on the knowledge of temperature and water saturation variations in the stone.

2. Material and methods

2.1. Stone sample properties

Tuffeau is a soft, porous, clayey, and fine-grained limestone used in the construction of most of the castles in the Loire Valley in France [11]. It is from the Turonian age, the upper Cretaceous period, approximately 88–92 million years ago. It is a light-weight stone showing a white colour.

The main mineral phases of tuffeau are 50% calcite (sparite, micrite, and marine fossils as coccoliths), 10% quartz, 30% opal (cristobalite–tridymite) and about 10% of clayey minerals and mica, resulting in a micro-porous fabric [11,12]. Previous results showed that tuffeau has negligible close porosity [12]. Similar observations were found for other sedimentary stones [2]. Thus, in this study, the vacuum saturation method was adopted to measure the stone's physical properties; total porosity, apparent density and skeletal density. The unconfined compressive strength and the tensile strength of the stone in both the dry and saturated states were measured using an Instron 4485 press machine. Table 1 summarises the characterisation of the studied stone for physical and mechanical properties. Fig. 1 presents the water retention curve of tuffeau [11,12]. The variations in the degrees of water saturation of tuffeau resulting from exposure to different conditions of relative humidity are presented. Measurements for water retention curves used three complementary techniques in order to apply different suctions linked to relative humidity thanks to Kelvin's law: saturated salt solutions (RH < 98%), osmotic solutions and tensiometric plates (RH > 98%) [11–13]. The variations of water saturation are very limited for relative humidity up to 76%, while significant increases in water saturation are observed when the relative humidity is close to 100%. In a fully saturated state, tuffeau exhibits high water-holding capacity, since it is characterised by high-fine porosity and contains a significant amount of clayey minerals.

2.2. Sample preparation

Tuffeau samples, 40 mm in diameter and 80 mm in height, were cored out perpendicularly to the bedding plane from a larger block. Attention was paid to selecting samples free from visible cracks and flaws.

Prior to testing, tuffeau samples were prepared in different conditions of relative humidity (0%, 76%, 98%, 99.99%, and 100%) corresponding to different degrees of water saturation (0%, 7%, 23%, 80% or 100%). These degrees of saturation were chosen to be representative of the water retention curve of tuffeau: dry and fully saturated states, and three other points required to describe the water retention curve (see Fig. 1). The different degrees of water saturation imposed on the tuffeau samples are based on the water retention curve which links the relative humidity (or suction) to the water content (and the degree of saturation). So, three consecutive techniques were used:

2.2.1. Preparing the sample with 7% and 23% of water saturation

The water saturation of 7% and 23% results from exposure at a relative humidity of 76% and 98%, respectively. The preparation of the sample was done in a climatic chamber with controlled temperature and relative humidity. A dry sample was exposed to a temperature of 20 °C and a relative humidity of 76%. The sample was left inside the chamber long enough to reach equilibrium (constant weight). At that time, the dilation of the sample was monitored using the strain meter (see Section 2.3). In fact, the dilation of the sample increased significantly in the first 24 h, and thereafter increased only slightly. Finally, after 96 h the sample showed no further increases in dilation, i.e. the measured strain data were always stabilized, indicating that the sample had already reached equilibrium with the environment inside the climatic chamber. At 76% RH, when the weight is stabilized, the sample

Table 1
Characterisation of the studied stone.

Stone property	Property value
Skeletal density, g/cm^3	2.57 ± 0.01
Apparent density, g/cm^3	1.30 ± 0.02
Total porosity, %	45.0 ± 0.52
Unconfined compressive strength, MPa	
Dry state	11.67 ± 0.33
Saturated state	4.83 ± 0.33
Brazilian tensile strength, MPa	
Dry state	1.30 ± 0.11
Saturated state	0.38 ± 0.08

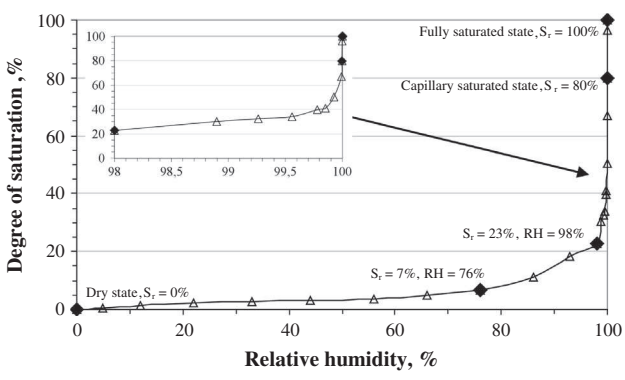

Fig. 1. Water retention curve of tuffeau [11,12].

contains about 7% of water saturation. The same procedure was followed for imposing 23% of water saturation on the sample by increasing the humidity inside the chamber to 98% till reaching equilibrium condition and keeping the temperature at 20 °C.

2.2.2. Preparing the sample with 80% of water saturation

The sample with 80% water saturation was obtained by water absorption by capillarity imbibition. It should be mentioned that the previous results presented by Beck [12] indicated that tuffeau reaches the mass saturation after about 2 h of imbibition which is equivalent to 80% of water saturation. According to the water retention curve (Fig. 1), this degree of saturation corresponds to 99.99% of relative humidity. The resulting sample is also referred to as a capillary saturated sample.

2.2.3. Preparing the sample with 100% of water saturation

The fully saturated sample was prepared by immersing the capillary saturated sample in water under a vacuum pressure of 1.0 kPa for 5 h, then the valve of the desiccator containing the immersed sample was closed and the sample was left for another 72 h to ensure it reached the full saturation condition. According to the water retention curve (Fig. 1), this degree of saturation corresponds to 100% of relative humidity, and all pore space of sample is filled by water.

After the samples achieved the required degree of water saturation, they were sealed with plastic film and kept inside a desiccator at room temperature for at least 24 h before the test.

2.3. Measuring the stone's mechanical properties

The experimental work in this study consists of measuring the mechanical properties of the tuffeau: strain, elastic modulus and Poisson's ratio in different environmental conditions. These properties were measured for samples preconditioned at different water saturation levels; 0%, 7%, 23%, 80% and 100%, and exposed to different temperatures; −8, 2, 20 and 40 °C in an attempt to simulate the extreme, but realistic, range of stone temperatures and humidities measured during 3 years in the field for stone temperature between 35.9 °C and −8.4 °C, and for stone humidity between 97% and 41% [6].

The measurements of stone strain were carried out by using a strain gauge. A 5 mm-long triaxial foil strain gauge, type KFG-5-120-D17 manufactured by KYOWA Measuring Instruments, Japan, was glued onto a smooth surface at the middle height of the sample. In order to protect the strain gauge against water during the sample preparation, a thin layer of protective coating (silicon adhesive type SG 250), specifically designed for waterproof electrical application, was put on the strain gauge and on the area about 5 mm around it. The wires of the strain gauge were connected to the National Instruments device (model NI9219-4Ch 24-Bit Universal Analog Input 60 VDC) via the 'data receiver box'. Data was recorded by the National Instruments software. The principle of the experimental layout is presented in Fig. 2.

In order to measure the strain, elastic modulus and Poisson's ratio of the tuffeau samples in different environmental conditions, samples were monitored during their exposure in the climatic chamber. The strains of the sample were recorded each 10 s. Fig. 3a shows the order of the stages during the measurements in different environmental conditions. At the beginning, the samples were put inside the temperature-controlled chamber at 20 °C. Then the temperature was changed to 40 °C. Once the sample reaches equilibrium at the new temperature (i.e. stabilisation of the recorded strain data), the strain variation of the sample is calculated as the difference between the recorded strain data at 20 °C and at 40 °C. To measure the elastic modulus and Poisson's ratio at a temperature of 40 °C, the sample was compressed using the cell placed inside the climatic chamber, via the hydraulic pressure system. The applied pressure, up to 2.5 MPa, was controlled by the hydraulic pressure controller unit with a precision of 0.001 MPa. During loading, the temperature of the chamber was kept constant and the strains of the sample were recorded. The resulting stress–strain relationships were used to calculate the elastic modulus and Poisson's ratio of the stone sample. The same protocol mentioned above was followed for measuring the strain, elastic modulus, and Poisson's ratio of the sample when the temperature changed from 20 °C to 2 °C and from 20 °C to −8 °C. The whole mechanical characterisation was performed in the elastic range of the stress–strain relationship of tuffeau.

In order to investigate the global effects both of temperature and of water saturation on the strain of the sample, it was necessary to select a reference point at which the strain of the sample was adjusted to zero. The reference point of zero strain was selected for the sample in the dry state (i.e. zero water saturation) with a temperature of 20 °C. However, the cycles presented in Fig. 3a can only be used to provide the value of strain variation corresponding to any variation of temperature, for a given constant water saturation. In order to study the combined effect both of temperature and of water saturation on the strain of stone, it is important to carry out another series of experimental tests concerning the strain measurements due to the variation in water saturation but at a constant temperature of 20 °C (Fig. 3b). The two experimental plans can be linked together to obtain the strain response at any variation in temperature and water saturation. It is worth mentioning that the strain measurements shown in Fig. 3b were carried out on the sample prepared with a different water saturation by following the procedure presented in Section 2.2, with the exception that the strain data were recorded continuously even when the sample evolved from dry to fully saturated condition.

Since there was no damage during loading, the same sample was used for the whole experimental field of the first experimental plan (i.e. all the different conditions of temperature and relative humidity). This solution of a single-sample campaign allows the standard deviation to be limited to that induced by the experimental procedure, since heterogeneity between samples cannot affect the results. However, because the last environmental conditions of the first experimental plan damaged this sample (see paragraph 4.1), a second sample was used to achieve the second experimental plan. In order to check that both samples give consistent behaviour, and to test the validity of the model obtained by linking both experimental plans, the second sample, which was undamaged at the end of the second experimental plan, was also used to perform extra tests in the environmental conditions: 30 °C and S_r = 80%. The result of this validation is presented in paragraph 4.2.3.

3. Application of the design of experiments method

In the literature, numerous experimental works have focused on studying the single effect of temperature or of water saturation on the mechanical properties of the porous material [14–18]. These studies found good correlations between the measured mechanical properties on the one hand and temperature and water saturation on the other hand. The thermal–hygric dilation of the sample can be simply characterised by calculating the linear thermal dilation coefficient (α_t) in the dry state resulting from the change in temperature and the linear hygric dilation coefficient (α_h) at 20 °C resulting from the change in water saturation (Eq. (1)).

$$\text{Strain (m/m)} = \text{Constant} + \alpha_t \cdot T + \alpha_h \cdot S_r \quad (1)$$

where α_t is the linear thermal dilation coefficient, °C^{-1}, α_h the linear hygric dilation coefficient, T the temperature of sample, °C, S_r is the water saturation of sample, %

Usually, the elastic modulus and Poisson's ratio are measured in the dry state, at 20 °C (Eqs. (2) and (3)). These are the conditions for the characterisation of the stone's properties used in the previous works [4–7].

$$\text{Elastic modulus} = \text{value of elastic modulus for dry sample at } 20\,^{\circ}\text{C} \quad (2)$$

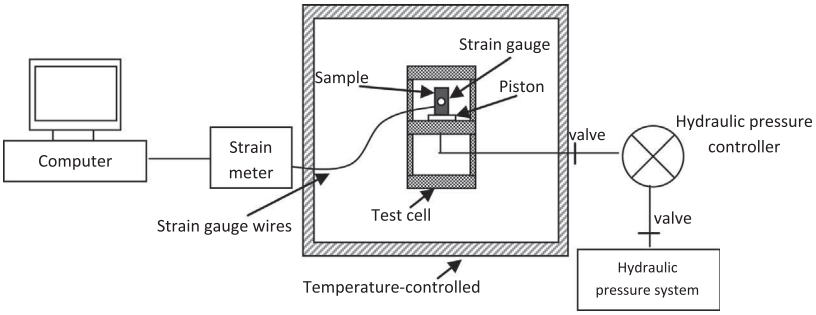

Fig. 2. Scheme of the layout of the experimental set-up.

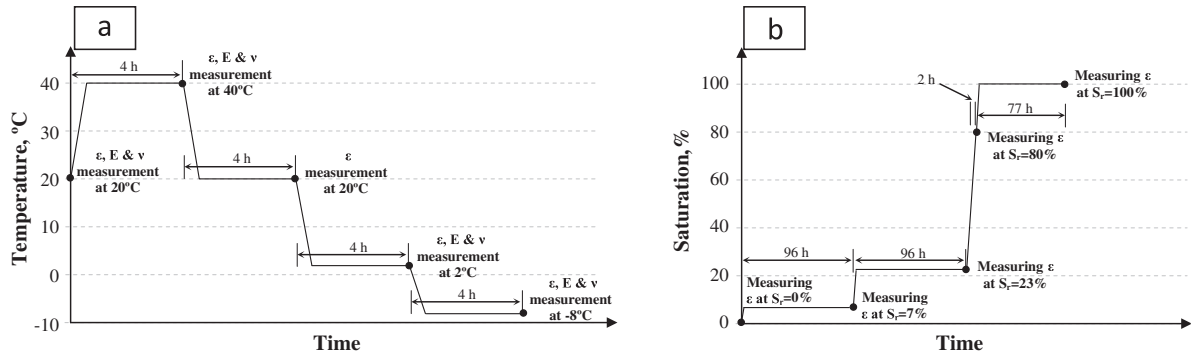

Fig. 3. Outline showing the stages followed in: (a) first experimental plan: strain, elastic modulus and Poisson's ratio measurements for the samples with different temperatures at constant water saturation, and (b) second experimental plan: strain measurements for the sample with different water saturation at constant temperature of 20 °C.

$$\text{Poissons ratio} = \text{value of Poisson ratio for dry sample at } 20\ ^\circ\text{C} \tag{3}$$

However, as this study was focused on a rigorous and fine definition of the stone's strain and mechanical properties as a result of the coupled effect of temperature and water saturation variation, a more precise analysis was required. Previous studies [19–21] concluded that the best way to quantify the coupled effects of several parameters on the material's response can be achieved by using the design of experiments (DOE). DOE is a branch of applied statistics that deals with planning, conducting, analyzing and interpreting controlled tests to evaluate the parameters (here: temperature and water saturation) that control the value of responses (here: elastic modulus, Poisson's ratio, and strain). Here, the structure of the DOE chosen to conduct the experimental investigation was complete factorial. This means that every possible combination between the levels of the different parameters is analyzed. This solution requires numerous trial experiments but makes it possible to quantify each interaction. This research used DOE methodology to create a mathematical relationship that assesses the coupled effect of temperature and water saturation variation on the elastic properties and the strain of tuffeau. Modelling consisted in generating empirical equations describing the systematic variation of the studied properties: strain, elastic modulus and Poisson's ratio, based on two different parameters (temperature and water saturation). The DOE method allows statistical validation of the obtained empirical models. The statistical considerations in this method followed the mathematical logic presented by Linder [22]. This methodology includes the following stages:

3.1. Identifying the parameters to be studied and the number of levels for each parameter

Two parameters were studied; the first one was the temperature with four different levels: −8, 2, 20 and 40 °C. The second parameter was the water saturation with five levels: 0%, 7%, 23%, 80% and 100%.

3.2. Coding the levels of the parameter

The second step consists in coding the levels of the parameters. This change is used to centre and reduce the magnitude of the parameter, thus allowing optimised and rigorous calculations. The limits of parameter coding depend on the number of levels for the given parameter, *the coding limits* = ±(*No. of parameter levels*−1)/2, that is, between ±1.5 for temperature and ±2 for water saturation.

A nonlinear regression analysis was used to distribute the actual coding values for the levels of both temperature and water saturation (see equations in Table 2). Table 2 lists the resulting coded values adopted in this study.

3.3. Constructing the polynomial model

The third step is to generate the polynomial models for the parameters of both temperature and water saturation. These polynomials, called orthogonal-Fisher polynomials, are composed of a constant and a series of polynomials of increasing degree up to the number of the level minus one (see Eq. (4)).

$$P_0 = 1, P_1 = x, P_{k+1} = P_1 \cdot P_k - \frac{k^2(n^2-k^2)}{4(4k^2-1)} \cdot P_{k-1} \quad k \geq 1 \tag{4}$$

where x is the relevant parameter, k is the degree of the polynomial, n the number of parameter levels.

Accordingly, the polynomials for temperature can be written as:

$$\text{Response}_{(t)} = \text{Const} + T_1 \cdot t + T_2 \cdot \left(t^2 - \frac{5}{4}\right) + T_3 \cdot \frac{5}{4}(t^3 - 2.05 \cdot t) \tag{5}$$

and for water saturation as:

$$\text{Response}_{(s)} = \text{Const} + S_1 \cdot s + S_2 \cdot (s^2 - 2) + S_3 \cdot \left(s^3 - \frac{51}{15}s\right) + S_4 \cdot \left(s^4 - \frac{31}{7}s^2 + \frac{72}{35}\right) \tag{6}$$

In order to estimate the coupled effect of temperature and water saturation on the mechanical properties of stone, the global model was created by multiplying the two previous equations. This model involved a constant and nineteen coefficients associated with each polynomial. Table 3 lists the names of the coefficients, and the degree and associated polynomials included in this model.

3.4. Determination of the coefficients of the model

The matrix formalism was used to represent the relationship between the measured responses [Y], the structure of the model (polynomials, named [X]), and the associated coefficients [A]:

$$[Y] = [X] \cdot [A] \tag{7}$$

where [X] is the model's matrix, [Y] is the measured response's vector–matrix, [A] is the unknown coefficient's vector–matrix.

The model matrix [X] contains the values of the polynomials for each experiment. The dimension of this matrix is (L, K), where K is the number of coefficients, and L is the number of the experiments.

Table 2
Coding of the levels for each parameter.

Variable	Temperature: t				Water saturation: s				
Value	−8 °C	2 °C	20 °C	40 °C	0%	7%	23%	80%	100%
Theoretical coding	−1.5	−0.5	0.5	1.5	−2	−1	0	1	2
Actual coding*	−1.442	−0.617	0.565	1.423	−1.930	−1.117	0.073	1.016	1.960

* Equation for temperature coding, coded $(t) = -6 \times 10^{-4} \cdot t^2 + 0.0789 \cdot t - 0.7726$.
* Equation for saturation coding, coded $(s) = 1.28 \times 10^{-5} \cdot s^3 - 0.0022 \cdot s^2 + 0.1309 \cdot s - 1.9298$.

Table 3
Details of the coefficients included in the global model.

Name of coefficient	Degree of polynomial		Associated polynomial
	Temperature	Saturation	
Constant	–	–	1
S_1	–	1	s
S_2	–	2	$s^2 - 2$
S_3	–	3	$s^3 - 51/15s$
S_4	–	4	$s^4 - 31/7s^2 + 72/35$
T_1	1	–	t
T_1S_1	1	1	t^*s
T_1S_2	1	2	$t^*(s^2 - 2)$
T_1S_3	1	3	$t^*(s^3 - 51/15s)$
T_1S_4	1	4	$t^*(s^4 - 31/7s^2 + 72/35)$
T_2	2	–	$t^2 - 5/4$
T_2S_1	2	1	$(t^2 - 5/4)^*s$
T_2S_2	2	2	$(t^2 - 5/4)^*(s^2 - 2)$
T_2S_3	2	3	$(t^2 - 5/4)^*(s^3 - 51/15s)$
T_2S_4	2	4	$(t^2 - 5/4)^*(s^4 - 31/7s^2 + 72/35)$
T_3	3	–	$(t^3 - 2.05t)$
T_3S_1	3	1	$(t^3 - 2.05t)^*s$
T_3S_2	3	2	$(t^3 - 2.05t)^*(s^2 - 2)$
T_3S_3	3	3	$(t^3 - 2.05t)^*(s^3 - 51/15s)$
T_3S_4	3	4	$(t^3 - 2.05t)^*(s^4 - 31/7s^2 + 72/35)$

The vector matrix $[Y]$ includes the measured values of the response for each experiment. The vector matrix $[A]$ contains the unknown coefficients required to define the model. Solving this equation consists in obtaining $[A]$. Calculation of the vector matrix $[A]$ requires the inversion of matrix $[X]$, which is not square. As a consequence, the least-square adjustment method was applied, using Eq. (8):

$$[A] = \left([X]^t \cdot [X]\right)^{-1} \cdot [X]^t \cdot [Y] \tag{8}$$

3.5. Statistical analysis

The last step required to obtain the final version of the model consists in testing the statistical significance of the effect of each coefficient so as to retain only significant coefficients. If the mean effect of the coefficient k is lower than the experimental dispersion, this means the coefficient k is insignificant and should be deleted. The Fisher–Snedecor test (Eq. (9)) was used to verify whether the mean effects produced by the coefficient k were larger than the experimental variance (σ^2) with a confidence level of (α).

$$F(\alpha) = \frac{X_{A_{k^2}}}{\sigma^2} \tag{9}$$

The mean effect of coefficient $X_{A_{k^2}}$ can be calculated as:

$$X_{A_{k^2}} = A_{K^2} \|X_k\| \tag{10}$$

where A_k is the value of the coefficient k, $\|X_k\|$ is the value relative to the coefficient k in the diagonal of the square matrix $([X]^t \cdot [X])$

The higher the F-value of the coefficient, the more significant is the effect of the coefficient. For the confidence level $\alpha = 5\%$, the degree of freedom of the coefficient which is 1 and the degree of freedom of the variance $(v > 30)$, the reference F-value is 4.17. Any F-value over this threshold means the effect of the coefficient is statistically significant with a 5% risk of error, so the associated coefficient must be kept for the model's definition.

4. Results and discussion

4.1. Experimental results of the stone's mechanical properties

4.1.1. Strain of sample

Both the sample strain data measured at a constant water saturation with different temperatures (1st experimental plan) and the strain data measured at a constant temperature with different levels of water saturation (2nd experimental plan) were linked together and are presented in Fig. 4. The results plotted in Fig. 4 represent the average of the axial, lateral and diagonal strain measurements. In the figure, the reference state corresponding to a zero strain was taken at a temperature of 20 °C and water saturation of 0.0%.

Irrespective of the water saturation, a rise in the temperature from 20 °C to 40 °C resulted in increasing the strain, while the opposite was observed when the temperature fell from 20 °C to 2 °C. This occurs as a result of the well-known and expected thermal dilation of the mineral components of the sample. Similarly, increasing the water saturation of the sample from 0% to 100%, or at any intermediate step, results in increasing the strain. This is due to the hygric dilation.

The coupled effects can be seen in the case of reducing the temperature from 20 °C to −8 °C. The following observations can be made:

- The fully saturated sample, i.e. $S_r = 100\%$, showed significant increases in its strain. This behaviour relates to the increases in volume of the sample resulting from ice growth.
- The opposite case was found for the dry sample since there was no frozen water; thus, a decrease in the sample strain was observed due to shrinkage of the minerals at −8 °C.

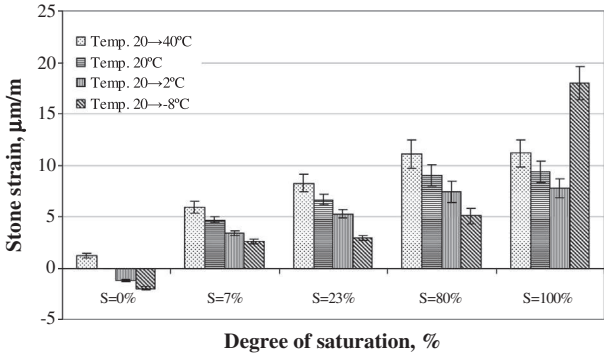

Fig. 4. Effect of water saturation on values of stone strain at different changes in temperature.

– The three intermediate conditions correspond to the partially saturated sample prepared with water saturation of 7%, 23% and 80%. Although the sample contained water, it showed contraction, i.e. decreases in the sample strain, when exposed to sub-zero temperatures. Here, the ice crystallisation pressure caused by ice growth was probably dissipated in the air-filled pores. Indeed, the three partially saturated tests did not result in cracking the sample after freezing, even at 80% of water saturation. This indicates that these levels of water saturation were below the critical one at which the sample starts to degrade during freezing [23,24]. Added to the thermal dilation effect, the observed contraction can be attributed to the effect of the migration processes for the unfrozen pore water from the smallest pores toward the larger ones during freezing [25].

4.1.2. Elastic modulus

For each test condition presented in Fig. 3a, the elastic modulus was measured three times. An average value of the three measurements of elastic modulus is shown in Fig. 5. The results indicate when the sample was in the dry state or in a state with a low level of water saturation, i.e. degree of saturation of 7% or 23%, and for all applied temperatures, the elastic modulus was weakly affected by changes in the degree of water saturation. This behaviour is due to the small amount of water in the pores.

The elastic modulus for both the fully and capillary saturated sample was found to increase noticeably as the temperature decreased. Considering the reference sample temperature as 20 °C, the results in Fig. 5 indicate that increasing the temperature of the sample from 20 °C to 40 °C decreases its elastic modulus by about 6% and 12% for the vacuum and capillary saturated sample, respectively. This was found to be in good agreement with previous studies [16–18] that concluded the elastic modulus of rock decreases with increasing temperature.

When the sample temperature fell from 20 °C to −8 °C, there was a gain in elastic modulus by about 70% for the capillary saturated sample. This can be attributed to the growth of ice within the pore structure. The fully-saturated sample exhibits wide cracks after the test at −8 °C. We may reasonably claim that these cracks were generated just after freezing at −8 °C and before loading the sample, because the compressive stress is limited to 2.5 MPa, which is 50% of the lowest measured strength (see Table 1). This issue is discussed in the session dedicated to the results for the Poisson's ratio.

Concerning the influence of water saturation on the elastic modulus, the results presented in Fig. 5 show that, regardless of the temperature, the elastic modulus decreases when increasing the water saturation up to 23%. Then, the sample exhibited slight increases in the elastic modulus at water saturation of 80% and 100%. These findings were found to be in good agreement with other studies [26,12], where the ultrasonic pulse velocity was measured for tuffeau stone at different degrees of water saturation. Such an increase may be a consequence of the high water saturation and the presence of a superficial insulation that limits drainage. In these conditions, the water within the pores of the stone is submitted to pressure during loading, and this pressure may not be instantly balanced, since the sample is sealed. Such pressure contributes to an apparent improvement of the matrix's properties. This phenomenon is called partially un-drained conditions and is well-known in soil mechanics. On the other hand, the frozen sample at −8 °C showed decreasing modulus when increasing the water saturation up to 23%. For further increases in water saturation up to 80%, the sample exhibited significant increases in the moduli. This can be attributed to the presence of a sufficient amount of frozen water that strengthens the sample.

4.1.3. Poisson's ratio

The Poisson's ratio of the cylindrical tuffeau sample was measured at the same time and with the same procedure followed for measuring the elastic modulus. The measurements were carried out three times for each test condition. The average of the three measurements is presented in Fig. 6. The Poisson's ratio of the sample does not seem to be significantly affected by the temperature increase. The effect of water saturation on the Poisson's ratio seemed to increase slightly when increasing the water saturation. For the Poisson's ratio, all the measurements but one were in the range 0.201–0.334. There was an unexpected measurement for the particular condition relative to full saturation and −8 °C with a value over 0.5, which is the theoretical maximum for this mechanical property. As for elastic modulus measurement, this may be attributed to the damage to the stone resulting from freezing prior to loading. A significant amount of unfrozen water may migrate to the cracks during loading, generating an anisotropic expansion and thus an artifact measurement of the Poisson's ratio.

4.2. Estimating the mechanical stone properties

The three mechanical stone properties considered in this study; strain, elastic modulus and Poisson's ratio, were considered as different responses of the material as a consequence of change in temperature and in water saturation. From this point, the DOE method was used to represent the evolution of these responses as a function of the controlled parameters (t, s) using polynomial equations.

4.2.1. The models of stone strain, elastic modulus and Poisson's ratio

The global model presented in Table 3 consists of one constant plus 19 coefficients. This model takes into account both the single

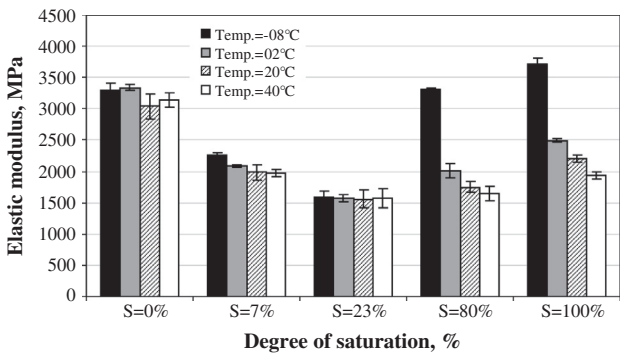

Fig. 5. Effect of water saturation on values of elastic modulus at different temperature.

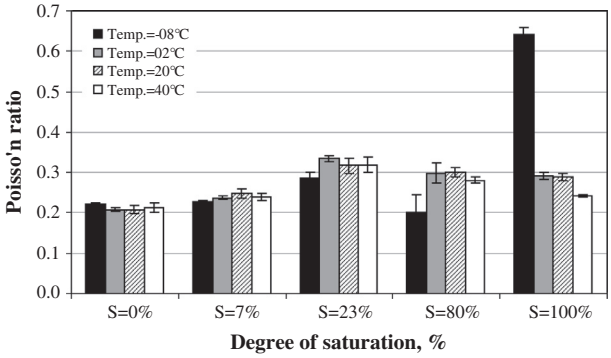

Fig. 6. Effect of water saturation on the values of Poisson's ratio at different temperature.

and the coupled effects of temperature and water saturation on the stone's response. However, the model does not take into account the artifact value of the elastic modulus and Poisson's ratio measured on the fully saturated sample frozen at −8 °C. Therefore, the related models for the elastic modulus and Poisson's ratio can be presented with one constant plus 18 coefficients.

Based on statistical analysis of the variance of the models, it is possible to identify the coefficients which have no significant effects on the stone's response. The significance of the coefficients of the models was ranked according to their calculated *F*-values (see Fig. 7). The higher the *F*-value of coefficient is, the greater the significance of the coefficient. Once the insignificant coefficients are removed, the stone strain can be represented with the constant and 15 of the 19 available coefficients (see Fig. 7). The models for both the elastic modulus and the Poisson's ratio can be represented using the constant and 15 significant coefficients out of the total 18 available coefficients.

Table 4 lists the values of the significant coefficients included in the three models. Eqs. (13)–(15) represent the simplified final forms of the models used, respectively, for estimating the strain, elastic modulus and Poisson's ratio of the stone. The values to be used in the related equations are the values of the coded levels of the parameters in accordance with Table 2.

$$\begin{aligned}\text{Strain}_{(t,s)} = [&61.898 + 5.202t + 18.854s - 4.09t^2 + 1.519s^2 \\ &- 0.489ts - 3.944t^2s + 1.584ts^2 + 8.16t^3 + 0.565s^3 \\ &+ 4.54t^3s + 0.965ts^3 + 5.53t^2s^2 - 2.36s^4 - 4.08t^3s^2 \\ &+ 3.26t^2s^3 - 2.7t^3s^3] \cdot (10)^{-5}\end{aligned} \quad (11)$$

$$\begin{aligned}\text{Elastic modulus}_{(t,s)} = &1570.775 + 17.303t + 19.098s \\ &+ 6.02t^2 + 248.808s^2 - 94.496st \\ &+ 11.67t^3 + 61.634st^2 - 92.936s^2t \\ &- 100.175s^3 - 19.486st^3 + 58.033s^3t \\ &+ 191.29s^2t^2 - 127.7s^2t^3 + 80.14s^3t^2 \\ &+ 21.89s^4t - 75.66s^3t^3\end{aligned} \quad (12)$$

$$\begin{aligned}\text{Poisson's ratio}_{(t,s)} = &0.325 - 0.021t + 0.033s - 0.011st \\ &- 0.53s^2 + 0.021s^2t - 0.017st^2 \\ &+ 0.016t^3 - 0.003s^3 + 0.012st^3 \\ &- 0.009s^2t^2 + 0.003s^3t + 0.008s^4 \\ &- 0.008s^2t^3 + 0.005s^3t^2 - 0.004s^4t \\ &- 0.005s^3t^3 + 0.004s^4t^2\end{aligned} \quad (13)$$

In order to highlight the new contribution of the models proposed in this study, the stone responses estimated by using the models presented in Eqs. (13)–(15) were compared with the responses determined usually in simple way using Eqs. (3)–(5). The thermal dilation coefficient presented in Eq. (1) was calculated from the difference between two values of the sample strain measured in the dry state (S_r = 0%) at two different temperatures(−8 to 40 °C), while the hygric dilation coefficient was calculated from the difference between two values of the sample strain measured at two different degrees of water saturation (S_r = 0% and S_r = 100%) at 20 °C. Accordingly, the values of the thermal and hygric dilation coefficients were found to be equal to 6.6E−6 and 9.3E−6, respectively. By applying the boundary condition; *strain* = 0.0 *at* T = 20°C, *at* S_r = 0.0%, the constant in Eq. (1) was found to be equal to −132.1E−6 (see Eq. (14)). The experimental measurements for the values of the elastic modulus and Poisson's ratio, obtained for the sample in dry state (S_r = 0%) at temperature of 20 °C, are also presented in Eqs. (15) and (16) respectively.

$$\text{Strain} = [-132.1 + 6.6T + 9.3S_r] \cdot 10^{-6} \quad (14)$$

$$\text{Elastic modulus} = 3040 \quad (15)$$

$$\text{Poisson's ratio} = 0.209 \quad (16)$$

4.2.2. Significance of the studied parameters

Based on the *F*-values obtained from the Fisher–Snedecor test, it was possible to find the significance of the studied parameters and whether they affect individually or jointly the estimated stone

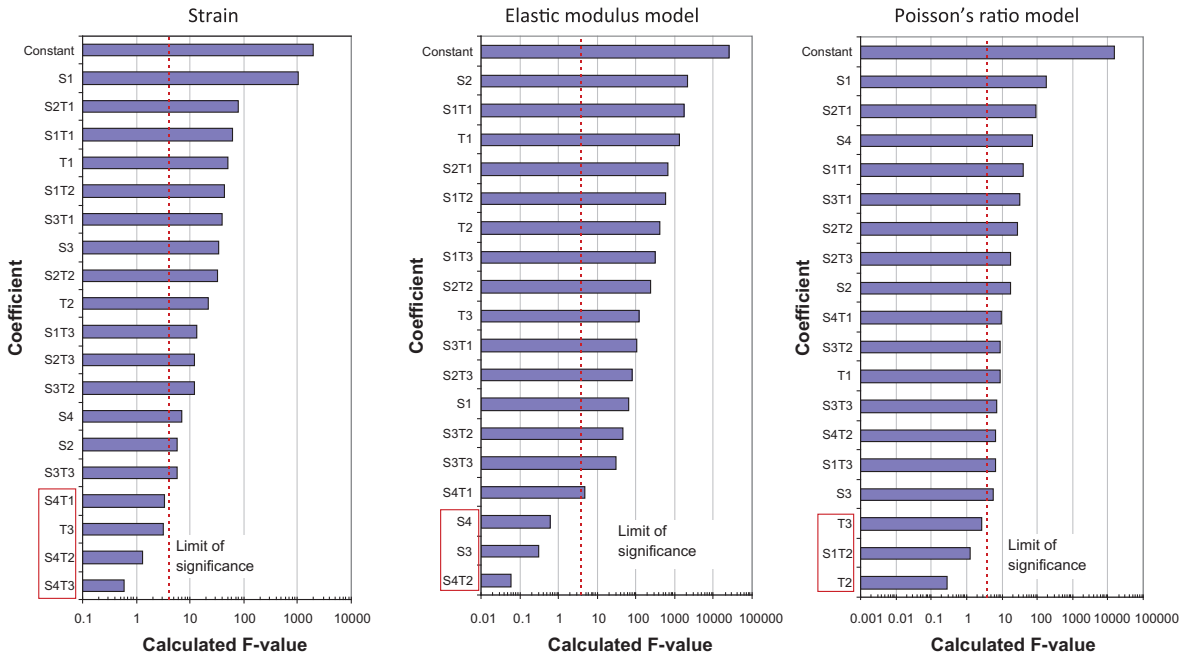

Fig. 7. Ranking the coefficients' significance for the three models.

Table 4
Coefficients values of the three models.

Stone strain model		Modulus of elasticity model		Poisson's ratio model	
Name of coefficient	Value of coefficient	Name of coefficient	Value of coefficient	Name of coefficient	Value of coefficient
Constant	5.8E−04	Constant	2554.14	Constant	0.274
T_1	8.4E−05	T_1	−553.97	T_1	−0.006
T_2	7.0E−05	T_2	388.6	S_1	0.022
S_1	3.0E−04	T_3	−243.73	S_1T_1	−0.01
S_1T_1	−6.7E−05	S_1	96.14	S_1T_3	−0.005
S_1T_2	7.1E−05	S_1T_1	−464.48	S_2	−0.006
S_1T_3	−4.6E−05	S_1T_2	334.11	S_2T_1	−0.013
S_2	−2.0E−05	S_1T_3	−276.73	S_2T_2	0.009
S_2T_1	−6.8E−05	S_2	487.92	S_2T_3	−0.008
S_2T_2	5.5E−05	S_2T_1	−257.78	S_3	0.003
S_2T_3	−4.1E−05	S_2T_2	191.29	S_3T_1	−0.007
S_3	4.6E−05	S_2T_3	−127.7	S_3T_2	0.005
S_3T_1	−4.6E−05	S_3T_1	−97.07	S_3T_3	−0.005
S_3T_2	3.3E−05	S_3T_2	80.14	S_4	0.013
S_3T_3	−2.7E−05	S_3T_3	−75.66	S_4T_1	−0.004
S_4	−2.4E−05	S_4T_1	21.89	S_4T_2	0.004

responses. The summation of the *F*-values of all coefficients related to the single or to the coupled parameters refers to the degree of significance of the parameters' effectiveness. Fig. 8 presents the ranking of the parameters for the three models included in this study according to their significance.

Concerning the stone strain model, the most dominant effect was the single effect of water saturation. The coupling between water saturation/temperature and the single parameter of temperature were ranked in second and third order of significance, respectively, with much less magnitude than the single effect of water saturation. The significance ranking of the parameters for the Poisson's ratio model were still in the same sequence compared to the strain model. However, the single effect of water saturation and the coupling between water saturation/temperature seemed to be of the same magnitude, while the single effect of temperature was very limited. For the elastic modulus model, the two single parameters and the coupling between them had strong effects on the estimated elastic modulus. However, the effects of the coupling between water saturation/temperature were found to be slightly higher than the effects of other single parameters.

4.2.3. Validation of the models

The validity of the proposed models can be assessed by examining the ability of the postulated models to fit the experimental data. Fig. 9 shows the comparison between the measured and the modelled stone response data. The proposed models give excellent accuracy of the estimated stone response compared to the experimental one. The slope of the relationship between the modelled values and the experimental ones is very close to 1, with an error of 0.79%, 0.04% and 0.47% for the strain, elastic modulus and Poisson's ratio, respectively.

The dashed lines drawn in Fig. 9 are the confidence interval corresponding to the relative experimental uncertainties. The modelled relative uncertainties of the three responses: strain, elastic modulus, and Poisson's ratio are 0.172, 0.06, and 0.062 respectively. They were compared with the relative uncertainties of the measured responses: 0.122 for strain, 0.057 for elastic modulus, and 0.059 for Poisson's ratio. The relative uncertainty of the model was calculated as the square root of the sum of error between each of the three measurements and the modelled value relative to the mean measured response of the three measurements. For the Poisson's ratio and elastic modulus, the model's relative uncertainty was not significantly higher than the experimental one, suggesting that the modelling did not introduce any error. For the strain, the model's relative uncertainty was 41% higher than the experimental one. This is due to the fact that some mean strain values were close to zero, so in these cases even a very slight deviation resulted in high relative error. However, the overall fit was very satisfactory, as can be seen in Fig. 9a.

Finally, in order to check the reliability of the proposed model of strain that builds on both experimental plans presented in Fig. 3, and so two different samples, the second sample was exposed to an extra environmental condition corresponding to a point within the experimental range, but on an interpolated point (i.e. 30 °C and S_r = 80%). Its strain was measured and found to be equal to 1.003E−3. This value is to be compared with the value obtained with Eq. (11) (i.e. 0.963E−3). The difference is less than the experimental deviation, suggesting that the developed model represented by Eq. (11) is reliable.

4.2.4. Graphical representation of the models and discussion

The obtained models are usually generated as a way to describe the effects of the studied parameters (temperature and water saturation) on a particular measured stone response based on the experimental results. These models can be displayed as a surface plot. Fig. 10 shows the three surface plots of the stone's

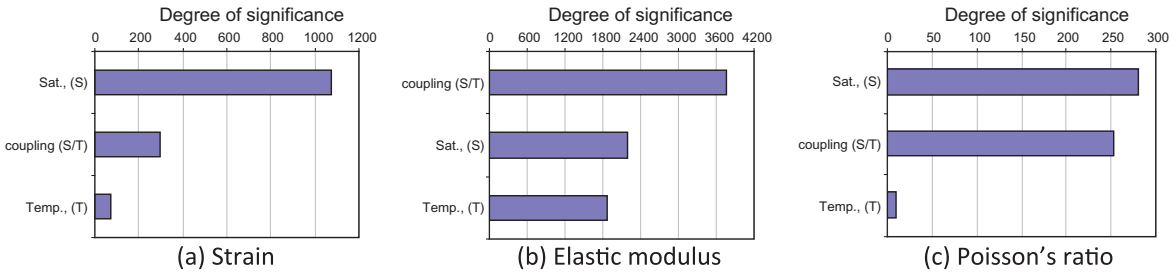

Fig. 8. Ranking the parameters in the form of the single or coupling effect on the measured response of (a) strain, (b) elastic modulus and (c) Poisson's ratio.

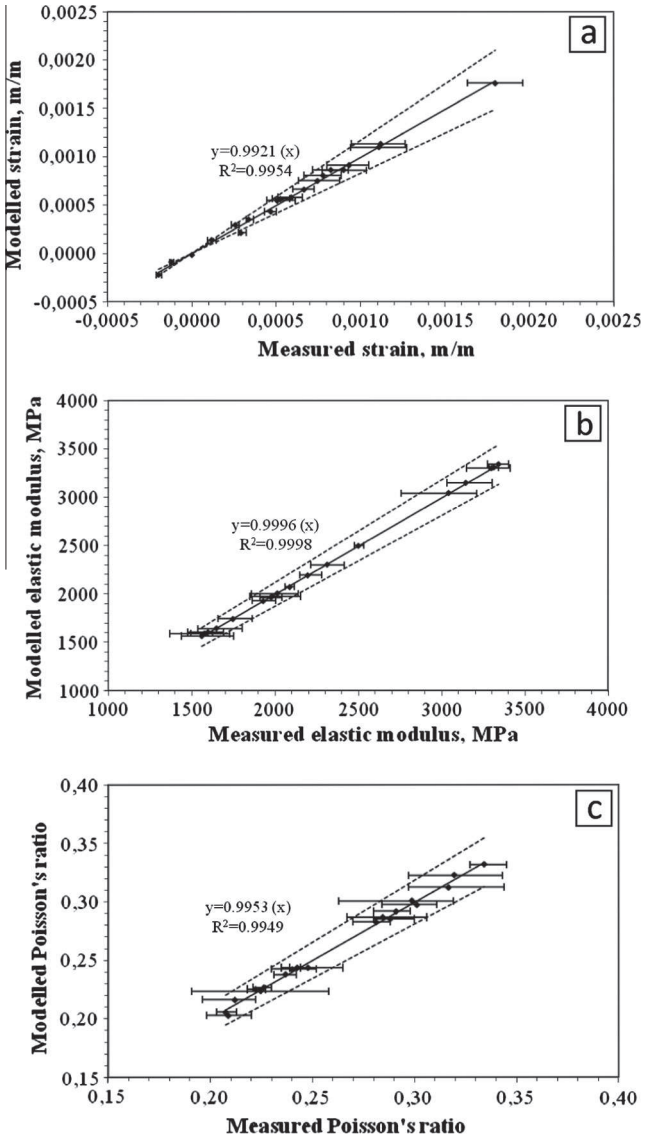

Fig. 9. Comparison between the experimental and modelled stone response of: (a) strain, (b) elastic modulus and (c) Poisson's ratio.

response–temperature–water saturation relationship as presented in Eqs. (13)–(15), respectively.

The surface plots of both the elastic modulus and the Poisson's ratio were truncated so as to avoid representing the value related to the artifact test condition (i.e. $T = -8$ °C and $S_r = 100\%$). This is because, as mentioned before, the results obtained under this experimental test condition were found to be incorrect (the sample was damaged by freezing) and so not taken into account during the model calculations. Thus, the proposed models cannot simulate these specific conditions.

Fig. 10 allows comparison of the proposed models with the calculation of elastic properties at dry state. The strain measurements in dry state seem to be simply bilinear, whereas the proposed model describes the measured strain with greater precision. Both approaches give the same value at the three boundaries conditions due to the calculation: ($T = -8$ °C; $S_r = 0\%$), ($T = 40$ °C; $S_r = 0\%$), ($T = 40$ °C; $S_r = 100\%$). There is no significant difference in the dry state, which corresponds to the usual characterisation conditions. However, since the water saturation is just over 0%, the difference becomes significant. The maximum difference occurs at around 10% of water saturation, which corresponds to about 80% of relative humidity (see Fig. 1). The stone data showed that 80% of

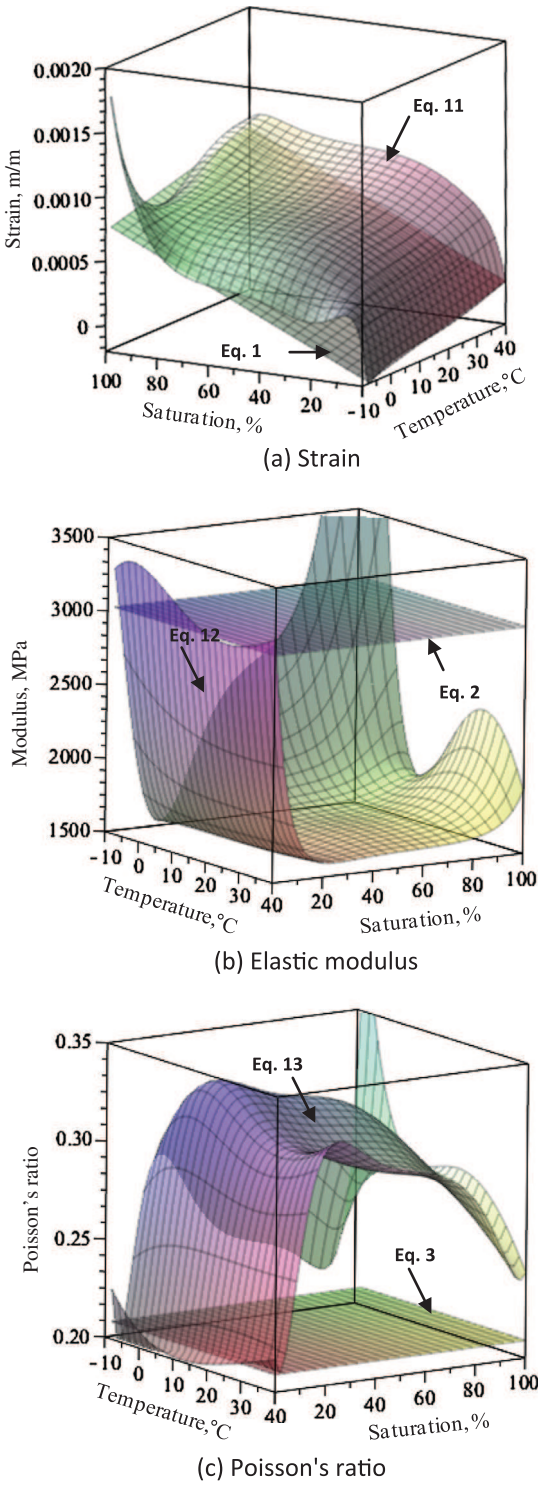

Fig. 10. 3D Graphical representation of the models of: (a) strain, (b) elastic modulus and (c) Poisson's ratio as a function of temperature and water saturation.

relative humidity is quite a usual outdoor environmental condition [6], proving that the bilinear representation of strain is globally inaccurate. For the elastic modulus, both approaches give the same value at 20 °C and the dry state due to the calculation. More generally, the curves are quite similar for the dry state. Since the state is not dry, the two curves are totally different. For most of the experimental range, the value of the elastic modulus in dry state is twice the actually measured one, suggesting that this property is globally inaccurate. Finally, for the Poisson's ratio, the same

analysis can be made; the two approaches give similar values for the dry state but globally differ in the rest of the experimental range.

Indeed, the values of the Poisson's ratio and elastic modulus obtained at S_r = 10% (i.e. RH = 80%) are more representative of the full experimental range compared to the dry state, knowing that the temperature effect is in second order over freezing point.

5. Conclusion

Temperature and water saturation play a crucial role in affecting the mechanical properties of tuffeau, a widespread soft porous limestone widely quarried in France.

The relationship between variations in elastic behaviour (i.e. strain, elastic modulus and Poisson's ratio), temperature and water saturation was experimentally explored and successfully represented by equations using the design of experiments (DOE) method on two complementary experimental plans.

The resulting models are statistically validated in the range of −8 °C to 40 °C for temperature and 0–100% for water saturation. However, the model cannot be used to simulate the particular conditions of −8 °C and S_r = 100%, since this condition damaged the tested sample due to freezing.

By ranking the significance of the single and coupled effects of temperature and water saturation variation, the stone strain was found to be affected most by the single effect of water saturation. The Poisson's ratio was the most dependent on the single effect of water saturation, followed by the coupled effects of temperature/water saturation. The elastic modulus depends on the effects of all three parameters.

The equations of the models for stone strain, elastic modulus and Poisson's ratio can be plotted in a 3D graphical representation and compared with the elastic properties at dry state. These properties are accurate in the dry state but inaccurate for most environmental conditions (outdoor state of buildings). As material characterisation is the first step in the assessment of damage risk due to climatic conditions through hygrothermal stress calculation, the proposed models represent an essential contribution to any further research involving the simulation of outdoor conditions on the mechanical behaviour of stones. Based on the proposed coupled hygrothermal characterisation, it is now possible to calculate hygrothermal stress using the mechanical approach relative to the effect of restrained hygrothermal dilations. This new approach includes the effect of temperature and water saturation not only on the strain variation, but also on the elastic modulus and the Poisson's ratio. Hence, this methodology can be applied as a data source to determine the stresses in building stones induced by cyclic variation in environmental conditions. This approach enhances the study of the durability of materials used in the construction and maintenance of buildings.

References

[1] Tarik Ozkahraman H, Bolatturk A. The use of tuff stone cladding in buildings for energy conservation. Constr Build Mater 2006;20(7):435–40.

[2] Vázquez P, Alonso FJ, Carrizo L, Molina E, Cultrone G, Blanco M, et al. Evaluation of the petrophysical properties of sedimentary building stones in order to establish quality criteria. Constr Build Mater 2013;41:868–78.

[3] Yurdakul M, Akdas H. Modelling uniaxial compressive strength of building stones using non-destructive test results as neural networks input parameters. Constr Build Mater 2013;47:1010–9.

[4] Bonazza A, Sabbioni C, Messina P, Guaraldi C, De Nuntiis P. Climate change impact: mapping thermal stress on Carrara marble in Europe. Sci Total Environ 2009;407:4506–12.

[5] Ponziani D, Ferrero E, Appolonia L, Migliorini S. Effects of temperature and humidity excursions and wind exposure on the arch of Augustus in Aosta. J Cultural Heritage 2012;13:462–8.

[6] Al-Omari A, Brunetaud X, Beck K, Al-Mukhtar M. Effect of thermal stress, condensation and freezing–thawing action on the degradation of stones on the Castle of Chambord, France. Environ Earth Sci 2013. http://dx.doi.org/10.1007/s12665-013-2782-4.

[7] Al-Omari A, Brunetaud X, Beck K, Al-Mukhtar M. Effect of environmental conditions on the degradation of stones in the Castle of Chambord. 31èmes Rencontres de l'AUGC, E.N.S. Cachan, 29–31 May; 2013b.

[8] Weiss T, Siegesmund S, Kirchner D, Sippel J. Insolation weathering and hygric dilatation: two competitive factors in stone degradation. Environ Geol 2004;46(3–4):402–13.

[9] Benavente D, Cultrone G, Gomez-Heras M. The combined influence of mineralogical, hygric and thermal properties on the durability of porous building stones. Eur J Mineral 2008;20(4):673–85.

[10] Koch A, Siegesmund S. The combined effect of moisture and temperature on the anomalous expansion behaviour of marble. Environ Geol 2004;46(3–4):350–63.

[11] Beck K, AL-Mukhtar M, Rozenbaum O, Rautureau M. Characterisation, water transfer properties and deterioration in Tuffeau: building material in the Loire Valley-France. Build Environ 2003;28(9–10):1151–62.

[12] Beck K. Etude des propriétés hydriques et des mécanismes d'altération de pierres calcaires à forte porosité. Ph.D. Thesis. University of Orleans, France; 2006.

[13] Fredlund DG, Rahardjo H. Soil mechanics for unsaturated soils. New York: John Wiley éd.; 1993. p. 517.

[14] Shoukry SN, William GW, Downie B, Riad MY. Effect of moisture and water saturation on the mechanical properties of concrete. Constr Build Mater 2011;25:688–96.

[15] Kodama J, Goto T, Fujii Y, Hagan P. The effects of water content, temperature and loading rate on strength and failure process of frozen rocks. Int J Rock Mech Min Sci 2013;62:1–13.

[16] Dwivedi RD, Goel RK, Prasad VVR, Sinha A. Thermo-mechanical properties of Indian and other granites. Int J Rock Mech Min Sci 2008;45:303–15.

[17] Wu G, Wang Y, Swift G, Chen J. Laboratory investigation of the effects of temperature on the mechanical properties of sandstone. Geotech Geol Eng 2013. http://dx.doi.org/10.1007/s10706-013-9614-x.

[18] Lam dos Santos JP, Rosa LG, Amaral PM. Temperature effects on mechanical behaviour of engineered stones. Constr Build Mater 2011;25:171–4.

[19] Brunetaud X, Linder R, Divet L, Duragrin D, Damidot D. Effect of curing conditions and concrete mix design on the expansion generated by delayed ettringite formation. Mater Struct 2007;40:567–78.

[20] Brunetaud X, Divet L, Damidot D. Impact of unrestrained delayed ettringite formation-induced expansion on concrete mechanical properties. Cem Concr Res 2008;38:1343–8.

[21] Pavoine A, Brunetaud X, Divet L. The impact of cement parameters on Delayed Ettringite Formation. Cement Concr Compos 2012;34:521–8.

[22] Linder R. Les plans d'expériences, un outil indispensable à l'expérimentateur. Presse de l'École Nationale des Ponts et Chaussées; 2005.

[23] Al-Omari, Brunetaud X, Beck K, Al-Mukhtar M. Experimental study on the role of freezing–thawing in the degradation of stones in the Castle of Chambord. In: Proceedings of International Conference on Built Heritage. Milano, Italy; 2013c.

[24] Chen TC, Yeung MR, Mori N. Effect of water saturation on deterioration of welded tuff due to freeze–thaw action. Cold Reg Sci Technol 2004;38:127–36.

[25] Prick A. Dilatometrical behaviour of porous calcareous rock samples subjected to freeze–thaw cycles. Catena 1995;25:7–20.

[26] Beck K, Al-Mukhtar M. The mechanical resistance properties of two limestones from France, tuffeau and Sébastopol. In: Prikryl R, editor. Book of Proceedings of Dimension Stone 2004: New Perspectives for a Traditional Building Material. A.A. Balkema Publishers (ISBN 90 5809 675 0). p. 97–102.

Appendix 3

INTERNATIONAL JOURNAL OF CIVIL AND STRUCTURAL ENGINEERING
Volume 4, No 3, 2014

Research article ISSN 0976 – 4399

Hygrothermal stress and damage risk in the stones of the Castle of Chambord-France

Asaad Al-Omari[1,2], Xavier Brunetaud[1], Kevin Beck[1], Muzahim Al-Mukhtar[1]
1- CNRS-Centre de Recherche sur la Matière Divisée, 1 Rue de la Ferollerie, 45100 Orléans, France
2- Department of Civil Engineering, College of Engineering, Mosul University, Al-Majmooah Street, Mosul, Iraq
muzahim.al-mukhtar@univ-orleans.fr
doi:10.6088/ijcser.201304010039

ABSTRACT

The aim of this paper is to assess the risk of climate-induced damage to stone through the calculation of hygrothermal stresses. The stone studied is tuffeau, the main building stone of the Castle of Chambord. The climate is assessed though measurement of the stone temperature and relative humidity using sensors inserted into the stones of the castle. The mechanical properties required for stress calculation are the elastic modulus, the Poisson's ratio and the hygrothermal strain. A numerical model based on restrained strain was used to estimate the hygrothermal stresses, which were analysed through the calculation of their daily variation, or alternatively by comparison with core behaviour. The parameters studied include the depth in the stone, the orientation of the walls, the alternative calculation methodology, and an optional correction of stone data due to sensor accuracy. Results show that the risk of damage to the stone exposed to climate fluctuations can be significant: joint cracking due to tension near the stone surface, and surface buckling due to compression for stones already subjected to spalling, leading to crack propagation. The risk decreases with depth, and is maximal on the south wall. Sensor accuracy for high relative humidity proved to be a significant issue.

Keywords: Damage risk assessment, hygrothermal stress, spalling, tuffeau, Castle of Chambord.

1. Introduction

Sustainable conservation of the built heritage involves studying the stresses experienced by materials of the monument in question, as this can provide key information to reduce the progress of damage, and to choose appropriate solutions for restoration.

Cultural heritage buildings are made of stone that must withstand the stresses induced by the loads of the structure itself, and on a more local scale, the stresses induced by surface phenomena: salt or ice crystallization, and thermal and hygric dilation. These surface phenomena are induced by interaction between local climate conditions and the properties of the stones. The monitoring of field temperature and humidity data, added to an appropriate characterization of the stone properties, are therefore prerequisites for such work.

Recently, several studies have investigated the mechanism that leads to degradation of the stones in the Castle of Chambord. Some of these studies involved the multi-scale experimental physical, chemical, and mechanical characterization of stone behaviour, in addition to laboratory ageing tests (Al-Omari et al., 2013b; Janvier-Badosa et al., 2013, 2010).

Received on January, 2014 Published on February 2014

Others concerned the organization of all the data collected in a 3D documentation platform, the so-called digital health record, to be used as a diagnostic tool and decision support in the conservation and restoration planning phase (Stefani et al., 2013).

Several previous studies explored the impact of climatic conditions on the decaying processes of stones (Al-Omari et al., 2013a; Bonazza et al., 2009a and b; Ponziani et al., 2012; Eklund, 2008; Camuffo, 1998; Camuffo and Sturaro, 2001; Moropoulou et al., 1995; Viles, 2005). The work presented in this study is part of a research program on the degradation mechanisms of building stones in the Castle of Chambord. The paper focuses on assessing the risk of damage to the stone at different depths due to variation in the local climatic conditions through calculation of the induced hygrothermal stress, building on two previous studies (Al-Omari et al., 2013a, 2014). The first one aimed at assessing different damage processes such as thermal stress, condensation, and freezing-thawing cycles that could lead to degradation of the stone. The second one involved the coupled hygrothermal characterization of the stone elastic properties (i.e. elastic modulus, Poisson's ratio and hygrothermal strain). The present paper focuses on the calculation of stresses from restrained dilations. While previous attempts of stress calculation were limited to the effect of restrained thermal dilation (σ_T), with standard material characterization, the present one treats the coupled hygrothermal stress ($\sigma_{T\text{-}H}$) based on the coupled hygrothermal characterization of stone elastic properties. Moreover, the main application of this paper is not limited to the calculation of compressive stresses, but also covers tensile stresses, which may be more critical as the tensile strength of stone is weaker than the compressive strength.

2. Site, methods, climate data, and material characterisation

2.1 Site, the Castle of Chambord

The Castle of Chambord, Figure (1) is one of the most famous castles in the world as it is an emblem of French Renaissance architecture. It blends traditional French medieval forms with classical Renaissance structures. Its construction began in 1519, and reached completion in 1547, then changed little until 1639, when Louis XIV restored and furnished the castle. Further restorations took place at different periods in the 20th century. The Castle of Chambord has been part of the UNESCO World Heritage list since 1981.

This study focuses on the stones located in the walls of the east tower of the Castle, for three main reasons, Figure (1). Firstly, most of the stones in the walls of the east tower are original (not restored). Secondly, the east tower includes many highly degraded stones, with two main patterns of degradation: biological colonization (different types of lichens and mosses) and stone detachment in the form of stone spalling and exfoliation (Janvier-Badosa et al., 2013). Lastly, the semi-circular shape of the east tower makes it possible to study two different wall orientations, north- and south-facing, and thus to assess the effect of the wall orientation on the spatial distribution of the hygrothermal stresses induced within the stone.

2.2 Local climatic conditions

The Castle of Chambord is located in a rural area about 150 km to the south-west of Paris, approximately 84 m above average sea level. The area surrounding the castle is subjected to a mild humid temperate climate with moderately warm summers and no dry season. The meteorological data recorded during 1997-2012 at Bricy Air-Base station, about 45 km NE of the castle of Chambord, Figure (1), revealed that the average annual temperature is 11.4 °C,

while daily variations are often in excess of 20 °C and 70% for stone temperature and stone humidity, respectively (Al-Omari et al., 2013a).

The digital thermal-humidity sensors FHAD-46x were used to measure the stone temperature (accuracy 1.3% for a temperature range from -20°C to 80°C) and stone humidity (accuracy 1.8% for humidity between 0%-90%). These sensors were installed on the stone surface and inserted at different depths (15, 30, 50 and 250 mm) inside the stones on both the north and south walls. The measurements of stone data lasted three years, from June 2009 to May 2012. The readings were recorded every 30 minutes, giving a total of 52560 values for temperature and humidity for each case studied (at different depths within the stone and at two different orientations).

An example of stone data is presented in Figure (2). It shows the daily maximum and minimum values of temperature and relative humidity, at 15 and 250 mm depth inside the stones located on the south wall, during one year. The recorded data revealed that the highest temperature and humidity variations occur at a depth of 15 mm inside the stone. At this depth, the daily difference between the extreme values of temperature and humidity can exceed 20°C and 30%, respectively, whereas at a depth of 250 mm, low or negligible variations were observed for both temperature and humidity (i.e. below 3°C for temperature and below 0.5% for humidity).

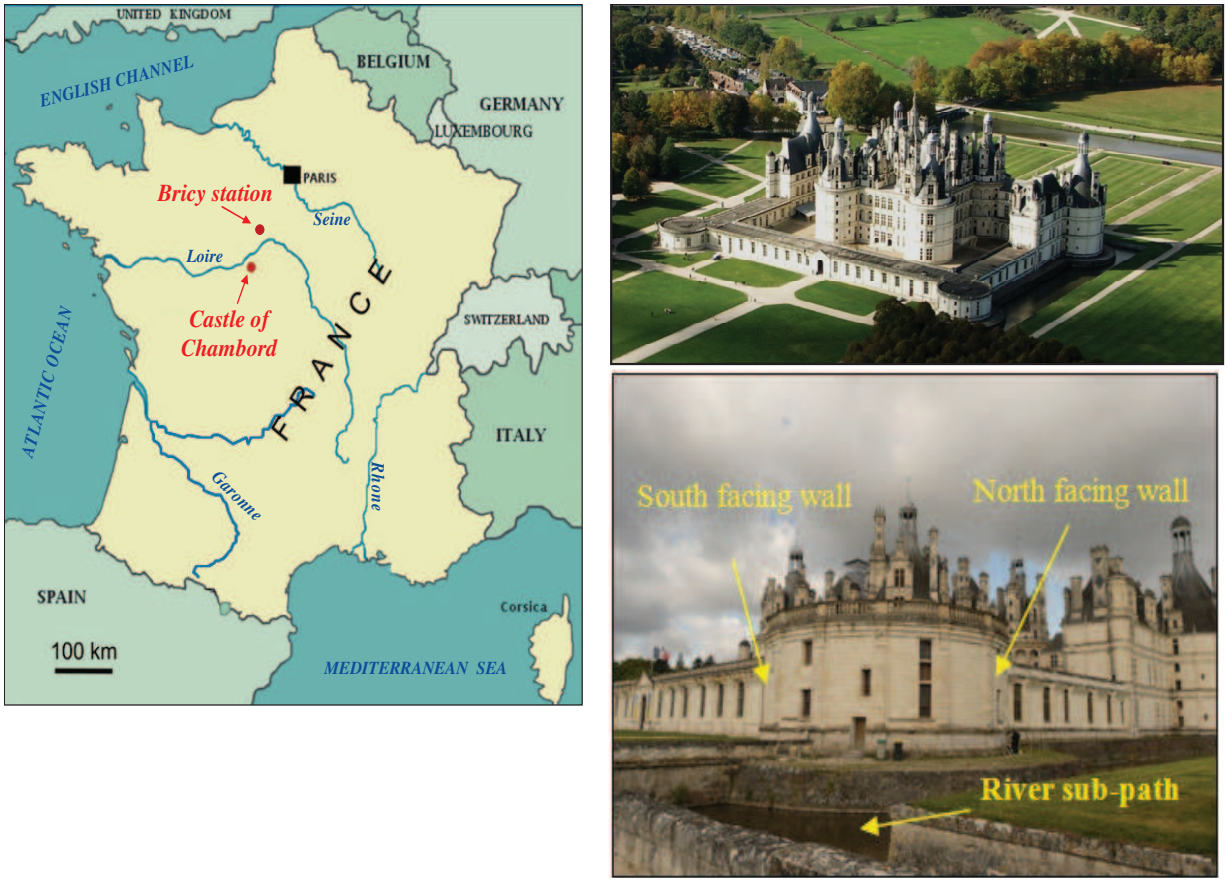

Figure 1: Geographical setting of the Castle of Chambord (*left*); the Castle of Chambord-aerial view "copyright: Domaine national de Chambord" (top right); the east tower of the castle (bottom right)

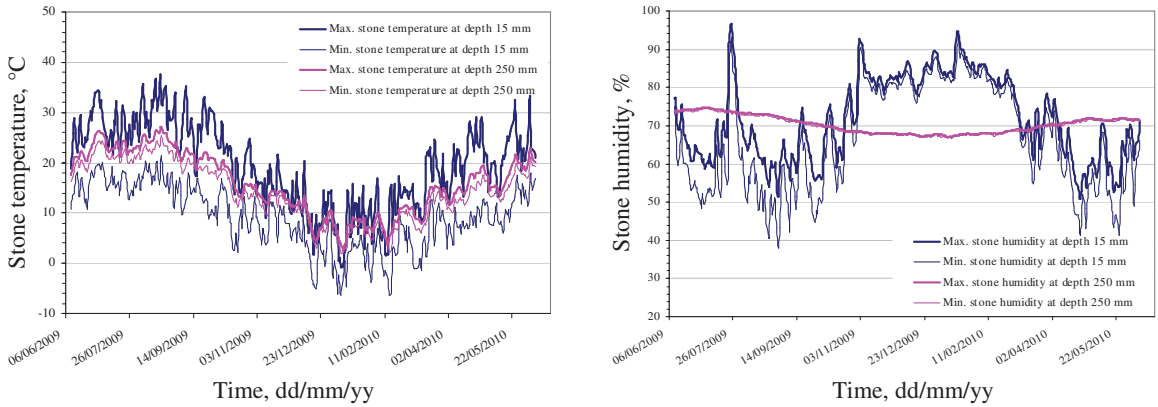

Figure 2: Daily maximum and minimum values of temperature (left) and relative humidity (right) at 15 and 250 mm depth, on the south wall for the period from June 2009June 2009 to June 2010

2.3 Material characterisation

The Castle of Chambord was mainly constructed in a soft-porous limestone, called tuffeau. This limestone dates from the Turonian age, the upper Cretaceous period, approximately 88-92 million years ago. Tuffeau was widely used in a number of castles in the Loire Valley because it is fine-grained, lightweight, shiny white in colour, and can be easily cut. It is characterized by a multi-scale pore size distribution, variable mineral composition and heterogeneous petrophysical properties (Beck et al., 2003). According to Folk's classification, tuffeau can be classified as a siliceous limestone that contains maritime fossils (coccoliths), reflecting its sedimentary origin. This highly porous limestone (porosity about 45%) is composed of 50% calcite and 30% silica in the form of opal cristobalite-tridymite, 10% quartz, and 10 % of clayey minerals (Dessandier, 2000), and is highly sensitive to moisture, Figure (3). Nowadays, tuffeau is still quarried in the area close to the Loire River.

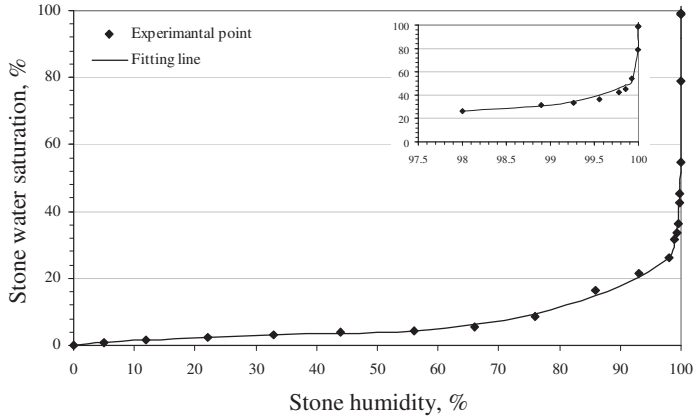

Figure 3: Relationship between stone humidity and degree of water saturation, (Beck, 2006)

The unconfined compressive strength (UCS) of tuffeau ranged between 12 MPa and 4.8 MPa for dry and fully saturated samples, respectively, while the indirect tensile strength values, measured by means of the Brazilian test, were 1.5 MPa for dry samples and 0.5 MPa for saturated samples (Beck, 2006). The relationships between the strength of tuffeau and water

saturation were fitted using logarithmic mathematical equations, as shown in Figure (4). These correlations are used later in this paper to estimate the strength of tuffeau at any water saturation.

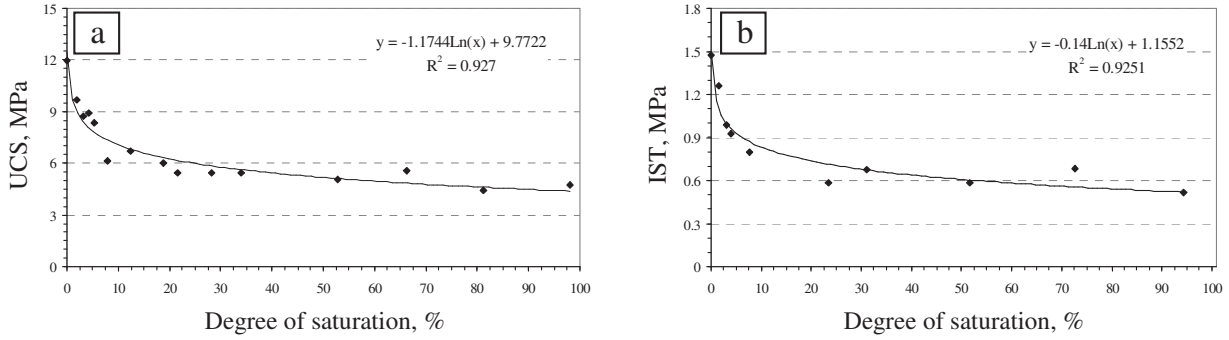

Figure 4: Correlation between degree of water saturation and Unconfined Compressive Strength, UCS (a), and Indirect Tensile strength, ITS (b), (Beck, 2006)

The elastic parameters (see section 2.4) used for calculation of the induced $\sigma_{T\text{-}H}$ can be obtained using Eqs.1, 2 and 3, at any stone temperature in the range from -8ºC to 40ºC and at any stone humidity between 0% and 100% (Al-Omari et al., 2014). These limits represent the extreme, but realistic, range of stone temperature and humidity measured in the field. The symbols (s and t) used in Eqs.3, 4 and 5 are the coded values obtained by the Design of Experiment (DOE) methodology used in this study. The coded values at different levels of stone temperature and stone water saturation (i.e. stone humidity) are listed in Table (1).

$$\varepsilon_{T\text{-}H} = [\,61.898 + 5.202t + 18.854s - 4.09t^2 + 1.519s^2 - 0.489ts - 3.944t^2s + 1.584ts^2 + 8.16t^3 + 0.565s^3 + 4.54t^3s + 0.965ts^3 + 5.53t^2s^2 - 2.36s^4 - 4.08t^3s^2 + 3.26t^2s^3 - 2.7t^3s^3\,] \cdot (10)^{-5} \quad \text{Eq.1}$$

$$E_{T\text{-}H} = 1570.775 + 17.303t + 19.098s + 6.02t^2 + 248.808s^2 - 94.496st + 11.67t^3 + 61.634st^2 - 92.936s^2t - 100.175s^3 - 19.486st^3 + 58.033s^3t + 191.29s^2t^2 - 127.7s^2t^3 + 80.14s^3t^2 + 21.89s^4t - 75.66s^3t^3 \quad \text{Eq.2}$$

$$\upsilon_{T-H} = 0.325 - 0.021t + 0.033s - 0.011st - 0.53s^2 + 0.021s^2t - 0.017st^2 + 0.016t^3 - 0.003s^3 + 0.012st^3 - 0.009s^2t^2 + 0.003s^3t + 0.008s^4 - 0.008s^2t^3 + 0.005s^3t^2 - 0.004s^4t - 0.005s^3t^3 + 0.004s^4t^2 \quad \text{Eq.3}$$

Table 1: Coding of the levels for stone temperature and stone water saturation (Al-Omari et al., 2014)

Variable	Temperature levels					Water saturation levels				
Value: T or S	-8ºC	2ºC	20ºC	40ºC		0%	7%	23%	80%	100%
Coding*: t or s	-1.442	-0.617	0.565	1.423		-1.930	-1.117	0.073	1.016	1.960
*Equation for temperature coding, $t = = -6.10^{-4}.T^2+0.0789.T-0.7726$ *Equation for water saturation coding, $s = 1.28.10^{-5}.S^3-0.0022.S^2+0.1309.S-1.9298$										

2.4 Methods

The mathematical model (Eq.4) presented in previous studies (Bonazza et al., 2009a; Ponziani et al., 2012; Al-Omari et al., 2013a) was used to calculate the thermal stresses (σ_T) induced in the stone due to the daily variation in stone surface temperature. This equation refers to the mechanical response of a semi-infinite medium to restrained thermal dilation. The resulting stress is calculated in the plane subjected to zero strain (i.e. the plane of the walls in the case of the Castle of Chambord). In the direction perpendicular to this plane, the strain is assumed to be free so the resulting stress is zero.

$$\sigma_T = \frac{E \cdot \alpha \cdot \Delta T}{1 - \upsilon} \qquad \text{Eq.4}$$

where:

E : The elastic modulus, Pa
α : The linear thermal expansion coefficient, $^{o}K^{-1}$
ΔT : The daily variation in stone surface temperature, °K
υ : The Poisson's ratio

In the present study the $\sigma_{T\text{-}H}$ generated inside the stones due to the variation in temperature and humidity were calculated by modifying Eq.4 to take the form below:

$$\sigma_{T-H} = \frac{E_{T-H} \cdot \varepsilon_{T-H}}{1 - \upsilon_{T-H}} \qquad \text{Eq.5}$$

Where the three elastic parameters - elastic modulus ($E_{T\text{-}H}$), Poisson's ratio ($\upsilon_{T\text{-}H}$) and strain ($\varepsilon_{T\text{-}H}$) - included in the modified model are functions of stone temperature and stone humidity. Since positive hygrothermal strain means positive dilation, the restriction of this positive strain generates compression. Consequently, when the result of Eq. 5 returned positive stresses, it corresponded to compression, while negative stresses meant tension.

The $\sigma_{T\text{-}H}$ stresses were calculated for each value of temperature and humidity collected (i.e. every 30 min during three years for each depth and wall orientation). The calculated $\sigma_{T\text{-}H}$ stresses were analyzed through two methods. The first one is called "daily variation in hygrothermal stresses". In this case the risk of damage induced to the stone due to the $\sigma_{T\text{-}H}$ was estimated with the methodology presented in previous work (Al-Omari et al., 2013a; Bonazza et al., 2009a; Ponziani et al., 2012). This method consisted in identifying the daily variation in stone stresses, i.e. the difference between the maximum and minimum stone stresses. This was done in an attempt to quantify the variations that may generate fatigue to the stones. These daily variations in stone stresses were divided by the lowest UCS calculated each day to represent the actual stress level as a proportion of the strength. In order to calculate the daily lowest UCS, the maximum stone humidity for each day was selected. Then Figure (3) was used to obtain the maximum stone saturation based on the maximum stone humidity. Finally, the minimum unconfined compressive stone strength was determined by using the formula presented in Figure (4-a).

The second method is called "maximum and minimum differential hygrothermal stresses". This new alternative consisted in computing the maximal and minimal stresses resulting from

the daily variation in stone temperature and stone humidity, assuming a zero level of stress at 250 mm depth. These stresses were calculated by subtracting the stresses generated near the surface (at 15, 30 and 50 mm depth) from the stress measured at 250 mm depth. This depth is assumed to correspond to the mean state of the stone as it is very slightly affected by climatic variations (see Figure 2), allowing creep effects to stabilize.

In addition to these two methods, another parameter was studied: the correction of stone data. Since the accuracy of the sensors is not guaranteed in the 90-100% humidity range, the hypothesis that every value above 90% of humidity could be 99.99% (i.e. capillary saturation) was systematically tested. This hypothesis is supported by observations in the field: after heavy rainfall with significant wind, the humidity near the surface of stones is always randomly in the range 90-98 %, even if the surface is visually water saturated.

3. Results

3.1. Calculation of hygrothermal stresses

The results of both methods for stress calculation are presented in this section. For each result, two different hypotheses are presented: results based on actual stone data and results based on corrected stone data. Then, the damage risk assessment is presented for each method, and for each set of stone data.

3.1.1 Daily variation in hygrothermal stresses

The $\sigma_{T\text{-}H}$ calculated using Eq.5 was analyzed. Based on the original values of stone humidity, the daily variations in the $\sigma_{T\text{-}H}$ at three depths (15, 30 and 50 mm) inside the stones of both north and south walls, over a one-year period (June 2009June 2009 to June 2010), are presented in Figure (5). Figure (6) presents the same results when the calculations of the $\sigma_{T\text{-}H}$ were based on the adjusted stone humidity. The adjustment of the stones' humidity values resulted in an increase in the values of the daily variation in stone stresses, especially for the stone of the south walls.

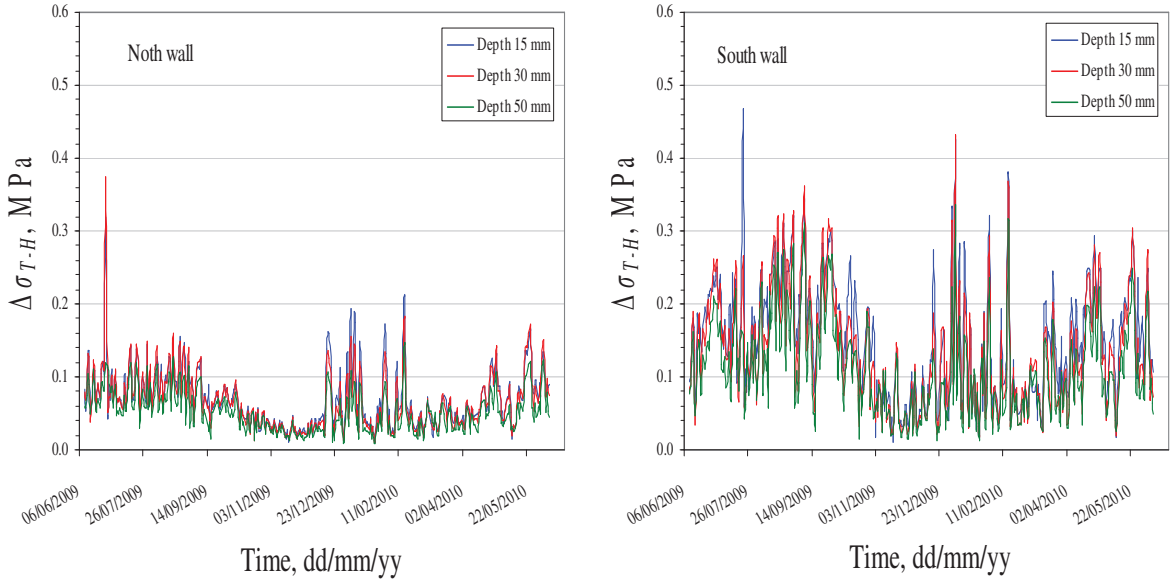

Figure 5: Daily variations in hygrothermal stresses at different depths inside the stone for the period from June 2009 to June 2010 on both, north wall (left), and south wall (right), **based on the original stone humidity**

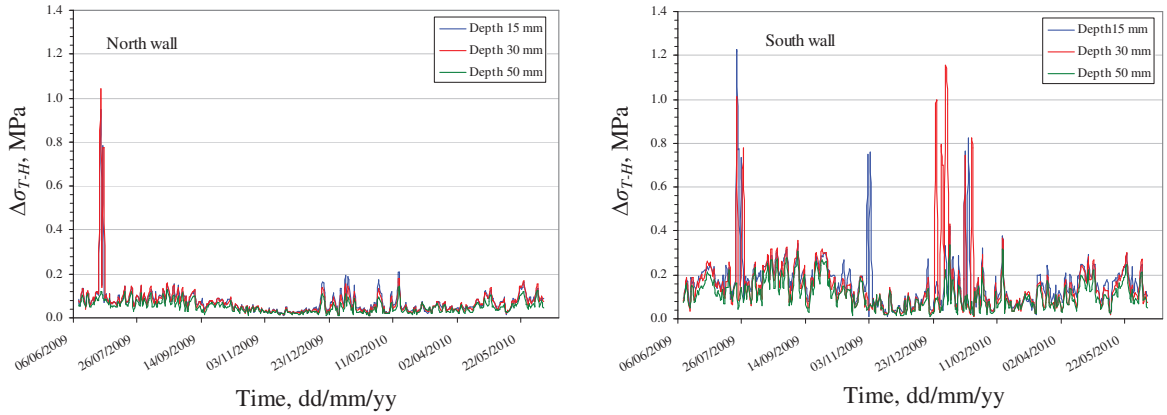

Figure 6: Daily variations in hygrothermal stresses at different depths inside the stone for the period from June 2009 to June 2010 on both, north wall (left), and south wall (right), **based on the adjusted stone humidity**

3.1.2 Maximum and minimum differential hygrothermal stresses

Using the first method, it was possible to distinguish two extreme stresses (maximum and minimum) each day for each depth. By comparing these two extreme stresses and the reference stress at 250 mm depth the maximum and minimum differential stresses were calculated. When this differential stress was positive, it was compression, and tension when negative. The results of the analysis, based on the original stone humidity measurements, showed that, for both the north and south walls, the compression and tension stresses respectively reached 0.4 MPa and 0.3 MPa, Figure (7). The results in Figure (8) indicate that the adjustment of the stone humidity had little impact on the tensile stresses, while a clear effect was observed for the compressive stresses. The maximum/minimum stresses and the reference stress can both be positive as shown with the orange circles and both negative as shown with the black circles in Figure (7).

3.2. Damage risk assessment

3.2.1. Damage due to daily variation in hygrothermal stresses

The $\sigma_{T\text{-}H}$ stresses were compared with the minimum stone strength to assess the risk of damage to the stones located in the Castle of Chambord. In this case the daily variation in $\sigma_{T\text{-}H}$, for each day over the three-year period, was divided by the daily minimum stone strength. Figures (9 and 10) present an example of these daily variations during one year (from June 2009 to June 2010); the calculations were done by following the two bases adopted in the analysis, i.e. original and adjusted stone humidity.

In this study, the damage to stone was estimated by comparing the σT-H with the maximum sustainable load. The maximum sustainable loads for the stone were obtained by dividing the unconfined compressive strength by a safety factor (Bonazza et al. 2009a; Ponziani et al., 2012; Al-Omari et al., 2013a). Table (2) lists the annual percentages of days with a daily variation of $\sigma_{T\text{-}H}$ exceeding the maximum sustainable loads at different safety factors, over the three-year period for the north and south walls, and for the original set of humidity data. Table (3) presents the same results as those in Table (2) but the analysis is based on the adjusted stone humidity. The results show that, irrespective of the safety factor, the damage risk due to the daily variation in $\sigma_{T\text{-}H}$ is several times higher for the analysis based on the adjusted stone humidity than for the analysis based on the original one.

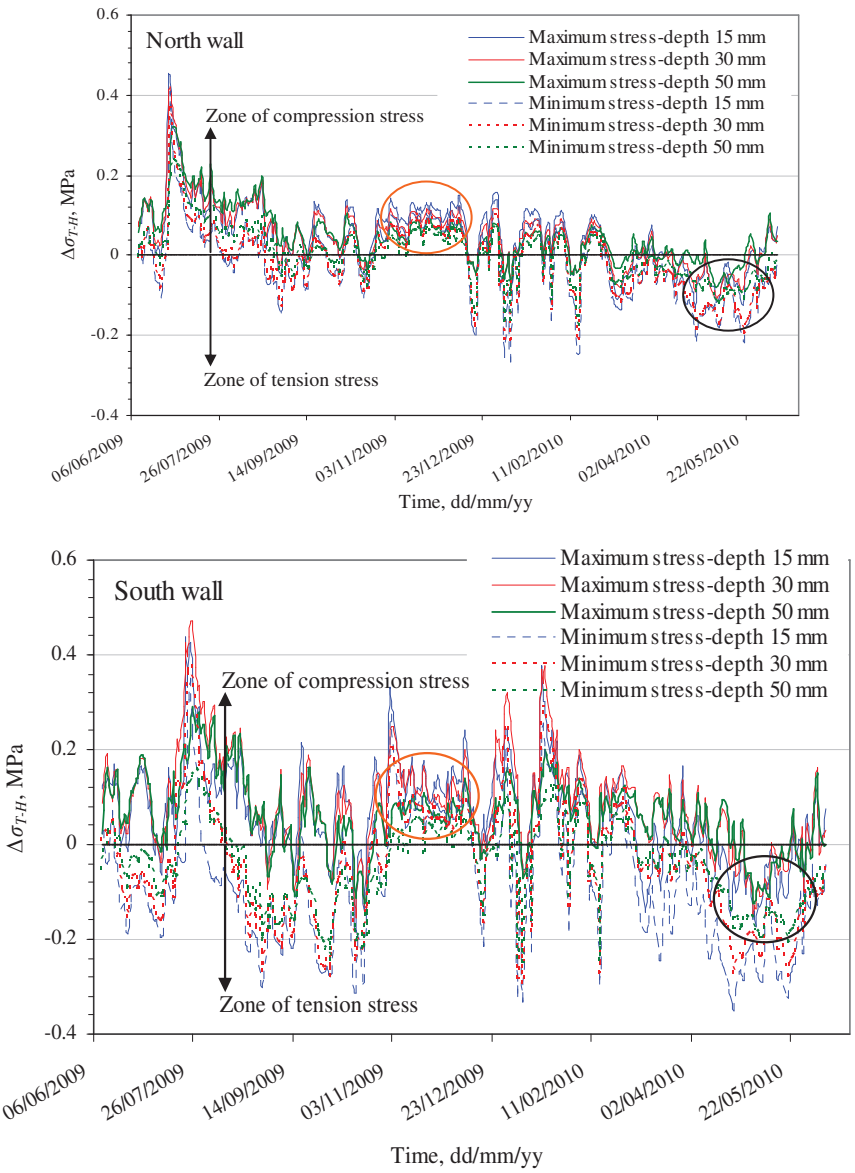

Figure 7: Maximum and minimum hygrothermal stresses at different depths inside the stone for the period from June 2009 to June 2010 on the north wall (top) and the south wall (bottom)**, based on the original stone humidity**

Table 2: Annual percentage of days with daily variation in hygrothermal stresses exceeding the sustainable load over the 3-year period (June 2009 to June/2012) for both north and south walls, depending on the safety factor, based on the original stone humidity

Safety factor	North			South		
	15 mm	30 mm	50 mm	15 mm	30 mm	50 mm
1	--	--	--	--	--	--
2	--	--	--	--	--	--
4	--	--	--	--	--	--
8	--	--	--	--	--	--
12	--	--	--	0.10	--	0.05
16	0.06	0.03	--	0.27	0.13	0.16
20	0.17	0.17	0.08	0.71	0.59	0.47

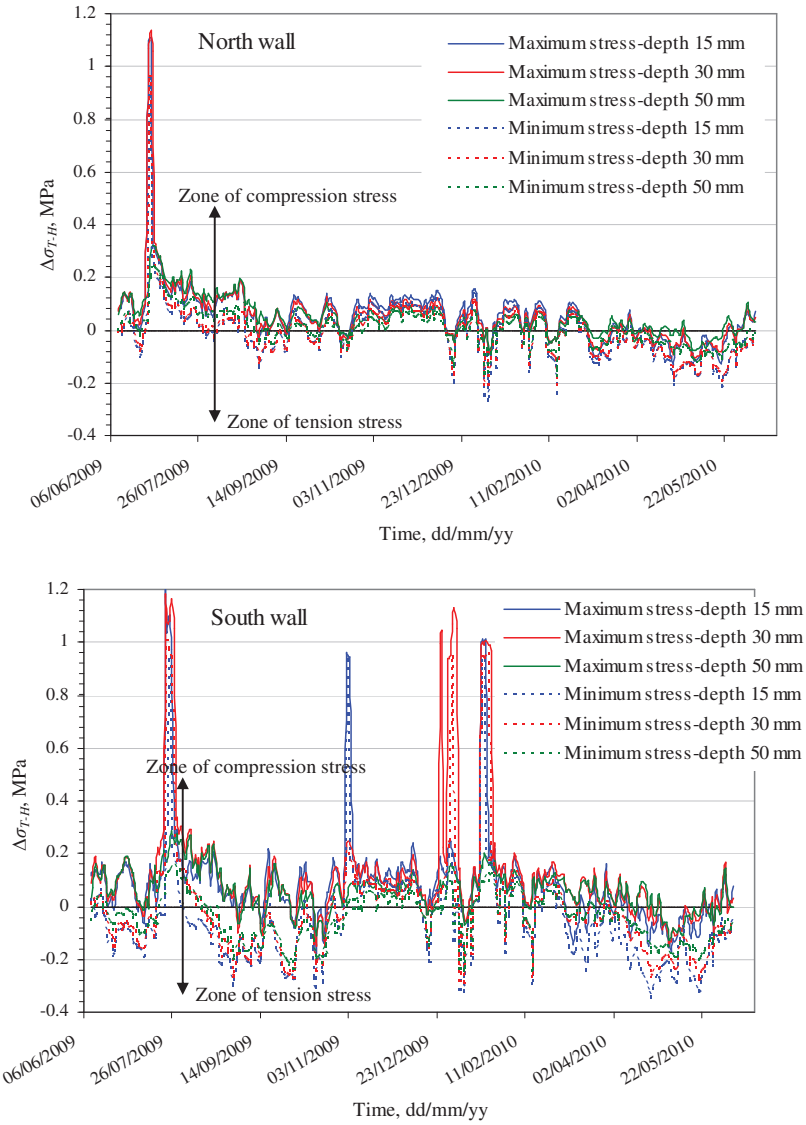

Figure 8: Maximum and minimum and tension hygrothermal stresses at different depths inside the stone for the period from June 2009 to June 2010 on the north wall (top) and the south wall (bottom), **based on the adjusted stone humidity**

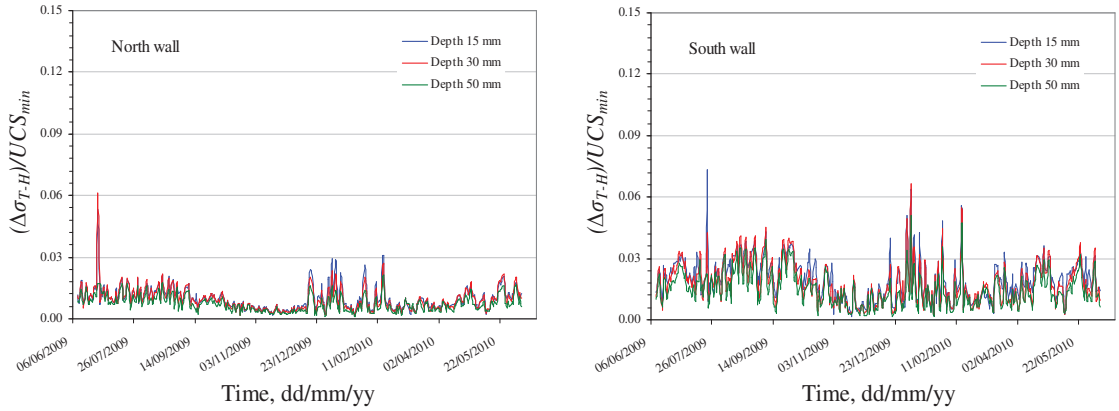

Figure 9: Proportion of daily variations in hygrothermal stresses to the minimum compression strength at different depths inside the stone for the period from June 2009 to June 2010 on both, north wall (left), and south wall (right), **based on the original stone humidity**

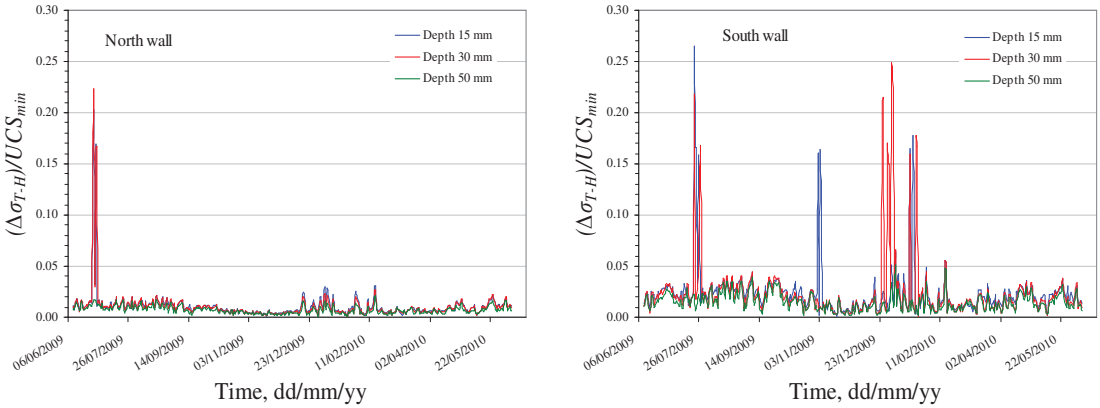

Figure 10: Proportion of daily variations in hygrothermal stresses to the minimum compression strength at different depths inside the stone for the period from June 2009 to June 2010 on both, north wall (left), and south wall (right), **based on the adjusted stone humidity**

Table 3: Annual percentage of days with daily variation in hygrothermal stresses exceeding the sustainable load over the 3-year period (June 2009 to June/2012) for both north and south walls, depending on the safety factor, based on the adjusted stone humidity

Safety factor	North			South		
	15 mm	30 mm	50 mm	15 mm	30 mm	50 mm
1	--	--	--	--	--	--
2	--	--	--	--	--	--
4	--	--	--	0.02	--	--
8	0.88	1.14	0.12	1.51	1.79	--
12	0.94	1.20	0.15	1.63	1.93	0.05
16	1.02	1.27	0.16	1.70	2.09	0.16
20	1.14	1.39	0.25	2.09	2.40	0.47

3.2.2. Damage due to maximum and minimum differential hygrothermal stresses

The calculated compression and tension σ_{T-H}, based on the original stone humidity, were divided by the compressive and tensile strength, over the period from June 2009 to June 2010 for both the north and south walls, and are shown in Figure (11). Both the compressive and tensile strengths were obtained by using relationships presented in Figure (4) with the actual stone saturation values. Figure (12) presents the same approach with σ_{T-H} based on the adjusted stone humidity. The damage to stone was estimated by comparing the σ_{T-H} in compression and in tension with the compressive and tensile sustainable loads. The stone sustainable loads were obtained by dividing the compressive and tensile strength over a suitable safety factor. The analysis based on the original stone humidity, Table (4), lists the annual percentages of days with damage risk to the stone when compression and tension σ_{T-H} exceed the sustainable loads both in compression and in tension conditions at different safety factors over the period of three years for the north and the south walls. Table (5) presents the same results as Table (4) but the analysis is based on the adjusted stone humidity.

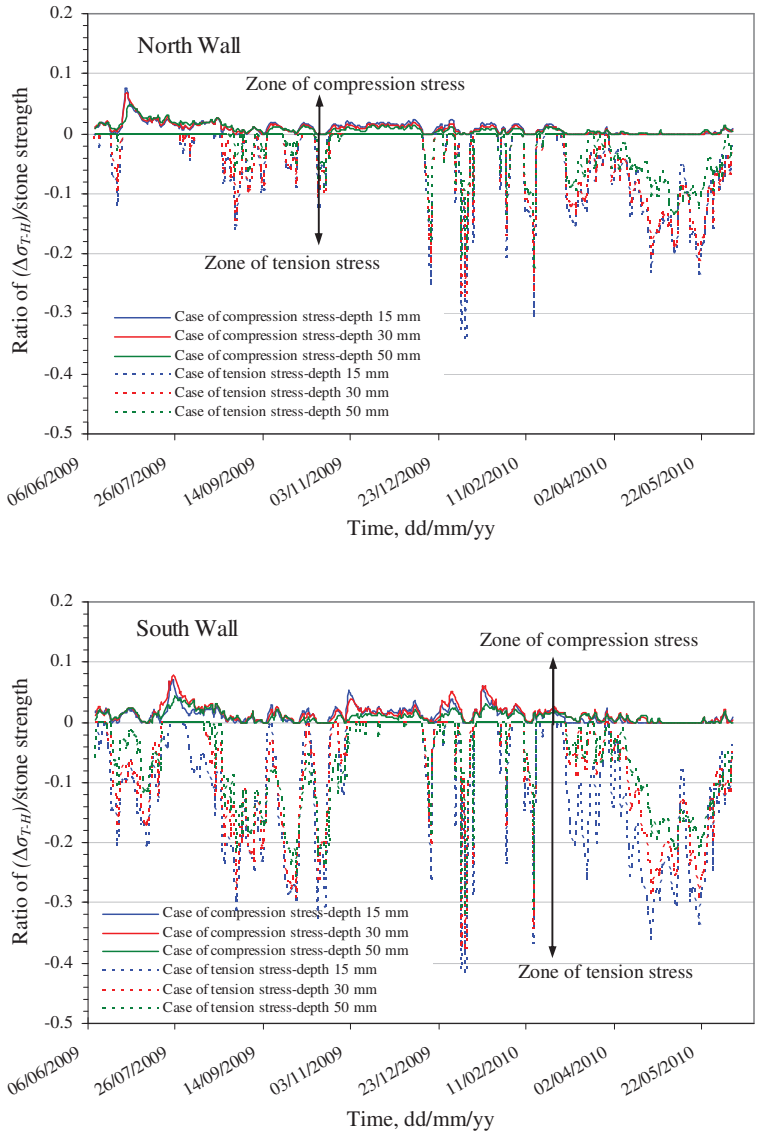

Figure 11: Proportion of compression, tension hygrothermal stresses to compressive, tensile stone strength at different depths inside the stone for the period from June 2009 to June 2010 on the north wall (top) and the south wall (bottom), **based on the original stone humidity**

Table 4: Annual percentage of the damage risk when the compression, tension hygrothermal stresses exceed the stone compressive, tensile strength over the 3-year period for both north and south walls, analysis based on the original stone humidity

Safety factor	**Case of tension stress**						**Case of compression stress**					
	North			South			North			South		
	15 mm	30 mm	50 mm	15 mm	30 mm	50 mm	15 mm	30 mm	50 mm	15 mm	30 mm	50 mm
1	--	--	--	--	--	--	--	--	--	--	--	--
2	0.7	0.6	0.61	--	0.1	0.2	--	--	--	--	--	--
4	3.9	3.0	2.1	16.8	8.53	2.2	--	--	--	--	--	--
8	26.3	18.9	5.7	54.6	43.0	30.9	--	--	--	--	--	--
12	42.8	38.2	19.7	68.4	60.1	46.9	--	--	--	0.4	0.02	--
16	55.0	51.6	34.3	76.3	69.9	58.9	0.3	0.3	--	0.8	1.03	--
20	63.4	60.7	45.3	82.1	75.8	66.2	0.7	0.5	--	1.7	3.14	--

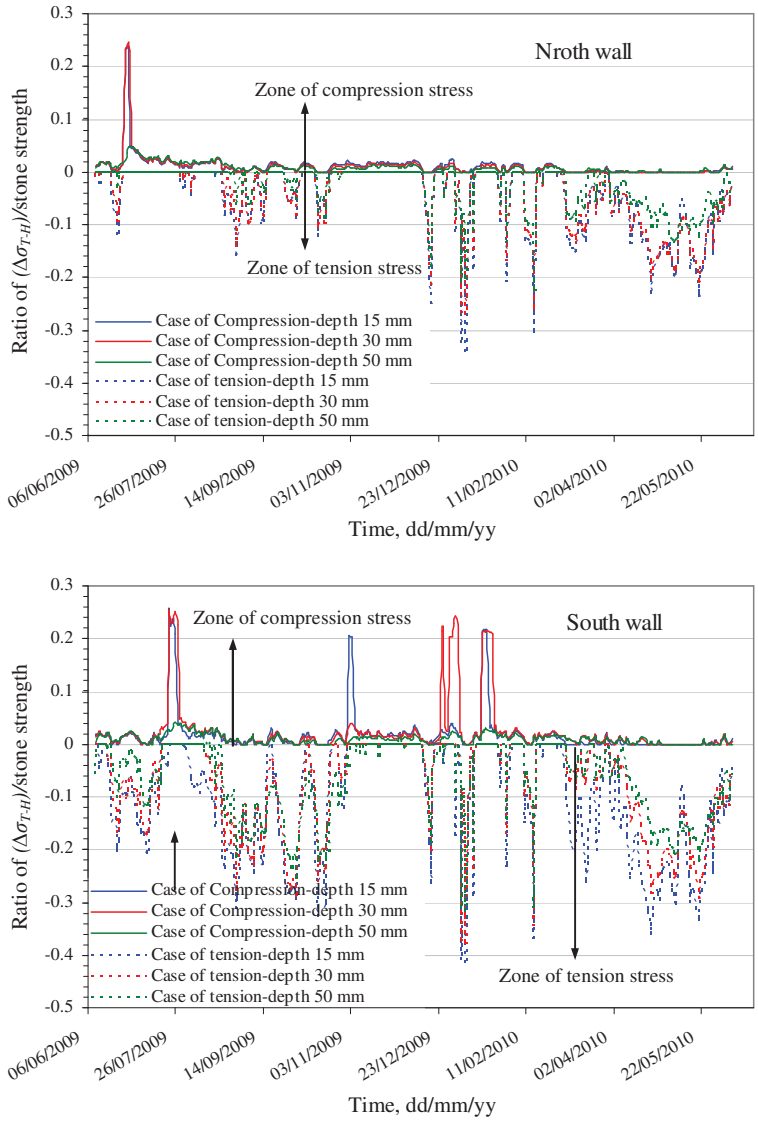

Figure 12: Proportion of compression, tension hygrothermal stresses to compressive, tensile stone strength at different depths inside the stone for the period from June 2009 to June 2010 on the north wall (left), and the south wall (right), **based on the adjusted stone humidity**

Table 5: Annual percentage of the damage risk when the compression, tension hygrothermal stresses exceed the stone compressive, tensile strength over the 3-year period for both north and south walls, analysis based on the adjusted stone humidity

Safety factor	Case of tension stress						Case of compression stress					
	North			South			North			South		
	15 mm	30 mm	50 mm	15 mm	30 mm	50 mm	15 mm	30 mm	50 mm	15 mm	30 mm	50 mm
1	--	--	--	--	--	--	--	--	--	--	--	--
2	0.5	0.5	0.5	--	0.06	0.17	--	--	--	--	--	--
4	2.9	2.2	1.6	12.6	6.39	1.64	--	--	--	0.14	0.22	--
8	19.7	14.1	4.3	41.0	32.2	23.2	4.86	4.68	0.15	2.60	3.54	--
12	32.2	28.7	14.8	51.3	45.0	35.2	4.92	4.73	0.17	2.69	3.63	--
16	41.4	38.7	25.7	57.2	52.3	44.2	4.94	4.76	0.18	2.74	3.68	--
20	47.4	45.3	34.0	61.6	56.8	49.6	4.96	4.81	0.19	2.85	4.33	--

4. Discussion

The damage risk assessment performed in this study has thrown light on the effect of local factors such as the wall orientation or the depth inside the stone. These two local factors are discussed in this section. Moreover, as two different methods were used for stress calculation, in addition to the correction of stone data, these two methodological factors are also discussed.

4.1. Wall orientation

The fluctuations in the calculated $\sigma_{T\text{-}H}$ presented in Figures (5-12) were found to be higher in the stones in the South wall compared to the North wall. These findings can be attributed to the effect of direct insulation. The stones in the south wall are subjected to direct sun rays, leading to increased amplitude in the daily measurements of stone temperature and humidity. For example, the preliminary analysis of the stone data measured at the south wall showed that the daily variation in stone temperature and in stone humidity can exceed 20ºC and 30% respectively, while in the north wall these variations did not exceed 14ºC and 25%, respectively. The results presented in Tables 2 and 3 show that the stone orientation significantly affects the damage risk. The stones in the south wall are subjected to an increased damage risk compared with the stones in the north wall. This also holds for the compression and tension stresses calculated with the alternative methodology (Tables 4 and 5). This effect of wall orientation cannot be supported by in-situ observations since the dates of restoration are different for each span of the tower. However, this calculation tends to conclude that stones oriented southwards require finer monitoring and may require more frequent restoration compared to northward-facing stones.

4.2. Depth inside the stone

The results presented in Tables (2-5) show that, irrespective of the wall orientation, the methodology or the optional data correction, the damage risk decreases with depth. The decrease is significant from 15 mm to 30 mm and becomes even higher from 30 to 50 mm. As for wall orientation, this can be attributed to the lower amplitude of variation in temperature and humidity with depth. This is a consequence of the very fine porosity of tuffeau which results in a low thermal conductivity and low hygric diffusion coefficient. Of course, in-situ visual observations preferentially show surface damage, so no objective conclusion can be drawn from such observations. However, characterization of spalling revealed the presence of a crack network parallel to the surface, whose opening decreases with depth, suggesting that damage decreases with depth (Janvier-Badosa et al., 2013). This observation supports the hypothesis that hygrothermal stresses could contribute to the damage process of spalling, as proposed by (Benavente et al., 2008; Colas et al., 2011).

4.3. Methodology of calculation

In this study, two methodologies were adopted in the analysis of the induced $\sigma_{T\text{-}H}$; by calculating $\sigma_{T\text{-}H}$ as the difference between the daily maximum and minimum stresses (reference method), and by identifying the compression and tension stresses based on the comparison of the daily maximum and minimum stresses at depths up to 50 mm with the stone stresses at 250 mm depth (alternative method). Figures 5 and 6 show the $\sigma_{T\text{-}H}$ obtained by the reference method. Because no stress sign can be extracted with the reference method, all the calculated stresses are assumed to be compression. The alternative method is able to differentiate compression stresses and tension stresses, as shown in Figure 7. The compression stresses calculated with the alternative method were found to be slightly higher than the

compression stresses calculated by the reference method, especially for the stone in the north walls. As the tensile strength of tuffeau is much lower than its compressive strength, the calculation of tension stresses may be more critical. The data in Figure (7) showed that the tension stresses calculated with the alternative method reach 0.35 MPa, which corresponds to a non-nil damage risk with a safety factor of 2 and over. As for compression stresses, the risk is non-nil with a safety factor of 12 and over for the original set of stone data and 4 and over for the optional data correction, see Tables (4 and 5). Hence, the first damage is expected to occur for tension stresses, which would result in cracking of the stone/mortar interface. For high compression stresses, the main risk would be surface buckling. This type of instability could be a major factor for crack propagation or plate split-up when the cracks are parallel to the surface, especially if the thickness of the plate is low compared to its width, as for spalling (i.e. from 1 to 2 cm thick compared to 60 cm wide stones). Hence, tension damage would result in joint cracking while compression damage would result in spalling propagation or split-up. This mechanical analysis proves that it is relevant to calculate both tension and compression stresses, and so to promote the use of the alternative method.

4.4. Stone data correction

As the correction is only performed for days with relative humidity higher than 90%, and because it corresponds to days with heavy rain and wind, this data correction seems to be relevant. From the results presented in Figures (5 and 6) with the reference method, the effect of the stone data correction concerns only a few days in any given year. However, even in this situation, the damage risk is significantly higher for the results with the adjusted stone humidity (see Tables 2 and 3). The same is true of the results of the alternative method, but only for compression stresses. This is due to the fact that the data correction concerns only days with very high relative humidity that would result in positive hygric dilation if the strain were free and so compression since the strain is restrained. As a result, this correction only slightly affects the tension stress calculation, as can be seen in Figures (11 and 12) and Tables (4 and 5). The fact remains that stone data correction provides a significantly increased damage risk, from a minimal safety factor of 12 for compression stresses with the original set of data to only 4 for the same stresses with the adjusted stone humidity (see Table 5). This marked difference in the result demonstrates that sensor accuracy needs to be finer for high humidity so as to prevent any underestimation of the damage risk by compression.

5. Conclusion

This paper aimed to assess the risk of stone damage through the calculation of hygrothermal stresses, using a numerical model representing the effect of restrained dilation. To perform this analysis, it was necessary to first characterize the stone's hygrothermal elastic properties: elastic modulus, Poisson's ratio and hygrothermal strain. The climate data included in this calculation are the stone temperature and relative humidity, measured by sensors inserted into the stone at different depths. Particular attention must be paid when gathering core data; this was done here by inserting a sensor at 250 mm depth.

The reference method consisted in calculating the daily variation in hygrothermal stresses, and by dividing it by the minimal daily compressive strength of the stone. The damage risk was assessed by calculating the number of days with daily variation in stresses exceeding the maximum sustainable load, according to a given safety factor. The new alternative method proposed in this paper consisted in calculating the differential stresses between the surface sensors (15, 30 and 50 mm depth) and the core sensor (250 mm depth). This differential stress, either compression or tension, was divided by the compressive strength or the tensile strength,

respectively. As for the reference method, the damage risk was assessed by calculating the number of days with tension or compression stresses exceeding the corresponding strength, according to a given safety factor.

The parameters studied were: the depth of sensors (15, 30, 50 and 250 mm); the wall orientation (North or South); the methodology (reference or alternative) and the optional stone data correction (original set or adjusted humidity). The study of this correction parameter was motivated by the fact that the accuracy of the sensors used at the Castle of Chambord is not guaranteed from 90 % to 100 % of relative humidity.

The results proved that the risk of damage to the stone can be significant. The first risk of damage is expected to occur in tension near the surface of the stone exposed to climate fluctuations. This would result in joint cracking. For higher safety factors, a significant risk of compression can occur. This would result in surface buckling, especially for stones already subjected to spalling, leading to crack propagation up to split-up. The damage risk decreases with depth and is higher on the south wall than on the north wall. The alternative methodology proved to be relevant for the calculation of both compression and tension stresses, which is useful to assess the consequences of the damage. The optional stone data correction proved to be relevant since the damage risk is significantly higher with this correction compared to the original set of data. This reveals that sensor accuracy is a significant issue for this calculation, and sensors with finer accuracy for high humidity should be preferred to avoid any underestimation of damage risk, especially in compression.

6. References

1. Al-Omari, A., Brunetaud, X., Beck, K., and Al-Mukhtar, M., (2013a), Effect of thermal stress, condensation and freezing–thawing action on the degradation of stones on the Castle of Chambord, France, Environmental earth science, DOI:10.1007/s12665-013-2782-4.

2. Al-Omari, A., Brunetaud, X., Beck, K., and Al-Mukhtar, M., (2013b), Experimental study on the role of freezing–thawing in the degradation of stones in the Castle of Chambord, Proceedings of International Conference on Built heritage, Milano, Italy.

3. Al-Omari, A., Brunetaud, X., Beck, K., and Al-Mukhtar, M., (2014), Coupled thermal-hygric characterisation of elastic behaviour for soft and porous limestone, Construction and Building Materials, DOI: 10.1016/j.conbuildmat.2014.03.029.

4. Beck K. (2006), Etude des propriétés hydriques et des mécanismes d'altération de pierres calcaires à forte porosité. Ph.D. Thesis. University of Orleans, France.

5. Beck, K., Al-Mukhtar, M., Rozenbaum, O., and Rautureau, M., (2003), Characterisation, water transfer properties and deterioration in tuffeau: Building material in the Loire Valley, France, International Journal of Building and Environment, 38(9), pp 1151–1162.

6. Benavente, D., Cultrone, G., and Gomez-Heras M., (2008), The combined influence of mineralogical, hygric and thermal properties on the durability of porous building stones, European Journal of Mineralogy 20, pp 673–685.

7. Bonazza, A., Sabbioni, C., Messina, P., Guaraldi, C., and De Nuntiis, P., (2009a), Climate change impact: Mapping thermal stress on Carrara marble in Europe, Science of the Total Environment, 407, pp 4506–4512.

8. Bonazza, A., Messina, P., Sabbioni, C., Grossi, C.M., and Brimblecombe, P., (2009b), Mapping the impact of climate change on surface recession of carbonate buildings in Europe, Science of the Total Environment, 407, pp 2039–2050.

9. Camuffo, D., (1998), Microclimate for cultural heritage, Elsevier, Amsterdam.

10. Camuffo, D., and Sturaro, G., (2001), The climate of Rome and its action on monument decay, Climate Research, 6, pp 145–55.

11. Colas, E., Mertz, J.D., Thomachot-Schneider, C., Barbin, V., and Rassineux, F., (2011), Influence of the clay coating properties on the dilation behavior of sandstones, Applied Clay Science, 52(3), pp 245–252.

12. Dessandier, D., (2000), Guide méthodologique des monuments en termes de durabilité et compatibilité, in collaboration with Auger P., Haas H. and Hugues G. BRGM Report.

13. Eklund, S., (2008), Stone weathering in the monastic building complex on Mountain of St Aaron in Petra, Jordan, M.Sc. Thesis, University of Helsinki-Finland.

14. Janvier-Badosa, S., Beck, K., Brunetaud, X., and Al-Mukhtar, M., (2010), Characterization of stone weathering: a case study for Chambord castle, France, 8th International Symposium on the Conservation of Monuments in the Mediterranean Basin, Patras, Greece.
15. Janvier-Badosa, S., Beck, K., Brunetaud, X., and Al-Mukhtar, M., (2013), The occurrence of gypsum in the scaling of stones at the Castle of Chambord (France), Journal of Environmental Earth Sciences, DOI: 10.1007/s12665-013- 2865-2.

16. Moropoulou, A., Theoulakis, P., and Chrysophakis, T., (1995), Correlation between stone weathering and environmental factors in marine atmosphere, Atmospheric Environment, 29(8), pp 895–903.

17. Ponziani, D., Ferrero, E., Appolonia, L., and Migliorini, S., (2012), Effects of temperature and humidity excursions and wind exposure on the arch of Augustus in Aosta, Journal of Cultural Heritage, 13, pp 462–468.

18. Stefani, C., Brunetaud, X., Janvier-Badosa, S., Beck, K., De Luca, L., and Al-Mukhtar, M., (2013), Developing a toolkit for mapping and displaying stone alteration on a web-based documentation platform, Journal of Cultural Heritage, DOI: 10.1016/j.culher.2013.01.011

19. Viles, H.A., (2005), Microclimate and weathering in the central Namib Desert, Namibia, Geomorphology 67, pp 189–209.

Appendix 4

Critical degree of saturation: A control factor of freeze-thaw damage of porous limestones at Castle of Chambord, France

Asaad Al-Omari[1,2], Kevin Beck[1], Xavier Brunetaud[1], Ákos Török*[3], Muzahim Al-Mukhtar[1]

[1]CNRS-Centre de Recherche sur la Matière Divisée, 1 Rue de la Ferollerie, 45100 Orléans, France

[2]Department of Civil Engineering, College of Engineering, Mosul University, Al-Majmooah Street, Mosul, Iraq

[3]Department of Construction Materials and Engineering Geology, Budapest University of Technology and Economics, Budapest, Hungary

*corresponding author: torokakos@mail.bme.hu

Abstract

The paper analyses the petrophysical and mechanical properties of two porous limestones that were used in the construction and restoration works at the castle of Chambord in France, an UNESCO World Heritage site. The original construction material, the tuffeau limestone with a total porosity of 45±0.6%, and the replacement stone of later restorations, the Richemont limestone with a total porosity of 29±0.7% were subjected to freeze-thaw tests under laboratory conditions to evaluate the role of critical degree of saturation and pore-size distribution in frost damage. Laboratory tests were coupled with in situ measurements of temperature and relative humidity at stone surface at the castle of Chambord. In situ data show that the stones in the castle experienced several freezing-thawing cycles annually. The limestone samples under laboratory conditions were subjected to up to 50 freeze-thaw cycles under eight different degrees of saturations. The total porosity, tensile strength, ultrasonic pulse velocity, the mercury intrusion porosimetry and scanning electron microscopy techniques were employed to analyse the conditions of samples during the cycles. The experimental results show that when the degree of saturation of the two studied

limestones exceeds 80-85%, the freeze-thaw, damage occurs even after a few freeze-thaw cycles. The effect of freezing is very fast if the water saturation is sufficient. Moreover, results indicate that these stones have the same critical degree of saturation of about 85%, despite the differences in porosity. Finally, the results indicate that the increase in the number of freezing-thawing cycles has no effect on the critical degree of saturation, but the frost damage is mostly controlled by pore-size distribution rather than by total porosity. Accordingly, critical degree of saturation can be defined as an intrinsic stone property.

Keywords: Freeze-thaw cycles, critical degree of water saturation, meteorological data, tuffeau limestone, Richemont limestone

1. Introduction

Frost is one of the main causes of the damage in cultural built heritage in cold regions. The durability of stone structures against frost strongly depends on hydro-physico-mechanical parameters. It was demonstrated that intrinsic properties of the stones like total porosity, pore connectivity, pore size distribution, mechanical strength, mineralogy, grain-size, and environmental conditions affect both the stone's durability and mechanism of frost weathering (Bayram, 2012; Jamshidi et al., 2013; Mutlutürk et al., 2004; Takarli et al., 2008; Tan et al., 2011; Yavuz et al., 2006). Most of the previous experimental works dealing with the deterioration of stone under freezing-thawing conditions were performed on fully water saturated samples. However, natural stones are almost never fully saturated. Consequently, in order to understand the mechanisms of stone damage and simulating the real field problems, experiments with stones having various water contents are necessary (Matsuoka,

2001). It was also pointed out that effective microgelivation requires an initial degree of saturation in excess of 80% and it is followed by rapid freezing. However, Matsuoka (2001) also emphasized that rocks can uptake water during slow freezing, and thus, for a frost damage, a high initial water content is unnecessary. The role of porosity in the durability of porous stones have been studied in details taking into account the salt weathering susceptibility (Benavente et al. 2004, Yu and Oguchi 2010) and pore structure (Benavente et al. 2001). The frost damage of porous materials was also explained by the critical degree of water saturation (Fagerlund 1977a, 1977b). Sulphate attack is also considered as one of the main causes of damage observed on limestone buildings (Török 2003, Siegesmund et al. 2007, Kloppmann et al. 2011), however this research focuses on other aspects of limestone decay.This paper provides information on the mechanism of freezing-thawing related to stone deterioration by using the example of the castle of Chambord in France. It uses two approaches: i) the *in situ* monitoring of stone surface temperature and meteorological data in order to identify the risk of damage by freezing to two limestones, the tuffeau and Richemont, that were used in the construction and restoration of the castle, and ii) laboratory experiments aiming to determine the critical degree of saturation and pore-size distribution that triggers the freezing damage of these two stones. Stones used in the construction of monuments such as Chambord castle can gradually deteriorate over a long period of time in response to the action of water and local environmental conditions. The deterioration in castle of Chambord belongs to three main categories: biological colonizations (mosses and lichens), spalling (centimetre-thick) and flaking (millimetre-thick). The factors leading to these deteriorations have never been defined precisely.

2. The Castle of Chambord and its building stones

The Royal Castle of Chambord at Loire Valley, in France, an UNESCO World Heritage site since 1981 is located in a rural area at a distance about 150 km to SW of Paris, and at latitude of 47˚36□ N,and longitude of 1˚31□ E Its average elevation is about 84 m above sea level (Fig. 1). The area experiences a mild humid temperate climate with warm summers and no dry seasons.

The castle of Chambord is the largest castle in Loire Valley (155 m × 115 m) built between 1519 and 1547; and the main building stone used for the construction is tuffeau, a highly porous siliceous limestone with a total porosity of about 45% (Beck et al., 2003). The castle had experienced many restoration works especially during the last century. Accordingly, a lot of the original limestones were replaced. Janvier-Badosa et al. (2013b) mentioned that more than 50% and 28% of the original stones has been replaced on the south façade wall, the main Royal entrance and the east tower of the castle, respectively. Richemont stone, a moderately porous limestone with a total porosity of about 29%, is the main stone used in the restoration works at the walls of the castle. It was used as a replacement stone in between 1953 and 1962. The main stone degradation features at the castle of Chambord were identified as biological colonization, crack formation, and especially scaling of stone in forms of spalling and flaking (Beck and Al-Mukhtar, 2005; Janvier-Badosa et al., 2010; 2013a; 2013b).

According to Bricy Air-Base meteorological station, about 45 km NE to the castle of Chambord, (Fig. 1), the recorded data during 1997-2012 revealed that the mean annual temperature is 11.4±0.5°C with winter minimum of -16°C in February and summer maximum of 39°C in August. The mean annual precipitation is 400 mm with

maximums of 47.2 mm per day in summer in August. Therefore, the area under study is subject to high atmospheric temperature range, with daily temperature variations often in excess of 20°C (Al-Omari et al., 2013).

Fig. 1. Map showing the geographical setting of the castle of Chambord and Bricy Air-Base meteorological station (left). Ground plan of the castle showing the location of studied southern façade wall and the east tower (top left, after Janvier-Badosa et al., 2013b). Castle of Chambord-aerial view (bottom left).

Fig. 2. Monthly variations in the extreme values of mean air temperature and mean air relative humidity for the period 1997–2012.

3. Material and Methods

3.1. The studied stones

Two French stones were presented in this study: tuffeau and Richemont stone. Tuffeau is a soft-porous stone and dates from the Turonian age, the upper Cretaceous period, approximately 88-92 million years ago. It comes from the quarries at Tuorain/Anjou close to Loire river (NW France). It is used in many numbers of the castles in Loire Valley-France because of its light weight, special aesthetics with shine white and easy to form. Richemont is a fine-grained limestone has the same geological age as for tuffeau but with higher strength properties. It is obtained from the quarry in Charente-Maritime (W France).

The cylindrical samples of tuffeau and Richemont stone with a dimension of 40 mm in diameter and 40 mm in height were cored from large blocks of which the coring was perpendicular to the bedding plane. Samples were visually assessed and only the ones that were free from visible defects, cracks and flaws were used for the

129 experiments. In order to minimize the heterogeneity of the results, preliminary
130 ultrasonic pulse velocity tests were performed on the fresh cylindrical samples. Then
131 the samples with velocity value close to the average one were selected. A total of 128
132 cylindrical samples were prepared; 64 samples from each stone type. The samples
133 representing one lithotype were further divided into 8 groups containing 8 samples
134 each
135

136 **3.2. On site measurements and data analysis**

137 In order to assess the effect of freezing and thawing in the stones deterioration of the
138 castle of Chambord, field measurements were carried out to gather the comprehensive
139 information on the environment. The data from digital temperature sensors placed on
140 the surfaces of the ashlars together with the meteorological data for the surrounding
141 area were described to assess the role of conditions in enhancing freezing–thawing
142 degradation of the.
143 Digital temperature sensors type FHAD-46x were installed on the stone surface of the
144 wall of the east tower (Fig. 3). The data set include 30-minute readings for three years
145 period starting from June 2009. The analysis of the stone temperature data allows to
146 determine the number of freezing events that occurs on the surface of stone. The
147 temperature of 0 ºC was considered as the criterion for estimating the number of
148 freezing-thawing cycles (Al-Omari et al., 2013; Camuffo and Sturaro, 2001; Ponziani
149 et al., 2012). Moreover, the meteorological data: air temperature, relative humidity,
150 and rainfall obtained from Bricy Air-Base station over a long period (from 1973 to
151 2012) were analyzed and compared with the meteorological data for the period of the
152 monitored three years (from June-2009 to June-2012).
153

Fig. 3. General view of the east tower of the castle of Chambord showing the sensor installation on the stone surface.

The degradation of stone by freezing is mainly controlled by existing sufficient amount of water in the pores of the stone. In this study the availability of water on the stone surface prior to freezing was justified by two means: rainfall and condensation processes. The condensation on the surface of the stone was evaluated by using stone surface temperature data and air dew temperature data. The water vapour condenses on the stone surface when air dew temperature is higher than the stone surface temperature. For this purpose, both the stone data from sensor and the meteorological data from Bricy station were analyzed.

3.3. Laboratory tests analyses

Mineralogical composition and micro-fabric

The mineralogical composition of the two fresh stones was gathered by using two complementary techniques: X-Ray diffraction and thermo-gravimetric analyses (TGA-DTG). X-Ray diffraction test was performed using a Phillips Diffractometer with radiation of Cu Kα (λ = 1.5406 A). The goniometer speed was 0.025° (2θ) per six seconds of which the counts were recorded for the range of (2θ) angle between 4° and 60°. The quantitative analyses of minerals were performed by means of thermo-gravimetry by using Setaram (TG-DTA 92-18) apparatus. Samples were heated from room temperature to 1000°C at a constant speed of 2°C per minute. The visual conditions of stones during freezing-thawing tests were observed by using a digital camera. Thin-sections were also prepared by using resin impregnation in an attempt to characterize the petrographic features of the two studied stones, both for fresh and

179 for aging samples. For this purpose the Leica Optical Microscope type DVM2500-
180 VZ80 and the TableTop Microscope type TM3000 were used.
181
182 *Pore-size distribution*
183 The pore size distribution was measured by means of Mercury Intrusion Porosimetry
184 (MIP) test. The apparatus used was an Autopore IV 9520 micro-porosimeter which
185 satisfies the pressures in the range of 2.76 kPa up to 414 MPa and allows,
186 theoretically of measuring the pore diameter sizes from 0.003 μm up to 450 μm.
187
188 *Total porosity, apparent dry density and skeletal density*
189 The total porosity (n), dry bulk density (ρ_a) and skeletal density (ρ_s) of tuffeau and
190 Richemont stone samples were measured by applying the vacuum water saturation
191 method following the method described by RILEM (1984). The tests were achieved
192 by using vacuum pressure of about 0.1 kPa for a period of 24 hour. The tests were
193 carried out on 64 cylindrical samples of each lithotype. The same stone samples in
194 fresh state and after subjected to different number of freezing-thawing cycles were
195 included in these tests.
196
197 *Mechanical properties*
198 Ultrasonic pulse velocity (V_p) and indirect tensile strength (σ_t) (Brazilian test) were
199 used to assess the mechanical properties of stones. The direct method proposed by
200 (Kahraman, 2002) was applied to detect the ultrasonic pulse velocity of tuffeau and
201 Richemont stones. The tests were carried out on cylindrical stone samples under dry
202 laboratory conditions following the procedure described in (Norm AFNOR P94-411).
203 The property of ultrasonic pulse velocity was determined from the ratio of the length

of the sample to the transit time of the pulse. The PUNDIT pulse apparatus with two transducers having a frequency of 82 kHz was used to conduct the tests on the same samples prior to and after the freezing-thawing tests. The Brazilian tensile strength of the stone samples were measured following the methodology described in (Norm AFNOR P94-422) by using an Instron 4485 press machine with 200 kN force capacity and the load was applied on the tested samples with constant strain rate of 0.05 mm/min.

Freezing-thawing test

The freezing-thawing tests were carried out following the guidelines given in ASTM (D5312-04). The cylindrical samples (Ø 40 × 40 mm) of tuffeau and Richemont stone prepared at eight different degrees of saturation were used for the tests: 20, 40, 70, 80, 85, 90, 95 and 100%. After measuring the total porosity by vacuum water saturation method the samples were fully saturated, then they underwent free air drying at different periods in a room conditioned at 23±2°C of temperature and at 50±3% of relative humidity. The relationship that correlates the degree of saturation with water content of the porous material is: degree of saturation = [(specific gravity/void ratio) × water content]. As the specific gravity and the void ratio were constant during the tests, the mass of the wet samples leads to the determination of the required degree of saturation. During the drying periods, the mass of the wet samples were continuously monitored. The samples that reached the required degree of saturation were firmly sealed using parafilm to prevent the weight change prior to freezing-thawing test.

A Vö tsch-VT 4011 climate chamber was used for the freezing-thawing tests. All stone samples were frozen to -18°C and kept there for 12 hours. It was followed by a thawing phase with temperature of 32°C for another 12 hours. The change in chamber

229 temperature from/to the freezing-thawing conditions was controlled and took place
230 within 10 minutes and thus one freezing-thawing cycle lasted 24 hours. The graphic
231 illustration of the cycles is given on Fig. 4. Samples were subjected to 2, 4, 10, 16,
232 20, 30 and 50 freezing-thawing cycles, respectively and continuously monitored.
233 After the required number of freezing-thawing cycles, the samples were removed
234 from the freezing chamber and oven dried at 105 ºC for 24 hour.
235
236 **Fig. 4.** Schematic diagram of temperatures and time scales of one freezing-thawing cycle.
237
238 **4. Results**
239
240 **4.1. Climatic data**
241 In this study, the freezing events on the stone surface and in the atmosphere were
242 identified by analyzing the data measured in stones by using the sensors, and the
243 meteorological data recorded at Bricy air-Base station for the periods 2009-2012. The
244 statistical analysis of the meteorological data recorded at Bricy air-Base station
245 during 1973-2012 and 2009-2012 suggests that the trends during the two different
246 periods are similar (Fig. 5). Therefore, the data acquired for an annual period can be
247 considered as representative of the local climatic conditions in the studied area
248 including seasonal variation.
249
250
251 **Fig. 5.** Monthly variations in the extreme values of mean air temperature (top), and mean air relative
252 humidity (bottom) for the two observation periods: 2009–2012 and 1973–2012.
253

The meteorological data during the previous freezing periods was analyzed in an attempt to determine the days with rainfall and/or with condensation events on the stone surfaces. The variation of the maximum and minimum air and stone surface temperatures allow to identify the freezing-thawing events at the stone surface (Fig. 6a) and in the ambient air (Fig. 6b). The results of analysis of climate data had revealed that the events of the freezing-thawing cycles in the atmosphere during the years of 2009/2010, 2010/2011, and 2011/2012, were 45, 45 and 23, respectively. The number of freezing-thawing cycles occurred on the stone surface for the same period was smaller; 36, 28 and 15, respectively.

The frequencies of condensation events on the stone surfaces were calculated suggesting that the highest amount of condensation events occur within September and February (Fig. 7). The results of analysis indicated that at most days when freezing occurred the stone contained water either in a form of rainfall and/or by condensation.

These results make it possible to estimate the percentage of the damage risk on an annual basis, i.e., the frost events when stone was wet at the castle of Chambord (Table 1).

Fig. 6. Maximum and minimum air temperature variations during June/2011-June/2012 (F- indicates frost events) (top), maximum and minimum stone surface temperature variations during June/2011-June/2012 (bottom).

Fig. 7. Monthly frequency of condensation events on the stone surface, Castle of Chambord

Table 1

Damage risk of limestone at Castle of Chambord, (N_{F-T}) - number of freezing days with water on the stone surface by rainfall or/and by condensation; (P_{F-T}) - percentage of damage risk (%).

4.2. Laboratory observations

4.2.1 Petrographic characterization

Tuffeau is a siliceous limestone which has a homogenous micro-fabric of pale white colour which becomes greenish after wetting (Fig. 8a). It is composed of calcite 50% and 30% of silica in the form of opal cristobalite-tridymite. Crystalline quartz accounts for 10% (Dessandier, 2000). The minor minerals are represented by clays (glauconite) and by micas. These accessory minerals were found in smaller quantities than 10%. The predominant calcite phase is micrite with abundant coccoliths resulting in a micro-porous fabric (Beck et al., 2003). The sparitic and micritic calcite contains angular quartz grains of 100 μm as a maximum in size (Fig. 8c).

Richemont is white-beige fine-grained limestone with a bio-pelmicrite microfacies and contains some shell fragments (Fig. 8b). The colour changes to slightly reddish when the stone is wet. It is mainly composed of calcite 96-97%, and small quantities of clay minerals such as, smectite 2-3%, illite/mica 1%. Small amount of quartz was also found (Dessandier, 2000). The calcite crystals are also micritic providing a porous micro-fabric (Fig. 8d). Iron oxi-hydroxide was also recognized as brownish stains on the stone surface.

Fig. 8. Cylindrical samples of tuffeau (a) and Richemont (b) (arrows mark shell fragments) and their micro-fabrics obtained by using optical microscopy :tuffeau –(c) and Richemont –(d) (arrow points to iron-oxi-hydroxide).

306 *4.2.2 Visual appearance and microscopic observation*

307 The outer surfaces of the two stone samples subjected to different cycles of freezing-
308 thawing tests were visually observed in an attempt to quantify the amounts and sizes
309 of the frost-related cracks. It was noticed that during the aging tests tuffeau and
310 Richemont samples preconditioned with a degree of saturation at or below 85% did
311 not exhibit any visual cracks (Fig. 9). Meanwhile, the cracks start to appear at those
312 samples that have higher degrees of water saturation (i.e. $S \geq 90\%$). No direct
313 correlation was found between the size/intensity of the cracks and the number of
314 freezing-thawing cycles; in other words, the repeated freezing-thawing cycles did not
315 affect the damage processes of the samples. On the other hand, with increasing degree
316 of water saturation the size of cracks generally increased, but other test conditions
317 remained the same. Indeed, thin cracks were observed on samples with 90% of water
318 saturation. The width of these cracks was around 0.2 mm. Larger cracks reaching up
319 to 1.0 mm in size were observed on samples with 95% of initial degree of water
320 saturation. The widest cracks were detected on samples preconditioned at 100 % of
321 water saturation. These cracks with a width of more than 3.0 mm, were the precursors
322 of crumbling processes and loss of materials in the form of small pieces (Fig. 9a, c
323 and e).

324 Scanning electronic microscopy (SEM) studies revealed that no cracks were observed
325 on the fresh tuffeau and Richemont stone (Fig. 10a, d). For the aged samples micro-
326 cracks / micro-fissures were formed within the fabric of these stones. The micro-
327 cracks were visualized within the carbonate matrix (Fig. 10b, e) and some of those
328 even cut individual grains (Fig. 10c, f).

329

330

Fig. 9. The Cracked aging samples prepared at 100, 95 and 90% initial degree of water saturation at different conditions of freeze-thaw test.

Fig. 10. SEM images showing the micro cracks within the limestone developed after 10 freeze-thaw cycles. Tuffeau samples fresh (a) and with water saturation of 100 % (c, d) and Richemont samples fresh (d) and with water saturation of 100 % (e) and 95 % (f).

4.2.3 Physical properties and porous system

The measured physical properties, total porosity (n), dry bulk density (ρ_d) and skeletal density (ρ_s), for the fresh stones samples are listed in Table 2. These properties were obtained by using vacuum water saturation method.

Table 2

Physical properties for two fresh stones; total porosity (n), dry bulk density (ρ_d), and skeletal density (ρ_s).

Richemont stone has higher skeletal density than tuffeau. This is due to the presence of higher amount of calcite (96-97 %), and, accordingly, its skeletal density is very similar to that of the calcite (2.71 g/cm^3). The low skeletal density of tuffeau is related to the high amount of the low density opal (2.15 g/cm^3). Tuffeau represents high values of total porosity ranged between (43.6-47.2%) with a mean value of 45.2%, resulting in very low values of dry bulk densities compared to less porous Richemont.

Four different ranges of pore diameters, connected porosity, median pore access diameter, dispersion coefficient as obtained by MIP tests are presented in Table 3.

The MIP test revealed that tuffeau matrix includes wide ranges of pore access diameters; 0.003 μm and 20 μm. This is due to the presence of amorphous silicates and various sizes of carbonate crystals as well as to the presence of coccoliths. The dispersion coefficient for tuffeau is very high, which reflects the bimodal distribution of pore diameter with a mean peak at 8 μm and the second smaller peak at 0.1 μm. To the contrary, Richemont limestone has a pore size distribution restricted to the range of 0.02 to 4 μm of the pore diameters with the main peak of an incremental pore volume at 2 μm. The median pore access diameter with values of about 1.0 μm has a wide dispersion coefficient. It is important to note that the two limestones have the same percentage (about 50%) of the pores in the pore-size range of 1.0-10 μm. The values of connected porosity (n_c), obtained by MIP test, are slightly smaller than the ones measured by vacuum water saturation method. This reflects the fact that this technique is able to measure only limited ranges of pore sizes.

Table 3

Results of MIP test, fresh stones; (n_c) connected porosity, (D_m) median pore access diameter, (D_s) dispersion coefficient, and pore size distribution.

The porosity measured by vacuum water saturation method gives the fractional volume of all pore space (i.e., total porosity) inside a porous material. Thus, this physical property considers a good tool for detecting any slight change in the porous structure of the stone samples exposed to accelerated freezing-thawing test. For this purpose, the total porosity of the aging samples with freezing-thawing test were normalized to their initial values of the same samples but in fresh state. Then the normalized values were related to the initial degree of water saturation of the stone

384 samples as shown in Figs. 11. The results indicate that the normalized values of
385 porosity are different for the samples prepared with low water saturation and the ones
386 prepared with high water saturation. The considerable changes in the normalized
387 values were found for the samples with water saturation higher 85%.
388
389 **Fig. 11.** Normalized total porosity vs. degree of saturation after freezing-thawing test for tuffeau and
390 Richemont limestone.
391
392
393 The results of MIP tests of samples preconditioned at water saturation of 100 and of
394 90% subjected to 10 or 20 freezing-thawing cycles were analyzed and compared with
395 the results obtained from the fresh samples (Fig. 12). No significant differences in the
396 cumulative pore volumes and in the measured porosities of the freeze-thaw subjected
397 and of the fresh samples were observed. However it is also related to the fact that
398 range of pores and the detection limit of MIP apparatus allow the measurements of
399 pore sizes in a range of 450 and 0.003 μm thus, some of the cracks and very small
400 pores are not documented. These limitations can be overcome by detecting saturation
401 levels and normalized porosity values (Fig. 11,).
402
403 **Fig. 12.** Results of MIP of fresh and freeze-thaw cycles subjected samples of tuffeau and Richemont
404 limestone.
405
406 *4.2.4 Mechanical properties*
407 The samples of tuffeau have lower ultrasonic pulse velocity values (V_p) compared to
408 the ones of Richemont (Table 4), indicating the higher rate of porosity. The mean
409 values of V_p are app. 1600 m/s and 2600 m/s, for tuffeau and Richemont stone,

410 respectively. According to Anon (1979) the two stones are classified as low and very
411 low sound velocity.
412
413 **Table 4**
414 Mechanical properties of fresh limestones; ultrasonic pulse velocity (V_p), and indirect tensile strength
415 (σ_t).
416
417 The results of ultrasonic pulse velocity tests confirm that there is almost a threshold
418 degree of water saturation value at which the stone samples start to deteriorate when
419 subjected to freeze-thaw cycles and show a sudden decrease in pulse velocities with
420 respect to fresh samples (Fig. 13). The stone samples with initial degree of water
421 saturation below 85% represent minor and almost negligible changes in the ultrasonic
422 pulse velocity values. In contrast, the significant decreases in the ultrasonic pulse
423 velocity values were obtained for the other samples with higher initial degree of water
424 saturation. These findings were the same for both tuffeau and Richemont stone
425 samples.
426
427
428 **Fig. 13.** Ultrasonic pulse velocity of fresh and freeze-thaw cycles subjected specimens at different
429 degree of saturation, tuffeau (right) and Richemont limestone (left).
430
431
432 The fresh limestone samples have low tensile strength values. However, the tensile
433 strength for Richemont exceeds by about 40% that of the tuffeau; this could be
434 attributed to micro-fabric of the two stones. Richemont limestone is less

435 homogeneous than tuffeau as it is reflected in the standard deviations (S.D.) of
436 measured physico-mechanical properties in Tables 2 and 4.
437 The tensile strength of the samples prepared at different degree of saturation and
438 subjected to different number of freezing-thawing cycles indicates that the higher
439 tensile strength values belong to both fresh samples and freeze-thaw samples having
440 low water saturation (40, 70 and 80%). While lower tensile strength are attributed to
441 freeze-thaw samples with high water saturation level (90, 95 and 100%, Figure 14).
442 The dotted lines represent the best fitting lines for the two set-points of both the low
443 and the high tensile strength values of the stone samples. The slopes of the two dotted
444 lines differ. The blue dotted ones have higher slopes which are related to the more
445 weathered samples. The nick-point between the two slopes is located about 85% of
446 water saturation.
447
448 **Fig. 14.** Indirect tensile strength for fresh and aging samples, Tuffeau (right) and Richemont limestone
449 (left).
450
451 **5. Discussion**
452
453 The results of freeze-thaw tests of the two limestones show that signs of frost damage
454 are not visible on samples having water saturation of less than 85%. However,
455 indirect tensile strength values show minor changes when air dry samples and
456 moderately saturated (up to 80%) freeze-thaw subjected samples are compared (Fig.
457 14). The same trend was observed for ultrasonic pulse velocities (Fig. 13). Drastic
458 changes due to freeze-thaw cycles took place at saturation levels of higher than 85%.
459 These damage forms are visible in the form of micro-crack generation on both
460 limestones (Fig. 9.). More specifically, the micro-cracks appear both in the carbonate

461 matrix and in the carbonate grains as revealed by SEM (Fig. 10). The numerical
462 representation of frost damage is best obtained by comparing indirect tensile strength
463 values (Fig. 14) of samples with 80% and 90% of water saturation. To explain these
464 sudden changes at water saturation level of 85%, normalized porosity values are
465 analyzed with degree of saturation. From the graphic representation of total porosities
466 measured on samples after subjected to freeze-thaw tests it is clear, that a dramatic
467 increase in porosity can be pinpointed at saturation levels of 85% (Fig. 11). The
468 augmentation of porosity is attributed to the formation of visible micro-cracks (Fig.
469 9). The crack generation in fact reduces the strength and ultrasonic pulse velocity of
470 samples. This level of saturation, when major changes took place, is called a critical
471 degree of saturation (Sc) according to Fagerlund (1977a). It was defined as a
472 threshold moisture level promoting the frost damage of concrete (Fagerlund 1977b).
473 Previous studies suggested that the critical degree of saturation of French limestones
474 were between 58% and 93% (Prick 1997). The present study indicates that this is
475 around 85% for both studied limestones. Welded volcanic tuff samples showed
476 intense frost damage at saturation levels of higher than 70% (Chen et al. 2004). The
477 fact that the two limestones under investigation have almost the same critical degree
478 of water saturation invokes a question of how physical properties influence S_c values.
479 Tuffeau and Richemont limestone have very different properties in many aspects,
480 including bulk densities, total porosities (Table 2), ultrasonic pulse velocities and
481 indirect tensile strength (Table 4). The key factor in which the two limestones are
482 similar is the amount of macro-pores and the similar median pore access diameters
483 (Table 3). It seems that these parameters also influence the durability of the
484 limestones against frost. The pore-size distribution also controls the durability of
485 mortars (Falchi et al. 2013). In most previous studies one given condition of freezing-

thawing test was considered aiming to find the critical degree of saturation of limestones (Prick 1995) and tuffs (Chen et al. 2004). The obtained data set provided evidences that an increase in the number of freeze-thaw cycles (up to 50 cylces) had no effect on the minimum degree of saturation at which frost damage occur, i.e., the number of freeze-thaw cycles had fairly limited effect on the fatigue of the rock. In other terms the critical degree of saturation can be defined as an intrinsic property of stone. By using the meteorological and micro-climatic data obtained at Castle of Chambord (Fig. 6, Fig. 7. and Table 1) and the critical degree of saturation revealed by laboratory analyses, it is possible to explain the mechanism of stone damage. At castle of Chambord 4 to 10 annual events were identified (Table 1) when stone could be subjected to frost damage. For both limestones, a degree of water saturation of 85% can be set up as a warning level of frost damage. To conclude, when temperature drops below 0°C, and the limestone has higher degree of water saturation than 85%, limited number of freeze-thaw cycles can cause irreversible damage.

6. Conclusions

This study of porous limestones suggests that field observations of both ambient air temperatures and stone surface temperatures in combination with relative humidity data are needed to identify dew temperature at stone surfaces and to determine the availability of moisture within the pores. The moisture content has a crucial importance with regard to freeze-thaw damage of stones. The moisture in the pores of the stone is also related to precipitation events or elevated ground water, however dew temperature conditions can also contribute to the frost damage of stones by bringing water into the pore system via stone surface. Despite the differences in

several properties a similar critical degree of water saturation (S_c=85%) was found both for tuffeau and Richemont limestone, which suggests that a threshold limit of moisture content exists The similar behavior and sensitivity to frost damage of the two different limestones is explained with the similarities in proportion of pore sizes of 1.0-10 μm and the comparable medium pore access diameters. In contrast to predictions, the number of freeze-thaw cycles has limited influence on frost damage, since the main control factor is the critical degree of water saturation. Hence this latter parameter is considered as an intrinsic material property.

The results invoke that the critical degree of saturation determined under laboratory conditions with the combination of microclimatic data can be used to introduce a warning level to frost damage.

Finally, this study demonstrates that the damage of the stones related to freezing-thawing at the castle of Chambord is not clearly identified but must be considered when the different mechanisms of deterioration such as scaling and flaking are analyzed.

Acknowledgements

The authors acknowledge the financial support provided by Université d'Orléans for the visiting research grant to Ákos Török to Centre de Recherche sur la Matière Divisée (CNRS- CRMD).

References

535 Al-Omari, A., Brunetaud, X., Beck, K., Al-Mukhtar, M., 2013. Effect of thermal stress, condensation and
536 freezing–thawing action on the degradation of stones on the Castle of Chambord, France. Environmental Earth
537 Science DOI 10.1007/s12665-013-2782-4.

538 Anon., 1979. Classification of rocks and soils for engineering geological mapping. Part 1-Rock and soil materials.
539 Bull Int. Assoc. Geo., 19, pp. 364-371.

540 ASTM. (2004). Standard Test Method for Evaluation of Durability of Rock for Erosion Control Under Freezing
541 and Thawing Conditions. Standard D5312-04.

542 Bayram, F., 2012. Predicting mechanical strength loss of natural stones after freeze–thaw in cold regions. Cold
543 Regions Science and Technology 83-84, 98-102.

544 Beck, K., Al-Mukhtar, M., 2005. Multi-scale characterization of two French limestones used in historic
545 constructions. International Journal of Restoration of Buildings and Monuments 11,4, 219–226.

546 Beck, K., AL-Mukhtar, M., Rozenbaum, O., Rautureau, M., 2003. Characterization, water transfer properties and
547 deterioration in Tuffeau: building material in the Loire Valley–France. Building and Environment 28 ,9–10, 1151–
548 1162.

549 Benavente, D., García del Cura, M.A., Bernabéu, A., Ordóñez, S. 2001 Quantification of salt weathering in porous
550 stones using an experimental continuous partial immersion method. Engineering Geology, 59, 313–325.

551 Benavente, D., García del Cura, M.A., Fort, R., Ordóñez, S. 2004. Durability estimation of porous building stones
552 from pore structure and strength. Engineering Geology, 74, 113–127.

553 Camuffo, D., Sturaro, G., 2001. The climate of Rome and its action on monument decay. Climate Research 16,
554 145–155.

555 Chen, T.,C., Yeung, M.,R., Mori, N., 2004. Effect of water saturation on deterioration of welded tuff due to
556 freeze-thaw action. Cold Regions Science and Technology 38, 127–136.

557 Dessandier, D., 2000. Guide méthodologique des monuments en termes de durabilité et compatibilité, in
558 collaboration with Auger P., Haas H. and Hugues G. BRGM Report.

559 Fagerlund, G., 1977a. The critical degree of saturation method of assessing the freeze-thaw resistance of concrete.
560 Materials and Structures, 10, 58, 217–229.

561 Fagerlund, G., 1977b. The international cooperative test of the critical degree of saturation method of assessing
562 the freeze/thaw resistance of concrete". Materials and Structures, 10,58, 231–253.

563 Fagerlund, G., 1992. Effect of the freezing rate on the frost resistance of concrete. Nordic Concrete Research, 11
564 10–36.

565 Falchi, L. Müller, U, Fontana P, Izzo, F.C., Zendri E. 2013. Influence and effectiveness of water-repellent
566 admixtures on pozzolana–lime mortars for restoration application. Construction and Building Materials 49, 272–
567 280

568 Jamshidi, A., Nikudel, M.,R., Khamehchiyan, M., 2013. Predicting the long-term durability of building stones
569 against freeze-thaw using a decay function model. Cold Regions Science and Technology 92, 29-36.

570 Janvier-Badosa, S, Beck, K., Brunetaud, X., Al-Mukhtar, M., 2013a. The occurrence of gypsum in the scaling of
571 stones at the Castle of Chambord (France)., Environmental Earth Sciences, DOI: 10.1007/s12665-013-2865-2.

572 Janvier-Badosa, S., Beck, K., Brunetaud, X., Al-Mukhtar, M., 2010. Characterization of stone weathering: a case
573 study for Chambord castle, France. 8th International Symposium on the Conservation of Monuments in the
574 Mediterranean Basin, Patras, Greece.

575 Janvier-Badosa, S., Beck, K., Brunetaud, X., Al-Mukhtar, M., 2013b. Historical study of Chambord castle: basis
576 for establishing the monument health record. International Journal of Architectural Heritage 7, 247–260.

577 Kahraman, S., 2002. Estimating the direct P-wave velocity value of intact rock from indirect laboratory
578 measurements. International Journal of Rock Mechanics and Mining Sciences 39, 101-104.

579 Kloppmann, W, Bromblet P., Vallet, J.M., Vergès-Belmin, V., Rolland O., Guerrot C., Gosselin, C. 2011.
580 Building materials as intrinsic sources of sulphate: A hidden face of salt weathering of historical monuments
581 investigated through multi-isotope tracing (B, O, S). Science of the Total Environment 409, 1658–69.

582 Matsuoka, N., 2001. Microgelivation versus Macrogelivation: Towards Bridging the Gap between Laboratory and
583 Field Frost Weathering. Permafrost and Periglacial Processes 12, 299–313.

584 Mutlutürk, M., Altindag, R., Türkc, G., 2004. A decay function model for the integrity loss of rock when
585 subjected to recurrent cycles of freezing–thawing and heating–cooling, International Journal of Rock Mechanics
586 and Mining Sciences 41, 237–244.

587 Norme AFNOR, 2001. Référence NF P94-422. Détermination de la résistance à la traction. Méthode indirecte-
588 Essai brésilien. 7 p.

589 Norme AFNOR, 2002. Référence NF P94-411. Roches - Détermination de la vitesse de propagation des ondes
590 ultrasonores en laboratoire. 7 p.

591 Ponziani, D., Ferrero, E., Appolonia, L., Migliorini, S., 2012. Effects of temperature and humidity excursions and
592 wind exposure on the arch of Augustus in Aosta. Journal of Cultural Heritage 13, 462–468.

593 Prick, A., 1997. Critical degree of saturation as a threshold moisture level in frost weathering of limestones.
594 Permafrost and Periglacial Processes 8, 91–99.

595 RILEM Recommendations, 1984. Absorption of Water by Immersion under Vacuum. Materials and Structures,
596 RILEM CPC 11.3, Vol. 101, 393–394.

597 Siegesmund, S., Török, Á., Hüpers, A., Müller, C., Klemm, W. 2007. Mineralogical, geochemical and microfabric
598 evidences of gypsum crusts: a case study from Budapest. Environmental Geology,52, 2, 358-397

599 Takarli, M., Prince, W., Siddique, R., 2008. Damage in granite under heating/cooling cycles and water freeze–
600 thaw condition. International Journal of Rock Mechanics and Mining Sciences 45, 1164–1175.

601 Tan, X., Chen, W., Yang, J., Cao, J., 2011. Laboratory investigation on the mechanical properties degradation of
602 granite under freeze–thaw action. Cold Regions Science and Technology 68, 130–138.

603 Török Á. 2003. Surface strength and mineralogy of weathering crusts on limestone buildings in Budapest.
604 Building and Environment, 38, 9-10, 1185-1192.

605 Yavuz, H., Altindag, R., Sarac, S., Ugur, I., Sengun, N., 2006. Estimating the index properties of deteriorated
606 carbonate rocks due to freeze–thaw and thermal shock weathering, International Journal of Rock Mechanics and
607 Mining Sciences 43, 767–775.

608 Yu, S., Oguchi, C.T. 2010. Role of pore size distribution in salt uptake, damage, and predicting salt susceptibility
609 of eight types of Japanese building stones. Engineering Geology, 115, 226–236.

610

611

Table 1

Click here to download Table: Table 1.doc

Table 1

Damage risk of limestone at Castle of Chambord. (N_{F-T}) - number of freezing days with water on the stone surface by rainfall or/and by condensation; (P_{F-T}) - percentage of damage risk (%).

Year	N_{F-T}	P_{F-T}
2009-2010	20	5.5
2010-2011	19	5.2
2011-2012	13	3.5

Table 2
Click here to download Table: Table 2.doc

Table 2
Physical properties for two fresh stones; total porosity (n), dry bulk density (ρ_d), and skeletal density (ρ_s).

Property	tuffeau				Richemont			
	Max.	Min.	Mean	S.D.	Max.	Min.	Mean	S.D.
ρ_s (g/cm^3)	2.58	2.54	2.56	0.007	2.71	2.70	2.71	0.007
ρ_d (g/cm^3)	1.46	1.35	1.40	0.017	1.95	1.88	1.92	0.018
n (%)	47.20	43.60	45.20	0.580	30.70	27.80	29.00	0.670

Table 3

Table 3
Results of MIP test for two fresh stones; (n_c) connected porosity, (D_m) median pore access diameter, (D_s) dispersion coefficient, and pore size distribution.

Limestone type	n_c %	D_m µm	D_s	Pore size distribution, %				
				<0.01 µm	0.01-0.1 µm	0.1-1.0 µm	1.0 -10 µm	>10 µm
Tuffeau	44.58	1.81	13.7	6.22	12.55	20.29	52.02	8.92
Richemont	27.16	1.16	2.4	0.0	2.96	42.17	51.58	3.29

Table 4

Table 4
Mechanical properties of fresh limestones; ultrasonic pulse velocity (V_p), and indirect tensile strength (σ_t).

Property	tuffeau				Richemont			
	Max.	Min.	Mean	S.D.	Max.	Min.	Mean	S.D.
V_p, (m/s)	1740	1498	1624	48.0	2987	2415	2599	89.2
σ_t (MPa)	1.63	1.15	1.43	0.15	2.18	1.78	2.01	0.13

Figure 1
Click here to download high resolution image

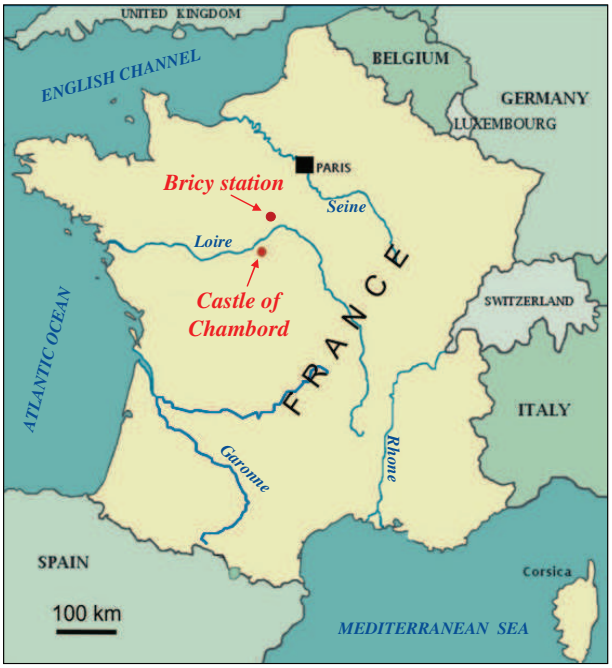

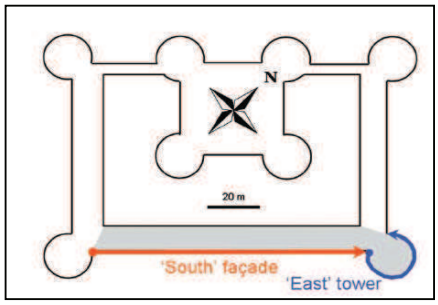

Figure 2
Click here to download high resolution image

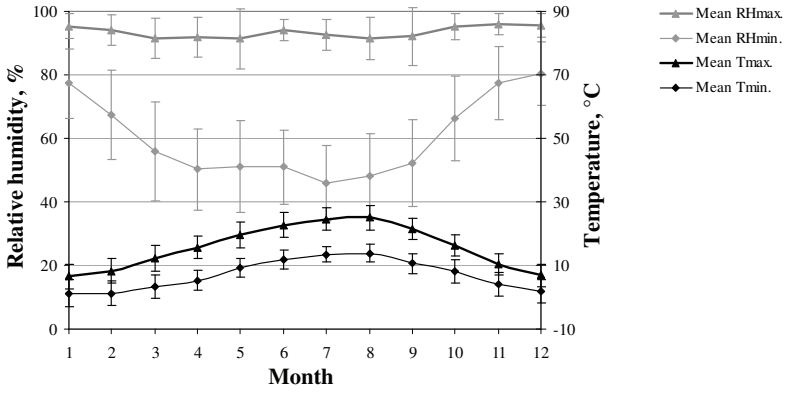

Figure 3
Click here to download high resolution image

Sensor at surface on the wall of the east tower

Figure 4

Click here to download high resolution image

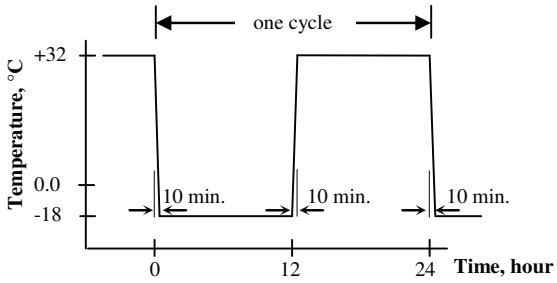

Figure 5
Click here to download high resolution image

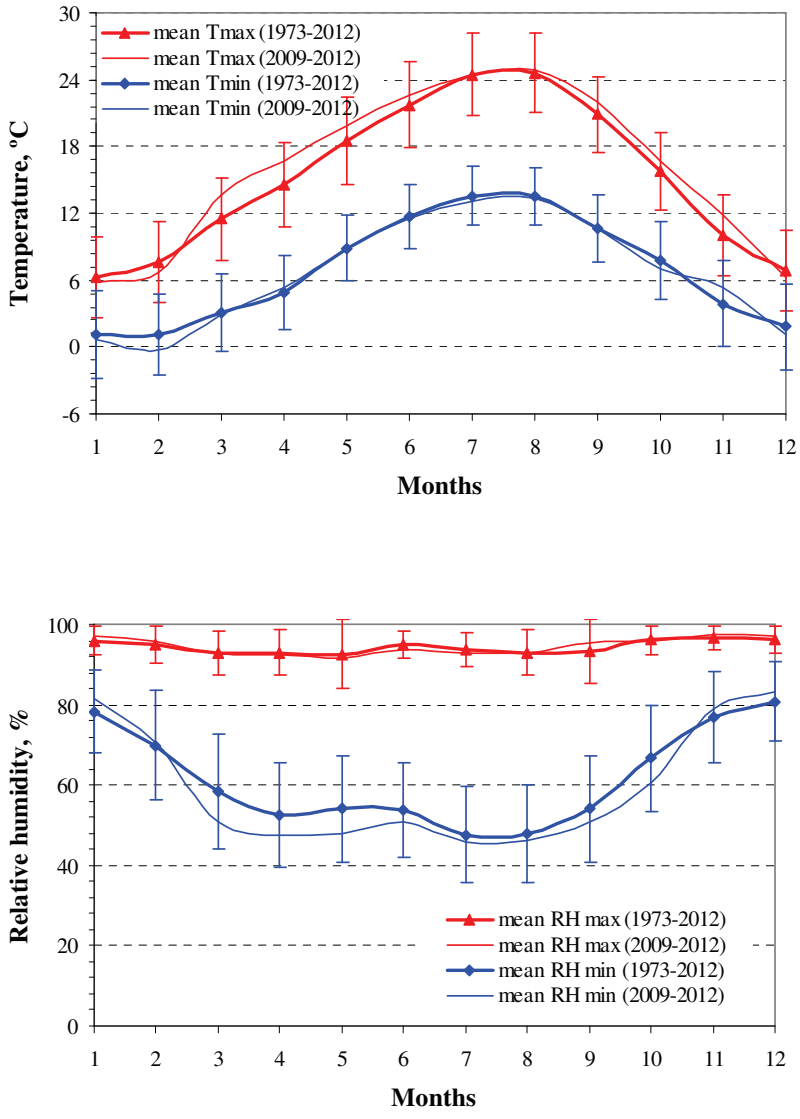

Figure 6

Click here to download high resolution image

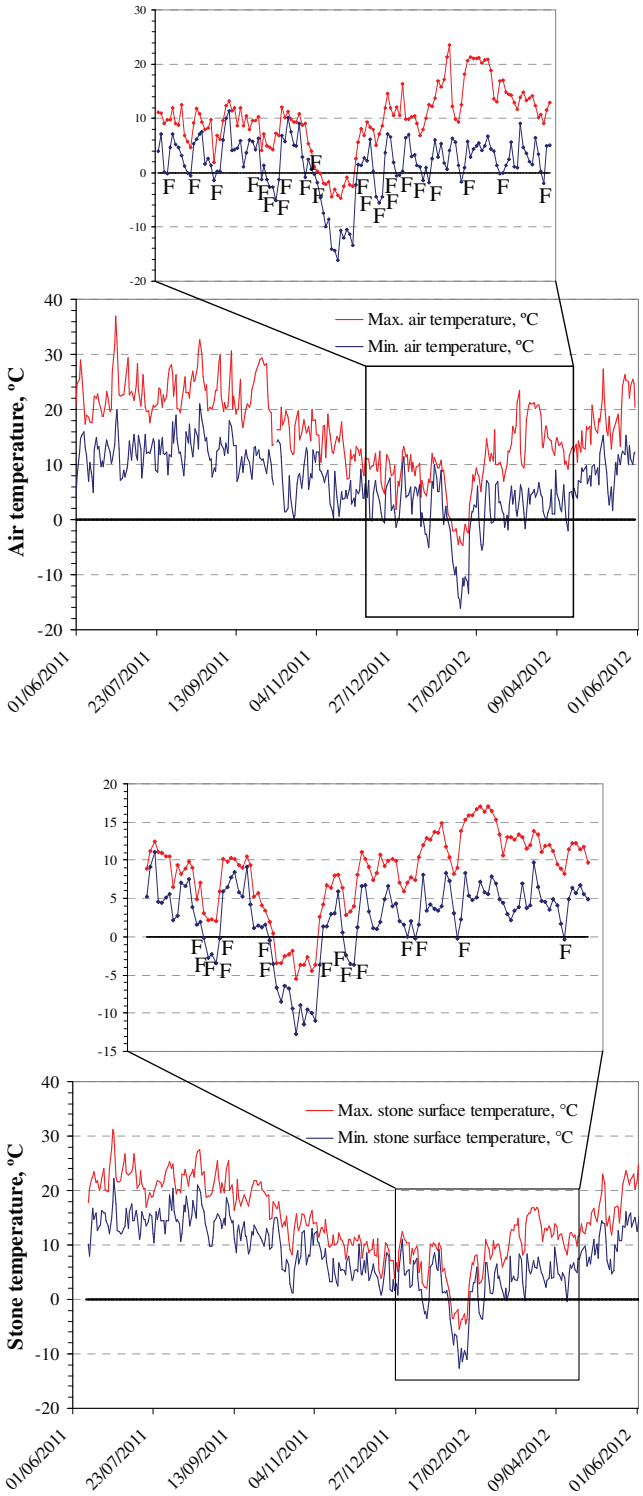

Figure 7
Click here to download high resolution image

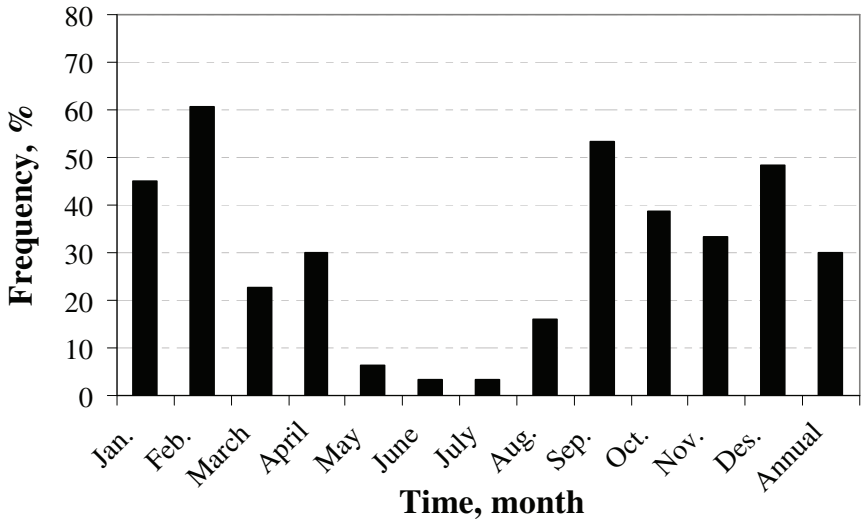

Figure 8
Click here to download high resolution image

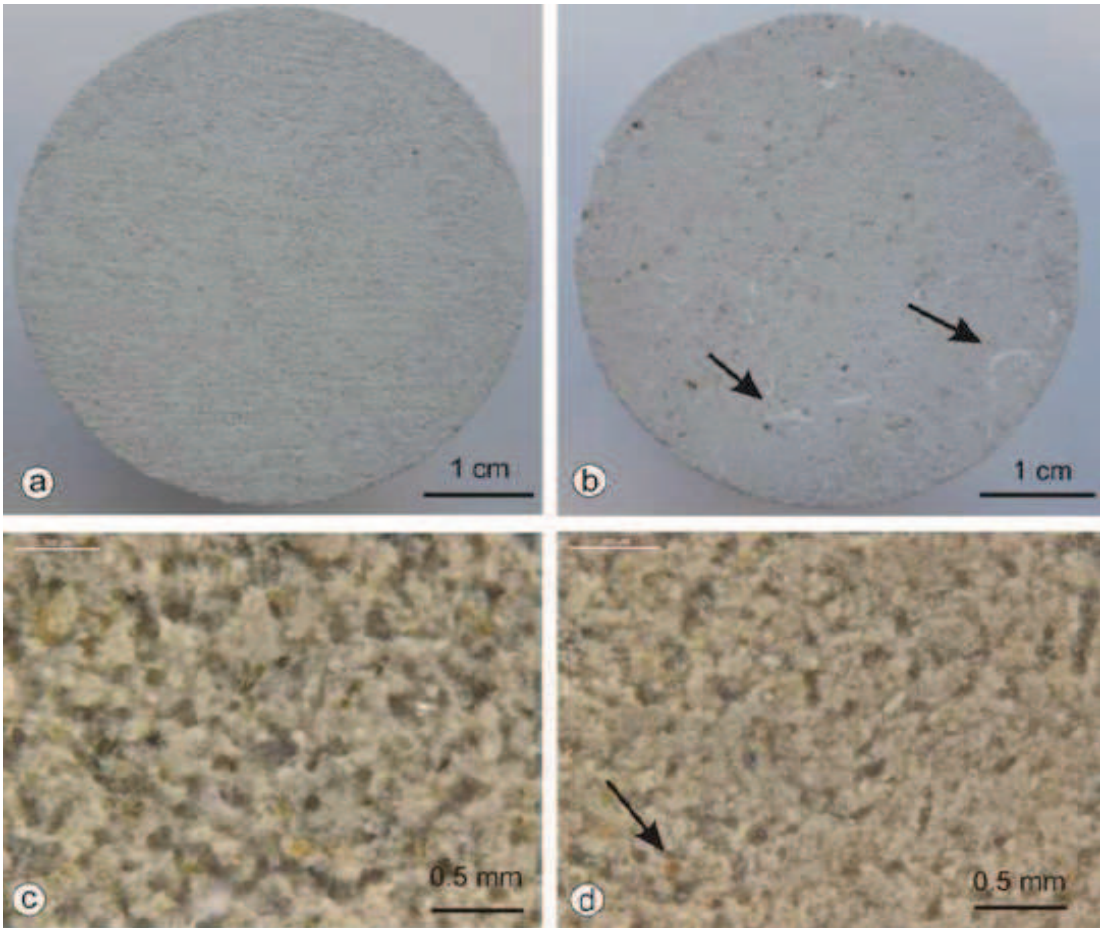

Figure 9
Click here to download high resolution image

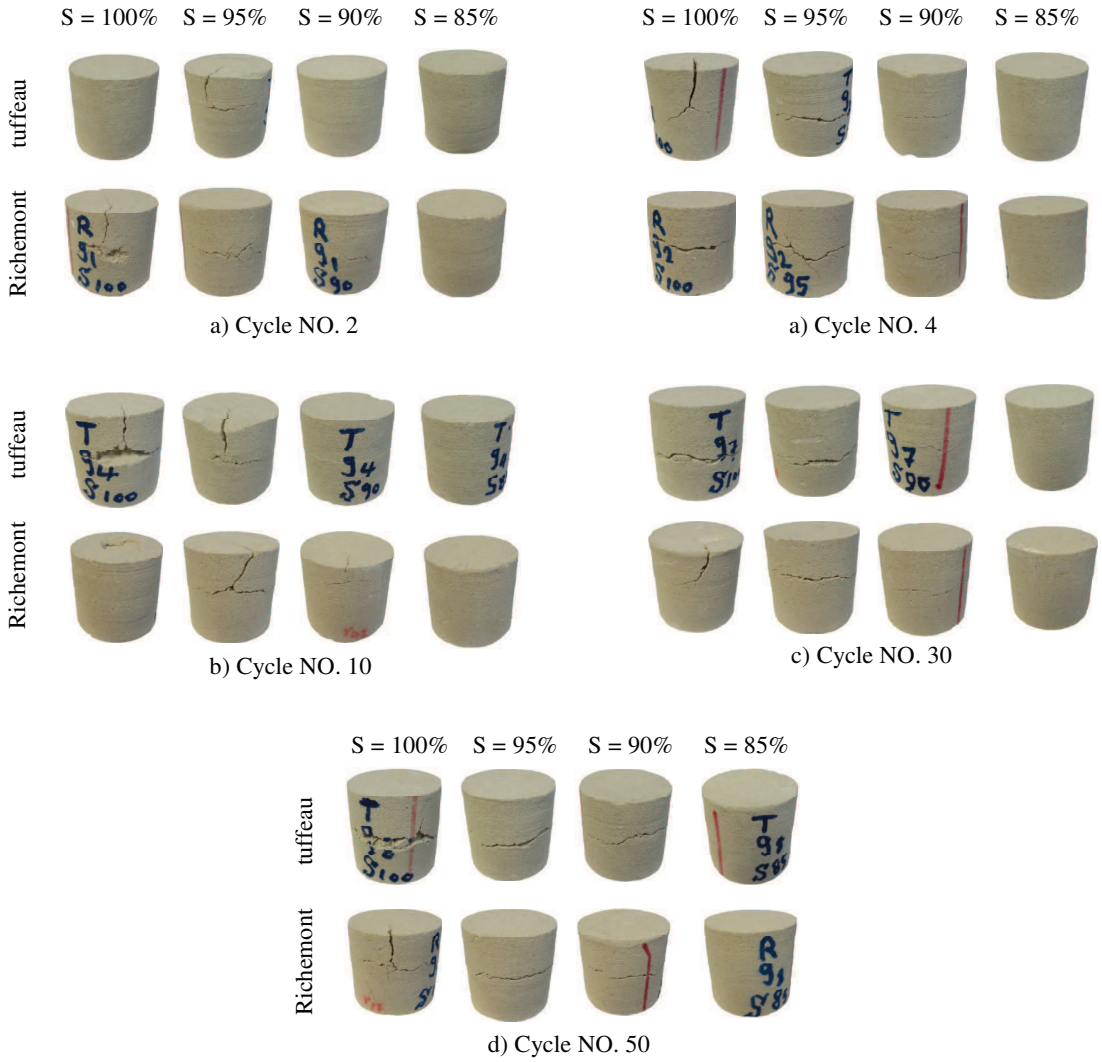

Figure 10
Click here to download high resolution image

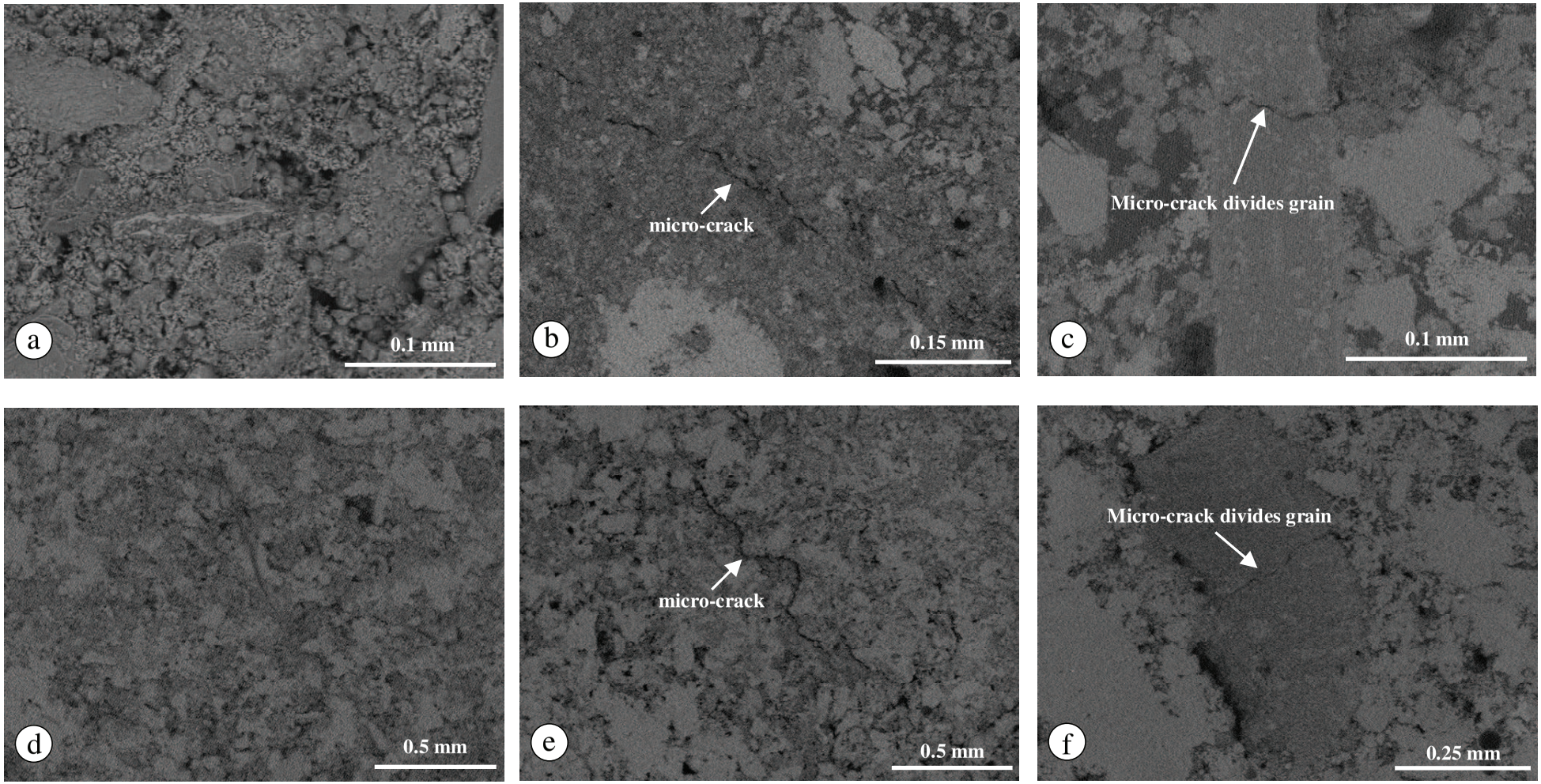

Figure 11
Click here to download high resolution image

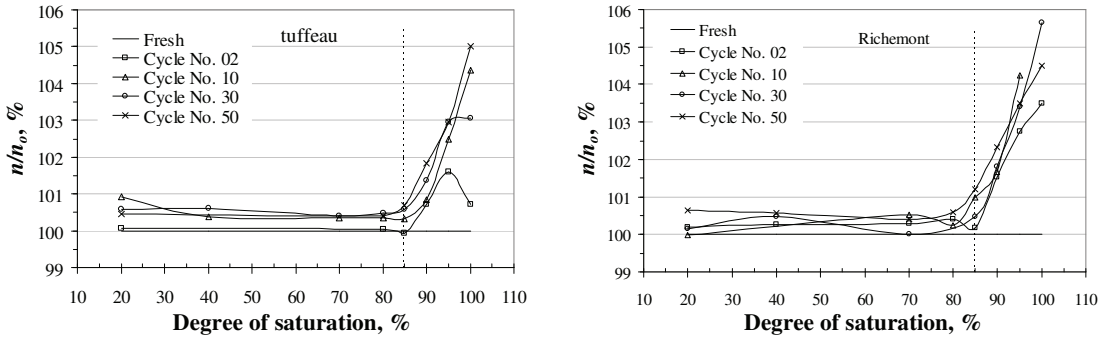

Figure 12
Click here to download high resolution image

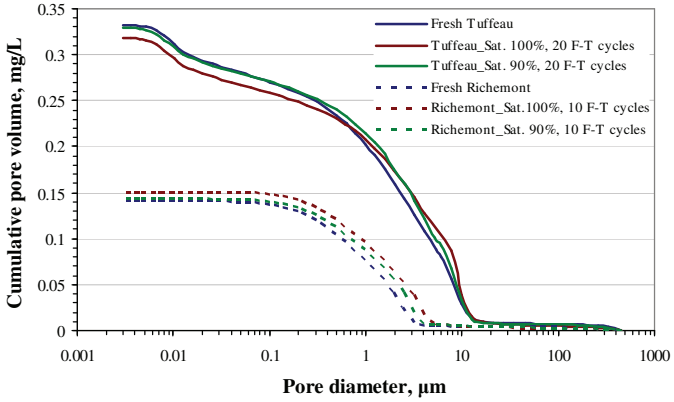

	Tuffeau		
	Fresh	**Aged sample, S:100%, C: 20**	**Aged sample, S:90%, C: 20**
Porosity %	44.58	43.02	44.37

	Richemont		
	Fresh	**Aged sample, S:100%, C: 10**	**Aged sample, S:90%, C: 10**
Porosity %	27.16	28.19	27.39

Figure 13
Click here to download high resolution image

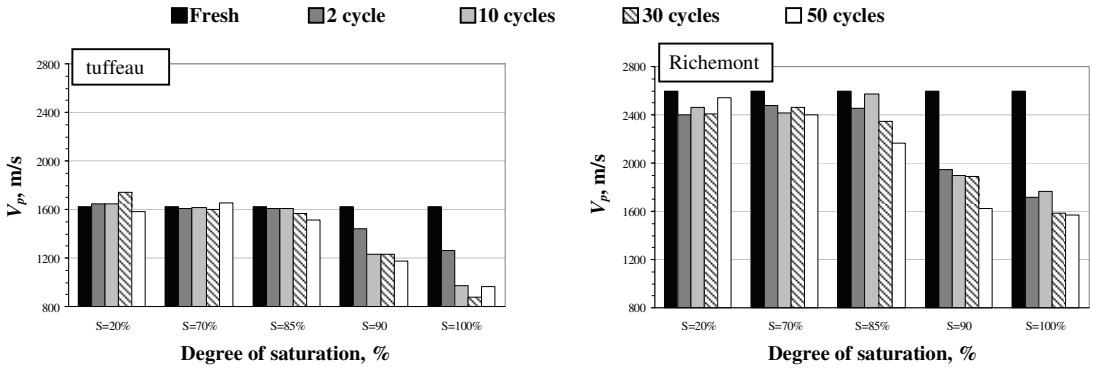

Figure 14
Click here to download high resolution image

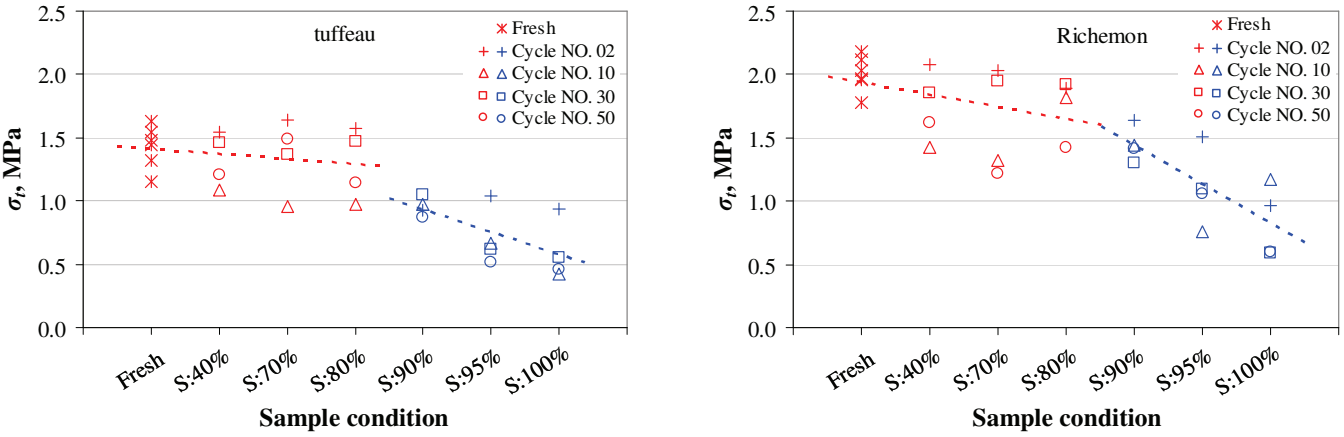

Asaad ALOMARI

Evaluation des risques d'altération d'origine thermo-hydro-mécanique des pierres du patrimoine bâti

Résumé

Cette étude traite du vieillissement des ouvrages en pierres calcaires en interaction avec leur environnement, en se basant à la fois sur la caractérisation des matériaux et des conditions climatiques locales. L'objectif de cette thèse est d'étudier le rôle des conditions climatiques sur la dégradation des pierres par une estimation quantitative du poids des différents processus physiques de dégradation : gel-dégel, condensation and dilatations hygro-thermiques empêchées. Deux sites majeurs ont été sélectionnés : le Château de Chambord en France et le site d'Al-Namrud en Irak, qui est une ancienne capitale assyrienne datant de 1280 BC. Les matériaux français étudiés sont le tuffeau et la pierre de Richemont, qui a été abondamment utilisée comme pierre de substitution durant les restaurations du 20ème siècle. Les matériaux irakiens utilisés sont issus de prélèvements sur des pierres d'origines altérées, des pierres d'origine saines, ainsi que la pierre candidate pour la restauration du site. L'approche choisie pour l'estimation du risque d'endommagement commence par la réalisation d'une campagne expérimentale de caractérisation multi-physiques et multi-échelles des pierres calcaires utilisées à Chambord, ajouté à la collecte des données météorologiques à Chambord grâce à une station et des mesures dans la pierre. L'estimation du risque d'endommagement est obtenue en combinant l'utilisation des données climatiques et de la caractérisation des matériaux, grâce au calcul de l'impact des différents processus physiques de dégradation, qui a nécessité plusieurs développements méthodologiques. La méthodologie proposée pour l'estimation du risque d'endommagement est ensuite appliquée au site d'Al-Namrud. Finalement, un carnet de santé numérique préliminaire du plus édifiant monument d'Al-Namrud – la Ziggurat – est réalisé pour son diagnostic de durabilité.

Mots clés : Pierres calcaires, estimation du risque d'endommagement, processus physiques de dégradation, données météorologiques, Château de Chambord, site d'Al-Narmud.

Risk assessment of thermo-hydro mechanical stone decay in built heritage

Abstract

This study deals with the ageing of limestone structures as a result of the interaction with their environment. It is based on the characterization of both the material and the local climatic conditions. The objective of this thesis is to study the role of climatic conditions in the degradation of stone by quantitative estimation of the weight of the different physical weathering processes: freezing-thawing, condensation and restrained hygro-thermal dilations. Two major historic sites were selected: the Château of Chambord in France and the site of Al-Nimrud City in Iraq, an ancient Assyrian capital, built in 1280 BCE. The French materials studied are tuffeau and Richemont stone, extensively used as a substitute for tuffeau restoration during part of the 20th century. The Iraqi materials studied are samples cored in situ in original weathered stones, original healthy stones, and the stone that could be used as a substitute for restoration. The approach chosen for damage risk assessment starts by the realization of a multiphysics and multiscale experimental characterization campaign of the limestone used at Chambord, added to the collection of meteorological data at Chambord thanks to a weather station supplemented by situ stone measurements. The damage risk assessment is obtained by the combined use of climate data and material characterization, through the calculation of the impact of the different physical weathering processes, which required some methodological developments. The proposed damage risk assessment methodology is then applied to Al-Nimrud site. Finally, a preliminary digital health record of the most prominent monument of Al-Nimrud - the Al-Ziggurat - is carried out to diagnose its durability.

Keywords: Limestone, damage risk assessment, physical weathering processes, meteorological data, Castle of Chambord, Al-Nimrud city

UNIVERSITE D'ORLEANS

Centre de Recherche sur la Matière Divisée CRMD FRE CNRS 3520, 1b rue de la Férollerie 45072, Orléans

cnrs